Special Issue for the 60th anniversary of the foundation of the Technical University of Košice

Foreword

This special issue of the Acta Polytechnica Hungarica is dedicated to the 60th anniversary of the foundation of the Technical University of Košice, which we cherish because of our long term beneficial and fruitful cooperation.

The Technical University of Košice belongs to our long term and stable foreign partners. The cooperation began long before the foundation of Óbuda University, with our previous institutions (Bánki Donát Polytechnic, Budapest Tech). An agreement of cooperation, which was signed in year 2000, has been the culmination of mutual relations. Its aim has been the enhancement of the partner relations and cooperation in education, research and science program, training of PhD students, exchange programs for teachers, organizing international scientific events and also in the cultural and social field.

Founders of the predecessor, the Technical College in Košice, founded in 1952, dreamed of building a university of spectacular quality. This dream has become a reality in the academic year 2012/2013, thanks to the valuable and hard work of their successors, when the Technical University of Košice celebrates 60 years of its existence. During this period, the university has created itself a profile of a top and recognized educational and research institution.

Faculties of the Technical University of Košice cover large spectrum of attractive study programs, whereas every faculty differs in its scientific profile and aim. In the present, main pillars consist of 9 faculties that cover wide range of fields of study and research paths: Faculty of Mining, Ecology, Process Control and Geotechnology (1952), Faculty of Metallurgy (1952), Faculty of Mechanical Engineering (1952), Faculty of Electrical Engineering and Informatics (1969), Faculty of Civil Engineering (1977), Faculty of Economics (1992), Faculty of Manufacturing Technologies with a seat in Prešov (1992), Faculty of Arts (1998), Faculty of Aeronautics (2005). The composition of faculties itself indicates that the university concentrates on fields that are progressive in global aspect (cybernetics, artificial intelligence, robotics, ICT). It does not even disregard classical science fields, e.g. mechanical engineering, civil engineering, electrical engineering, metallurgy, covers fields of aeronautics as well as economics and arts.

Employees of the university make significant efforts to enhance the scientific and research activities and the presentation of results in public, mostly in form of

quality scientific publications and innovative products. The Technical University of Košice has become one of the strongest repositories of highly qualified engineers for manufacturing companies and other institutions in its region.

We sincerely wish Technical University of Košice to continue the quality enhancement and gain even more intensive results and recognition in international scope in its scientific, research and other activities.

Imre J. Rudas
Rector
Óbuda University

Evolutionary Algorithm for Optimizing Parameters of GPGPU-based Image Segmentation

Sándor Szénási[1], Zoltán Vámossy[2]

[1] Óbuda University, Bécsi 96/B, H-1034 Budapest, Hungary, szenasi.sandor@nik.uni-obuda.hu

[2] Óbuda University, Bécsi 96/B, H-1034 Budapest, Hungary, vamossy.zoltan@nik.uni-obuda.hu

Abstract: The use of digital microscopy allows diagnosis through automated quantitative and qualitative analysis of the digital images. Often to evaluate the samples, the first step is determining the number and location of cell nuclei. For this purpose, we have developed a GPGPU based data-parallel region growing algorithm that is equally as accurate as the already existing sequential versions, but its speed is two or three times faster (implementing in CUDA environment), but this algorithm is very sensitive to the appropriate setting of different parameters. Due to the large number of parameters and due to the big set of possible values setting those parameters manually is a quite hard task, so we have developed a genetic algorithm to optimize these values. Our evolution-based algorithm that is described in this paper was used to successfully determine a set of parameters that compared to the results with the previously known best set of parameters means a significantly improvement.

Keywords: biomedical image processing, nuclei detection, GPGPU, CUDA, genetic algorithm

1 Introduction

Our work focuses on the segmentation of images containing hematoxilin-eosin stained colon tissue samples (Fig. 1). There are several procedures to identify the main structures in these images and a lot of them based on a reliable cell nuclei detection method (these procedures need the exact locations of the cells).

There are several image processing algorithms for this purpose [1][2][3][4][5], but some factors could increase the challenge. The size of the images can easily reach the order of few 100 Megabytes, therefore the image processing speed plays an important factor.

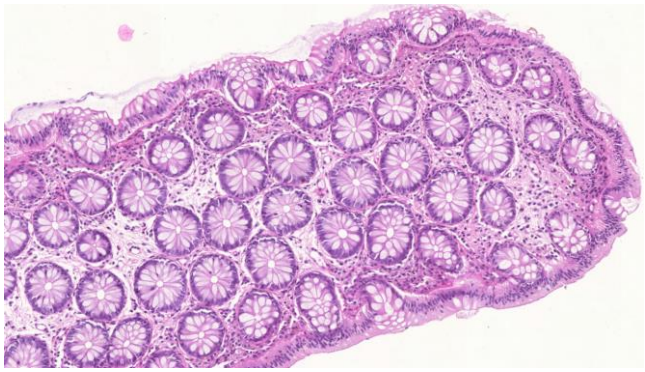

Figure 1
HE stained colon tissue

One of the most promising alternatives is the region growing approach; it can correctly separate structures but it is too slow for practical usage. Parallelizing the region growing algorithm aims at providing better execution times, while delivering the similar outcome produced by the sequential version [4]. We have developed a GPGPU based region growing algorithm [6], and implemented it in CUDA environment. The new method is 25–65% faster than the CPU based implementations and its accuracy is the same.

The different steps of the region growing algorithm (pre-processing, the region growing itself, separation of merged cells) require fairly much (in our implementation, twenty-seven) parameters which can be considered as independent variables since their effects on each other is unknown. Every parameter greatly affects the output of the algorithm, so to define an optimal set of parameters we have to treat all parameters simultaneously. Due to the large number of the parameters manual method is practically hopeless; we need an intelligent system [7] that finds the best values. Therefore we have developed a genetic algorithm, which tries to find the most optimum set of parameters from the available parameter collection.

2 Description of the Parallel Region Growing Algorithm

2.1 Detection of Seed Points

In the first step of region growing, we have to find the most intensive point of the image that complies with some. In case of the GPGPU implementation this means multiple points, becase we can execute multiple cell nucleus searches parallel. The adjacent seed points can cause problems (we must avoid overlapping cell nuclei),

which would require a lot of computational time to administer. We know the maximum radius of a cell nucleus, so we can presume that the searches started from two seed points (that are at least four times further apart than this known distance) can be handled as independent searches; so they can be launched in the same time.

A quick overview of our complex searching algorithm (full description about this algorithm is given in our previous paper [6]):

1. The points that matches the starting condition and that have the biggest intensity must be collected into an $S_{waiting}$ set (since we only store the intensity on 8 bits, it is likely that there will be more than one points). To achive this we can use the atomic operations of the GPGPU.
2. One element is selected from the $S_{waiting}$ set, and it is moved to the $S_{confirmed}$ set. We can use the GPGPU capabilities therefore every seed point is checked by a seperate thread.
3. In the $S_{waiting}$ set, we examine the next element: we check if any of the elements from the set $S_{confirmed}$ collide with the parallelized processing of this element (they collide, if the distance of the two points is below the critical threshold). If there is no collision, then this element is moved into the $S_{confirmed}$ as well, otherwise it stays where it is. We repeat step 3 until we run out of elements in the $S_{waiting}$ set, or we find no more suitable points, or the $S_{confirmed}$ set is full (its size is the same as the number of the parallelized region growing runs we want to execute simultaneously).
4. We launch the region growing kernel using the seed points that are in the $S_{confirmed}$ set.
5. After the execution of the kernel, we store the results, we delete the contents of the $S_{confirmed}$ set, and the elements from the $S_{waiting}$ set that no longer match the starting criteria.
6. If there are still elements left in the $S_{waiting}$ set, we continue with step 2. If it is empty, we continue the processing with step 1.

This iteration is continued until the thread runs out of seed points, or the required amount of points is enough for the starting of the next region growing.

2.2 Cell Detection with Parallel Region Growing

The region growing itself iterates three steps until one of the stop conditions is met. A quick overview of the region growing iterations (full description about this algorithm is in our previous paper [6]):

1. We have to check all the possible directions in which the contour can be expanded. This means the four-neighborhood of the starting point (in case of first iteration) or the pixels around the lastly accepted contour point (in case of further iterations). The examinations of these pixels are independent of each other, therefore we can process them in the same time: four threads

examine the different neighbors, whether they are suitable points for further expansion or not.

2. All of the contour points must be evaluated to decide in which direction the known region should be expanded. For this, we have to evaluate a cost function [4] for every point. It is important to notice that some parameters of the cost function change at the insertion of every new point, so they have to be re-calculated in every iteration for every points. This is well parallelizable calculation, every thread counts the cost of a single contour point.
3. The contour point with the smallest cost must be selected. We can use the *atomicMin* function to make the threads calculate the smallest cost. That contour point can be chosen to increase the region.

After every iteration, a fitness function is evaluated that reflects the intensity differences between the region's inner and outer contour, and the region's circularity. The process goes until the region reaches the maximum size (in pixels or in radius), and its result is the state where the maximum fitness was reached [6].

We can start several region growing parallel. In this case we have to assign a single block to the processing of one single cell nucleus.

3 Parameter Optimization Techniques

It can be reasonably simple to create a model of the problem itself: we have 27 mutually independent parameters with pre-defined target sets; we have a working region growing algorithm (and its implementation) that produces the list of cell nuclei (size, location, etc.) that can be found in a sample; and we also have an evaluation function [8] that determines an accuracy value that is defined by comparing the results of the aforementioned region growing algorithm with the slides that were annotated manually by qualified pathologists (further on, the "Gold Standard" or GS slides) available at our disposition. Our aim is to search a set of parameter values that gives us the best possible accuracy (which is a classical problem in the field of image segmentation [9]). This is a classic optimization task and as for such, we found several possible solution alternatives.

3.1 Enumerative Methods

The different search methods can be grouped into three distinct categories [10]: random, enumerative and calculus-based methods. The basic principle of the enumerative-based methods is to examine all possible solutions and then it selects the best from those [11]. This method could easily be adapted to our task; we should only list all possible combination of parameters, and then we could find the

best by using a simple linear search (thought it would be a good question that what resolution should be used to break up the different intervals into discrete values).

It is guaranteed that this solution finds the best solution, but due to the large number of possible combinations, this method is practically useless for us. Thought we can influence the number of possibilities at some level (by arbitrarily narrowing down the target sets or decreasing the resolutions of the intervals); but in the case of a typical real-world configuration the evaluation could probably take years. And since we do not have exact information about the results of the various parameters and about their effects on each other, we cannot even reduce the search space using different heuristic methods either.

3.2 Calculus-based Methods

The other important group of methods contains the calculus-based methods where the reasonably large search space does not necessarily mean large computational needs, because there is no need to search through the whole problem space. In these cases, we start off an arbitrarily selected point, and then the algorithm (after every single evaluation) continues in the direction that at the given moment results in the greatest immediate positive advantage (the classical examples of this approach are the Greedy [12][13] and the Hill-Climbing [14] methods).

Naturally we can implement this method to our problem as well: as a starting point, we can select any point in the parameter space, and then we can evaluate its immediate surroundings, and then we can move towards the point that has the biggest accuracy and continue our search from that place. These greedy algorithms can be reasonably fast in finding a result, but we can only guarantee that this result of parameter set will be a local optimum; however, we will have no clue about the relation of this local optimum with the global optimum. Since the parameters are loosely connected to each other, it is very likely that we will find many local maxima (points where the parameter set yields us reasonably good results but a slight modification will worsen these results).

The disadvantage of this method is that there is no possibility for a backtrack, so once the search has ran into such a local maximum, we can only get to a different result by re-starting the whole process from a different starting point.

The search is sensitive to its starting parameters, so of course it is possible to fine-tune the results if we simply start several different search processes from different starting points, and then we compare the results of these. However, due to the large number of parameters, there can be many different possible starting points, and within a finite time, we can only examine a very small fraction of these. Furthermore, the large number of parameters poses another problem: because of this, the examination of the neighborhood of a single point can have very high computational needs if we want to test the outcome of all possible directions (what

is more, due to the large number of parameters, we would be forced to simplify this process, so we would lose the biggest advantage of the hill-climbing algorithm: that is, we risk that it will not find the local maximum as it originally should).

3.3 Guided Random Search Techniques

The third group of search methods is the random search group: in a strict sense it simply means that we examine randomly selected points within the problem space and we always store the one that yields the best results. On its own it will be less effective for us, for two reasons. Firstly, its execution time can get pretty high. Secondly, it gives us absolutely no guarantee of finding any kind of local or global optima within finite time. However, in practice, we can use the guided random search techniques [15]: they basically examine randomly selected points, but they try to fine-tune the selection method using various heuristics.

Typical examples of these methods are the Tabu Search [16], the Simulated Annealing [17] and the Evolutionary Algorithms [15]. Out of these, the different evolution-based algorithms are the most interesting for us. The basis of these techniques is that various well-known biological mechanisms are used to execute various search and optimization algorithms. These algorithms share the same basic principle: newer and newer generations are calculated starting from an initial population (in our case, this means a starting set of parameters for the region growing algorithm); and the members of the new generations are expected to be more and more viable (in our case, this will represent parameter sets that yield more and more accurate results). In addition, we can define various stopping criteria as well, but this method can also be used even without those, because the individual generations can be checked on-the-fly, so the parameter set that actually yields the best results can always be accessed at any given moment.

In our case, this technique seems the most suitable, because our task fulfills the following criteria where the usage of the genetic algorithm is considered favorable:

- Search space with multiple dimensions, where the relations between the major variables are unknown.
- The traditional solutions give us unacceptable execution times.
- It is very difficult (or impossible) to narrow down the search space.
- One solution can be checked quickly, but finding an optimal solution is difficult.
- We do not necessarily need the global optimum, we merely want the best possible result.

```
Formulate the initial population()
Randomly initialize the population()
Repeat
   Evaluate the objective function()
   Find fitness function()
   Apply genetic operators (reproduction, crossover, mutation)
Until (¬Stopping_critera())
```

Algorithm 1
Typical structure of genetic algorithms

In addition to this, the genetic algorithms have several more advantages:

- They can be very well parallelized so they can be efficiently implemented in multi-processor environments. Since the method described above has reasonably big computational requirements (because of the fact that during the search process both the region growing itself and the evaluation too have to be executed for every set of parameters); it is essential that we can complete this process within the shortest possible time in a distributed environment.
- Compared to the hill-climbing method, it is more likely that we find a global maximum because due to the nature of its operation a genetic algorithm continues the search even if a local maximum is found: due to the mutations, there are nonstop changes even with a stable population. In addition to this, even thought we cannot guarantee that it will find the global maximum within a finite time, but there are several papers that show that the search itself generally converges towards an optimal result [18], [19], [20].
- After reviewing the publications in this topic we examined several genetic algorithms for optimizing parameters and usually these algorithms met the previously stated requirements [21], [22].

4 Construction of the Genetic Algorithm

4.1 Representation of Chromosomes

A genetic algorithm usually contains the steps of Algorithm 1. When creating a genetic algorithm, a decision must be made that which encoding form should be used with the data of the different instances (in our case, an instance is represented by a single chromosome so we use the two terms as equals). For this, the search space must be somehow mapped to the chromosome space. To do that, we have several possibilities, but the following aspects must be taken into consideration:

- We want to optimize a reasonably big set of parameters.

- These parameters can be considered as being independent from each other.
- Every parameter is a number; some of them are floating point numbers.
- The target sets of the different parameters are different.
- Most of the parameters can be surrounded with an upper and lower bound, but there are several parameters that have to comply with additional rules as well (e.g. only even numbers are allowed).

It is a very common approach that the parameter set is simply converted into a vector of bits (using the values of the parameters in base-two form). However, several researchers suggest [23] that we should not encode the floating point numbers in bits; the chromosomes should contain real (floating point) numbers. The advantage of this method is that we can easily apply problem-specific mutations and crossovers.

In our case we have a multi-dimensional search space; and according to this we have to store several genes inside a chromosome (these genes actually represent the parameters of the region growing algorithm). Since the relations between the individual genes are hard to describe, it is more feasible to choose a representation where every parameter is separately encoded according to its target set and where we can establish that the functionality of the different genes do not depend on their location inside the chromosome.

Of course, we can have chromosomes that are not viable (if not the crossovers, then the mutations will probably produce some of those). These instances are handled in a way so that they will have a fitness value of zero. This way (even thought they will be indeed evaluated) these chromosomes will most certainly not be included in the next generations.

4.2 Initial Generation for Genetic Algorithm

The initial generation is generated by randomly generated instances. There is a set of parameters that is already used in the live applications, but using this set as the initial generation came with no benefits at all, because the system found an even better set of parameters within only a few generations).

Some of the parameters have known upper and lower bounds [24]. In case of these parameters the actual values for the different instances were chosen using Gaussian distribution within these intervals. The known intervals are:

- Cell nuclei size: 34 – 882 pixels
- Cell nuclei radius: 4 – 23 pixels
- Cell nuclei circularity: 27.66 – 97.1
- Cell nuclei average intensity: 36.59 – 205.01 (RGB average)
- Seed point intensity: 0 – 251 (RGB average)

With some technical parameters it is not possible to perform such preliminary tests, in these cases the initial values of the parameters are distributed using the currently known best set of parameters. The intervals are generated in the ±10% surroundings of these aforementioned values using normal distribution. Of course, this does not guarantee that the optimal result will be within this interval, so it is advised to check both the final result of the optimization and the intermediate results as well: if the instances that yield good results have a parameter that is always around one of the arbitrarily chosen bounds, then it might be practical to further extend this interval. Despite this (due to the operation of the genetic algorithm, and due to the mutations) the genes can have values that are outside these starting intervals, so an initial generation generated with some unfortunate initial values can also find the good final result as well.

Every instance in the first generation was created using random parameter values, so with a great probability there are a large number of non-viable instances in this generation, which is not feasible for the further processing. Firstly, it is necessary that we have the biggest number of usable instances for the next generations so that we can choose the best candidates from multiple possible instances. Secondly, there is a bigger importance on the first generation, because it would be better if there could be the biggest number of different values for a parameter so that these multiple values can be taken into the next generations and this way there is a bigger chance that the given parameter's optimal value is carried along as well. For these reasons, the first generation is created with a lot more instances than the following ones, in our case that means 3000 chromosomes. The following generations will contain only 300 instances (both values were determined arbitrarily based on the experiences of the first test runs).

4.3 Processing Generations

We have to calculate the fitness value of all instances in the actual generation. In our case the fitness value is determined based on how well the parameters represented by the chromosome performs with the region growing algorithm. We need two main steps to calculate this:

1. First we have to execute the region growing cell nuclei detector algorithm with the given set of parameters. Since the parameters can behave differently on different slides, the region growing is executed for several slides.
2. The next step is the evaluation of the result of the region growing (the list of cell nuclei). For this, we compare these results (test result) with the manual annotations of the Gold Standard slides (reference result). By averaging the results of the comparisons we get the fitness value for the given chromosome.

4.3.1 Accuracy

We use the evaluation algorithm described in our previous paper [8] for comparing test and reference cell nuclei sets. This is based on the confusion matrix [25] that can be constructed using comparison the two result sets hits (another approach can be a fuzzy based model [26], [27]). The accuracy of the region growing is a simply calculated measurement number [25]:

$$Accuracy = (TP + TN) / (TP + TN + FP + FN) \quad (1)$$

Where *TP* means the number of *true-positive* pixels; *TN* is the number of *true-negative* pixels; *FP* is the number of *false-positive* pixels and *FN* means the number of *false-negative* pixels.

The pixel-level evaluation itself will not give us a generally acceptable result, because it will only show a small error even for big changes in densities, and our task is not only to determine if a pixel belongs to any object or not, but we have to locate the objects themselves (because it is not acceptable to detect one big nucleus instead of a lot of small nuclei).

4.3.2 Object Level Evaluation

Our measurement number does not based only on a pixel-by-pixel comparison; instead it starts by matching the cell nuclei together in the reference and the test results. One cell nucleus from the reference result set can only have one matching cell nucleus in the test result set and vice versa. After the cell nuclei matching, we can compare the paired elements.

The final result is highly depends on that how the cell nuclei are matched against each other in the reference and the test result sets. Due to the overlapping nuclei, this pairing can be done in several ways, therefore it is important that from the several possible pair combinations we have to use the optimal (the highest final score).

During the practical analysis [8] of the results we found out that on areas where cells are located very densely, we have to loop through a very long chain of overlapped cells, which results in groups that contain very much cell nuclei from the test and from the reference sets as well. We use a new backtracking search algorithm [28] to find the optimal pairings. This requires significantly fewer steps than the traditional linear search method.

The sub-problem of the backtracking search is finding one of the overlapping cell nuclei from the test results and assigning it to one of the reference cell nuclei. It is possible that there will be some reference cells with no test cell nucleus assigned to them and it is also possible that there will be some test cells with no assignment at all. The final result of the search is the optimal pairing of all the possible solutions. Full description of this algorithm is given in our previous paper [8].

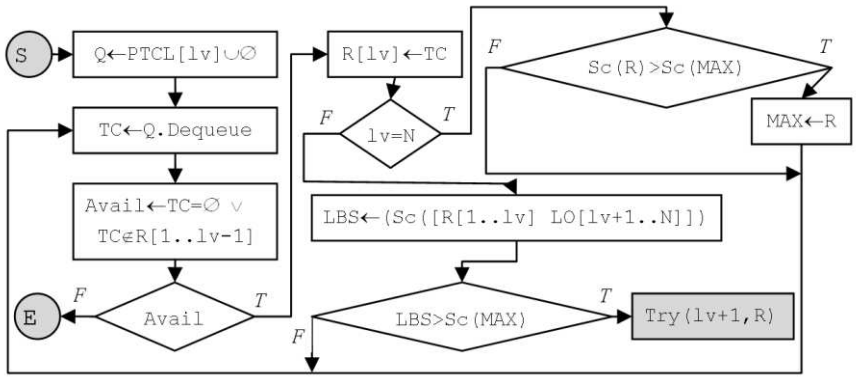

Algorithm 2

Backtracking core algorithm

Inputs and utilized functions:

- lv – The level currently being processed by the backtracking search.
- R – The array that holds the results.
- PTCL – An array for every reference cell with test cells from the group that overlap with the given reference cell.
- LO – For every reference cell nucleus LO represents the local optimal result, if we choose the best overlapping test cell. During the search, the algorithm will not move to the next level if it is found out that the final result will be worse if we choose the most optimal choices on all the following levels.
- Sc(X) – It returns the value for the pixel-level comparison using input X (which is a pair of a test and a reference cell nucleus).

Algorithm 2 will search and return the optimal pairing of a group containing test and reference cell nuclei. The i^{th} element of the MAX array shows that the i^{th} reference cell nucleus should be paired with the MAX[*i*] test cell nucleus.

The above algorithm algorithm should be execued for every group to get the optimally paired cells. After that, we can calculate the above mentioned accuracy. This will be the fitness value of the given chromosome.

4.4 Implementation of Genetic Operators

4.4.1 Implementing Selection Operator

The selection of the parent pairs can be performed using any available methods; the important feature is that instances with a bigger fitness value should be selected proportionally more times than the others. One of the best solutions for

this is the well-known roulette wheel selection method, where we generate an imaginary roulette wheel where every instance has a slot that is sized proportionally according to the fitness value of the given instance. When selecting the new parents, we spin the wheel and we watch which slot the ball is falling into [29].

The probabilities can be determined using the following formula:

$$P_i = (F_i - Min(F)) / \sum_k (F_k - Min(F)) \quad (2)$$

Where

- P_i: the probability to select the instance #i
- F_k: the fitness value for the instance #k
- Min(F): the smallest fitness value for the current generation

It is visible that by using this calculation method there is a side effect: the instances with the smallest fitness values are completely locked out from the next generation, but in the practical implementation this means absolutely no problem. However, this way we eliminate the biggest drawback of the roulette wheel method too that occurs if the fitness values for different chromosomes are too close. In addition, since it is possible that non-viable instances are in the generation as well (which means that after the evaluation there can be some chromosomes with the fitness value of zero) we have to remove these instances before calculating the probabilities so that these instances will not distort the minimum value in the equation.

The search space is reasonably large, so the occasionally occurring instances with good fitness value can disappear in the next generation due to the random crossovers. For this reason we use elitism [30]: the instances with the highest fitness values are carried along into the next generation (10% of the generation is selected this way). This method slightly decreases the number of trial runs per generation, but this way we guarantee that the best chromosomes are kept.

4.4.2 Implementing Crossover Operator

The most typical step of a genetic algorithm is the crossover. There are several known methods for this step; the simplest one is the single-point crossover: we simply cut the chromosomes in half using a random cut-point and we exchange the chromosome parts that are after the cut point [18]. This can naturally be done using two or more cut points as well, the most generic case being the uniform crossover where we generate a random crossover mask that simply defines for every bit which parent is used for the given bit of the descendant instance.

In our case the size of the population can be considered as reasonably small (because the evaluation of the single instances can be very time consuming, so we cannot use a large population); while the chromosomes are considered to be

reasonably large (27 parameters, several hundred bits altogether). Because of these we clearly have to use the uniform crossover method.

In the strict approach, the uniform crossover could be performed for every bit; but in our case this is not feasible. The reason for this is that there are some parameters that have to comply with some additional rules (e.g. divisibility), and the bitwise mixture of those can easily lead us to values that do not belong to the target set.

We only combine whole genes: for every gene we use a random number to determine which parent's gene is inherited.

We use the following probabilities:

$$P_a = (F_a - \text{Min}(F)) / (F_a + F_b - 2*\text{Min}(F)) \quad (3)$$

$$P_b = (F_b - \text{Min}(F)) / (F_a + F_b - 2*\text{Min}(F)) \quad (4)$$

Where

- P_a: the probability of gene of parent A is inherited
- P_b: the probability of gene of parent B is inherited
- F_a: the fitness value for parent A
- F_b: the fitness value for parent B
- Min(F): the smallest fitness value for the current generation

4.4.3 Implementing Mutation Operator

The size of the mutation cannot be defined in a general form (for every parameter), because the values of the parameters can be very different. With some parameters small changes in the actual value can have great effects, while other parameters are much less sensitive. For this reason, we rejected the bit-level mutation, because in some cases this can result in too drastic changes.

Some parameters are reasonably small integers, and we cannot use percentage-based mutations with those, because neither the small nor the medium-sized mutations would be enough to change the value even to the closest integer. For this reason these values change with discrete values according to the $\pm\varepsilon$ method described in [31]: small mutation means a change with one, medium mutation means a change with two, and a big mutation means a change with three; and there is a 50–50% chance that the change will be positive or negative.

During the mutation process we do not check if the new value complies with the given parameter's target set. If a mutation causes the parameter to have a wrong value, then the chromosome will have a very bad fitness value (if the parameter is out of bounds, then a zero fitness value) after the next evaluation, so similarly to the rules of nature, these non-viable instances will fall out from the next

generations. The number of such instances is quite small, so this does not deteriorate the results of the search.

By introducing an auxiliary verification step this could be resolved, but on one hand the development of an extra rule-set is difficult (since we do not know exactly the relations between the various parameters), on the other hand it would not be feasible to fix these rules. The reason behind this is that the mutations have an additional important role in the system: since in the starter generation we generated the parameter values between arbitrarily chosen interval boundaries, it is possible that due to a mistake in this process, the ideal gene was not even present in the initial generation. In this case, the mutation can help us so that the search continues to an undiscovered area that has great potentials and that was originally locked out due to a badly chosen interval (or an unlucky random number generation).

The probability of a mutation is 10%. The size of the mutation is a random number based on the parameter (generally there is a 60% chance for small, a 30% chance for medium-sized, and a 10% chance for large mutation).

5 Implementation Details

The actual implementation was done according to the following criteria:

- 27 parameter values are searched.
- The initial generation has 3000 chromosomes.
- Every following generation has 300 chromosomes.
- Every parameter set (every instance) is tested against 11 representative tissue samples.

With the genetic algorithms, usually the execution time is the only barrier for the accessibility of the optimal results. This is true in our case as well, because the evaluation of a single instance needs quite a lot of time: based on the first 1550318 evaluations, the average processing time for a single region growing is 1498ms, and it took another 8249ms to evaluate the results for a single image. Since we always have to examine 11 tissue samples, it takes about 107 seconds to examine a single chromosome, so the evaluation of a single generation takes about 8.93 hours.

Since we have to assume that we will process hundreds of generations, it is obvious that we have to speed up the whole process somehow; and an obvious method for this is a high-level parallelization. Out of these, the most basic method is the master-slave processing [29]. Since the testing of the single instances (the execution of the region growing and the evaluation of the results) can be considered as independent tasks, these can be efficiently parallelized in a distributed environment. In this case we work with a global population and the

parallelization is merely used only for the evaluation. To achieve this, a parallel execution environment was developed that uses client-server technologies to execute the genetic algorithm using the parallelized method described above.

A single central server manages the whole process. Basically, this program stores the population itself and this is where the basic genetic operations are executed. The main tasks of this module are:

- Generate an initial population.
- Generate any following generations (selection of parents, crossover, and mutation).
- Distribute the tasks towards the evaluator clients, then collect and process the results.

The number of clients that can connect to the server is not limited; the clients do not see the whole population and they take no part in the genetic operations, they only perform auxiliary operations for the evaluation. Their tasks are:

- Download the data that are necessary to process an instance (tissue images, parameters).
- Execute the region growing algorithm for every tissue sample using the downloaded parameter set.
- Evaluate the results of the region growing algorithm, and then send back the results of the evaluation to the server.

The system was designed with scalability in mind, because the number of available client computers greatly varies over time. In the worst case this can be as low as only a few clients, but sometimes (by taking advantage of the university's capabilities and using the occasionally free computer laboratories) it peaked at a little more than one hundred. The server is continuously online and produces the data packets that require further processing; the clients can join at any time and can operate for any length of time. The smallest atomic unit is the processing of a single chromosome.

Although there is no technical upper limit for the number of connected clients, we usually used 100 clients, which proved to be enough for our generation size of 300 instances. Increasing the number of clients does cause an increase in speed, but this increase is far from linear. The cause behind this is that evaluating the different instances always requires a different amount of time, and in nearly every generation there are some clients that receive a task unit that requires a lot more computational time than the others. So by the time these clients are finished with their one instance, the other clients can process two or even three of them. So even if we increased the number of clients, the bottleneck would still be the single client that received the most difficult instance.

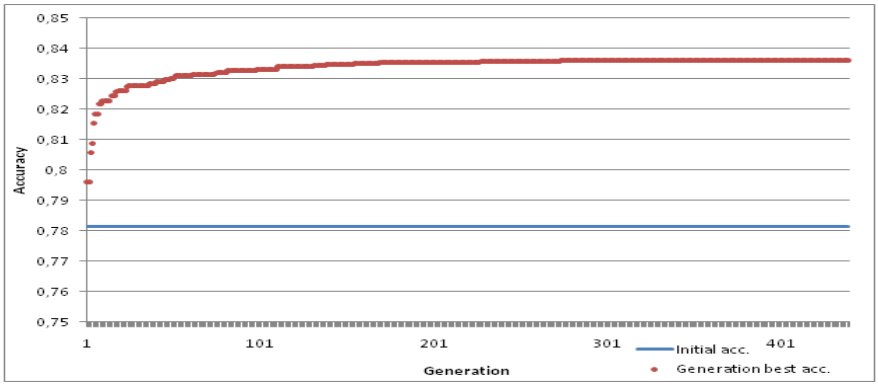

Diagram 1
Best accuracy by generations

The extensive description of our developed system (structure of the server and the client, description of the communication and the robust implementation) will be detailed in our next paper. In the followings, we present our results after 440 generations (this took approx. 3948 working hours; thanks to parallel processing capabilities this was only a weekend in practice).

6 Final Results

6.1 Examination of Generations

The best fitness values give us a monotonically increasing series of numbers because the chromosomes with the best fitness values are automatically carried along into the following generation as well. These values can contain useful information about the speed of our optimization.

We did not have any specific goals for this task, so we cannot mention any expected results that we wanted to get (with the exception of the 100% accuracy; although, reaching this seems impossible, because we have to consider that the region growing itself does not guarantee a perfect result, even if we find the optimal set of parameters). For these reasons, our aim is to get the best possible results, compared to our possibilities.

We can compare these values to the parameter set that was originally developed by Pannon University [4], which gave us the average accuracy of 78.1%. This can be considered as the acutally known best accuracy. Surpassing this value with any extent can be considered as a useful result.

Diagram 1 shows the best results for every generation, the horizontal line shows the 78.1% level. In the first generation we even had an instance that reached this

level; and later we managed to even improve this accuracy. By generation #273, the best accuracy reached at 83.6%; this means an upgrade of 5.5% compared to the previous best result.

We kept the algorithm running for even more time, but until we stopped it (at generation #440) it produced no generation that had better accuracy than this level.

6.2 Examination of the Stopping Condition

In the case of genetic algorithms it is usually very hard to determine an exact stopping condition. Our task is a great example for this as well, because we do not have a specific pre-defined final goal (final accuracy) that we wish to reach. It can be practical to examine the differences between the individuals of the consecutive generations; expecting that those will be more and more similar to each other, so by examining the deviation in the accuracy of the parameter sets represented by the various chromosomes, we could stop the search if it goes below a pre-defined limit. However, in our case this cannot be used, due to the fact that we use relatively big mutations. For this reason, we examined the parameters separately, and by checking the changes in their values, we made the decision whether to stop the algorithm or not.

Due to lack of space we cannot give extensive details about all the 27 parameters, so we only describe some more interesting specific examples. The changes of the parameters over time are shown on a similar to the previous ones: horizontal axis represents the generations, vertical axis represents the values of a single parameter in the chromosomes of the generations using grey dots, so in this case as well, the darker areas obviously mean overlapping values (all referenced diagrams are available on the following website: *http://users.nik.uni-obuda.hu/sanyo/acta835*). It can be stated that we noticed three distinct patterns in the changes of the various parameters:

Most of the parameters have settled to their respective ideal values reasonably fast (usually this happened around generation #100), and then their values did not change from this level. Obviously due to the mutations there were some values below or above this ideal level, but all of these turned out to exist only for a short period of time. Good examples for this pattern are parameters #1 and #2 (Diagram A.1 and A.2), and even thought the required time for the stabilization is a little higher, the same pattern is visible with parameters #3 and #6 (Diagram A.3 and A.4).

It is less common, but it does happen with some parameters that can also be known as a "typical example" of genetic algorithms, which is when different parameter values (alleles) compete with each other. In these cases, a few different parameter values remain viable for a reasonably long period of time, sometimes

even for 40–50 generations. During this time, some of them can get stronger (sometimes even two or three different values can remain dominant simultaneously). But eventually, some stable state was achieved with these parameters as well; good examples for this pattern are the parameters #13, #19 and #24 (Diagram A.5, A.6 and A.7).

In addition, we can find some examples for genes whose values did not settle, not even in the last generation (#400) when we stopped the algorithm. Examples for this pattern are the parameters #9 and #12 (Diagram A.8 and A.9).

It is visible that in these cases there were usually only two values in the end, and these cases are usually next to each other, so it basically does not matter which one we choose. For this reason, we should not continue the search just for the sake of these parameters.

6.3 Examination of the Number of Non-Viable Instances

Although this factor is less important for us, but it is practical to examine the number of non-viable instances inside the different generations.

During the creation of the first generation and later during the execution of the crossovers and the mutations we performed no verification whether or not the newly created instances' parameters are valid or not. This is because we had the assumption that the newly created non-viable instances will fall out at the next selection for parents, so hopefully there will be less and less non-viable chromosomes as the generations evolve.

Diagram 2 seems to verify this assumption: the first (initially created) generation's data is not shown, because there were 1879 (from 3000) non-viable instances in that generation. This number drastically decreased in the following 5 generations, and then it was stabilized around 13.2 items.

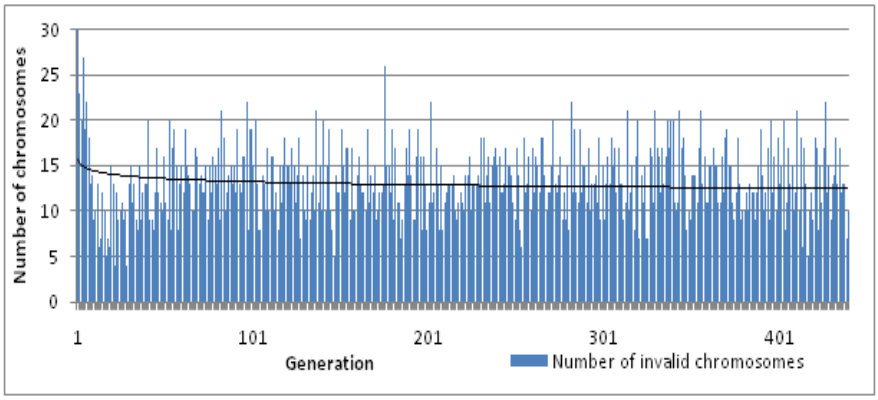

Diagram 2
Number of invalid chromosomes

Since the crossovers and especially the mutations can still create non-viable instances in the subsequent generations as well, we cannot expect that this number will furthermore decrease; but this is a tolerable amount, and the evaluation of those instances does not require too much resources.

6.4 Examination of the Control Group

Since the region growing and the evaluation have both high computational needs, we have to decrease the number of necessary processing steps as much as possible. One possible way of doing so is that we do not run the evaluation for every possible tissue samples (which would be altogether 41); instead we selected 11 tissue samples so that they reflect all different kinds of sample images and there is at least one example for every sample type (e.g. a lot of cell nuclei or only a few; sharp or blurred contours).

We executed the search only for this narrowed list, which (in addition to the faster evaluation of the instances) has the additional benefit that we could use the remaining sample images as control group. According to this, by executing the cell nuclei search algorithm for all possible samples, we got the following results:

- Average accuracy using the old (best known) set of parameters: 76.83%
- Average accuracy using the parameter set found by our evolution-based algorithm: 81.15%

Since these samples were not used during the optimization process, we can very well use them to estimate the improvement of accuracy with unknown samples, and in our case this improvement was 4.32%. In addition to this, it is clearly visible from both results that the selected 11 samples reflected the whole set of 41 samples reasonably well (76.83% – 78.1%).

Conclusions

We have developed a data-parallel GPGPU based region growing algorithm with improved seed point search and region growing iteration that is equally as accurate as the original sequential version, but it is suitable to process more than one cell nucleus at the same time, therefore its speed is 25–65% faster than the original CPU implementation. We have implemented the algorithm in CUDA environment (using Nvidia Fermi based GPGPUs). A possible improvement could be to implement the parallelization on a higher level, and develop the system so that it can be executed simultaneously on multiple GPUs (and in addition, on multiple CPU cores).

In the next step we have developed an evolution-based algorithm to find the optimal parameters for this new data-parallel version of the region growing method. This genetic algorithm was used to successfully determine a set of

parameters that could be used to achieve 81.15%, which means an improvement of 4.32% compared to the previously known best set of parameters.

One direction for further developments could be towards the specialized search techniques, because it is possible to arbitrarily select which tissue samples the clients should use for the evaluation and verification; so it might be feasible to narrow down this selection to include only the tissue samples of a given type, and this way it might be possible to find an even better set of parameters for the developed algorithms.

We have developed a new method (based on pixel level and object level comparisons) which is suitable to evaluate the accuracy of cell nuclei detector algorithms. In the next step we have successfully implemented this using an improved backtrack search algorithm to process high number of overlapping cells, which requires significantly fewer steps than the traditional linear search methods.

We have already developed a distributed framework for the execution of the genetic algorithm. The framework have lived up to our expectations, the execution time of 440 generations was fully acceptable.

References

[1] Z. Shebab, H. Keshk, M. E. Shourbagy, “A Fast Algorithm for Segmentation of Microscopic Cell Images”, ICICT '06. ITI 4th International Conference on Information & Communications Technology, 2006, ISBN: 0780397703

[2] J. Hukkanen, A. Hategan, E. Sabo, I. Tabus, “Segmentation of Cell Nuclei From Histological Images by Ellipse Fitting”, 18th European Signal Processing Conference (EUSIPCO-2010), 23-27 Aug. 2010, Denmark, ISSN 207614651219, pp. 1219-1223.

[3] R. Pohle, K. D. Toennies, “Segmentation of medical images using adaptive region growing”, 2001, Proc. of SPIE (Medical Imaging 2001), San Diego, vol. 4322, pp. 1337-1346.

[4] Pannon University, “Algoritmus- és forráskódleírás a 3DHistech Kft. számára készített sejtmag-szegmentáló eljáráshoz”, 2009

[5] L. Ficsór, V. S. Varga, A. Tagscherer. Zs. Tulassay, B. Molnár., “Automated classification of inflammation in colon histological sections based on digital microscopy and advanced image analysis”, Cytometry, 2008, pp. 230–237.

[6] S. Szenasi, Z. Vamossy, M. Kozlovszky, “GPGPU-based data parallel region growing algorithm for cell nuclei detection“, 2011 IEEE 12th International Symposium on Computational Intelligence and Informatics (CINTI), 21-22 Nov. 2011, pp. 493-499.

[7] I. J. Rudas, J. K. Tar, “Computational intelligence for problem solving in engineering”, 36th Annual Conference on IEEE Industrial Electronics Society (IECON), 7-10 Nov. 2010, pp. 1317-1322.

[8] S. Szenasi, Z. Vamossy, M. Kozlovszky, “Evaluation and comparison of cell nuclei detection algorithms“, IEEE 16th International Conference on Intelligent Engineering Systems (INES), 13-15 June 2012, pp. 469-475.

[9] S. Sergyán, L. Csink, “Automatic Parameterization of Region Finding Algorithms in Gray Images”, 4th International Symposium on Applied Computational Intelligence and Informatics, Timisoara, Romania, 17-18 May. 2007, pp. 199-202.

[10] Goldberg, David G, “Genetic Algorithms in Search, Optimization, and Machine Learning”, Addison-Wesley Longman Publishing Co., Boston, ISBN: 0201157675

[11] C. Carrick, K. MacLeod, “An evaluation of genetic algorithm solutions in optimization and machine learning”, 21st Annual Conference Canadian Association for Information Science CAIS/ACSI’93, Antigonish, 12-14 July 1993, pp. 224–231.

[12] T. H. Cormen, C. E. Leiserson, R. L. Rivest, “Introduction to Algorithms”, Mcgraw-Hill College, 1990, ISBN: 0070131430, Chapter 17 "Greedy Algorithms", p. 329.

[13] Z. Blázsik, Cs. Imreh, Z. Kovács, “Heuristic algorithms for a complex parallel machine scheduling problem”, Central European Journal of Operations Research, 2008, pp. 379-390

[14] J. L. Noyes, “Artificial Intelligence With Common Lisp”, D.C. Health and Company, 1992, ISBN: 0669194735, pp. 157-199.

[15] S. N. Sivanandam, S. N. Deepa, “Introduction to Genetic Algorithms”, Springer, 2008, ISBN: 9783540731894

[16] M. Gendreau, J.-Y. Potvin, “Handbook of Metaheuristics”, Springer, 2010, ISBN: 1441916636

[17] D. Bersimas, J. Tsitsiklis, “Simulated Annealing”, Statistical Science, vol. 8, no. 1, Institute of Mathematical Statistics, 1993, pp. 10-15.

[18] D. Whitley, “A genetic algorithm tutorial”, Statistics and Computing, vol. 4(2). 1994, pp. 65–85.

[19] C. Reews, “Genetic algorithms”, Coventry University, Heuristics in Optimization course, 2012

[20] M. Mitchell, “Genetic algorithms: An Overview”, Complexity, 1995, pp. 31-39.

[21] Y.-S. Choi, B.-R. Moon, “Parameter Optimization by a Genetic Algorithm for a Pitch Tracking System”, Proceedings of the 2003 international

conference on Genetic and evolutionary computation: PartII, GECCO'03, 2003, ISBN: 3540406034, pp. 2010-2021.

[22] A. Bevilacqua, R. Campanini, N. Lanconelli, "A Distributed Genetic Algorithm for Parameters Optimization to Detect Microcalcifications in Digital Mammograms", EvoWorkshop 2001, 2001, pp. 278-287.

[23] L. Budin, M. Golub, A. Budin, "Traditional Techniques of Genetic Algorithms Applied to Floating-Point Chromosome Representations", Proceedings of the 41st Annual Conference KoREMA, Opatija, 1996, pp. 93-96.

[24] S. Szenasi, Z. Vamossy, M. Kozlovszky, "Preparing initial population of genetic algorithm for region growing parameter optimization", 4th IEEE International Symposium on Logistics and Industrial Informatics (LINDI), 2012, 5-7 Sept. 2012, pp. 47-54.

[25] R. Kohavi, F. Provost, "Glossary of Terms", Machine Learning vol. 30 issue 2, Springer Netherlands, 1998, pp. 271-274., ISSN: 08856125

[26] E. Tóth-Laufer, M. Takács, I.J. Rudas, "Conjunction and Disjunction Operators in Neuro-Fuzzy Risk Calculation Model Simplification", 13th IEEE International Symposium on Computational Intelligence and Informatics (CINTI), Budapest, Hungary, 20-22 Nov. 2012, ISBN: 9781467352048, pp. 195-200.

[27] Zs. Cs. Johanyák, O. Papp, "A Hybrid Algorithm for Parameter Tuning in Fuzzy Model Identification", Acta Polytechnica Hungarica, vol. 9, no. 6, 2012, pp. 153-165.

[28] M. T. Goodrich, R. Tamassia, "Algorithm Design: Foundations, Analysis, and Internet Examples", John Wiley & Sons Inc., 2002, ISBN: 0471383651

[29] M. Mitchell, "An introduction to genetic algorithms", Bradfork Book The MIT Press, Cambridge, 1999, ISBN: 0262133164

[30] D. Gupta, S. Ghafir, "An Overview of methods maintaining Diversity in Genetic Algorithms", International Journal of Emerging Technology and Advanced Engineering, vol 2., issue 5., May 2012, ISSN: 22502459, pp. 56-60.

[31] K. Messa, M. Lybanon, "Curve Fitting Using Genetic Algorithms", Naval Oceanographic and Atmospheric Research Lab., Stennis Space Center MS., NTIS issue number 9212.

A Multicore Architecture Focused on Accelerating Computer Vision Computations

Liberios Vokorokos *, Eva Chovancová *, Ján Radušovský*, Martin Chovanec**

* Department of Computers and Informatics, Faculty of Electrical Engineering and Informatics, Technical University of Košice
Letná 9, 04001 Košice, Slovak Republic
eva.chovancova@tuke.sk, liberios.vokorokos@tuke.sk, jan.radusovsky@tuke.sk

** Institute of Computer technology, Technical University of Košice, Letná 9, 04001 Košice, Slovak Republic; e-mail: martin.chovanec@tuke.sk

Abstract: This paper deals with accelerating computer vision computations using a specialized multicore architecture. Computer vision is one of the fastest-evolving segments of computer science. Even though computer vision uses time-consuming methods, the processing can be accelerated using specialized multicore processor architectures. Single-core processors are a legacy, since they have reached their physical limits. The way to go is to use multicore architectures, which can be also used to accelerate computations in specialized areas such as computer vision. This paper describes a specialized multicore architecture that can be used to accelerate time-consuming calculations in the field of computer vision. The architecture proposed in this paper belongs to the Harvard architecture family.

Keywords: image; architecture; Harvard concept; Princeton concept; threshold; control unit; processing unit

1 Introduction

Computing and information systems have become an integral part of everyday life and also of research. In research, there is a demand for systems that provide more power, due to the time-consuming calculations involved.

The computing power of single-core processors – which are mostly examples of the Von Neumann architecture – may be increased by increasing the capacity of the individual components of the computer; this goes hand in hand with increasing the amount of available memory in the system. However, this method of gaining more computing power brings with it an increase in the costs of the development

of the individual components. It also reveals certain physical limits. The method of increasing the capacity of the individual components to obtain higher performance has been superseded; new developments tend to target multicore processors. Having multiple processors on a single chip brings the advantage of sheer processing power; nothing is free though. With multicore architectures, one may see different problems, such as power consumption and heat dissipation. The architecture must be designed so that the heat is distributed and there are no hot links. Distributed and shared on-chip caches must adhere to the rules of coherence to ensure data accuracy.

The present work analyses the various multicore architectures, based on which is designed a specialized multicore architecture for accelerating calculations in computer vision. The present work was supported by the Slovak Research and Development Agency under contract no. APVV-0008-10. This research is the result of the implementation of the "Research Centre for efficient integration of the renewable energy sources" project, ITMS: 26220220064, supported by the Research & Development Operational Programme funded by the ERDF.

2 Architecture Concept

When designing a specialized architecture, the concept choice is important. The basi concepts we have taken into account when designing our architecture were the following:

- the Harvard concept; and
- the Princeton concept.

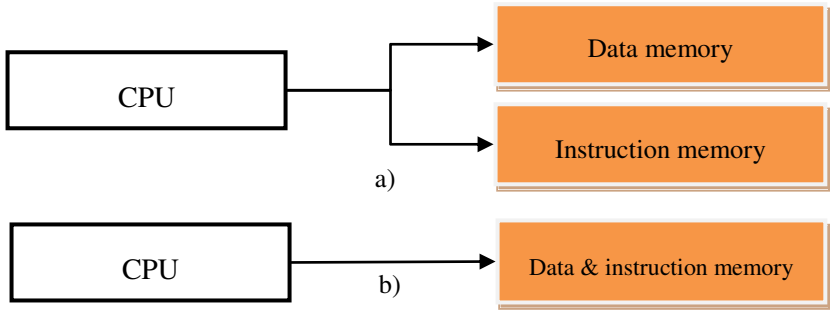

Figure 1
a) the Harvard architecture, b) the Princeton architecture

The Harvard concept (Figure 1a) is a computer architecture with a physically separated storage space and signal path for instructions and data. This means that it has a separate address space for both programs and data. Today, most processors have implemented a separate signal path due to performance reasons. [2] [6] [12]

In conjunction with a modified Harvard architecture, it is possible to support tasks such as reading the program implementation directly from the disk as data and then executing them. In the Harvard architecture, it is not necessary to share the memory properties, because the timing, the technology implementation and the structure of addressable memory may vary. In some systems, the instruction memory is larger than the memory for data, because the address of the instruction is wider than the address of data. One of the most notable examples of the Princeton concept is the Von Neumann architecture, which is simpler than the newer Harvard architecture. The Von Neumann architecture – in comparison with the Harvard concept – has only one memory (Figure 1b), which is used to store both data and instructions; this means that it contains a common set of data and instruction addresses. [12] [13]

Consequently, it is necessary to ensure that the processor does not interpret data as instructions, and vice versa. The CPU accesses the memory in the same way, both in the case of instructions or data. It uses the same addresses, data and control signals. This memory structure allows for the existence of self-modifying programs.

The Von Neumann architecture is a system that can store the program into the operating memory, and thus the instructions and data are stored in a RAM memory. This RAM memory enables both reading and writing operations. In the Von Neumann architecture, the CPU can read instructions or read/write data from/to the memory. These operations cannot be performed simultaneously because both the data and the instructions use the same memory. However, the Harvard architecture can load instructions and data at the same time because both are stored at their own memory. Therefore, the Harvard architecture is faster. [2] [6]

3 Multicore Processors

High-performance processor architectures are mostly represented by multiple processor cores on a single chip. These architectures have the potential to provide a higher maximum throughput; they scale better and provide higher performance than monolithic architectures. The current trend in technology development aims at new types of processors which should meet the need for higher performance without increasing power consumption and heat. [1] [3] [4]

Multi-core processor architectures allow us to achieve increased performance and to reduce heat by the integration of two or more processor cores in a single processor case. Today, processors sporting a large number of cores are being produced. These processors have the most logical structure – a two-dimensional grid; they apply control flow and data flow core architectures. Considering the definition of the processor, we can describe the multi-core processor as an

integrated circuit to which two or more processors (cores) connect. Such a design enables improved performance, reduced energy consumption and more efficient, simultaneous task processing. All of this has resulted in a development boom in the field of multi-core processors because single-core processors have reached their limits in terms of performance and speed. [1] [3] [4]

4 The Proposed Architecture

The proposed processor architecture is based on the analysis of multi-core processors and computer vision. Due to the advances in the development of multi-core processors and computer vision, i.e. the use of parallel algorithms, it is advisable to use multi-core processors to accelerate computations in this field. The use of specialized multi-core processors results in higher performance and faster data processing due to the fact that the image is distributed to the individual cores. It takes less time to process the same amount of data. [5] [7] [19]

4.1 Image Mapping

The proposed specialized processor allows for the use of several approaches when mapping the image; these differ in the distribution of the digital image, but also in the number of required cores. Figure 2 represents the way the digital image is mapped to the individual processor cores. This approach may be applied if the size of the digital image is 256×256 pixels, which is also the maximum size of the processed image. This size is given by the maximum capacity of data memory, which is large enough for testing purposes; nevertheless, it may be expanded in the future. With this approach, we divide the image into equally large parts that exactly correspond to the memory size of a single core. [5] [7]

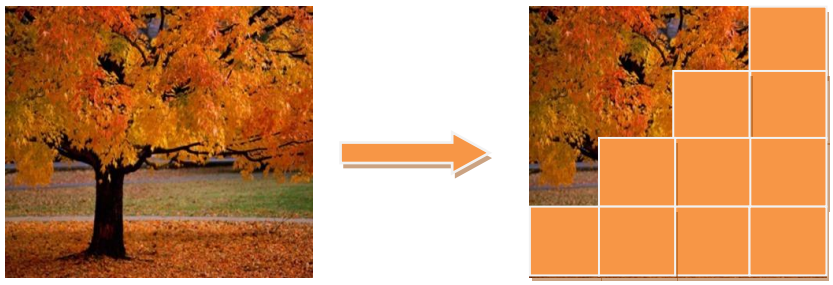

Figure 2
Image mapping (256×256 pixels)

If the image is smaller than 256×256 pixels, there are two ways to split the mapped image. The first – even – method uses all the processor cores, so all cores are equally busy, but they do not use their entire memory. The second method to use with a smaller picture is the uneven method. This method uses the entire memory capacity, but it is not as effective as the previous one, because it requires more time to process the same image than the even method.

Due to the memory capacity used for testing, the maximum input image size is 256×256 pixels, and since we have available 16 cores with a memory capacity of 256 points × 256 points × 3 bytes (RGB) × 4 banks = 786432 bytes. The image is stored in separate memory banks; therefore, we can load 4 different images simultaneously and process them sequentially. [5] [7]

4.2 Instruction Set

To execute various operations over the input images, we need a set of instructions representing the operations in question. Each of these instructions has a defined format (Figure 3), as follows:

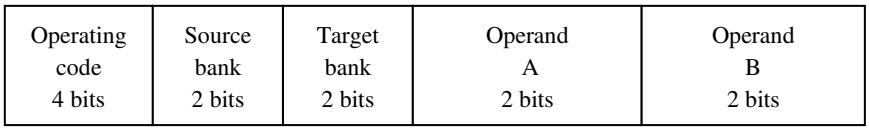

Figure 3
Instruction format

The instruction set shown in the following table contains a list of instructions and their parameters necessary for the execution of the instructions over the input data:

Table 1
Instruction set

	Operating code	Operand A	Operand B	Information
RGB → GS	00001	--	--	--
Thresholding	00010	Upper threshold	Lower threshold	Object boundaries calculation
Half thresholding	00011	Upper threshold	Lower threshold	Object boundaries calculation
Spectral thresholding	00100	Upper threshold	Lower threshold	Object boundaries calculation
Half-spectral thresholding	00101	Upper threshold	Lower threshold	Object boundaries calculation

Writing to register	00111	Upper threshold	Lower threshold	Object boundaries calculation

As is evident from Table 1, for the calculation of the various thresholding types, one has to specify operands A and B, i.e. the upper and lower threshold. We can define the object boundaries in a digital image using these thresholds and thus tell these from the background.

5 The Covitor Processor

The proposed processor – Covitor – is a processor with 16 cores specialized in digital image processing and using the instruction set described in the previous section. This processor is an instance of the Harvard architecture; it has its own data memory and its own instruction memory. Having two memories makes access to data and instructions faster. The cores of the Covitor processor are arranged as a 4×4 grid. The structural diagram of the Covitor processor appears in Figure 4.

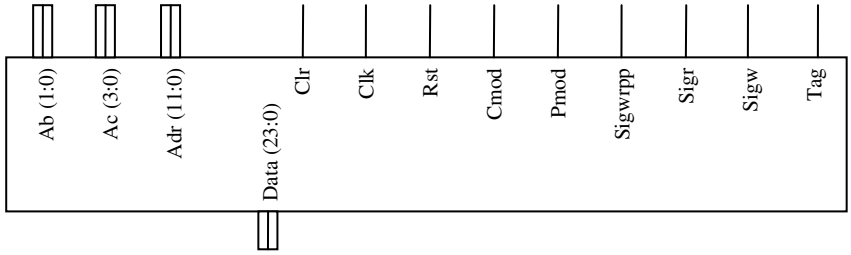

Figure 4
The structural diagram of the 16-core processor

The processor operates in two modes; the *Pmod* and *Cmod* instructions are used to set the system into programming or computing mode. In programming mode, the input values are read into the registers / into the memory and the system timing is set. Then the system switches to computing mode, which will run calculations based on the program – these are the instructions applied to the data.

The *done* signal marks the end of the data processing cycle, while the data are located at specific address in memory. If done is set to one, the cycle is terminated. The address is set to the subsequent address in the memory, and the next cycle of calculations starts. The Covitor processor contains two components listed below; their connections are defined by mapping:

- *Cores;*
- *Decoders.*

A *Core* is a universal processor core, mapped to 16 cores; the Decoder components are used to address the cores.

6 Processor Cores

The Covitor processor was designed as a multi-core processor with 16 cores. The architecture is a member of the Harvard architecture family; it has a separate memory for both instructions and data.

The instruction memory is located directly in the core. The data memory is larger than the instruction memory and it sits in the processing unit. The scheme of a core is presented in Figure 5.

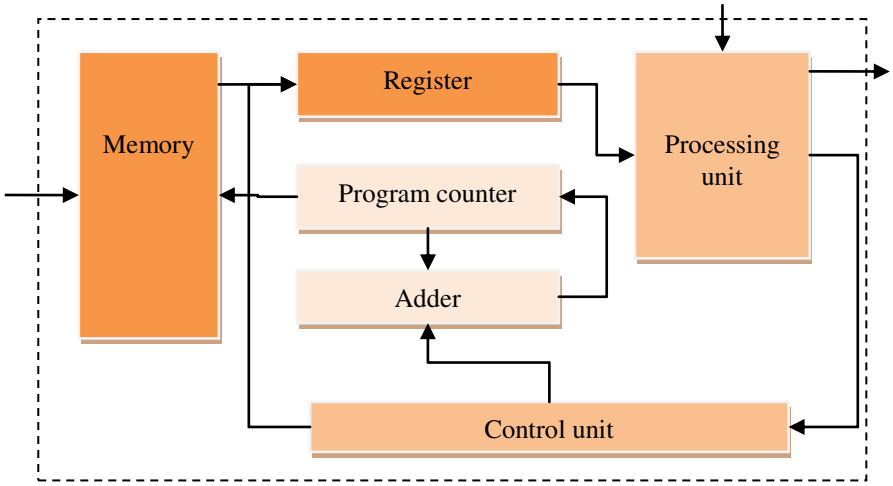

Figure 5
A processor core

By having 16 cores in a processor we achieve higher performance, which we need for faster image processing. This is expressed by the following formulae:

$$t_1 = \frac{m}{n} + d \qquad t_2 = \frac{m}{16n} + d \tag{1}$$

In these equations, m refers to the amount of pixels of a digital image, while n refers to the number of cores used. It is also necessary to calculate with the time needed for loading and distributing the data to each of the cores, which is expressed by the value of d. Each core of the Covitor processor consists of a memory, a register, a program counter, an adder, a control unit and a processing unit.

The processing unit includes an arithmetic logic unit. The digitized input image is loaded into the memory, located in a processing unit, and the instructions are loaded into the memory located in the core. The image processing is divided into four phases, controlled by the control unit. In the first phase, the instruction is loaded into the register. Then, in the second phase, a start signal is sent to the processing unit. In the third phase, the image processing starts, based on the particular instruction. The last, fourth phase is the stop signal itself, which terminates the processing cycle.

6.1 The Control Unit

The control unit is a finite state machine with four states describing image processing. The transitions between the states are performed by the control logic. In this logic, the signals from the control unit and the required conditions to make transitions are taken into account. The control unit controls the process by means of the R(0), R(1), R(2) and R(3) signals, which initialize the transitions between the various states of the finite state automaton. Figure 6 represents process control implemented using the above signals.

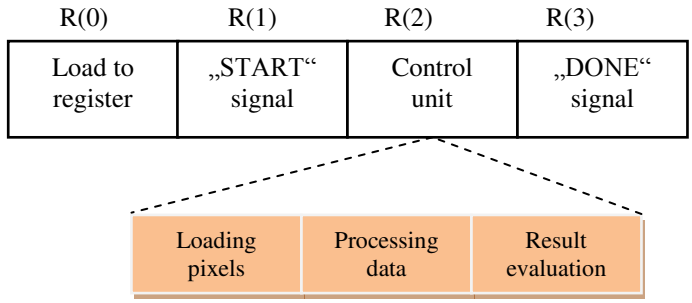

Figure 6
Process control

For the program to function properly, we have to switch to computing mode. If the program is in boot mode, the control unit will not start and image processing will not take place.

6.2 The Processing Unit

The processing unit is a part of the processor core; its main task is to implement the instructions processing the input data loaded in its internal memory. It also contains a partial logic circuit, controlling the termination of image processing. The implementation of the processing unit is based on the logic circuit presented in Figure 7.

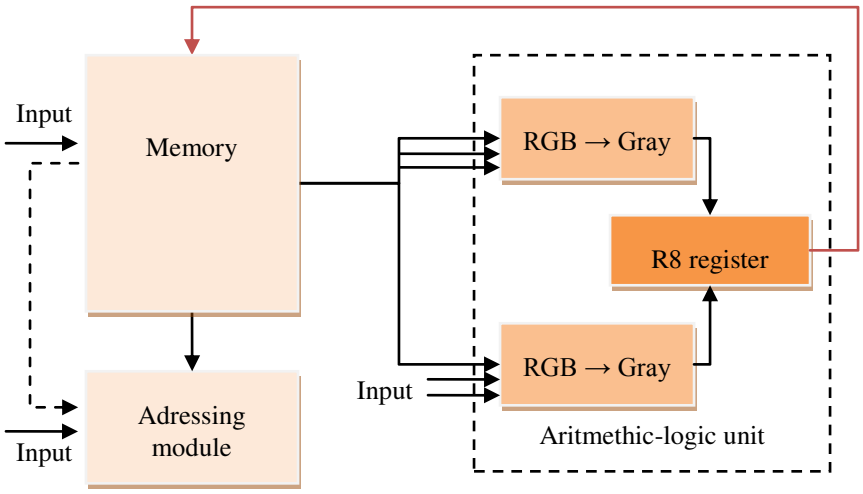

Figure 7
The processing unit

The processing unit is responsible for processing the image by thresholding or converting it from RGB to grayscale. The processing is started by a starting signal; this indicates the start of the process itself. The processing output is stored in the R8 output register, both after thresholding and also after conversion to greyscale.

We have created a set of rules to determine when and which results may be entered in the R8 register to ensure the accuracy of the data stored in the register. An important part of the processing unit is the addressing module; it determines the appropriate memory address, which is used to read further data for processing – as described lower in the text. A further important part of the processing unit is the arithmetic-logic unit, with two logic sub-circuits. One of these converts the digital image on the input from RGB format to grayscale. This RGB- grayscale conversion is based on the following equation:

$$grayscale = 0{,}3 * R + 0{,}59 * G + 0{,}11 * B \tag{2}$$

The second logic circuit is responsible for processing the image by means of various types of image thresholding operations. In our proposal, we use four thresholding types:

- *Simple thresholding;*
- *Half-thresholding;*
- *Spectral thresholding;*
- *Half-spectral thresholding.*

During thresholding, the input data of the digital image are compared with the upper and lower threshold values stored in the respective registers. Next, we perform a comparison to decide whether the given image point belongs to the subject or the background.

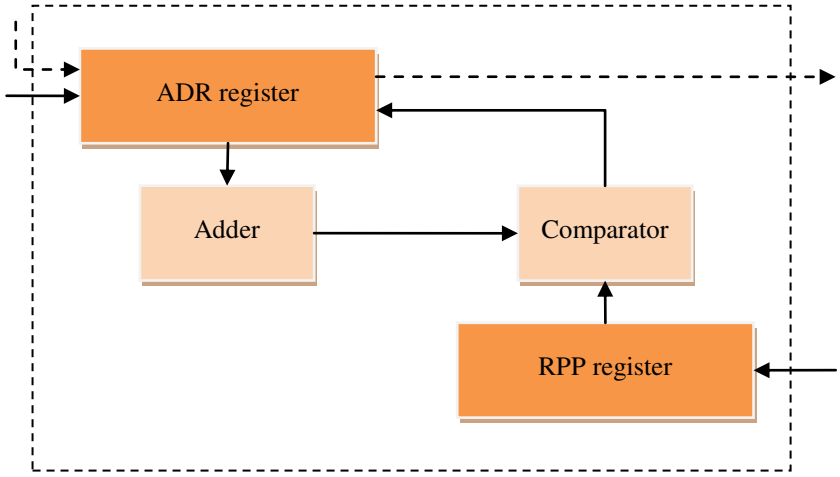

Figure 8
The addressing module

As mentioned above, the addressing module (Figure 8) is a significant part of the processing unit. The operation of this module is two-fold: its first task is to terminate the image processing when reaching the last address of the stored pixel data, while the second is to set the pixel addresses.

The ADR register stores a value that refers to the address from which data are taken for processing. If the input controlling R signal arrives, the adder increments the value stored in the ADR register. The incremented value is compared by the comparator with the value stored in the RPP register. If it is smaller or equal, the data processing continues with the next address in the sequence and the cycle repeats again.

7 Simulation

One way of speeding up image processing is to use multiple cores on a single chip; the load is spread over multiple cores, and thus each core has to process a smaller number of pixels.

In the simulation we have used different numbers of cores for image processing. We have seen that an increased number of cores allows us to process more pixels in the same period (Figure 9).

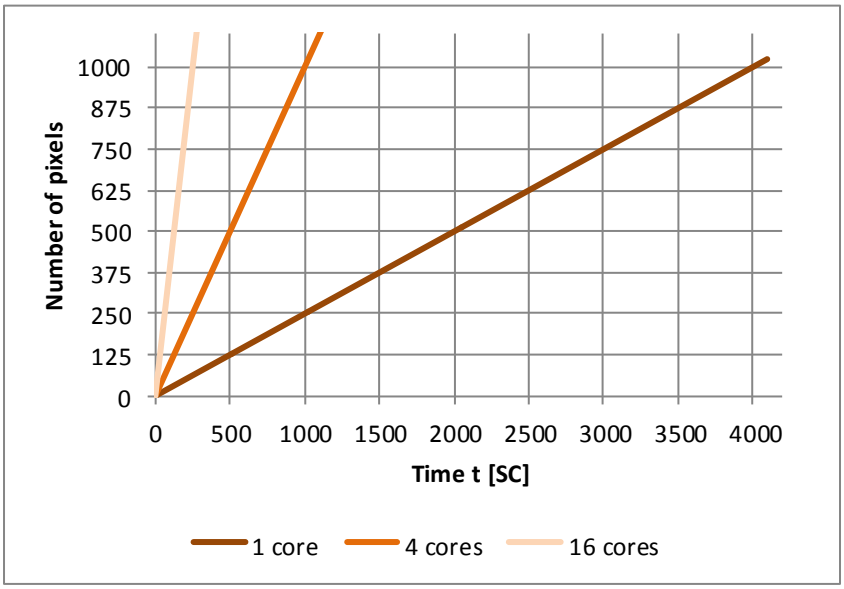

Figure 9
Image processing performed on multiple cores

As is evident from the graph, when processing the same image with 16 cores of a single chip, we need 16-times fewer machine cycles (SC) than we would need using a single core. In this simulation we used a 256×256 pixel image, so the total number of pixels processed was:

$$pixels = 256 * 256 = 65536 \tag{3}$$

The time required for processing the image using a single core is given by the following equation:

$$t = 256 * 256 * 4 \tag{3}$$

$$t = 262144SC \tag{4}$$

When processing the image using the Covitor processor, the total load spreads to 16 cores, which reduces the processing time. In the simulation, we have spread the load evenly due to a memory limitation (Figure 10 – the maximum amount of memory that can be processed by each core is evident from this figure).

We have imposed the image size limitation due to testing difficulties, though in the future it will be possible to expand the memory of the proposed processor to store and retrieve information about the image, i.e. process higher resolution images.

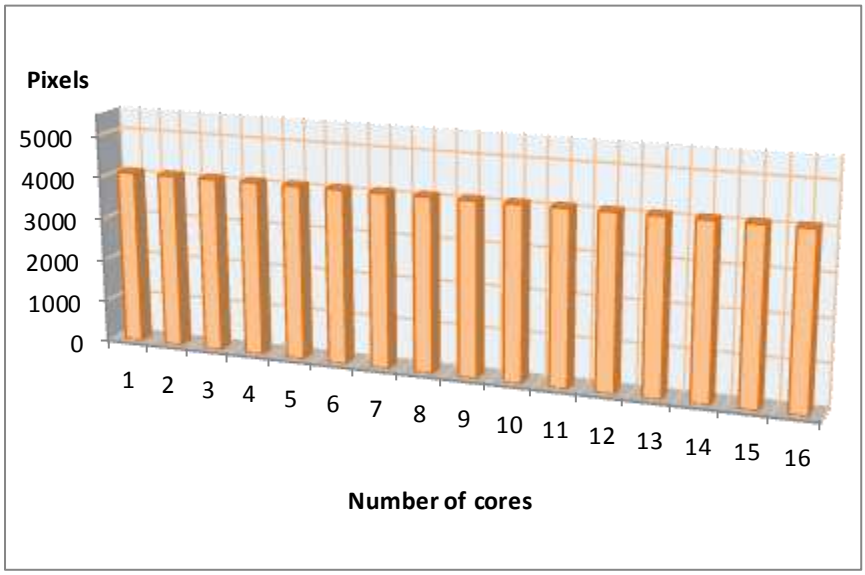

Figure 10
Even load distribution

Uneven load distribution may be used, too, on the condition that the processed image has a smaller resolution (64×64 pixels) than the maximum memory capacity (Figure 11).

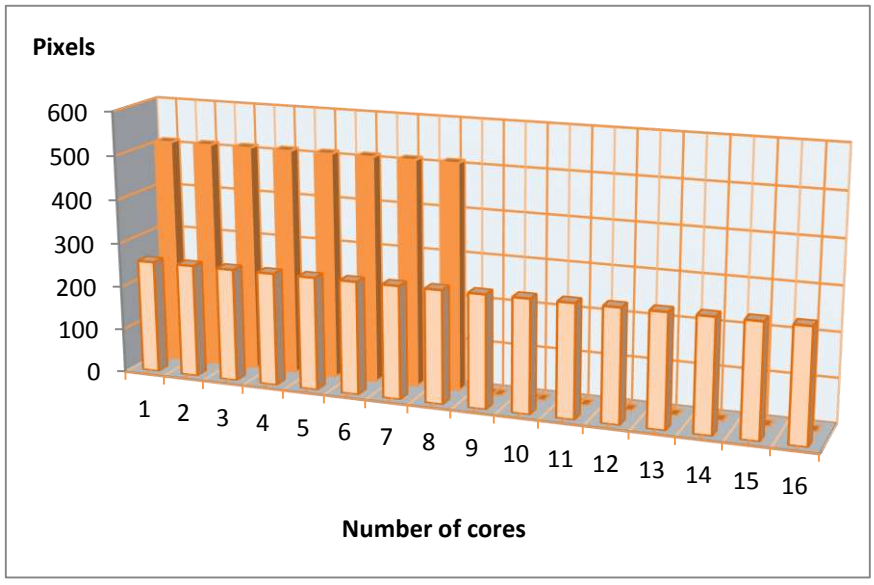

Figure 11
Load distribution with 64 × 64 pixel image resolution

When processing smaller resolution images, the load can be spread evenly or unevenly, as presented in the graph (Figure 11). In even load distribution, all cores are used, but only a part of their memory capacity. When applying uneven load distribution we use the whole memory capacity, but only some cores. In terms of efficiency, it is preferable to use even load distribution, because less time is needed to process the image than with the uneven load distribution.

The simulations we have implemented have demonstrated the correct functionality of the proposed architecture and the efficiency of image processing, too. We have also witnessed the acceleration of image processing computations.

Using multiple cores for image processing allows faster computation in linear proportion to the number of cores. This acceleration may be even 16-fold when using even load distribution.

When simulating image processing using the Covitor processor, we have witnessed that the acceleration depends on the load distribution type. Even load distribution is more efficient than uneven load distribution.

Conclusion

In our work we have designed and implemented a specialized multicore architecture focused on accelerating computer vision computations. The design of this architecture was based on the analysis of multicore processors, which has shown that the Harvard architecture is faster when accessing data and instructions stored in memory.

The speedup of the proposed architecture depends on the type of load distribution used; even load distribution is more effective than uneven distribution. The proposed data (image) memory has its limitations, though this can be overcome in future. This limitation is present due to testing reasons.

Moreover, the instruction set consists only of basic instructions that correspond to the various thresholding types and to RGB-grayscale transformation. This instruction set can be extended by instructions corresponding to image extraction by connected components (4- and 8-neighbours). These methods use the neighbour's pixels to perform computations, so the data might overlap. Therefore it is necessary to solve cache memory coherence problems. This specialized architecture may also process interactive algorithms.

Acknowledgements

The present work was supported by the Slovak Research and Development Agency under contract no. APVV-0008-10. The present research is the result of the implementation of the "Research Centre for efficient integration of the renewable energy sources" project, ITMS: 26220220064, supported by the Research & Development Operational Programme funded by the ERDF.

References

[1] G. Blake, R. Dreslinski, T. Mudge: „A Survey of Multicore Processors“, Signal Processing Magazine, IEEE, pp. 26-37, 2009, 1053-5888/09

[2] M. Jelšina: „Architektonické riešenie počítačového systému data flow KPI“ [Data-flow computer system architecture] Košice, Slovakia: Elfa, 2004, ISBN 80-89066-86-0

[3] B. De Ruijsscher, G. Gaydadjiev, J. Lichtenauer, E. Hendriks: „FPGA Accelerator for Real-Time Skin Segmentation“ 2006, ISBN 0-7803-9783-5

[4] P. Gepner, M. Kowalik: „Multi-Core Processors: New Way to Achieve High System Performance“, Proceedings of the International Symposium on Parallel Computing in Electrical Engineering PARELEC'06, Computer Society, 2006, ISBN: 0-7695-2554-7

[5] B. Chanda, D. Majumder: „Digital Image Processing and Analysis“, PHI Learning Pvt, 384 pages, 2004, ISBN 8120316185

[6] L. Vokorokos, N. Ádám, J. Trelová: „Sequential Threads In Data Flow Computers“, AEI '2010 : International Conference on Applied Electrical Engineering and Informatics, Venezia, Italy, September 5-13, Košice, Slovak Republic, 2010, pp. 54-58, ISBN 978-80-553-0519-6

[7] S. Klupsch, M. Ernst, S. Huss, M. Rumpf, R. Strzodka: „Real Time Image Processing Based on Reconfigurable Hardware Acceleration“, www.mpi-inf.mpg.de/~strzodka/papers/public/KlErHu_0 2fpga.pdf

[8] R. Kumar, V. Zyuban, D. Tullsen: „Interconnections in Multi-Core Architectures“, Proceedings of the 32nd International Symposium on Computer Architecture (ISCA’05), 2005, ISBN 1063-6897/05

[9] J. Nurmi: „Processor Design: System-On-Chip Computing for ASICs and FPGAs“, Springer, 2007, ISBN 978-1-4020-5530-0

[10] C. Rafael R. Woods: „Digital Image Processing“, Prentice Hall, 2008, ISBN, http://lit.fe.uni-lj.si/showpdf.php?lang=slo&type=doc&doc=dip&format=0, 0-13-168728-x

[11] V. Hlaváč: „Počítačové Vidění“ [Computer vision], Prague: Grada a.s., 252 pages, 1992, ISBN 8085424673

[12] L. Vokorokos: „Princípy architektúr počítačov riadených tokom údajov“ [Principles of data-flow computer architectures], Košice: Copycenter, spol. s r.o., 2002, p. 147. ISBN 80-7099-824-5

[13] L. Vokorokos, B. Madoš, A., Baláž, N. Ádam: „Architecture of Multi-Core Computer with Data-driven Computation Model“, Acta Electrotechnica et Informatica, pp. 20-23, 2010, ISSN 1335-8243

[14] R. Young: „How Computers Work“,Que Publishing, 2009, 464 pages, ISBN-10: 0789736136

[15] A. C. Bovik: „The Essential Guide to Image Processing“, Academic Press, 880 p, 2009, ISBN: 9780123744579

[16] J. Dennis, G. Gao: „An Efficient Pipelined Dataflow Processor Architecture“, Supercomputing '88 Proceedings of the 1988 ACM/IEEE conference on Supercomputing, s. 368-373, IEEE Computer Society Press Los Alamitos, ISBN:0-8186-0882-X

[17] M. Hill, M. Marty: „Amdahl’s Law in the multicore era“,EEE Computer Society Press Los Alamitos,Journal Computer, Volume 41, Issue 7, July 2008, Pages 33-38

[18] T. Mattson, R. Wijngaart, M. Frumkin: „Programming the Intel 80-Core Network-on-a-Chip Terascale Processor“, Conference on High Performance Networking and Computing, Proceedings of the 2008 ACM/IEEE conference on Supercomputing, 2008, ISBN: 978-1-4244-2835-9

[19] J. Parker: „Algorithms for Image Processing and Computer Vision“, Indianapolis, Ind.: Wiley Publishing, Inc., 2011

[20] N. Ádám, B. Madoš, A. Baláž: „ P-Double Operators in the Pipeline System of the DF-KPI Architecture“, INES 2012: IEEE 16th International Conference on Intelligent Engineering Systems: proceedings: June 13-15, 2012, Lisbon, Portugal. - Budapest: IEEE, 2012 P. 357-362. - ISBN 978-1-4673-2692-6

Speech Technologies for Advanced Applications in Service Robotics

Stanislav Ondáš[1], Jozef Juhár[1], Matúš Pleva[1], Martin Lojka[1], Eva Kiktová [1], Martin Sulír[1], Anton Čižmár[1], Roland Holcer[2]

[1] Department of Electronics and Multimedia Communications, FEI, Technical University of Košice, Park Komenského 13, 041 20 Košice, Slovak Republic
E-mail: {stanislav.ondas, jozef.juhar, matus.pleva, martin.lojka, eva.kiktova, martin.sulir, anton.cizmar}@tuke.sk

[2] ZŤS VVÚ KOŠICE a.s., Research, Development, Design & Supply Company, Slovakia, Južná trieda 95, 041 24 Košice, Slovakia
E-mail: roland.holcer@ztsvvu.eu

Abstract: The multimodal interface for controlling functions of the complex modular robotic system, which can be deployed in difficult conditions as are rescue works, natural disasters, fires, decontamination purposes was designed. Such interface involves several fundamental technologies such as speech recognition, speech synthesis and dialogue management. To enable human operator to cooperate with designed robotic system, the sophisticated architecture was designed and described technologies were implemented. The automatic speech recognition system is introduced, which is based on Hidden Markov models and enables to control functions of the system using a set of voice commands. The text-to-speech system was prepared for producing feedback to the operator and dialogue manager technology was adopted, which makes it possible to perform the information exchange between operator and robotic system. The system proposed is enriched with acoustic event detection system, which consists of a set of five microphones integrated on the robotic vehicle, the post-processing unit and detection unit.

Keywords: service robots; speech technologies; speech recognition; speech synthesis; multimodal interface

1 Introduction

The field of service robotics is growing rapidly due to the increasing need of automation, safety and time saving. Robotic systems are mainly deployed in industry and nowadays we see robot applications s for healthcare or home usage too [1], [2]. A special effort is devoted to design and development of robotic systems for independent living of elderly people [3], [4].

It can be concluded, that in such "advanced" applications, successfulness of robotic devices depends critically on the reliable, user-friendly and intuitive interface, which enables "cooperation" between a user and a robotic system. The other important reason for paying close attention to designing a so-called "human-machine interfaces" (HMI) is, that so complex systems have a lot of various functionalities, which can be difficult to control by "old school" interfaces, as are keyboard, buttons, joystick etc. Usage of more natural form of an interface, which enables human-like interaction involving speech, vision and other channels, can provide more usable, intuitive and ergonomic interface.

Speech together with auditory perception can be identified as the most important channels to exchange ideas and thoughts among people. This dominance relates to the fact, that speech is an acoustic representation of language, which relates to the representation of the world in a human mind. The other important attribute of human speech is its capability to replace other modalities, when they are not available (e.g. in telephony interaction). These attributes make speech the most important modality in HMI. Therefore speech technologies become widely used in advanced robotic applications.

To enable human-robot speech communication, a several technologies, which can be labeled as "speech technologies", need to be involved. The automatic speech recognition together with text-to-speech synthesis is the most important. But mentioned technologies alone are not enough for successful human-robot interaction. Some dialogue logic need to be integrated which will be able to hold information about dialogue state and will decide about next step in the interaction (next dialogue state). Previous sentence is the definition of dialogue management technology, which creates a core of spoken dialogue systems [5]. To close the communication ring of human-machine interaction, natural language understanding and generation technologies should be mentioned too.

When we are talking about speech technologies, another technology can be mentioned, whose relation to speech technologies is based on analyzing the audio signal and on similar processing mechanisms – acoustic event detection. Acoustic event detection processes the input audio signal and classifies incoming sounds. In robotics, recognition of dangerous sounds and alerting the operator can be very useful due to the fact that robots often work in distant (or closed) environment. If the operator cannot see the robot directly, the video stream from robot's camera is the only medium for accessing information about environment, in which the robot moves. Extending robot with a set of microphones and acoustic event detection system can bring possibility of collecting additional information from this environment [6].

Although these technologies are being researched and implemented for a long time, their language dependency together with applying in new applications and situations creates a new space for their researching, designing and development. It is also true, that there are a lot of problems, which were not solved successful yet,

e.g. robustness of speech recognition, naturalness of speech synthesis or the complexity of dialogue management. Therefore, the paper proposed introduces the work, which has been done in the area of speech technologies for Slovak language for deployment in robotics applications in *Laboratory of speech technologies in telecommunications* on the *Department of Electronics and Multimedia Communications FEI TU* in Košice.

In Section 2, the complex modular robotic system for service robotics development is presented on functional prototype described in the following section. Next, the description of technologies of speech recognition, speech synthesis, audio events detection, and multimodal interaction developed for the service robot prototype, is provided. Finally the future work is described and discussed.

2 Complex Modular Robotic System

The complex modular robotic system and particular modules have been designed and are being developed within a range of three projects. The first project, named "*The complex modular robotic system of middle category with highest intelligence*" (funded by the Ministry of Education, Science, Research and Sport of the Slovak Republic MŠ SR- 3928/2010-11), continues in our earlier cooperation with ZŤS VVÚ Košice a.s. company, described in [7]. Next projects are being performed in cooperation with our partners from industry and universities in range of Research & Development Operational Program funded by the ERDF - *Research of modules for intelligent robotic systems* (ITMS project code 26220220141) and *Competence Center for Innovation Knowledge Technology of production systems in industry and services* (ITMS project code 26220220155).

Mentioned projects are focused on the design and development of the complex system of intelligent modules to be used for development of robotic systems. Such complex robotics systems will be deployed in difficult conditions such as rescue works, natural disasters, fires, decontamination purposes and so on.

The mobile robotic platform (3D model in Figure 1), developed by ZŤS VVÚ a.s. Košice, able to move autonomously in rugged terrain with the speed about 3-5 km/h and elevation of 45°, of usable capacity of 400 kg is intended to be the output of the work within the aforementioned projects. The robotic vehicle will bear several superstructures (extensions):

- the robotic arm with 6 degrees of freedom and nominal load 200 kg
- the extricate system with expansion force 20 kN
- the decontamination system for removing of toxic substances

The following systems for control and navigation will be included into the robotic platform:

- systems for intelligent teleoperator control
- systems for autonomous performance of tasks of advanced cognitivity
- systems for multi-sources navigation

Figure 1
3D model of the complex modular robotic system

Although the introduced robotic system will be able to perform several tasks totally autonomously, a lot of other tasks need some cooperation with a human operator. The usage scenario of such systems is, that the mobile robotic platform (vehicle) has wireless connection with the control panel computer, which can be encapsulated into the robust briefcase (e.g. in [7]). Such control panel provides an interface between operator and robotic vehicle, which enables controlling the vehicle by joystick, keyboard or buttons, and the information from vehicle are depicted on display.

Adding the possibility of controlling selected functions by speech can significantly increase usability of the robotic system, due to the fact, that a large range of system's functions is difficult to control only by hands. The situation is very similar as for in-vehicle systems, because driver should pay attention to driving, what means, that his gaze watches the traffic and his hands are on the steering.

Therefore, modules, which enable cooperation with robotic system through speech interaction, need to be designed and integrated. The analysis of usage scenarios has shown the need of designing the more sophisticated multimodal interface (will be described in Section 3.1), because the interaction with robotic systems requires besides speech recognition and speech synthesis technologies also controlling the graphical output, transformation the speech commands into the system's actions, and some approach for acknowledgement of recognized commands (e.g. using "dead-man" button of the joystick) [8].

3 Technologies for the Robotic System Speech Control

3.1 The Robot Functions Multimodal Interface Architecture

For enabling usage of the speech modality for cooperation with robotic systems, a complex solution needs to be designed. Such solutions are usually not only unimodal and often present their output in graphical manner accompanied by speech output. Nowadays, a lot of systems enable also to control the system by touchscreens in combination with speech. Therefore user interfaces for cooperation with robots can be seen as a multimodal interactive system. The key components can be identified - input processing engines (automatic speech recognition, gesture recognition, touch recognition, etc.), multimodal fusion and fision components, dialogue manager, and output presentation engines (text-to-speech system, graphical output system). The proposed speech and multimodal technologies modules were realized and tested on the evaluation board provided, which is the computational center of the modular robotic system.

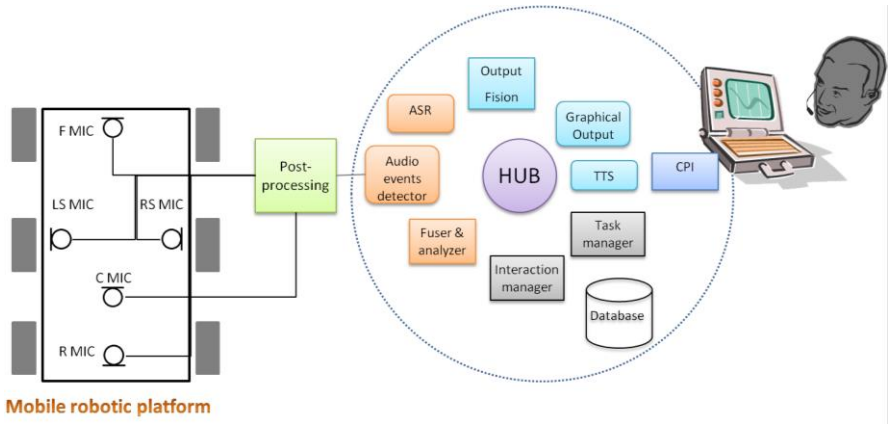

Figure 2
The robot speech interface

The newly designed robot multimodal interface (Figure 2) is de facto an asymmetric multimodal system, where speech is an input modality, and speech and graphical output are the output modalities. The system's input is extended with the acoustic event detection system, which carries the information about acoustic surrounding of the robot to the operator.

The Galaxy hub-server infrastructure [9] was adopted to construct the base structure of the system. The system designed consists of Galaxy hub process and nine servers:

- **Automatic speech recognition server** transforms speech signal into the corresponding text representation.
- **Audio events detector** serves for detecting of audio events as are gun shots or broken glass.
- **Fuser & analyzer** enable fusing several inputs into the corresponding events and perform analysis of incoming inputs. It transforms text representation of input into events, which represent voice commands for robotic system.
- **Output fision server** will serve for planning and fision of system outputs.
- **Text-to-speech server** performs speech synthesis, which transforms text output to speech signal.
- **Graphical output server** prepares text and graphical outputs, which should be presented to the user.
- **Interaction manager** is a part of the dialogue manager. It manages interaction by selecting appropriate tasks.
- **Task manager** is a part of the dialogue manager. It controls realization of simple tasks from which the interaction consists.
- **Control Panel Interface** (CPI) module was designed as an interface between the robot speech interface and control panel software.

To enable the control of the robot vehicle through voice commands, we decided to take an advantage of wireless close-talk headset to ensure as good SNR as possible. Usage of vehicle-integrated microphones directly for speech recognition purpose is not effective, because the acoustic surrounding of the robotic vehicle and also its own sound (from engine, movement, etc.) cause interferences to the input speech channel. Usage of wireless headset enables operator moving or standing close to the robot vehicle and expressing the voice commands as though directly to the robot. Of course, the signal from headset is still to be transmitted to the briefcase central control panel.

3.2 Automatic Speech Recognition

The Automatic speech recognition server is the most important part of the speech interface. Its performance (accuracy) determines successfulness of interaction. A lot of specific requirements can be identified on speech recognition technology for controlling the service robots, such as high accuracy, noise robustness, low hardware requirements, or the capability to run on specific hardware and software configurations. The ASR server was created by integrating an open-source solution into the Galaxy server. The advantage of using such approach is in the possibility to deliver audio stream both through Galaxy broker channel and directly through TCP/IP, also from remote locations.

For controlling robotic system by voice, rather than large vocabulary continues speech recognition system, the simpler recognition system being able to recognize isolated words and phrases should be used. Such systems are more accurate and also more robust, because of limited complexity and easier identification of start and end of commands.

The appropriate parameterization, acoustic and language models was designed and prepared for speech recognition process.

The most used parameterization, based on MFCC (Mel-frequency cepstral coefficients) was selected. The vector of parameters consist of twelve static MFCC coefficients, zero coefficient (0), delta (D), acceleration or acceleration coefficients (A) and subtraction of cepstral mean (Z) – (MFCC_D_A_Z_0) and its length is 39 values.

Acoustic models were trained on the telephone speech database SpeechDatE-SK [10] using training procedure from the COST-249 project [11]. Three states phoneme-based Hidden Markov models were prepared. We prefer phoneme models to triphone models for this task, because of their lower computation requirements. The accuracy of prepared models is higher than 95% (if SNR>20dB) for speech commands used for controlling SCORPIO service robot developed previously [7].

In case of the recognition system for recognizing a limited set of commands, the deterministic language model in form of context-independent grammar can be more effective and usable. The first step to building deterministic language model is performing analysis of system functions, which are considered to be controlled by voice. The analysis has shown that, there are six cooperation scenarios between robotic system and operator, which relate to:

- Movement of the robot
- Obtaining values from robot's sensors
- Turning on/off robot's devices and functions
- Manipulation with robotic arm
- Controlling of decontamination and extricate system
- Controlling of robot's legs

A set of commands was designed for each scenario. Approximately 200 voice commands were constructed and the speech grammar was prepared, which defines a recognition network. When the operator wants to control a specific part of the system, they need firstly to say the name of that part, e.g. "arm" or "decontamination system". Then they can start pronouncing commands for activated part, e.g.: "move right" or "lift the right front leg".

The pronunciation dictionary was also prepared, which contains all words from recognition grammar and their phonetic transcription.

3.3 Acoustic Event Detection

Short audio segments which can represent a potential threat or other interesting events are considered as acoustic events. The possibility to monitor acoustic scene of robotic vehicle surrounding and to detect acoustic events significantly improve usefulness of the robotic system, especially in situation, when robotic vehicle is not visible (and not audible) for operator and it moves in remote (long distance) or closed environments. Usually the operator watches mainly the output of the camera in direction of vehicle movement and some events can occur wherever in environment. Almost every physical event has its own acoustic accompaniment, which can be detected from acoustic signal, e.g. breaking glass, explosions, crash, gunshot, calling for help or crying. Acoustic event detection systems (AEDS) enable to detect mentioned events and can be able to detect also direction to the source of incoming sounds.

The acoustic event detection system was designed for earlier described complex modular robotic system, which is intended to serve for monitoring of acoustic environment around the robotic vehicle and for delivering information about possibly interesting or dangerous events that occurred within this surrounding. AEDS consists of a set of microphones on the robotic vehicle; the post-processing unit and acoustic events detector (see Fig. 2).

The set of five microphones was designed, where four microphones are localized on every side of the vehicle and fifth microphone is placed in center of the vehicle and serves as reference microphone. This deployment enables to detect also the direction of incoming sound. The reference microphone will be used for compensation of the robot's own produced noise.

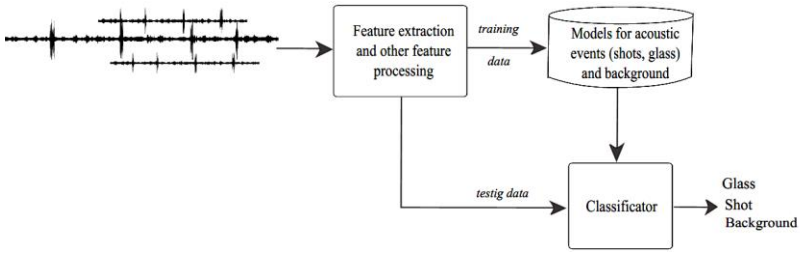

Figure 3
Acoustic event detection

The post-processing unit performs a compensation algorithms for noise reduction and enables to estimate the direction of incoming sound. Robot's own noise is compensated in all channels using the central, reference microphone.

The third part of the AEDS is the detection system, which consists of the feature extraction and processing unit, and classification unit. Its principal scheme is depicted in the Fig. 3.

The feature extraction unit transforms input acoustic signal into the sequence of feature vectors, which are then send to the classification unit. The output of the system has a form of so-called "alerts", which inform the operator about recognition of specific acoustic event.

Different algorithms can be used to describe the nature of acoustic signals. Some of them are inspired by the descriptors defined in MPEG-7 standard or they are speech-based, such as MFCC (Mel-Frequency Cepstral Coefficients), or they are based on other temporal and spectral features. Deeper analysis was performed in [12], [13]. An exhaustive search for suitable parametric representation of selected set of acoustic events (gunshot and breaking glass) was performed. In our experiments we investigated different parametric representations of the selected acoustic events [14], [15], [16], [17]. Our research was concentrated mainly on the gunshots and breaking glass detection. Many tests were performed using various feature extraction algorithms and also with using of mutual information-based feature selection [16].

There are several approaches to audio event classification. Usage of Hidden Markov models (HMMs) [18], [19], Support Vector Machines (SVMs) [20] [21] or GMM binary trees [22] [23] are the most popular.

Due to our previous experiences, classification based on HMM (Hidden Markov Model) was designed and implemented. Basically the classificator is based on Hidden Markov Models (HMM) with modified Viterbi search algorithm that includes our segmentation function [24]. In more detail, our classificator uses HMMs with dictionary of audio events combined and converted into Weighted Finite-Sate Transducer (WFST) as a search network [25]. Classificator is receiving extracted input features vectors and building up possible hypotheses that are corresponding with input audio signal. When classification ends using our segmentation algorithm the most probable hypothesis is outputted. Then it continues with processing of the rest of the signal until next segmentation.

Two types of models were trained – model which represents background sounds (noise of the environment), and models which represent foreground events, that we need to detect. Ergodic HMM models for background, gunshot and sound of breaking glass were trained. Models in range of one to four states with 1 to 1024 PDFs (Probability Density Function) were prepared and tested.

A lot of experiments were performed with several types of parameterization, as are Mel-spectrum coefficients, Logarithmic Mel-spectrum coefficients, classical MFCC and other. Promising results were obtained with speech inspired features MELSPEC_DAZ (Mel-spectrum coefficients) and FBANK_DAZ (Logarithmic Mel-spectrum coefficients) with first (D) and second time derivation (A) and with cepstral mean normalization (Z). The perfect recognitions were achieved for SNR levels higher than 0dB [18]. The results achieved from the experiments are depicted in the following Fig. 4. The detection performance is limited by various factors, e.g. weather condition, SNR, sound similarities, overlapping events, etc. SNR impact was investigated in the works [15], [17].

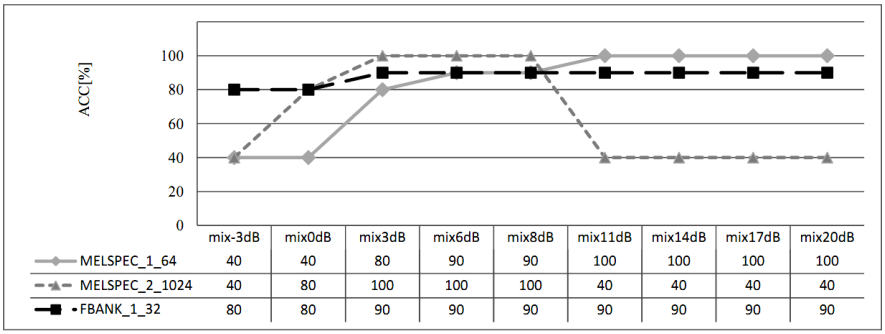

	mix-3dB	mix0dB	mix3dB	mix6dB	mix8dB	mix11dB	mix14dB	mix17dB	mix20dB
MELSPEC_1_64	40	40	80	90	90	100	100	100	100
MELSPEC_2_1024	40	80	100	100	100	40	40	40	40
FBANK_1_32	80	80	90	90	90	90	90	90	90

Figure 4

Accuracy of the audio events classification for different parameterizations and several SNR levels

To test newly-designed segmentation mechanism for classification process and to see if it interferes with detection accuracy, we conducted simple test on extended JDAE – TUKE database, described in [26]. Database contains (48 kHz, 16-bit per sample) recordings: 463 realizations of shots from commonly used weapons, 150 realizations of glass breaking and approximately 53 minutes of background sound. For testing purposes the database contains 13 glass breaking and 46 shots realizations. HMM models were trained using HTK environment [27] on MFCC feature vectors with zero, delta and acceleration coefficients resulting into 39 dimensional feature vectors. The segmentation algorithm was set to segment classification process and output results when the most probable hypothesis ending with background model and has lasted for 100ms time. For segmentation algorithm enabled and disabled we have achieved the same results 96.36% of accuracy. There was one missed alarm and 4 false alarms were produced [14].

3.4 Speech Synthesis

Text to speech (TTS) systems represent one of the most important parts of the speech interaction with robotic interface. Speech synthesizer enables to provide backchannel and information to the operator. It can be used also for indicating an occurrence of detected audio events.

The main objective of advanced speech synthesis nowadays is to use these artificial voices in various spheres of life without any limitation to their use in different situations. The essential requirements, which should be achieved in each TTS system, are the highest possible intelligibility, fluency and naturalness of speech at the output of this system.

The development of Slovak TTS systems for robotic interface is concentrated into two basic techniques of speech synthesis. The first voices, which were developed for this purpose, were based on the diphone concatenation method within the *Festival* TTS engine. In this case, it was necessary to create the voice data for

Festival (Slovak male and female diphone database) and additionally extend it using its embedded scheme scripting interface to incorporate the Slovak language support. The voices obtained by this approach can convert arbitrary text to speech with the quality corresponding to the diphone concatenation method [28]. Evaluation of voices using subjective and objective methods was conducted and from the obtained results it is clear that voices have acceptable intelligibility and fluency of speech at the output, but naturalness of speech significantly lags. The main advantages of this method are relatively small computing demands and small memory footprint, because the diphone concatenation method implemented in *Festival* uses LPC coefficients. Another advantage is the possibility to convert the obtained voices to the Festival-lite format, and we can use them with the *Flite* engine (cmuflite.org) which represents a small, fast run-time synthesis engine designed for small embedded machines.

Our recent research is focused on the creation of the new series of Slovak voices, which are based on the HMM-based speech synthesis method. This method uses the context-dependent HMM models, which are trained from speech corpus, as generative models for speech synthesis process [29]. We carried out some experiments with a relatively small database of Slovak language and the first female voices were built. The HMM-based TTS systems were developed by using several tools which are intended for this purpose. The quality of newly created voices was tested jointly with diphone voices and we can say that the HMM-based voices achieved much better results than diphone voices, even though the size of the input speech corpus in the case of HMM-based voices was not too large (speech corpus contained only 30 minutes of pure speech) [29]. Therefore, our work is now focused on building a bigger phonetically balanced speech corpus of male and female voice and we have to take into account that in case of development of the speech synthesis system for robotic interface, it is necessary to consider the fact, that we will probably synthesize short sentences or confirmation of commands, not long sentences nor a set of sentences. So the final speech database of both voices will consist of several variations of shorter sentences and confirmation.

3.5 Management of Interaction

The distributed dialogue manager, developed for communication with virtual agent [30], was adopted in simplified version also for management of interaction with the robotic system. The adopted solution is the distributed dialogue manager which consists of two agents – Interaction manager with user&history module included and Task manager. These agents cooperate over the common data space. Interaction is driven by events, which are represented by triggers and data objects. They could be caused by system, user or data. Triggers initiate small tasks. If user is passive, dialogue manager can invoke new tasks (system-initiative dialogue) by putting a new trigger into the trigger queue. The approach designed enables also

building transition networks or state machine, which enables to create trees or networks, where tasks are nodes of such structure. Each transition holds also decision condition, which must be true, to use the concrete transition from one task to another.

The interaction manager is responsible for event loop mechanisms, which consist of initialization of the Interaction Pool, event-selection algorithm and destroying the pool. During the initialization phase initial set of triggers, which invokes a welcome task and the next tasks according user experience level are included to the trigger queue. Event-selection algorithm checks trigger queue and selects the next trigger, which will be handled by the Task Manager. Interaction manager has two algorithms for selection of triggers. The first one searches for the first unhandled trigger in the trigger queue. When the trigger handling is finished, the second algorithm passes the transition network and searches for the next node (task), which should be processed. The transition condition is checked to evaluate if the transition is possible.

The task manager is responsible for performing the particular tasks, which were selected by the interaction manager. The task handling mechanism has three fundamental algorithms – data object values collection, cooperation with external data and output concepts generation. Each task can have a general prompt, which introduces particular task. Tasks can require filling zero or more data objects, which are attribute-value pairs for holding information obtained from user, related to particular task. When specific (or all) data objects has filled their values, task manager can perform specific function, e.g. writing data to the database, consult database and obtain information for user, or it can perform transition to other task or simply nothing.

The approach proposed for management of interaction enables to control interaction in simple, effective and variable manner. The interaction can be controlled solely by the user (user-initiative interaction) by his utterances, from which triggers are extracted and conveyed into the trigger queue. Manager also enables strictly system initiative dialog, where the dialog flow is determined by transition network (system-initiative interaction). The mixed-initiative dialogues are allowed by combining previous scenarios too.

3.6 The Interaction

Four tasks (*ObtainCom, GiveBCh, AckCom, SendCom*) as well as transition network (Fig. 5) were prepared for controlling the interaction with the complex robotic system.

Each task performs specific small interaction. *ObtainCom* task serves for obtaining voice command from the operator. According to user's experience level, it can prompt the user to say the command, or to leave him to be active and the system only waits for the command. *GiveBch* (Give backchannel) task repeats the

recognized command to inform operator about what was recognized. Then, the interaction is moved to the AckCom (Acknowledge command) task, where the system waits (during the specified time interval) on acknowledgment of the command. If the command is confirmed, SendCom (Send command) task is invoked and command is sent to the central control panel software, which performs it.

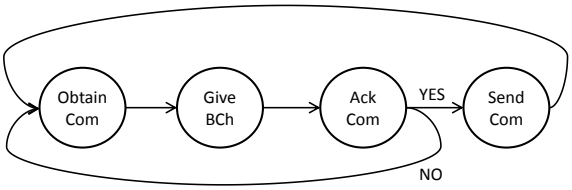

Figure 5
The transition network of tasks for controlling the robot using voice commands

Two examples of interaction are described below. The scenario no. 1 shows the base version, where the system firstly prompts the operator to say the command. The scenario no. 2 shows the scenario, when the operator is active and also the situation, when the command is not recognized correctly and the operator needs to repeat it.

Scenario 1:

S: Say your command. (*ObtainCom* task)

U: Robot, turn right. (*ObtainCom* task)

S: Robot, turn right. (*GiveBCh* task)

U: *(User pushes "dead man" button on the top of the joystick within a specified time interval)* (AckCom task)

System perform required task. (*SendCom*)

Scenario 2:

U: Robotic arm, base position. (*ObtainCom* task automatically invoked)

S: Arm, base position (*GiveBCh* task)

U: *(User pushes "dead man" button on the top of the joystick within a specified time interval)* (*AckCom* task)

System performs the required task. (*SendCom*)

U: Front camera (*ObtainCom* task)

S: Rear camera (*GiveBCh* task)

U: Front camera (*ObtainCom* task)

S: Front camera (*GiveBch* task)

….

As it is presented, the transition network enables to concatenate several tasks together, but the flow of the interaction is more flexible, because the user can in each state simply say the new command, and the first task (*ObtainCom*) is invoked.

Each task can be simply modified to change its prompts or data objects. The flexibility is assured by the possibility to access the database, where tasks as well as transition network are defined. The database can be modified also on the fly, which enables immediately react on situation.

Conclusion

The modules for implementation of speech technologies enabling cooperation of the human operator and the complex modular robotic system were introduced and evaluated on evaluation board provided. Presented modules are organized in the multimodal interface for controlling functions of the robotic system. All modules work well in laboratory conditions. However, to evaluate usability of the interface and to find possible sources of problems, tests and evaluation in real outdoor environment will be performed after final prototype of the whole robotic system will be introduced.

The special attention will be paid to the robustness of the speech recognition system [31] as well as to cognitive multimodal interaction aspects [32], to ensure ergonomics and usability of designed interface. Our further work will be also focused on design and development of the interface application for touchscreens of modern mobile tablet environment.

Acknowledgement

The research presented in this paper was supported partially (50%) by Research & Development Operational Program funded by the ERDF through project *Research of modules for intelligent robotic systems* (ITMS project code 26220220141) and partially (50%) by *Competence Center for Innovation Knowledge Technology of production systems in industry and services* (ITMS project code 26220220155).

References

[1] Broadbent E., Stafford R., MacDonald B., “Acceptance of Healthcare Robots for the Older Population: Review and future directions”, International Journal of Social Robotics, 1 (4), pp. 319-330, 2009

[2] Boissy P., Corriveau H., Michaud F., Labonté D., Royer M.-P., “A Qualitative Study of In-Home Robotic Telepresence for Home Care of Community-Living Elderly Subjects”, Journal of Telemedicine and Telecare, 13 (2), pp. 79-84, 2007

[3] Shibata T., Wada K., “Robot Therapy: A New Approach for Mental Healthcare of the Elderly - A mini-review”, Gerontology, 57 (4), pp. 378-386, 2011

[4] McColl D., Louie W.-Y.G., Nejat G., "Brian 2.1: A Socially Assistive Robot for the Elderly and Cognitively Impaired" IEEE Robotics and Automation Magazine, 20 (1), art. no. 6476702, pp. 74-83, 2013

[5] McTear M. F., "Spoken Dialogue Technology: Enabling the Conversational User Interface", ACM Computing Surveys, 34 (1), pp. 90-169, 2002

[6] Kotus J., Lopatka K., Czyzewski A., "Detection and Localization of Selected Acoustic Events in Acoustic Field for Smart Surveillance Applications", Multimedia Tools and Applications, p. 17, online first, 2012

[7] Ondas S. et al., "Service Robot SCORPIO with Robust Speech Interface", International Journal of Advanced Robotic Systems. Vol. 10, art. no. 3, pp. 1-11, ISSN: 1729-8806, 2013

[8] Vaughan B., Han J. G., Gilmartin E., Campbell N., "Designing and Implementing a Platform for Collecting Multi-Modal Data of Human-Robot Interaction", Acta Polytechnica Hungarica, Special Issue on Cognitive Infocommunications, Vol. 9, No. 1, pp. 7-17, 2012

[9] Seneff S., Hurley E., Lau R., Pao C., Schmid P., Zue V., "Galaxy-II: a Reference Architecture for Conversational System Development.", In Proceedings of the 5th International Conference on Spoken Language Processing – of ICSLP'98, Sydney, Australia, pp. 931-934 ,1998

[10] Pollak P. et al., "SpeechDat(E) Eastern European Telephone Speech Databases" Proceedings of LREC Satellite workshop XLDB, Athens, Greece, pp. 20-25, 2000

[11] Johansen F. T. et al., "The COST 249 SpeechDat Multilingual Reference Recogniser" LREC - International Conference on Language Resources and Evaluation, Athens, Proceedings Vol. 3, pp. 1351-1355, 2000

[12] Kim H. G., Moreau N., Sikora T., "MPEG-7 Audio and Beyond: Audio Content Indexing and Retrieval," New York: Wiley & Sons, p. 304, 2005

[13] Toh A. M., Togneri R., Nordhoolm S., "Investigation of Robust Features for Speech Recognition in Hostile Environments." Asia-Pacific Conference on Communications, Perth, art. n. 1554204, pp. 956-960, 2005

[14] Vozarikova E., Juhár J., Čižmár A., "Acoustic Events Detection Using MFCC and MPEG-7 Descriptors," Multimedia Communications, Services and Security, Springer, Vol. CCIS 149, pp. 191-197, 2011

[15] Vozarikova E., Pleva M., Vavrek J., Ondáš S., Juhár J., Čižmár A., "Detection and Classification of Audio Events in Noisy Environment," Journal of Computer Science and Control Systems, 3(1), pp. 253-258, 2010

[16] Vozarikova E., Juhár J., Čižmár A., "Performance of Basic Spectral Descriptors and MRMR Algorithm to the Detection of Acoustic Event," Multimedia Communications, Services and Security, Springer, Vol. CCIS 287, pp. 350-359, 2012

[17] Kiktova E., Lojka M., Pleva M., Juhar J., Cizmar A., "Comparison of Different Feature Types for Acoustic Event Detection System," Multimedia Communications, Services and Security, Springer, Vol. CCIS 368, pp. 288-297, 2013

[18] Zhou X., Zhuang X., Liu M., Tang H., Hasegawa-Johnson M., Huang T., "HMM-based Acoustic Event Detection with AdaBoost Feature Selection," Multimodal Technologies for Perception of Humans, Springer, Vol. LNCS 4625, pp. 345-353, 2008

[19] Ntalampiras S., Potamitis I., Fakotakis N., "On Acoustic Surveillance of Hazardous Situations," ICASSP: IEEE International Conference on Acoustics, Speech and Signal Processing, Taipei, pp. 165-168, 2009

[20] Bach J.-H., Kayser H., Anemuller J., "Audio Classification and Localization for Incongruent Event Detection," Detection and Identification of Rare Audiovisual Cues, Springer, Vol. SCI 384, pp. 39-46, 2012

[21] Giannakopoulos T., Kosmopoulos D., Aristidou A., Theodoridis S., "Violence Content Classification Using Audio Features" 4th Helenic Conference on AI, SETN, Heraklion, LNCS 3955, pp. 502-507, 2006

[22] Atrey P. K., Maddage N. C., Kankanhalli M. S., "Audio-based Event Detection for Multimedia Surveillance," ICASSP: IEEE International Conference on Acoustics, Speech and Signal Processing, Vol. 5, pp. V813-V816, 2006

[23] Vavrek J., Vozáriková E., Pleva M., Juhár J., "Broadcast News Audio Classification Using SVM Binary Trees," TSP: 35th International Conference on Telecommunications and Signal Processing, Prague, July 3-4, art. no. 6256338, pp. 469-473, 2012

[24] Pleva M., Lojka M., Juhar J., Vozarikova E., "Evaluating the Modified Viterbi Decoder for Long-Term Audio Events Monitoring Task" Elmar - International Symposium: Electronics in Marine, art. no. 6338500, pp. 179-182, 2012

[25] Lojka M., Juhár J., "Fast Construction of Speech Recognition Network for Slovak Language," Journal of Electrical and Electronics Engineering, Vol. 3, No. 1, pp. 111-114, 2010

[26] Pleva M., Vozáriková E., Doboš L., Čižmár A., "The Joint Database of Audio Events and Backgrounds for Monitoring of Urban Areas," Journal of Electrical and Electronics Engineering, Vol. 4 (1), pp. 185-188, 2011

[27] Young S., Kershaw D., Odell J., Ollason D., Valtchev V., Woodland P., The HTK Book Version 3.4, Cambridge University Press, 2006

[28] Sulír M., Juhár J., Ondáš S., "Speech Synthesis Evaluation for Robotic Interface", Complex Control Systems, Vol. 11(1), BAS, pp. 64-69, 2012

[29] Zen H., Oura K., Nose T., Yamagishi J., Sako S., Toda T., Masuko T., Black A. W., Tokuda K., "Recent Development of the HMM-based Speech Synthesis System (HTS)" APSIPA ASC: Asia-Pacific Signal and Information Processing Association Annual Summit and Conference, Sapporo, pp. 121-130, 2009

[30] Ondáš S., Juhár J., "Design and Development of the Slovak Multimodal Dialogue System with the BML Realizer Elckerlyc" CogInfoCom 2012: 3rd IEEE International Conference on Cognitive Infocommunications, December 2-5, Košice, pp. 427-432, 2012

[31] Staš J., Hládek D., "Recent Progress in Language Modeling and Continuous Speech Recognition of the Slovak Language", SCYR: Scientific Conference of Young Researchers of Faculty of Electrical Engineering and Informatics, FEI TU, Košice, pp. 339-342, 2011

[32] Baranyi P., Csapó A., "Definition and Synergies of Cognitive Infocommunications", Acta Polytechnica Hungarica, 9 (1), pp. 67-83, 2012

Innovative Operating Memory Architecture for Computers using the Data Driven Computation Model

Liberios Vokorokos, Branislav Madoš, Norbert Ádám, Anton Baláž

Department of Computers and Informatics, Faculty of Electrical Engineering and Informatics, Technical University of Košice, Letná 9, 042 00 Košice, Slovakia
{liberios.vokorokos, branislav.mados, norbert.adam, anton.balaz}@tuke.sk

Abstract: This paper deals with the data flow computing paradigm, with the characteristics of program execution control using a flow of data instead of a flow of instructions. Data flow computing represents an important alternative to the control flow computing paradigm, which is currently the mainstream computing paradigm represented by architectures mostly based on the Von Neumann principles, in which the flow of program execution is controlled by a flow of instructions. This paper also deals with the tile computing paradigm – a modern approach to designing multi-core microprocessors with components laid out in two-dimensional grids with various geometries of cores, memory elements and interconnection networks with architectures using both data flow and control flow program execution control. In this paper we introduce a data flow computer architecture designed at the Department of Computers and Informatics, Faculty of Electrical Engineering and Informatics, Technical University of Košice, Slovakia, employing the principles of tile computing. Efficient data flow architectures applying a different approach to the control of program execution flow also demand a different operating memory design. As the part of our effort to build data flow computer architectures, we have designed an innovative memory architecture that fulfils the specific needs of data flow computer architectures. In the final section of the paper we describe the functions and operations possible with this kind of memory.

Keywords: tile computing; data flow computing; data driven architecture; data flow graph; operating memory

1 Introduction

In the previous decades – starting from the middle of the last century – we have witnessed a tremendous expansion of the computer and electronics industry, connected to a long-term, unprecedented increase in the communication and computing performance of integrated circuits, accompanied with the increase of

memory chip capacities. This trend was driven by the increase of the number of basic building blocks [1] integrated onto the silicon chips and also by the increase of the density of their integration. This situation has brought the industry to the opportunity to gradually increase the communication and computing performance of superscalar monolithic uniprocessors. Unfortunately, it is not easy to use this opportunity to appropriately increase the computing performance of monolithic uniprocessors parallel to the increase of the number of transistors integrated on chips.

Microprocessor designs reflect the problem outlined above using the multi-core approach or single-chip multiprocessors [2]. Commercially available microprocessors are integrating more than one complex superscalar core on a single chip.

Other strategies are promoting downsizing of the superscalar core reducing its complexity and footprint in favour of the possibility to integrate even more cores on the chip. The core complexity ratio and the number of cores integrated onto the chip can therefore become an important parameter of multi-core microprocessor architectures. The future will bring the integration of not only tens, but hundreds and even thousands of cores. Integrating memory onto a single chip with the processing elements may become a further step in avoiding bottleneck problems related to accessing operating memory.

Researchers evaluate various layouts of cores, memory elements and especially interconnection networks, along with various program execution organization and control approaches [3]. Not only control flow driven architectures, along with Very Long Instruction Word (VLIW) approaches are being used, but the possibilities of architectures using the data driven computation model, called data flow architectures, are being continually investigated, too [4] [5] [6] [7] [8] [9] [10] [11].

A very important approach to microprocessor architecture design is tile computing, introduced in [12]. One can describe tile computing as the use of standardized components – including processing elements (small and simple processing elements, arithmetic and logic units or more complex cores), memory elements and modules, as well as various types of communication networks – in easily and highly scalable microprocessor and computer-on-a-chip architectures, where scaling the architecture up requires only minimal changes to the components in use and the architecture as such.

Tens of cores are being integrated not only in experimental architectures, but also in commercially available microprocessors – with more than hundred cores in some cases.

There are commercially available, as well as research and experimental processors and computer-on-the-chip architectures, in which the control of program execution is done by means of a control flow and a data flow; besides general

purpose architectures there are also specialized designs, such as digital signal processors.

Architectures range from 16 to 121 cores, such as TilePro64 (Figure 1), TeraScale, VGI, TRIPS, Monarch and others [13] [14] [15] [16] [17] [18].

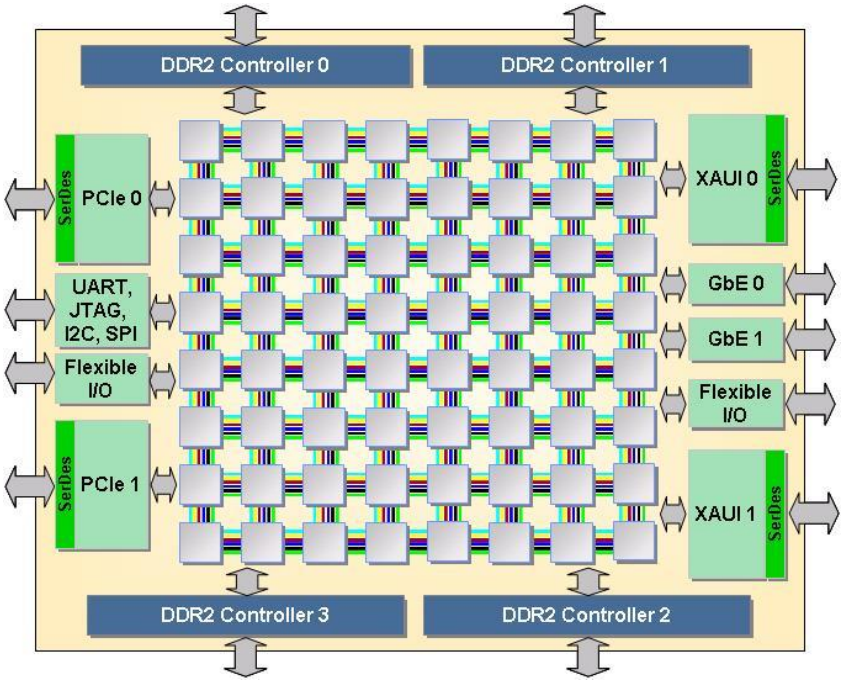

Figure 1
Tilera TilePro64 Block Diagram. Source: Tilera Corporation.

2 The Proposed Architecture

The architecture of the dataflow computer, proposed as a part of our research is a 32-bit computer-on-the chip with program execution driven by the flow of operands, according to the dataflow computing paradigm. The architecture was designed with the principles of tile computing in mind, with the aim to prepare a highly scalable design that could be scaled up in terms of integration of further processing elements and other components of the architecture on the chip with minimal changes to the design. One may scale this architecture up not only by redesigning the chip, but also by using the proposed computer-on-the-chip in a multichip configuration – in which chips are placed in a bi-dimensional grid layout, forming a consistent array of processing elements.

2.1 Elements of the Chip

The proposed computer architecture utilizes small elements with a simple design to allow the integration of as many elements as possible, in accordance with the number of transistors available on the chip. The basic element of the architecture is the Processing Element (PE), executing the dataflow program. Each processing element contains an integrated operating memory, used as the Activation Frames Store (AFS). All PEs are in a bi-dimensional grid, forming a Processing Array (PA). Other components integrated on the chip are Input/Output Elements (I/O) interconnecting PEs with the neighbouring components of the computer (Fig. 2).

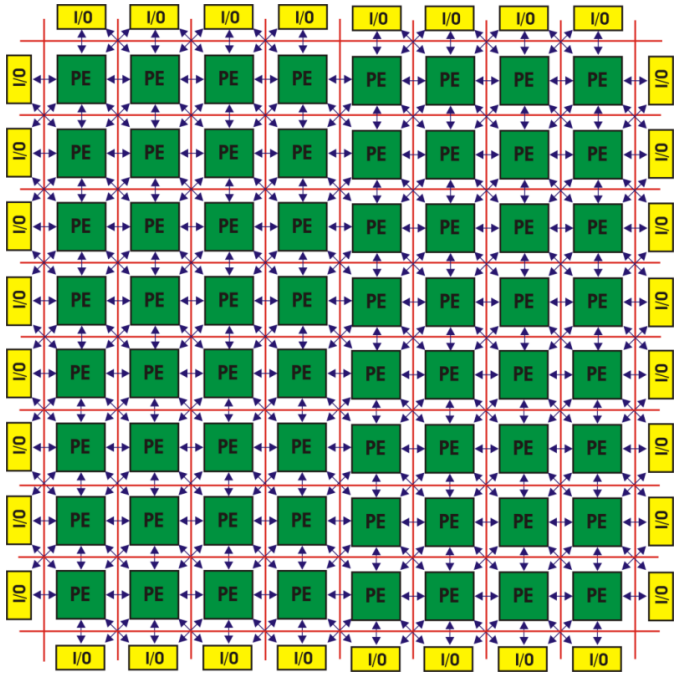

Figure 2
The processing array containing 64 processing elements, located in a two-dimensional, 8 × 8 layout, 32 input/output elements, communication channels intended for short-range communication (SCN) and the bus intended for global communication (GCN).

In the prototype built using Xilinx Field Programmable Gate Array (FPGA) technology, 64 processing elements (PE) are accompanied with 32 input/output elements (IO). The ratio (R) of the number of the integrated processing elements and the input/output elements may be calculated using formula (1). The ratio increases with the value of *n*.

$$R = \frac{n^2}{4n} \tag{1}$$

where

n is the number of PEs forming the edge of PA

2.1.1 Processing Elements

Each processing element (Figure 3) has a simple design and it consists of the following:

- an *Activation Frames Store (AFS):* a unit consisting of the operating memory developed as the part of the present research. The AFS has a capacity of 1024 × 144 bits. It is not only used as the instruction store but it also performs the Fetch phase of instruction cycle and it is capable of other operations, as described in section 3 of this paper.
- an *Arithmetic and Logic Unit (ALU):* the unit performing the Execute phase of the instruction cycle of integer arithmetic and logic operations.
- a *Control Unit (CU):* the unit controlling the execution of instructions and the communication with the neighbouring elements.

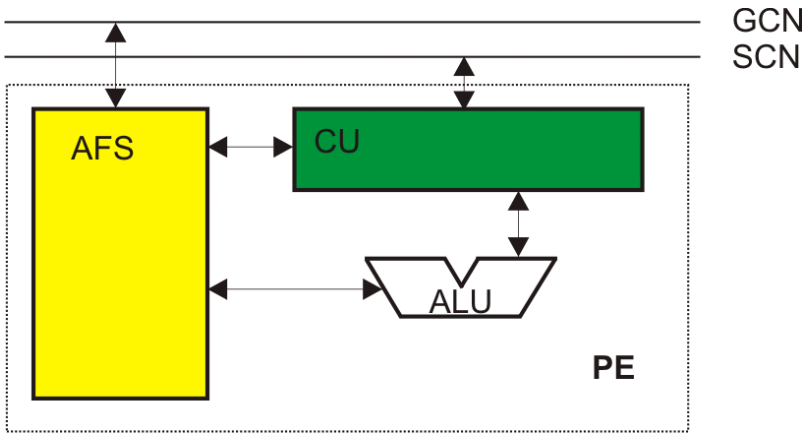

Figure 3

The structure of the processing element (PE), consisting of the Activation Frames Store (AFS), the Arithmetic and Logic Unit (ALU) and the Control Unit (CU), connected to the Global Communication Network (GCN) and a set of Short-range Communication Network (SCN) channels

Each activation frame stored in the AFS is addressable and all activation frames of all PEs integrated on the chip form a virtual cube of addressable space of the computer with addresses consisting of three components: X(2:0), Y(2:0) and Z(9:0). The X and Y components of the memory address, integrated in the processing element of the processing array and the Z component represents the address of the activation frame in the AFS of the particular PE. Each PE is allowed to address only activation frames stored in operating memory integrated in the particular PE; it is not allowed to address activation frames of other PEs.

2.1.2 Input/Output Elements

Processing elements situated on the edges of the processing element array are connected to the input/output elements surrounding this processing array. Each input/output element allows communication with other components of the computer system, when serving as the entry point of operands produced beyond the processing array, or as the exit point, when operands are leaving processing array and are used as inputs of other components of the computer system.

In a multichip configuration, two input/output elements, each on different chip form an I/O bridge that interconnects two processing elements of different chips and allows the transmission of operands between the chips. An I/O bridge forms an interconnection with the same function as a local network communication channel (Figure 4).

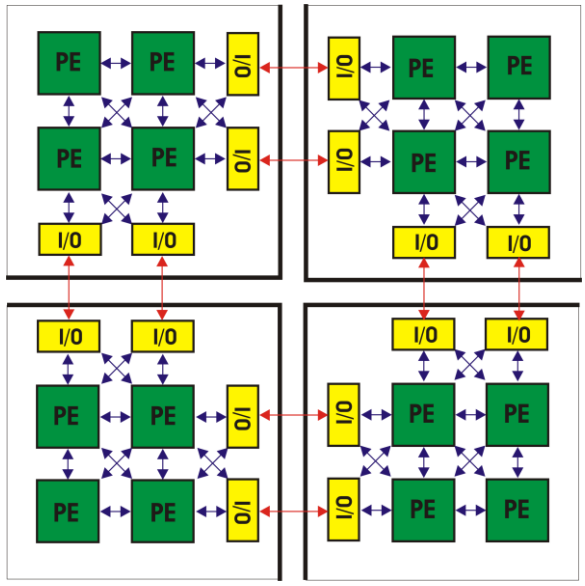

Figure 4
The multichip computer configuration allows scaling the computer beyond the borders of the chip. This figure presents four chips in a bi-dimensional layout, interconnected by I/O elements.

2.2 Communication Networks

To produce an efficient computer architecture design with the tile computing principles in mind, one also has to focus on the efficient communication of computer components. In the proposed architecture we have created two types of communication networks: for short-range and global-range communication.

Short-range communication (SCN) is performed by means of communication channels interconnecting each PE with each of its eight neighbouring elements. This allows pairs of chip elements to communicate in parallel; the high bandwidth short-range parallel communication of chip elements is implemented as follows: each PE is allowed to communicate with one of its neighbouring elements by passing tokens. A token consists of a 32-bit operand accompanied by a 10-bit target activation frame address and a 1-bit target operand flag (Figure 5). Short-range communication is used in *Compute Mode*, when the data flow program is executed.

Figure 5
Each token consists of a 32-bit operand (OP), a 1-bit target operand flag (AB) and a 10-bit activation frame address in the AFS (ADR)

Global-range communication (GCN) is implemented as a bus interconnecting all PEs, allowing data flow graph mapping onto the operating memory of each PE in three different manners developed as the part of the present research, as described below. This communication network is used in *Load Mode*, when the data flow graph is mapped onto the operating memory of each of the processing elements.

2.3 Data Flow Graph Mapping

A unique characteristic of the proposed architecture is that in *Load Mode* it is possible to map the data flow program as a data flow graph into the activation frames stores of the processing elements; this is done by means of the global range communication network, utilizing three different approaches. One can switch among these dynamically, immediately after each activation frame is mapped.

The first mode is *sequential mapping;* this allows mapping the instructions onto activation frames in the traditional way: one activation frame at once. Concurrent instruction mapping to the different AFS's of different PEs is not possible. All three components (X, Y and Z) of the activation frame are used.

The second mode, *global multi-mapping* allows mapping the same instruction onto all AFS's of all PEs in the PA concurrently in one machine cycle; the activation frame is addressed using the Z component of the address only.

The third mode, *mask multi-mapping mode* allows concurrent mapping of the same instruction into the AFS's of selected PEs of the PA. The PEs may be selected using a mask. The Z-component of the address, along with two 8–bit vectors representing the mask are used to specify which activation frames are targeted.

One may switch between the data flow graph mapping modes during the process to optimize the execution time of data flow graph mapping process. The mapping techniques are described in detail in [19].

2.4 Activation Frame

Instructions are represented as 144-bit vectors, mapped as activation frames onto the activation frame stores of the particular processing elements at time of data flow graph mapping, when the computer and the memory are in *Load mode*. Each instruction vector consists of components specified in Figure 6.

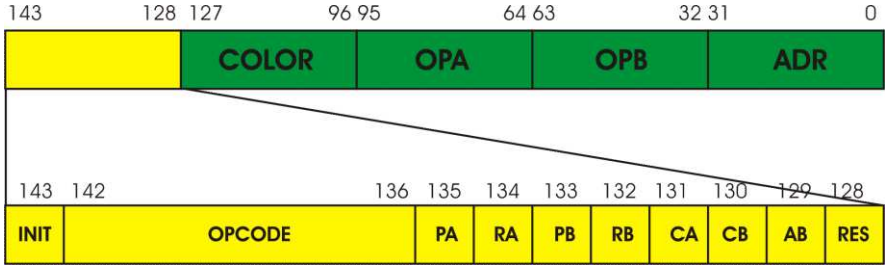

Figure 6
Instructions are represented by 144-bit vectors stored in activation frames

where:

INIT is a 1-bit instruction execution flag;

OPCODE is the 7-bit operation code of the instruction;

PA is a 1-bit flag indicating that operand A is required for instruction execution;

RA is a 1-bit flag indicating the availability of operand A;

PB is a 1-bit flag indicating that operand B is required for instruction execution;

RB is a 1-bit flag indicating the availability of operand B;

CA is a 1-bit flag indicating immediate operand A;

CB is a 1-bit flag indicating immediate operand B;

AB is a 1-bit flag indicating the target operand instructions;

RES is a 1-bit reserved flag;

COLOR is a 32-bit subgraph tag;

OPA is the 32-bit operand A;

OPB is the 32-bit operand B;

ADR is 32-bit target address of the instruction.

3 The Memory Subsystem of Processing Elements

The conventional concept of using operating memory in the control flow model – utilizing Random Access Memory (RAM) – has the advantage of simple design, high integration density of memory elements and low power consumption; however, it appears to be less useful for use in data flow computing. One of the basic operations of a data flow computer is to search for the next executable instruction stored in memory; therefore – in the worst case – all memory must be searched sequentially. This kind of operation requires logic beyond the memory and can be extremely time-consuming.

A solution to this problem is Content Addressable Memory (CAM), typically used in active network devices – for searching in routing tables [20] or in cache memory [21], for example. CAM has been designed with the aim to allow search of the entire memory in a single operation and it allows much faster search operations for immediately executable instructions, in comparison to RAM. However, Unlike RAM (having simple storage cells), each CAM bit is accompanied by a comparator to detect a match between the stored bit and searched bit and an additional circuit to evaluate if all bits of the data word match. This additional circuitry increases the physical size of the CAM chip, or – in other words – decreases the density of the memory elements, increases manufacturing costs and power consumption of the memory, as it is discussed in [22] [23]. With Ternary Content Addressable Memory (TCAM) it is possible to use not only 1 and 0 values, but also X as the "Don't care" value for one or more bits in the data word to make searches more flexible.

In our research, we are proposing a memory (Figure 7) philosophically based on TCAM. This memory incorporates not only memory cells, but also combinational logic to perform search operations, with which the immediately executable operation can be found, making use of parallel searches of the whole memory. We have altered the CAM concept and incorporated a priority generator into the memory to select the matching data word with the lowermost memory address. At any given time, there is only a single data word – representing the activation frame containing the immediately executable instruction – in the output of the memory.

One can write to the memory in an addressed fashion: a specific part of the data word will be stored at the specified address. This is used to store operands during program execution.

Another important feature of the proposed computer architecture is the ability to initialize or de-initialize subgraphs of the data flow graph with/without the preservation of operands. This is required to evaluate if the activation frame is part of the subgraph – that is why this operation must be performed on each activation frame stored in memory. After the evaluation, the instructions, which are part of the target subgraph, are initialized or de-initialized, according to the instruction type. All of those operations are performed on each activation frame stored in the activation frame store in parallel in a single machine cycle, by means of the built-in combinational logic circuit.

The memory operations of the proposed memory can be divided into two main groups, according to the operating mode of the memory and the computer: *Load mode (L)* and *Compute mode (C)*.

Operations performed in the traditional manner – including reading and writing of a specific activation frame using an address – are the first group of operations (I) performed in *Load mode*, when memory behaves as conventional RAM.

Another group of operations are data-flow-specific operations (II): these are performed on particular activation frames stored in memory (IIa) using an address or a specific attribute of the activation frame; or they are performed on all activation frames stored in memory in parallel (IIIa). The two aforementioned operation subgroups are available only in *Compute mode* and they are performed in connection with particular instructions of the data flow graph during data flow graph execution.

I. Load mode

1. Read;
2. Write.

II. Compute mode (data flow specific operations)

a. Operations on a single activation frame:

1. Writing operand A;
2. Writing operand B;
3. Reading the activation frame.

b. Operations on all activation frames:

1. Data flow graph initialization;
2. Data flow subgraph initialization with operands;
3. Data flow subgraph initialization without operands;
4. Data flow graph de-initialization;
5. Data flow subgraph de-initialization.

Instead of having separate Load and Compute inputs to control the two groups of operations, we have defined the $L/\overline{C}$ control signal. If the $L/\overline{C}$ input is set, the memory is in *Load mode,* otherwise it is in *Compute mode*. In *Load mode,* the $R/\overline{W}$ signal determines the particular operation of reading and writing, respectively (Figure 7).

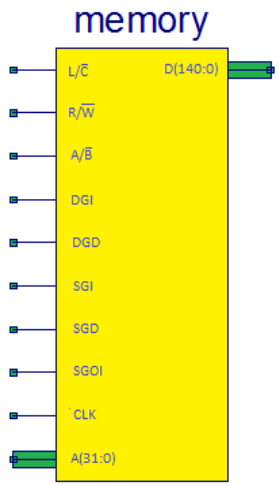

Figure 7
The schematic symbol of the data flow computer memory

3.1 Read Operation

The cycle of reading the activation frame memory is performed by setting the $L/\overline{C}$ and $R/\overline{W}$ signals to 1. The activation frame is addressed in the traditional manner, as used in RWM memory, with the A_α address present at the address input (A), while the activation frame can be read at the memory data output (DO).

$$L/\overline{C}.R/\overline{W}) \, DO := M[A_\alpha] \tag{2}$$

3.2 Write Operation

The cycle of writing operates on a memory address provided by the PE. The PE applies the address to the address input (A), the activation frame vector to the data input (DI) and sets the $L/\overline{C}$ signal to 1 and the $R/\overline{W}$ signal to 0. Then, the PE transfers the data to the activation frame during the positive transition of the next Ti pulse, which can also change the address and checks if there is another memory request. In this mode, the data flow graph is mapped onto the operating memory

of the processing element sequentially for subsequent execution. No data flow program activation frame is executed until $L/\overline{C}$ is set, even if there are executable instructions in the memory.

$$L/\overline{C} \,.\, \overline{\overline{R/W}}\,) \, M[A_\alpha] := DI \tag{3}$$

3.3 Writing Operand A

The process of writing operand A to the memory can be performed in *Compute Mode*, which is indicated by setting both the $L/\overline{C}$ and the $R/\overline{W}$ signals to 0. The activation frame is addressed at the addressing input of the memory (A) and the set $A/\overline{B}$ signal indicates that operand A will be stored in the activation frame. Operand A must be present in the appropriate part (bits 95:64) of the memory data input (DI) during writing.

$$\overline{\overline{L/C}} \,.\, \overline{\overline{R/W}}.A/\overline{B}\,) \, M[A_\alpha] := DI(95:64) \tag{4}$$

3.4 Writing Operand B

A change of the $A/\overline{B}$ signal to 0 indicates the process of writing operand B to the memory, when the $L/\overline{C}$ and $R/\overline{W}$ signals are set to 0. Operand B must be present in the appropriate part (bits 63:32) of the memory data input (DI) during writing.

$$\overline{\overline{L/C}} \,.\, \overline{\overline{R/W}}.\overline{\overline{A/B}}\,) \, M[A_\alpha] := DI(63:32) \tag{5}$$

3.5 Evaluation of Instruction Executability

An important operation that the memory performs on each stored activation frame is the evaluation of instruction executability. Each activation frame contains information as to whether the instruction is initialized or not (the INIT bit of the activation frame vector is set when the instruction is initialized). After mapping the data flow program into the operating memory and during program execution, instructions can be in an initialized state (i.e. they are ready for being executed, assuming that their operands are present), or the instructions are de-initialized (i.e. the instructions were executed or they have been prepared for subsequent initialization). Another condition of instruction executability is that the instruction operands must be present. Unary instructions require only a single operand – operand A – while binary instructions need operands A and B. The operand presence requirement is indicated by the PA and BB bits of the activation frame vector. If the operand is present, the RA and RB bits are set, respectively.

An instruction is executable, if the following conditions are fulfilled: INIT is set, RA = PA and RB = PB. The evaluation can be performed by a small logic circuit, as stated in Figure 8.

$$Y = INIT \wedge ((RA \oplus PA) \wedge (RB \oplus PB)) \tag{6}$$

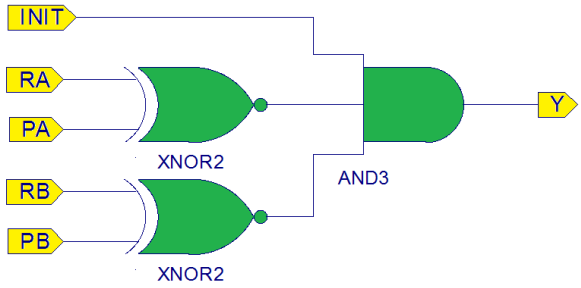

Figure 8
A logic circuit for evaluating instruction executability

The Y signal is set if the instruction is executable. If more than one instruction is executable at the same time, the memory evaluates the situation and selects (utilizing the priority generator) a single executable activation frame with the lowest memory address.

3.6 Reading the Activation Frame

Reading the activation frame in *Compute mode* is controlled by the operating memory itself and there is no need to activate the address input of the memory (A). The $L/\overline{C}$ control signal is set to 0 and the $R/\overline{W}$ signal is set to 1 during activation frame reading. At any time during program execution, the data output of the memory activation frame contains the activation frame vector of an instruction that is executable immediately. After the execution of the instruction, this frame is de-initialized and another frame is selected for execution. Executability evaluation is performed on each activation frame in parallel via the logic circuits described above. If more than one activation frame is executable concurrently, the priority generator is used select the appropriate one.

Selecting the executable activation frame is very important for proper and effective program execution in data flow computers. It requires a lot of time when using traditional operating memories.

$$\overline{L/\overline{C}} . R/\overline{W}) \, DO := M[A_{\alpha}] \tag{7}$$

3.7 Data Flow Graph Initialization

Every time the data flow graph is executed, the data flow graph may be initialized. The DGI input of the memory is set and the initialization operation is performed in parallel on each activation frame vector stored in memory, by setting its INIT bit. All operands stored in memory are removed. This operation may be used to activate another iteration of the data flow graph execution, without the need for data flow graph mapping.

$$\overline{\overline{L/C}}.\mathrm{DGI}) \, \mathrm{M}[\mathrm{A}_{\alpha}](0) := 1 \tag{8}$$

3.8 Data Flow Subgraph Initialization with Operands

Every time the data flow graph is executed, the data flow subgraph may be initialized. The SGOI input of the memory is set and the subgraph colour ($\mathrm{DFG}_{\mathrm{color}}$) is indicated at the appropriate memory data input.

$$\overline{\overline{L/C}}.\mathrm{SGOI}) \, \mathrm{DI} := \mathrm{DFG}_{\mathrm{color}} \tag{9}$$

A logic circuit acting as a comparator connected to each activation frame evaluates if the memory operation is valid for the given activation frame. If this condition is fulfilled ($\mathrm{Y}_{\mathrm{SGOI}}$ = 1), the activation frame is initialized and the operands present are preserved. By this initialization, the subgraph is prepared for another execution iteration.

$$\mathrm{L}_{\mathrm{SGOI}} \mid \mathrm{Y}_{\mathrm{SGOI}} = 1 \tag{10}$$

3.9 Data Flow Subgraph Initialization without Operands

The initialization of the data flow subgraph can be performed by setting the SGI memory input to 1. The subgraph colour is indicated at the appropriate data input of the memory.

$$\overline{\overline{L/C}}.\mathrm{SGI}) \, \mathrm{DI} := \mathrm{DFG}_{\mathrm{color}} \tag{11}$$

The comparator, connected to each activation frame, checks if the memory operation is valid for the given activation frame. If this condition is fulfilled ($\mathrm{Y}_{\mathrm{SGI}}$ = 1), the activation frame is initialised. Operands present are removed. Now, the data flow subgraph is ready for another iteration of execution.

$$\mathrm{L}_{\mathrm{SGI}} \mid \mathrm{Y}_{\mathrm{SGI}} = 1 \tag{12}$$

3.10 Data Flow Graph De-Initialization

If the DGD memory input is set to 1, de-initialization is performed on each activation frame vector stored in memory in parallel, by resetting their INIT bits. All operands stored in memory are preserved. This operation may be used to deactivate the data flow graph execution immediately, using the KG (Kill Graph) instruction that is part of instruction set of the architecture.

$$\overline{\overline{L/C}}.DGD) M[A_{\alpha}](143) := 0 \quad (13)$$

3.11 Data Flow Subgraph De-Initialization

Setting the SGD memory input to 1 indicates the de-initialization process of the data flow subgraphs having the specific colour presented at the appropriate data input of the memory. This operation may be used to deactivate the data flow subgraph execution immediately, using the KSG (Kill SubGraph) instruction that is part of instruction set of the architecture.

$$\overline{\overline{L/C}}.SGD) M[A_{\beta}](143) := 0 \quad (14)$$

The comparator connected to the activation frame checks if the operation is valid for the given activation frame. If this condition is fulfilled, the activation frame is de-initialized by resetting the INIT bit, while the operands present are preserved. The data flow subgraph is now ready for another initialization.

$$L_{SGD} \mid Y_{SGD} = 1 \quad (15)$$

Conclusions

The presented data flow computer architecture with tiled organization of processing elements is the result of the research performed at the Department of Computers and Informatics, Faculty of Electrical Engineering and Informatics, Technical University of Košice, Slovakia. Within the present research, we propose a memory with activation frame store functionality based on Ternary Content Addressable Memory (TCAM), which behaves as conventional RAM in *Load Mode* and CAM in *Compute Mode* and is capable of executing operations specific for the proposed data flow computer architecture. This memory represents an innovative approach to the construction of data flow computers; in future research it may serve as a basis to solve problems of data flow computers that limit their field use.

Acknowledgements

This work was supported by the Slovak Research and Development Agency under contract No. APVV-0008-10. The project is being implemented at the Department

of Computers and Informatics, Faculty of Electrical Engineering and Informatics, Technical University of Košice, Slovakia.

References

[1] Gy. Györök, M. Makó, J. Lakner: „Combinatorics at Electronic Circuit Realization in FPAA“, In: Acta Polytechnica Hungarica. Vol. 6, No. 1 (2009), pp. 151-160, ISSN 1785-8860

[2] B. Grot, J. Hestness, S. W. Keckler, O. Mutlu: „Express Cube Technologies for On-Chip Interconnects“, Proceedings of the 15th International Symposium on High-Performance Computer Architecture, February 14-18, 2009, Raleigh, North Carolina

[3] J. Kopják, J. Kovács: „Timed Cooperative Multitask for Tiny Real-Timeembedded Systems“, IEEE 10th Jubilee International Symposium on Applied Machine Intelligence and Informatics (SAMI 2012) Herl'any, Slovakia, 2012, pp. 377-382

[4] J., B. Dennis, R. P. Misunas: „A Preliminary Architecture for a Basic Data Flow Processor“, Proceedings of the 2nd Annual Symposium on Computer architectures., 1974

[5] A. Veen: “Dataflow Machine Architecture”, ACM Computing Surveys, December 1986, pp. 365-396

[6] P. Fanfara, E. Danková, M. Dufala: “Usage of Asymmetric Encryption Algorithms to Enhance the Security of Sensitive Data in Secure Communication”, 2012. - 1 CD-ROM. In: SAMI 2012: 10th IEEE Jubilee International Symposium on Applied Machine Intelligence and Informatics : proceedings : Herľany, Slovakia, January 26-28, 2012. - Budapest : IEEE, 2012 S. 213-217. - ISBN 978-1-4577-0195-5

[7] V. V. Vlassov, A. V. Kraynikov, B. A. Kurdikov: "A Data Flow Computer System". In: Izvestiya LETI (Proceedings of Leningrad Electrotechn.Inst.), St. Petersburg, Vol. 436, 1991, pp. 3-7

[8] L. Vokorokos: “Data Flow Computer Principles” (in Slovak), Copycenter, spol. s.r.o., Košice, Slovakia, 2002. ISBN 80-7099-824-5

[9] A. Arvind, D. E. Culler: "The Tagged Token Dataflow Architecture (preliminary version)".Tech. Rep. Laboratory for Computer Science, MIT, Cambridge, MA, 1983

[10] T. Shimada, K. Hiraki, K. Nishida, S. Sekigughi: "Evaluation of a Prototype Dataflow Processor of the SIGMA-1 for Scientific Computations", In: Proc. 13th Annual Symposium On Computer Architecture, 1986, pp. 226-234

[11] N. Ádám: „Single Input Operators of the DF KPI System“, In: Acta Polytechnica Hungarica. Vol. 7, No. 1 (2010), pp. 73-86, ISSN 1785-8860

[12] E. Waingold et al.: “Baring it All to Software: RAW Machines”, IEEE Computer, Sep. 1997, Technical Report, MIT Cambridge, Massachusetts, USA

[13] Tilera Corporation: TILEPro64 Processor Product Brief, 2011

[14] Sriram Vangal, et al. "An 80-Tile Sub-100-W TeraFLOPS Processor in 65-nm CMOS," l. IEEE Journal of Solid-State Circuits, Vol. 43, No. 1, Jan 2008

[15] V. P.Sirini, J. Thendean, S. Z.Ueng, J. M. Rabaey: “A Parallel DSP with Memory and I/O Processors. In Proceedings SPIE Conference 3452, pp. 2-13, 1998

[16] S. Swanson, K. Michelson, A. Schwerin, M. Oskin, “WaveScalar”, Proc. of the 36th International Symposium on Microarchitecture (MICRO-36 2003) 2003, pp. 291-302, ISBN 0-7695-2043-X

[17] Garnacki, J., J. a M. D. V,: MONARCH a High Performance Embedded Processor Architecture with Two Native Computing Modes, in High Performance Embedded Computing, 2002

[18] K. Mai, T. Paaske, J. Nuwan, R. Ho, W. Dally, M. Horowitz: “Smart Memories: A Modular Reconfigurable Architecture”, ISCA 00, Vancouver, British Columbia, Canada, ACM 1-58113-287-5/00/06-161

[19] L. Vokorkos, B. Madoš, A. Baláž, N. Ádám: „Architecture of Multi-Core Computer with Data Driven Computation Model“, In: Acta Electrotechnica et Informatica. Roč. 2010, č. 4 (2010), s. 20-23. - ISSN 1335-8243

[20] A. J. McAuley and P. Francis: "Fast Routing Table Lookup Using CAMs", IEEE INFOCOM 1993, pp. 1382-1391, March 1993

[21] A. Efthymiou and J. D. Garside: "An Adaptive Serial-Parallel CAM Architecture for Low-Power Cache Blocks", In Proc. of the ISLPED, pp. 136-141, 2002

[22] H. Miyatake, M. Tanaka, and Y. Mori: “A Design for High-Speed Low-Power Cmos Fully Parallel Content-Addressable Memory Macros,” IEEE J. Solid-State Circuits, Vol. 36, pp. 956-968, Jun. 2001

[23] I. Y.-L. Hsiao, D.-H. Wang, and C.-W. Je:, “Power Modelling and low-Power Design of Content Addressable Memories,” in Proc. IEEE Int. Symp. Circuits and Systems (IS- CAS), Vol. 4, May 2001, pp. 926-929

Innovative Approaches in Modeling, Control and Diagnostics of Small Turbojet Engines

Rudolf Andoga*, Ladislav Madarász*, Ladislav Főző**, Tobiáš Lazar*, Vladimír Gašpar*****

*Technical University of Košice, Faculty of Aeronautics, Department of Avionics, Rampová 7, 04200 Košice Slovakia, e-mail: rudolf.andoga@tuke.sk

**Technical University of Košice, Faculty of Aeronautics, Department of Aviation engineering, Rampová 7, 04200 Košice Slovakia, e-mail: ladislav.fozo@tuke.sk

***Technical University of Košice, Faculty of Informatics and Electrical Engineering, Department of Cybernetics and Artificial Intelligence, Letná 9, 04200 Košice Slovakia, e-mail: ladislav.madarasz , vladimir.gaspar@tuke.sk

Abstract: The article presents a survey of research and main results achieved in the Laboratory of intelligent control systems of aircraft engines during its five years of existence at the Technical university of Košice celebrating its 60th anniversary. The main areas of scientific interest and results are presented in the fields of innovative approaches in modeling, control and diagnostics of turbojet engines utilizing adaptive and intelligent algorithms. The researched methodologies have been tested and validated on the experimental engine small turbojet engine MPM-20 in laboratory conditions and selected results are presented in the article.

Keywords: turbojet engine; mathematical modeling; intelligent control; diagnostics; artificial intelligence

1 Introduction

A turbine engine in its general principle is a complex nonlinear systems with many parameters that are linked with each other through complex thermodynamic bindings. Thermodynamic processes and the need to operate such engines in various conditions presents a vast set of problems that are opened to solutions. Demands on the modern engines lie mainly in efficiency of their operation (output vs. fuel consumption) and safety. The traditional automatic control and diagnostics algorithms are being exhausted and brought to their limits in this area and opens a field of non traditional innovative approaches in this area [1, 2, 7]. The problem with such algorithms that are often non-deterministic in their nature

or very complex is their operational testing. While in simulation environment such algorithms can produce reliable results, testing in realworld environment with changing conditions may become problematic and expensive in case of failures [3, 6, 8].

The Laboratory of Intelligent Control Systems of Aircraft Engines has been established to deal with the afore mentioned problems at the Technical University. The laboratory has just recently achieved its first milestone of a humble 5^{th} anniversary aiming to become a scientifically important act within the frame of the Technical University of Košice that is celebrating its 60^{th} anniversary this year. This laboratory is a joint venture of three departments: Department of Avionics, Department of Aviation Engineering and the Department of Cybernetics and Artificial Intelligence. The main idea is to design implement and test progressive modeling, control and diagnostic algorithms in realworld conditions on an object of a turbojet engine. As our object the turboshaft engine TS-20/21 was chosen as it was phased out of service and is still in supply from old aircraft in non flying conditions. The engine has been adapted with an exhaust nozzle creating a small turbojet engine MPM-20/21. Such small engine has similar thermodynamic properties and normal sized engine, is affordable to obtain and thus suitable for laboratory experiments with progressive algorithms [1, 10, 15, 20].

The main aim of the laboratory is to do research in three basic areas of cybernetics: modeling, control and diagnostics of complex systems with additional evaluation of efficiency of such research and application of advanced methods in the area of turbojet engines. The obtained knowledge is to be used in modern control systems of small turbojet engines, however it can be expanded to normal sized engines and also other classes of similar complex systems [10, 21, 22].

Apart the mentioned areas of research and results in the last years work has been done in the area of alternative fuels research aimed at bio fuels, ethanol and hydrogenium tested on the object of small turbojet engine. The results have shown usability of such fuels up to certain concentrations (generally around 40%) and adverse effects on different engine parts were also researched. The other area of tests were carried out to asses the possibility of magnetic field (aura) measurement to evaluate the state of an engine. Pilot experiments were done and have shown some methodological approaches and pilot influence of engine temperature field on manifestation of its magnetic aura. Valid results were also achieved in modeling of temperature channel sensors in order to estimate turbojet engine temperatures infront of the turbine, the results were used in such estimation for the RD-33 engine. All the results from the previous research that are not covered within the presented article have been described in the sources [1, 10, 13, 14].

2 The Laboratory of Intelligent Control Systems of Aicraft Engines

The Laboratory of intelligent control systems of aircraft engines can be found in the campus of the Faculty of Aviation at Technical University in Košice The laboratory consists of two test rooms and two control rooms specially built for testing of turbo compressor engines. One of the testing and control rooms is shown in Figures 1 and 2. The room contains the object of small turbojet engine MPM-20 with its respective control computer and power supply unit. The other control and testing room contains a small turbojet TJ-100 engine with its control computer [10].

Figure 1
MPM-20 engine in the testing room

Figure 2
The control room and control computer

The whole structure of the measurement and control system for the MPM-20 engine is shown in Figure 3. The hydromechanical control and sensing has been transformed into fully digital control of the engine. This allows us to collect all the data from the engine in digital form with specified precision; test and implement models and control aglorithms of the engine [10].

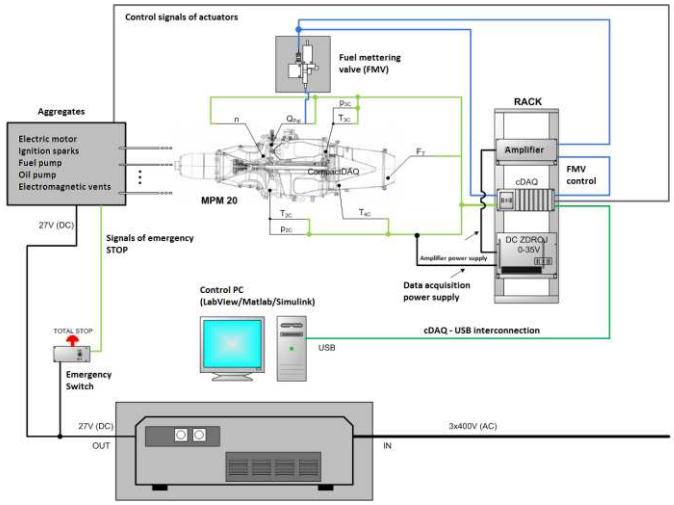

Figure 3
Structure of the engine's measurement systems

3 Modeling of Small Turbojet Engines

Aircraft turbo-compressor engines represent multivariable objects of control with existence of crossbindings between inputs and outputs invoked by complex thermo dynamic processes ongoing in inner parts of the engine and dominating load. Except those relations, other can occur by synthesis of control elements that can seriously influence functionality and integrity of the whole mechatronic object (engine and aircraft) [12, 18]. The active part of the engine is represented by its turbine and the passive part is its compressor. The general aim of multivariable objects control is to obtain optimal quality and stability of the whole control circuit. To obtain this aim it is necessary to build efficient simulation models aimed on control system design. If the control system has to bring a new quality the model used for its synthesis has to also have high quality expressed by its precision compared to real-world data. To obtain this aim a set of non-equal models serving for different purposes has been built. The following chapters illustrate the taken approaches in modeling of the MPM-20 engine for the purpose of its control and diagnostics system design.

3.1 A Small Turbojet Engine MPM-20

In order to build a simulation model of any object, it is necessary to know its properties (dynamic and static) and it structure. The MPM-20 engine in its present form is a one shaft single stream engine with radial compressor and bound combustion chamber with single stage uncooled turbine with fast exhaust geometry. The engine has been modeled in 3D environment and a render of this model can be seen in Figure 4 [10].

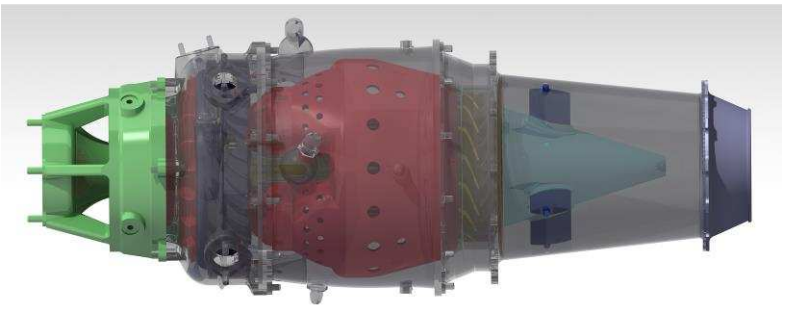

Figure 4
3D model of the MPM-20 engine

3.2 Analytic Modeling of the MPM-20 Engine

Static properties of turbojet engines can be calculated under equilibrium engine conditions, dynamic properties can be calculated during non-equilibrium conditions, while utilizing basic physical parameters depedencies in different cut of the engine. Resulting model can be called an analytic one and is used to precisely model thrust, fuel consumption, pressures and temperatures of the engine at different altitudes and velocities in selected cuts of the engine. This approach is called analytic modeling approach and its main benefit is its ability to calculate parameters that cannot be directly measured at conditions that are not obtainable in a laboratory [4, 8, 15].

While considering a steady operation of the engine, every element of the engine contains same thermodynamic processes. Such operation can be described by [15]:

- Algebraic equations computing the mass flow equilibrium of gasses travelling through all cuts of an engine, control laws and output equations. If such system of equations is sloved in equilibrium operating point, the result will present a steady operational state that an engine stablizies on.

- Graphic depiction that utilizes expert knowledge of individual constructional parts of an engine (compressor, combustion chamber, turbine, etc) and interactions between them. The graphs can be obtained by experimental measurement or analytic computation with later transformation into a tabular form with description of every regime [4, 16, 17].

Every operational regime of a turbojet engine has to satisfy the equation of continuity that describes dependencies between air mass flow through compressor the compressor, turbine, combustion chamber and exhaust system [4, 16, 17]:

$$Q_{VS} = Q_k = Q_{SK} = Q_T = Q_{tr} = Q \tag{1}$$

Also the condition (or assumption) of fast and non-distortive shaft has to be satisfied:

$$n_k = n_T = n \tag{2}$$

where [16]:

Q_{VS} – air mass flow of in the input system,

Q_k – air mass flow of air in compressor

Q_{SK} – air mass flow in the combustion chamber,

Q_T – gass mass flow on the turbine,

Q_{tr} – gass mass flow in the exhaust nozzle,

n_k – speed of the compressor,

n_T – speed of the turbine.

When solving the equations in equilibrium, thus computing a static analytic model the speed of the engine has to be constant in time [4, 16, 17].

$$\frac{dn}{dt} = 0 \tag{3}$$

This condition is satisfied when the output of the turbine is equal as power consumed by the compressor and other auxiliary systems of the engine

$$W_{KC} = \eta_m W_{TC} \tag{4}$$

Where [4, 6, 16, 17]:

η_m – mechanical effectiveness of the engine,

W_{KC} – technical work of the compressor,

W_{TC} – technical work of the turbine.

The complete algorithm that computes all operational points in steady state of a single stream engine can be found in [4, 16].

Transitional or non-steady operation of an engine is determined by variable complex thermodynamic processes in each node of a turbojet engine. Operation of the engine in such conditions can be described by a set of non-linear differential equations. Such equations describe non-steady processes in the engine where the operational point of the engine is changing either by fuel flow mettering or flight regime change.

This transitional regime is defined by difference of work of the turbine and power consumption by the compressor. This creates different moments of the turbine M_T and compressor M_K. In this case, acceleration or deceleration of the engine is defined by the elementar moment equation [4, 16]:

$$M_T - M_K - M_{ag} = J\frac{d\omega}{dt} \tag{5}$$

where

$\frac{d\omega}{dt}$ - angular acceleration,

J - moment of inertia of all rotating masses reduced to the shaft of the engine

M_{ag} - moment needed for actuation of aggregates and overcoming of friction.

The speed of the MPM-20 engine can be computed as $\omega = \frac{\pi n}{30}$ and the power output can be computed from the equation $P = M\omega$, after inclusion of mechanical efficiency, the elementar equation of transient operation is created:

$$P_T\eta_m - P_k = J\frac{\pi^2}{900}n\frac{dn}{dt} \tag{6}$$

In solution of the previous equation, the difference in speed is computed after a preset time step Δt and this algorithm is continuously repeated until the engine settles itself on a new equilibrium point.

Complete analytic model has been computed for MPM-20 engine and implemented in Matlab GUI environment. Such analytic model is called engine deck and can be used for parameters estimation and computation of many non measurable engine characteristics with many variable environmental (air temperature, pressure, humidity, velocity, aerodynamic angles, etc.) and inner parameters (friction, efficiency coefficients, mechanical losses, etc) [4].

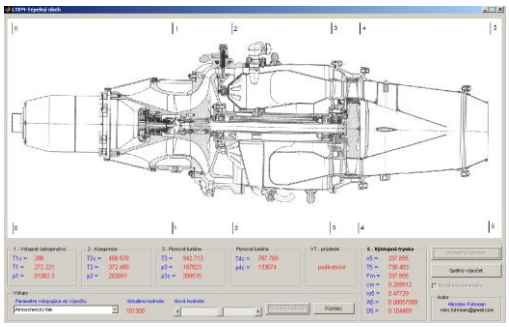

Figure 5
Matlab GUI analytic model

The analytic model will help us in design of complex control algorithms, can be used to design news systems for the engine like variable exhaust nozzle, can be used to calculate operational envelope of the engine and used as a nominal diagnostic model for the engine. Simulations with the analytic model are depicted in the following Figure 6 [4].

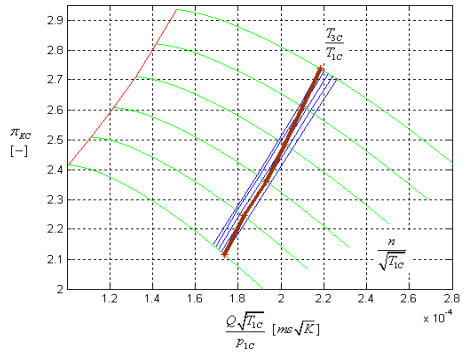

Figure 6
Compressor characteristics as computed by the analytic model

3.3 Experimental Engine Modeling

While the analytic models are suitable for computation of many different engine parameters, they are not able to simulate complex dynamic dependencies of individual parameters. Dynamic models used to simulate operation of turbojet engines have a more limited set of parameters and concetrate on complex dynamic dependencies between them. In this case for the MPM-20 engine we will consider exhaust gas temperature - T_{4c}, compressor pressure - P_{2c}, engine speed - n as parameters dependand on fuel flow - Q_{pal} parameter. Interconnections between the parameters however are not stationary, so the model changes structure in different

operating conditions, it can be stated that operating point will be defined as a functional of the following parameters [10]:

$$O_p = f\,(Q_p, N_1, T_{4c},\ P_2, t) \tag{7}$$

Because the functional (8) defines a complex multidimensional nonlinear space, it is very difficult to create a qualitative dynamic model of such functional. To solve this problem a methodology of situational modeling is proposed. This means to decompose the model into certain operating regions where we can consider the structure of the model to be stationary. By such decomposition we can obtain a set of models defining the operation of the engine [10].

$$O_{pi} = f_i\,(N_1, T_4, P_2),\ i=1\ldots n \tag{8}$$

where n is the situational frames count. Decomposition can be done by means of using expert knowledge or clustering (classification algorithms). To exclude time from the model we propose an intelligent selector that will select appropriate model for the given conditions. The architecture of the model is shown in Figure 7 with decomposition of the model into three structurally different submodels representing start-up, steady operation and shutdown of the engine.

Inputs of the classifier are defined by outputs of individual models while the total input to the model is only its fuel flow parameter – however other parameters (like environmental parameters can be used to improve selection of the active situational frame. The gating signal from the classifier can be defined as [10]:

$$O_u = [x_1,\ \ldots\ ,\ x_n] \tag{9}$$

where n is the number of situational model frames and $x_i = \{0;1\}$,in our case $n=3$. So the classifier switches

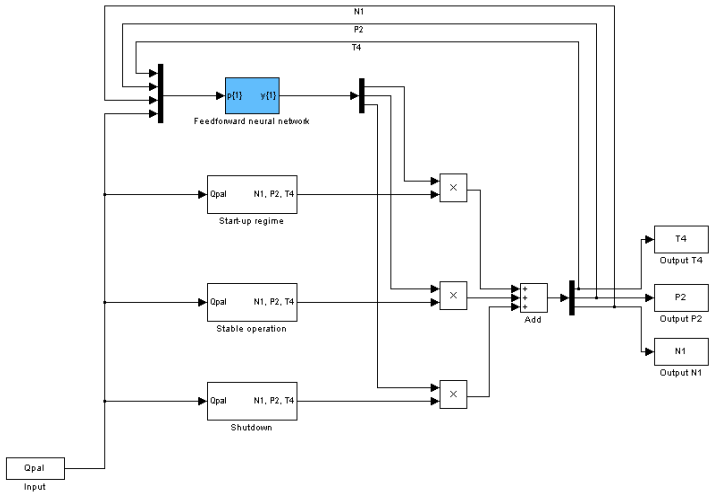

Figure 7

The structure of situational control model implemented in Matlab/Simulink

The classifier neural network utilizes state variables produced by the individual models, while the input parameter is only the fuel flow. The situational classifier will have its output in the following form:

$$O_u = [x_1, \ldots, x_n] \tag{10}$$

where n is the number of situational model frames and $x_i = \{0;1\}$,in our case $n=3$.

The models were tested separately with fuel supply inputs measured during different engine runs. Startup model utilizes feedforward neural networks with input time delays composed of two hidden layer and is trained by SCG algorithm [15]. The equilibrium operational state model is composed of three models using Takagi Sugeno (TSK) fuzzy inference systems to model individual parameter dependencies and the shut-down model uses neural networks of identical structure as the startup model trained with other data. Results of the average errors during those 15 runs show very good results as illustrated in Table 1, where MAE is mean absolute error averaged through 15 runs, MAAE is maximum absolute average error from those 15 runs and the errors are also expressed in percents (MAPE, MAAPE).

Table 1
A summary of the MPM-20 model simulations

Parameter	$MAE_{i=1\ldots15}$	$MAAE_{i=1\ldots15}$	$MAPE_{i=1\ldots15}$	$MAAPE_{i=1\ldots15}$
N(rpm)	67	275	0.14	0.61
T_{4C}(°C)	13	56	1.1	2.7
P_{2C}(at)	0.065	0.071	1.7	1.88

The maximum absolute percentage error is at 1.7% for P_{2C} parameter and the maximum percentage absolute error for T_{4C}(°C) is at 2.7% and this shows that the model produces a very accurate dynamic prediction in its all operational states.

4 Intelligent Engine Control Systems

Methods of artificial intelligence increase the quality of control processes. However this quality is conditioned only by careful analysis of the system they are applied to [12, 18, 19]. At low control level (as by control of turbojet engines), we deal mostly with raw data – therefore approaches utilizing pricniples of subsymbolic artificial intelligence will be used in design of intelligent full authority digital engine control (iFADEC). From modeling and selected preliminary control systems design we are aiming mainly at [21, 22]:

- neural networks,
- fuzzy inference systems.

These approaches are to be combined also with traditional control approaches into an adaptive hybrid control algorithm scheme utilizing the concept of situational control [12, 19]. The concept is shown in the framework architecture in Figure 8 with four controllers for different situational states the controlled engine can find itself.

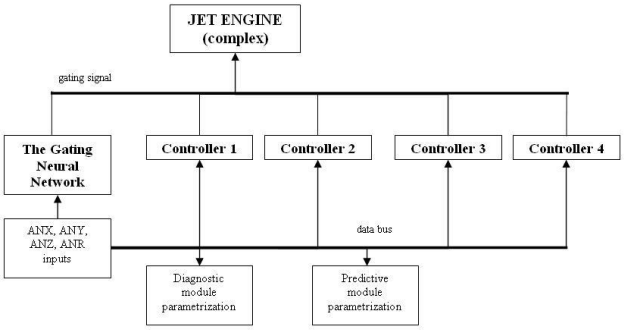

Figure 8

The structure of situational control model implemented in Matlab/Simulink

The basic concept of the situational control system is to decompose all operational states of an engine into time spaced situational frames while every situational frame would have at least one corresponding control algorithm assigned to it. Special attention is aimed at handling of critical areas of operation.

In the concept we propose dynamic (time delayed) neural network in the form of situational classifier with a corresponding set of controllers to handle individual situational frames. In design the concepts of traditional situational control and formatter control of complex systems were used [2,14]. The resulting physical architecture including analyzers of input (X), state (Z), output (Y) and desired (R) parameters is shown in the Figure 9

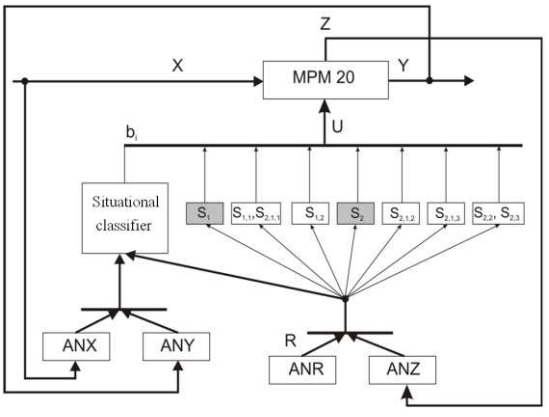

Figure 9

The structure of situational control model implemented in Matlab/Simulink

Blocks designated as $S_{i,j,k}$ represent controllers for different situational frames, where the system is decomposed into three basic frames horizontally and further decomposed into three levels vertically.

The primary situational decomposition of the engine states is shown in Figure 10 [1, 10].

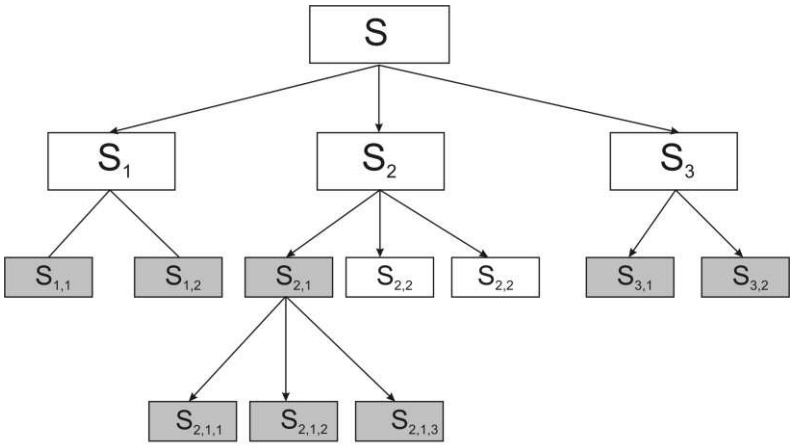

Figure 10
Decomposition of situational frames into a situational graph [10]

The blocks in the figure 10 have the following meaning [1, 10]:

S_1 – startup of the engine:

$S_{1,1}$ –temperature problem, $S_{1,2}$ –pressure $P_{2c\ problem}$

S_2 – steady state of operation:

$S_{2,1}$ – steady atypical state:

$S_{2,1,1}$: low compression, $S_{2,1,2}$ – low fuel flow, $S_{2,1,3}$ – unstable speed,

$S_{2,2}$ – acceleration,

$S_{2,3}$ – deceleration

S_3 – shutdown

$S_{3,1}$ – stall of the engine

$S_{3,2}$ – error by run-down

The grey blocks in Figure 10 represent atypical operational conditions with specialized control algorithms and approaches to handle them.

5 Small Turbojet Engine Diagnostic/Backup System

The small turbojet engine MPM-20 also serves us for testing purposes of redundant backup/diagnostic systems. The designed architecture of such system has been tested for a single engine parameter the speed of the engine. This parameter is crucial as it defines thrust and power output of the engine and is the primary controlled parameter. The main way to measure the speed of the engine is the **optical sensor**, while the other ways are synthetic model values [10, 13]:

- **successive integration dynamic model**,
- **a neural network**.

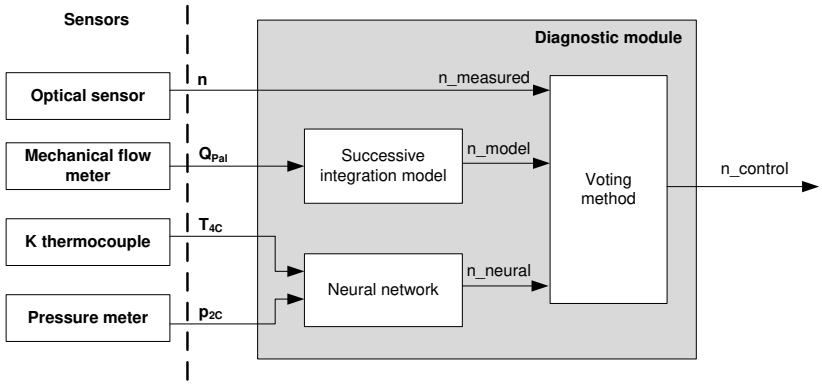

Figure 11
The structure of the diagnostic module

The basic designed architecture of a simple single parameter diagnostic system is shown in the figure 11. Reliability of the model is secured through independence of input parameters while utilizing virtual engine models to compute the speed. There are two basic errors that can occur with the optical sensor [10, 13]:

- **A random value –** caused by electro-magnetic environment disturbance,
- **Sensor failure** – it can be caused by a loss of power, loss of communication channel, loss of reflex area on the compressor blade.

The designed backup/diagnostic system is utilizing adaptive voting majority methods and its principal implementation is shown in Figure 12. The system can exclude faulty speed computation/measurement from its output and can also indicate its own total failure utilizing precise dynamic engine models. The resulting speed of the engine is represented by the average value of all means of speed computation/measurement I_c.

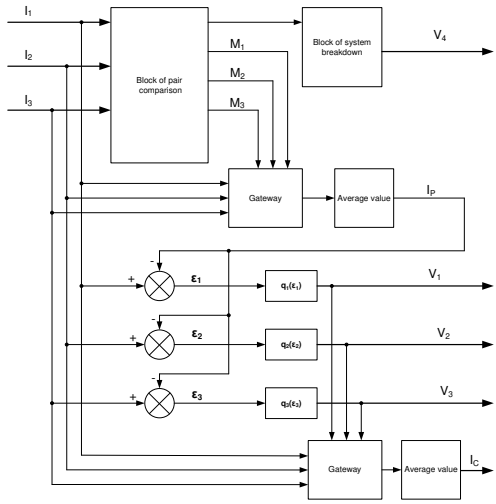

Figure 12
The structure of the diagnostic module

The designed diagnostic/backup system has been experimentally tested with the MPM-20 engine during its operation within running on speed of 43500 RPM. During the test all input had simulated errors; this is shown in Figure 13. During the test even real error of the optical sensor occurred at time of 30 seconds. The output of the diagnostic/backup system however was not influenced and has operated as desired. Further expansion of the system will lead into a highly redundant diagnostic/backup system utilizing the presented concept, where all important engine parameters (temperatures, pressures, fuel flow, thrust) will be mutually backed up, thus creating a highly redundant backup system.

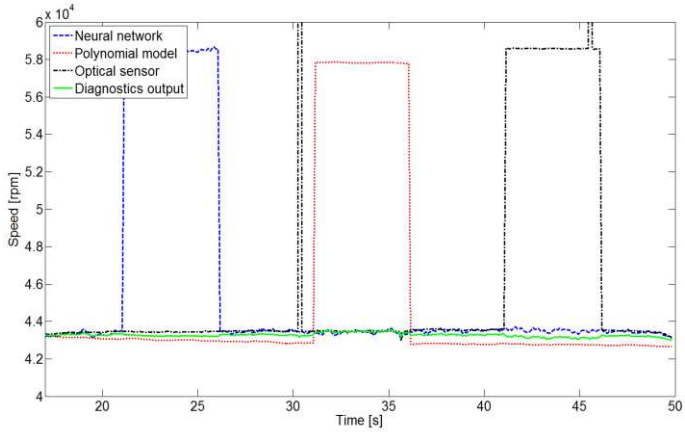

Figure 13
Diagnostic/backup system test results

6 Physical and Mathematical Modeling in the Research of the Efficiency of Technical Systems

A special emphasis has been recently put on evaluation of efficiency of research and object operation in the Laboratory of intelligent control systems of aircraft engines. A methodology for efficiency evaluation is being developed in conditions of the laboratory on the object of a small turbojet engine, whereas the resulting knowledge is generalized for complex technical systems [11]. Efficiency of a complex technical systems is estimated according to characteristics that are used to evaluate its utility parameters. The efficiency is considered one of the characteristic parts of the utility that brings up the physical and economical character. The testing procedure in each phase of efficiency evaluation is always connected to analysis [9]. Simple illustration of this process is depicted in Figure 14 [11].

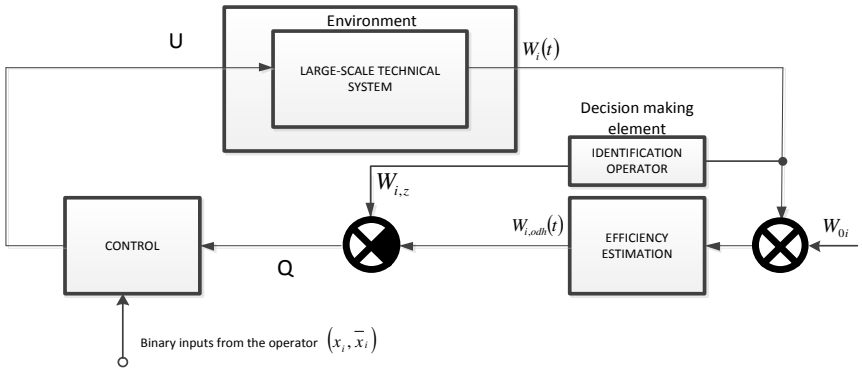

Figure 14
Efficiency estimation using feedback

Description:

W_{0i} - starting value of the efficiency in the i-th phase (time independent),

$W_i(t)$ – real-time value of the efficiency (reached ecciciency in i-th phase),

$W_{i,odh}$ (t) – estimation of efficiency in i-th phase,

$W_{i,Z}$ – requested efficiency value (time independent), after i-th phase,

U – efficiency control.

According to Fig. 14 it is possible to evaluate the output effect, which quantifies reached efficiency in i-th phase, using the following formula:

$$Q_i = 1 - \left(W_{i,Z} - W_{i,odh}\right). \tag{11}$$

However, this formula has only limited effect because it disregards expenses, connected with reaching the requested efficiency. Expenses may be represented by various parameters. Usually they are expressed as required time, required wages, required new knowledge, financial expenses for test evaluation, etc [9]. It is possible to consider expenses as the part of the efficiency function is we consider the general efficiency formula:

$$E = \frac{Q}{S}, \tag{12}$$

where:

E - general efficiency criterion,

Q - output system effect,

S - expenses needed to reach the output effect.

Both methods reflect the iterative character of testing that is carried out according to detailed theoretical planning of each experiment, its methods and expectations. The iterative process of continuous efficiency increase of the experimental identification can be observed in Figure 15.

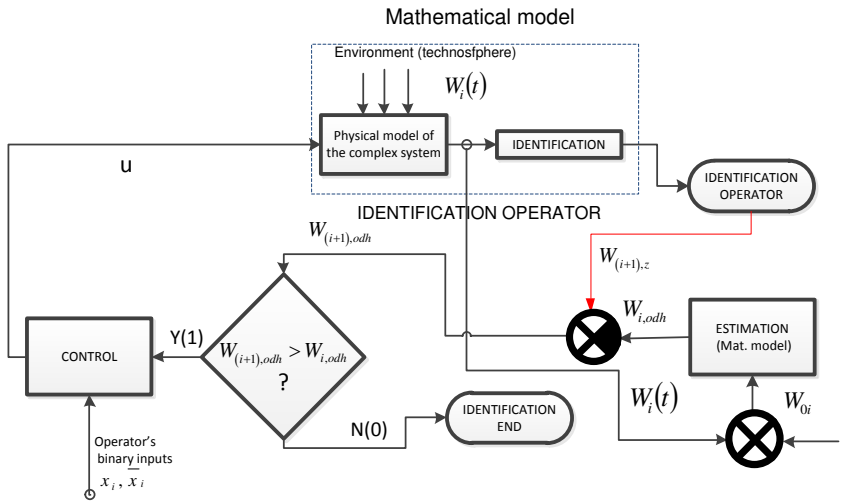

$W_{(i+1),Z}$ – predicted efficiency value (aposterior information is efficiency independent).

Figure 15

Complex system identification process with the possibility of efficiency increase

Conclusions

The article overviewed the main approaches and ideas developed in the Laboratory of intelligent control systems of aircraft engines. The scope of research in the laboratory is aimed at progressive methodologies applicable in modeling, control and diagnostics of jet engines but the ideas have also potential to be generalized for other classes of large scale systems. Obtained results show that application of modern adaptive methodologies can bring new quality, reliability and efficiency of operation of such systems. Research in the laboratory is aimed at modular designs that can utilize different control concepts combining the adaptive and classical approaches combined in such structures.

Acknowledgement

The work presented in this paper was supported by VEGA, Grant Agency of Ministry of Education and Academy of Science of Slovak Republic under Grant No. 1/0298/12 – "*Digital control of complex systems with two degrees of freedom*" and grant No. 1/1117/11 – *"Integration of automatic flight control algorithms with control algorithms of aircraft turbocompressor engines"*. The work presented in this paper was also supported by KEGA under Grant No. 018TUKE-4/2012 – "*Progressive methods of education in the area of control and modeling of complex systems object oriented on aircraft turbo-compressor engines*.

References

[1] Adamčík, F., Bréda R.: *The Determination of Input Parameters for Non-Contact Temperature Measurement of the LTJE*, In: Acta Avionica. Roč. 13, č. 22 (2011), s. 77-80. - ISSN 1335-9479

[2] Beneš, J. (1974), *Teorie systémů (řízení komplexů)(Theory of systems)*, 200 pp. Academia, nakladatelství ČSAV, 1974, Czech. Rep.

[3] Boyce P. Meherwan: Gas Turbine Engineering Handbook, Third Edition, Elsevier 2006, 935 pp., ISBN 0-88415-732-6

[4] Főző, L.(2008). *Use of Mathematical Model of Steady and Nonsteady Operation of MPM20 Turbojet Engine by Design of Anytime Control Algorithms* (in Slovak), Dissertation thesis, Dept. of Cybernetics and AI, Faculty of Electrical Engineerin and Informatics, Technical University of Košice, 144 p., September 2008, Slovakia

[5] Harris, Ch., Hong, X., Gan, Q. (2006) Adaptive Modelling, *Estimation and Fusion from Data*, Springer, ISBN 3-540-42686-8, p. 323, 2006

[6] Jaw C. L., Mattingly D. J.: *Aircraft Engine Controls Design, System Analysis, And Health Monitoring*, American Institute of Aeronautics and Astronautics, 2009, p. 361, ISBN 978-1-60086-705-7

[7] Jonathan S., L., Turso, J., A., Shah, N., Sowers., T., S., Owen, K., A. (2005) *A Demonstration of a Retrofit Architecture for Intelligent Control and Diagnostics of a Turbofan Engine*, NASA/TM -2005-214019, USA

[8] Kulikov G., Thompson A.: *Dynamic Modelling of Gas Turbines Identification, Simulation, Condition Monitoring and Optimal Control*, Springer 2004, 337 p., ISBN 1852337842

[9] Krineckij, E., Aleksandrovskaja: *Letnye ispytancija sistem upravcenija letatelnymi apparatami*, MOSKVA, Mašinostoje 1975, p. 46

[10] Lazar, T., Madarász, L. (Eds.): *Inovatívne výstupy z transformovaného experimentálneho pracoviska s malým prúdovým motorom (Inovative Outputs from the Transformed Experimental Laboratory with a Small Turbojet Engine)*. elfa, s.r.o. Košice, 348 p. ISBN 978-80-8086-170-4 (2011)

[11] Lazar, T., Madarász, L., Gašpar, V.: *Procesná analýza odhadu efektívnosti identifikácie MPM s inteligentným riadením (Process analysis of efficiency estimation of MPM identification with intelligent control)*, elfa s.r.o, ISBN 978-80-8086-200-8, p. 160, 2013

[12] Linke-Diesenger, A. (2008). *Systems of Commercial Turbofan Engines: an Introduction to Systems Functions*, Springer, ISBN 978-3-540-73618-9

[13] Madarász, L., Andoga R., Főző, L., Lazar. T.: *Situational Control, Modeling and Diagnostics of Large Scale Systems*, In: Towards Intelligent Engineering and Information Technology, Rudas I. J., Fodor, J., Kacprzyk, J. (Ed.), p. 153-164., ISBN 978-3-642-03737-5, Springer-Verlag, Berlin.`

[14] Madarász, L.: *Metodika situačného riadenia a jej aplikácie (Methodology of situational control and its applications)*, 212 p. ISBN 80 – 88786 – 66 – 5, Elfa Košice, 1996

[15] Moller, M. F. (1993) *A Scaled Conjugate Gradient Algorithm for Fast Supervised Learning*, Neural Networks, Vol. 6, pp. 525-533, 1993

[16] Považan J (1999): *Konštrukcia matematických modelov leteckých turbokompresorových motorov (Construction of Mathematic models of Aircraft Engines)*, VLA M.R.Š. v Košiciach, ISBN 80-7166-030-2, Slovakia

[17] Ružek, J., Kmoch, P. (1979) *Teorie leteckých motoru I. (Theory of Aircraft Engines)*, 373 pp, 1979, Czech Rep.

[18] Wiseman, M. (2005). *Intelligent Engine Systems*, NASA CR/-2005-213964, USA

[19] Tar, J. K., Rudas, I. J., Kósi, K., Csapó, A., Baranyi, P.: *Cognitive Control Initiative*. 3rd IEEE International Conference on Cognitive Infocommunications. December 2-5, 2012, Košice, Slovakia. pp. 579-584, ISBN 978-1-4673-5185-0

[20] Chebre M., Meroufel A., Bendaha Y.: *Speed Control of Induction Motor Using Genetic Algorithm-based PI Controller*, Acta Polytechnica Hungarica, Vol. 8, No. 6, pp. 141-153, 2011

[21] Precup R.-E., Tomescu M.-L., Petriu E. M., Preitl S., Dragos C.-A.: *Stable Design of a Class of Nonlinear Discrete-Time MIMO Fuzzy Control Systems*, Acta Polytechnica Hungarica, Vol. 9, No. 2, pp. 57-76, 2012

[22] John, S., Pedro J. O.: *Hybrid Feedback Linearization Slip Control for Anti-Lock Braking System*, Acta Polytechnica Hungarica, Vol. 10, No. 1, pp. 81-99, 2013

Robust Controller in the Structure of Lateral Control of Maneuvering Aircraft

Róbert Bréda*, Tobiáš Lazar*, Rudolf Andoga*, Ladislav Madarász**

*Technical university Košice, Faculty of Aeronautics, Department of Avionics, Rampová 7, 04021 Košice, Slovak Republic, robert.breda@tuke.sk, tobias.lazar@tuke.sk, rudolf.andoga@tuke.sk

**Technical university Košice, Faculty of Electrical Engineering and Informatics Department of Cybernetics and Artificial Intelligence Letná 9, 042 00 Košice, Slovak Republic, ladislav.madarasz@tuke.sk

Abstract: Efficiency in the process of aircraft control is expressed as the adaptability of the control system to the changes in the physical properties of the object. As a criterion of efficiency there exists an indicator by which the rules of selecting the best ways of solving control problems are determined. The contribution is describing the method of analyzing, synthetizing the designed parameters of a robust controller for lateral control of aircraft utilizing assisting damping automated devices (ADAD). The design of the controller parameters was done using Matlab program with the demo version of the lateral control of a maneuvering aircraft and the synthesis of the suggested controller is based on applying the H_∞ and μ methods.

Keywords: robust controller; multiplicative uncertainty; singular values; assisting damping and automatic devices (ADAD)

1 Introduction

Controlling the flight of an aircraft represents a process that takes place within a closed circuit, termed as the man - machine - loop, or an automated flight control system. When controlling an aircraft, it is about evaluation of information on the real motion of the aircraft and the subsequently well - organized utilization of selected forces and momenta acting on the aircraft to ensure the required movement of its center of gravity and angular positioning of the aircraft around it.

Currently used methods of aircraft control involves those of PID regulation, robust control and progressive methods of the Fuzzy logic. In the past, PID controllers were used as autopilots, based on simple laws up to the advanced systems of

control further developed into structures with multivariable coefficients in compliance with flight conditions, [13]. Today, advanced systems are used, which enable implementation of more complex laws of control and invariance of preset coefficients in time. When applying robust controllers, aircraft control systems make use of relatively widely used methods of H_∞ and μ synthesis. For example, the control system of the highly maneuverable F - 16 VISTA fighter, where control in the lateral and directional axes is ensured within the internal loop by method of dynamic inversion and the external control loop is made applying the method of μ synthesis. The control system in the longitudinal axis is also divided into the internal loop, H_∞ which is performed at of minimal order and the external loop by method of the μ synthesis, [1]. Methods of analysis and synthesis enable design of the parameters of a robust controller for lateral motion of a maneuvering aircraft, with the H_∞ and μ synthesis methods applied in the Matlab program environment.

2 Robust Control of Multi - Dimensional Systems

The theory of robust control of dynamic systems is typical for modeling, analysis of the object features when controller synthesis is to be done with an incomplete and imprecise mathematical description of the process. The problem of robust stabilization can be solved by optimal control methods such as based on the minimization of norms of transfer functions of the feedback system. The notion of designing a robust controller will be understood as a procedure and resulting in the design of a controller, which ensures robust features of the closed control loop at prescribed magnitudes of uncertainties, [3, 4]. Multidimensional MIMO systems by their specific features belong to the class of hard-to-stabilize systems, using the feedback from the output variable. Problems in the design of robust controllers consist in the interactional links existing between the separate subsystems of the multidimensional system and the one of „gains“ of the multidimensional system changing between the minimum and the maximum value of the singular value of the system matrix. Multidimensional systems are substantially sensitive to the changes in the parameters than the uni - dimensional SISO systems, and therefore the design of controllers stabilizing the process or the design of robust controllers is rather difficult. Any kind of precise model of the system is only approximating the behavior of the real system. The primary role of the feedback is to eliminate the effect of uncertainty, indefiniteness, as well as to obtain the required quality in control as defined by the appropriate norms. The term „robust“ is considered for such calculation procedures, which at small changes, or errors in the input data guarantee even the proportionately smallest variations in the output results.

Robustness is a measure to which a system is tolerant to certain limits to structured or non - structured uncertainties. Non - structured uncertainty is characterized as additional dynamics, which is not part of the model and can be of additive or even multiplicative in nature.

Real system is represented by $G(s)$, nominal system by $G_0(s)$, Δ_a stands for additive uncertainties – unknown information on the true value and phase of perturbation and Δ_m for multiplicative uncertainty. For additive uncertainty it holds:

$$G(s) = G_0(s) + \Delta_a(s) \tag{1}$$

For multiplicative uncertainty at the system input it holds:

$$G(s) = G_0(s)\left[I + \Delta_m(s)\right] \tag{2}$$

For multiplicative uncertainty at the system output it holds:

$$G(s) = \left[I + \Delta_m(s)\right]G_0(s) \tag{3}$$

Structured uncertainty is represented by the uncertainty of the parameter or the set of system parameters, and it also may be of additive or multiplicative in nature. Let l be a parameter of a real system, and l_0 is the nominal parameter, then for the separate uncertainty it holds:

$$l = l_0 + \Delta_a \tag{4}$$

$$l = l_0\left(1 + \Delta_m\right) \tag{5}$$

2.1 Method of Structured Singular Values

The analysis of structured singular values (μ), based on the „small gain theorem“, is used to evaluate the robustness of the system. In order to find the optimal controller of the aircraft control system, it might be necessary to make use the very methods of structured singular values $(\mu\ synthesis)$, [1]. The purpose of the μ synthesis is to find the controller, which minimizes the upper limit of structured singular values, see Fig. 1.

$P(s)$ is the object of control, $K(s)$ controller, w_0 input uncertainty, w_i output multiplicative function that ensures classification of the uncertainty, $\Delta(s)$ parameter of uncertainty.

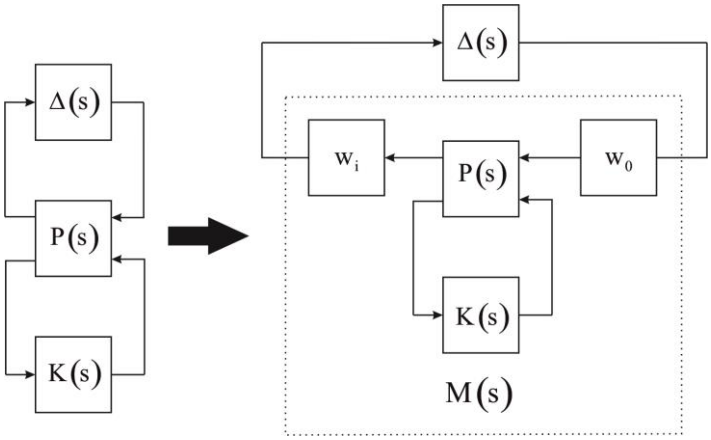

Figure 1
Block diagram of the method of structured singular values

Equivalent representation of the block of uncertainty is:

$\Delta(s) = w_0 \Delta(s) w_i$, where for the norm of uncertainty it holds that $\|\Delta(s)\|_\infty \leq 1$

The theory of small gains guarantees that if $M(s)$ and $\Delta(s)$ are stable, then the uncertain system will remain stable, if for all the frequencies it holds that $0 \leq \omega \leq \infty$.

$\bar{\sigma}(M(j\omega)\Delta(j\omega)) \leq 1$, which can be expressed as $\|M(s)\Delta(s)\|_\infty \leq 1$.

The inequality can be written as $\|M(s)\Delta(s)\|_\infty \leq \|M(s)\|_\infty \|\Delta(s)\|_\infty$ because it is known that $\|\Delta(s)\|_\infty \leq 1$

Then, the satisfactory condition to the stability is: $\|M(s)\|_\infty \leq 1$

To design the controller, it is necessary to define the uncertainties, which at the design of the aircraft control system and can be divided as uncertainties in:

- state matrix of the aircraft linear model,
- efficiency of operating elements – actuators,
- in - flight measurement of parameters,
- neglecting tensile design of the aircraft.

Constraints such as the dynamics of operating elements, noise and filters used for processing of the input signals coming from sensors may also be included in the model.

2.2 The H_∞ Method

Method H_∞ is aimed to find the controller with $\boldsymbol{y}(t)$ inputs and $\boldsymbol{u}(t)$ outputs, i.e. the one, which eliminates transfer functions between $\boldsymbol{w}(t)$ and $\boldsymbol{z}(t)$ as shown in Figure 2.

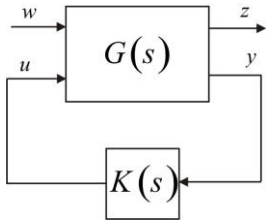

Figure 2
Block diagram of the H_∞ method

The linear system on which the method is applied can be generally described by the equation as:

$$\begin{aligned}
\dot{\boldsymbol{x}}(t) &= \boldsymbol{A}\boldsymbol{x}(t) + \boldsymbol{B}_1\boldsymbol{w}(t) + \boldsymbol{B}_2\boldsymbol{u}(t), \\
\boldsymbol{z}(t) &= \boldsymbol{C}_1\boldsymbol{x}(t) + \boldsymbol{D}_{11}\boldsymbol{w}(t) + \boldsymbol{D}_{12}\boldsymbol{u}(t), \\
\boldsymbol{y}(t) &= \boldsymbol{C}_2\boldsymbol{x}(t) + \boldsymbol{D}_{21}\boldsymbol{w}(t) + \boldsymbol{D}_{22}\boldsymbol{u}(t).
\end{aligned} \tag{6}$$

where:

$\boldsymbol{x}(t)$ is an n - dimensional state vector of the system, $\boldsymbol{w}(t)$ m_1 - dimensional vector of faulty variables, $\boldsymbol{u}(t)$ m_2 - dimensional vector of input variables, $\boldsymbol{z}(t)$ is the p_1 - dimensional vector of variables magnitudes the magnitude of which must be minimized and $\boldsymbol{y}(t)$ is the p_2 - dimensional vector of output or the measured variables. Prior to the synthesis of the controller, it is necessary to select in advance the weight functions, and also to measure the important signals, which affect the system on principle. Having extended the system by weight functions and constants, one can proceed to the design of the controller as it.

Norm H_∞ for the real matrix $T(x)$ is defined:

$$\|T\|_\infty = \sup_{\mathrm{Re}(s)>0} \|T(s)\| = \sup_{\omega} \|T(j\omega)\| = \sup_{\omega} \bar{\sigma}\left[T(j\omega)\right] \tag{7}$$

where:

$\bar{\sigma}\left[T(j\omega)\right]$ denotes the largest singular value of $T(j\omega)$ depending on the frequency.

To find the controller based on the methods as above, one can make use of the „Robust Control Toolbox“ program of the Matlab environment, which enables generating a model in compliance with the equation, defining the uncertain state area, synthesis of the controller applying the H_∞ or the μ method the one of synthesis and also reduction of the order of controller in case when it becomes apparent that the controller obtained is significantly slowing down the time of simulation [7].

3 Non - Linear Mathematical Model of the Aircraft Motion

Generally, a non-linear model of an aircraft consists of: model of dynamics for the determined class of aircraft in the environment, model of the power plant, model of the dynamics of operating elements, model of the atmosphere, shown in Figure 3 [2]. When modeling aircraft dynamics, the following assumptions are adopted:

- aircraft structure is perfectly stiff, eliminating the aero - elastic vibrations of the structure during flight,
- aircraft weight with momenta of gyro/inertia will remain constant in the process of modeling, not assuming transfer of fuel between tanks when in flight
- standard atmosphere as by ISA.

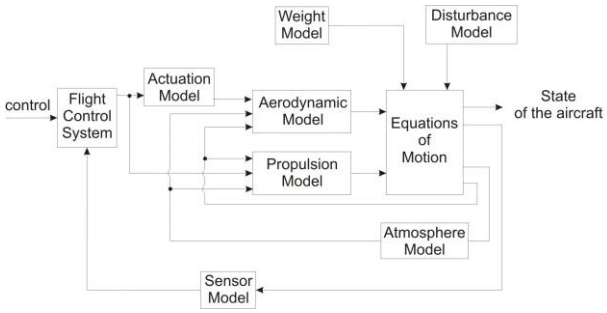

Figure 3
Block diagram of a non - linear model of an aircraft

3.1 Lateral Movement Equations for the Aircraft

Environmental influence causes the movement equations of aircraft to become non - linear and their coefficients variable. Solution of such equations and their practical realization in modelling is source of substantial difficulties. In order to overcome them, the method of linearization is employed, which by selecting an operational state shows the outputs within the assumed linearization limits. It means that the process of the dynamic flight is decomposed into increments related to the referential points, which represents the starting point for determining further movement of the aircraft. Then the linear equations of motion for lateral and directional motions of the aircraft comprise the equations for force Y, momenta L and N, [8]. For the lateral motion of the aircraft, equations of motion can be defined, which comprise three dynamical and two kinematical equations.

$$\begin{aligned} m\dot{v} - \dot{Y}_v v - \left(\dot{Y}_p + mW_s\right) p - \left(\dot{Y}_r - mU_s\right) r - mg\phi\cos\Theta_s - mg\psi\sin\Theta &= \dot{Y}_\xi \xi + \dot{Y}_\zeta \zeta, \\ -\dot{L}_v v + I_{xx}\dot{p} - \dot{L}_p p - I_{xz}\dot{r} - \dot{L}_r r &= \dot{L}_\xi \xi + \dot{L}_\zeta \zeta, \\ -\dot{N}_v v - I_{xz}\dot{p} - \dot{N}_p p + I_{zz}\dot{r} - \dot{N}_r r &= \dot{N}_\xi \xi + \dot{N}_\zeta \zeta, \\ \dot{\phi} &= p, \\ \dot{\psi} &= r. \end{aligned} \quad (8)$$

The lateral motion of the aircraft is described by the system of five linear differential equations of the first order with five unknown variables v, p, r, ψ, ϕ. The equations are referenced to the body frame of the aircraft, see Fig. 4 [10]. Linear differential equations for the lateral motion of the aircraft are written as state-space equations:

$$\begin{pmatrix} \dot{v} \\ \dot{p} \\ \dot{r} \\ \dot{\phi} \\ \dot{\psi} \end{pmatrix} = \begin{pmatrix} y_v & y_p & y_r & y_\phi & y_\psi \\ l_v & l_p & l_r & l_\phi & l_\psi \\ n_v & n_p & n_r & n_\phi & n_\psi \\ 0 & 1 & 0 & 0 & 0 \\ 0 & 0 & 1 & 0 & 0 \end{pmatrix} \begin{pmatrix} v \\ p \\ r \\ \phi \\ \psi \end{pmatrix} + \begin{pmatrix} y_\xi & y_\zeta \\ l_\xi & l_\zeta \\ n_\xi & n_\zeta \\ 0 & 0 \\ 0 & 0 \end{pmatrix} \begin{pmatrix} \xi \\ \zeta \end{pmatrix} \quad (9)$$

$$\boldsymbol{y}(t) = \boldsymbol{I}\boldsymbol{x}(t) = \begin{pmatrix} 1 & 0 & 0 & 0 & 0 \\ 0 & 1 & 0 & 0 & 0 \\ 0 & 0 & 1 & 0 & 0 \\ 0 & 0 & 0 & 1 & 0 \\ 0 & 0 & 0 & 0 & 1 \end{pmatrix} \begin{pmatrix} v \\ p \\ r \\ \phi \\ \psi \end{pmatrix} \quad (10)$$

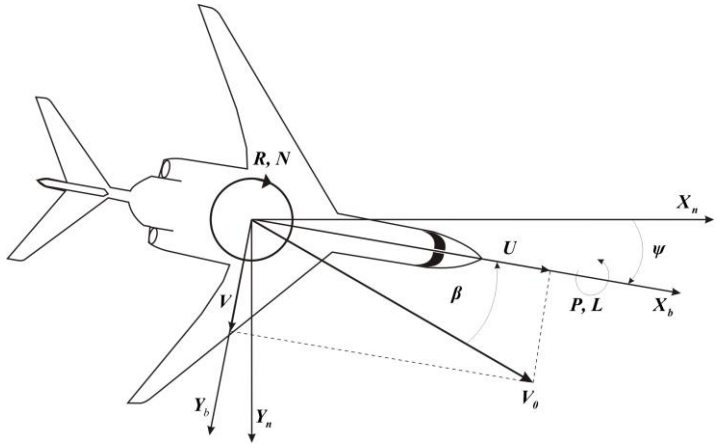

Figure 4
Lateral motion of the aircraft in coordinate systems

Dynamics of the aircraft lateral motion is characterized in damping mode - in pitching and spiral motions. Spiral motion has a great time constant, can be of mildly divergent. It is characterized by changes in the angles of banking and headings at small changes in directional movement. The damping - pitching motion is rapid and stable and describes the aircraft response to the lateral deflection of the control stick. Dutch Roll is an oscillating, poorly attenuated motion describing the aircraft response onto deflecting the pedals of directional control. The nature of the longitudinal relaxation and lateral fluctuation is unpleasant for the pilot, as it requires constant application of the means of aircraft control. Assesment of characteristic variables of oscillations and fluctiations helps to evaluate the quality of responsiveness and stability of aircraft motion which results from pilot's control actions. The frequency of oscillations and fluctuations is related to flight regime, in which the speed, altitude, acceleration multiples and the Mach number are determinant for its stability and controllability [12].

Table 1
Requirement for the value of damping by rapid movement, Dutch Roll

Level	$min\ \zeta_d$	$\min\ \zeta_d\omega_d\,(rad/s)$	$\min\omega_d\,(rad/s)$
1	*0.4*	*0.4*	*1.0*
2	*0.02*	*0.05*	*0.4*
3	0	− − −	*0.4*

Controllability of highly maneuverable aircraft is ensured by assisting damping and automatic devices (ADAD) the tasks of which is, following pilot action, to shorten, via the feedback action of the control surfaces, the time of tion from the original position to the next one without excessive motions. They all support

efficiency of performing the manoeuver at the prescribed value for flight safety and aircraft structure. The ADAD functions are ensured via measuring aircraft position and motion at a prescribed dynamics.

3.2 Design of a Robust Controller for Pilot - controlled Landing by the Directional Control of the Aircraft

The presented methods of analysis and synthesis help determine the parameter of the controller illustrated in Fig. 5 with a block K for the lateral motion of the aircraft. Input variables of the controller are the actual parameters of aircraft position with reference to the directional axis introduced by the pilot with the control stick handle and pedals [6]. Aircraft parameters measured by sensors:

- roll rate p, around the longitudinal axis X,
- yaw rate r, around the vertical axis Z,
- normal acceleration Nz, along the vertical axis Z,
- sideslip angle β.

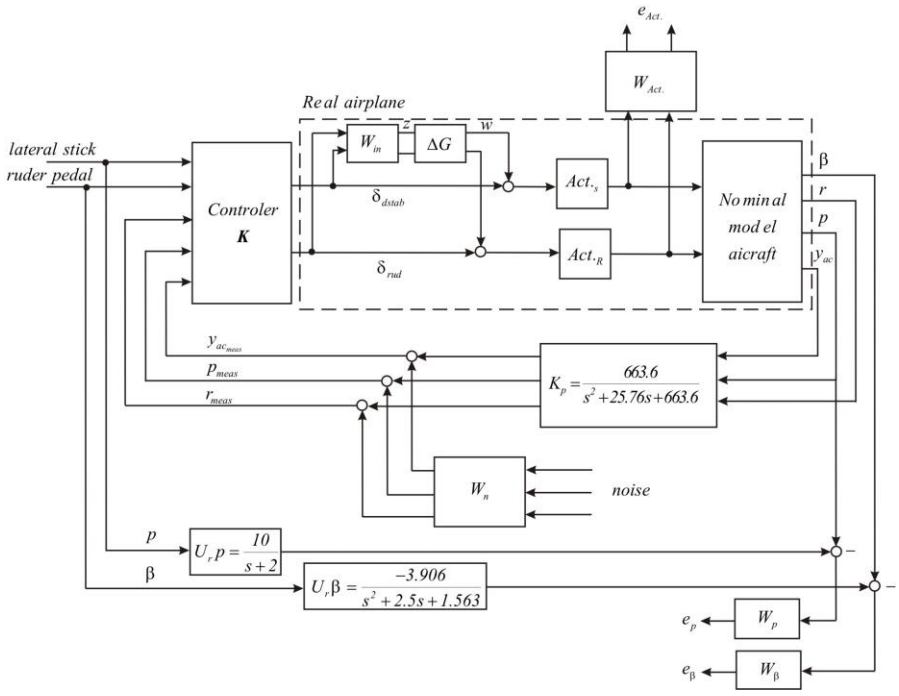

Figure 5
Integration of the robust controller in the structure of lateral movement control of the maneuvering aircraft

Input data are standing for angle of attack $\alpha = 10,5^{\circ}$ and landing speed $v = 140\ knots$. The aircraft control circuit features shaping filters, where the required shape of speed for roll rate p caused by the pilot is adjusted by the filter with transfer function: $U_r p = \frac{10}{s+2}$. Quality of lateral control is increased by a filter of second order adjusted by transfer function: $U_r \beta = \frac{-3.906}{s^2 + 2.5s + 1.563}$. Smooth shape of transient characteristics of time responses without excessive oscillations is precondition to qualitatively sound responses of the aircraft, its controllability, without reducing energy potential. Aircraft reactions measured by sensors are: roll rate and yaw rate $p,\ r$ and lateral acceleration $y\ a_c$.

Output signals of sensors are passing pass through a three - channel shaper - a filter with transfer function $K_p = \frac{663.6}{s^2 + 25.76s + 663.6}$, $K_p = K_r = K_{y_{-ac}}$ and sums of positive element are fed onto the input of the robust controller K, which makes up the assisting attenuating automatic device (ADAD). The ADAD functions are ensured via measuring the position of aircraft with a prescribed dynamics.

Servo elements of the ADAD are the rudder actuators with prescribed data:

- stabilizer deflection: $\pm 20^{\circ}$ degrees, motion speed: $\pm 90^{\circ}/sec$,
- rudder deflection: $\pm 30^{\circ}$ degrees, motion speed: $\pm 125^{\circ}/sec$.

Measurement of aircraft movement around the $X,\ Z$ axes and in the direction of Z axis is performed by sensors of angular velocities /gyro/ and accelerations with prescribed features. Noisy signals of normal accelerations and angular velocities are separated from the useful by filters, which also ensure shaping for further use. Input frequency measured by the sensor at aircraft turn is $f = 12,5\ Hz$, sensor dynamics of $f = 25\ Hz$, damping $\zeta = 0,7$. Flight of the aircraft in the direction is influence by natural fluctuation at a frequency of $f = 4,1\ Hz$.

3.3 Determining the Weight Functions of the Controller

Algorithms of robust control minimize action of the feed-back loop by reducing its gain by the frequency of aircraft fluctuation $H_{\infty_{nominal}}$. To determine the true frequency of fluctuation, weight functions are used, when the pulses to obtain weight responses on the aircraft are generated by interceptors, operated by pilot´s control stick handle until the aircraft reaction is achieved in the form of weight function $p,\ r, y_{a_c}$, the signals of which enter the joint filter - the shaper. The numeric values of the filters and models have been taken from [7].

Additive noises are eliminated by another joint filter-shaper, which is synthetized by setting up a diagonal matrix of the known values of active elements (interceptor, rudder, angular velocities, positions) [7]:

$$Wact = diag\left(\left[1/90, 1/20, 1/125, 1/30\right]\right) = diag\left(\left[0.0111, 0.5, 0.008, 0.0333\right]\right) \qquad (11)$$

Of the matrix mentioned, the transfer functions are formulated, which are equations of shaping filters of the upper - values marked as Wn in Fig. 6, which combines filters $Wn_1 = 0.025$, $Wn_2 = \frac{0.0125s + 0.0125}{s + 100}$, $Wn_3 = 0.025$ characteristics of the spectral performance function are illustrated in Fig. 6.

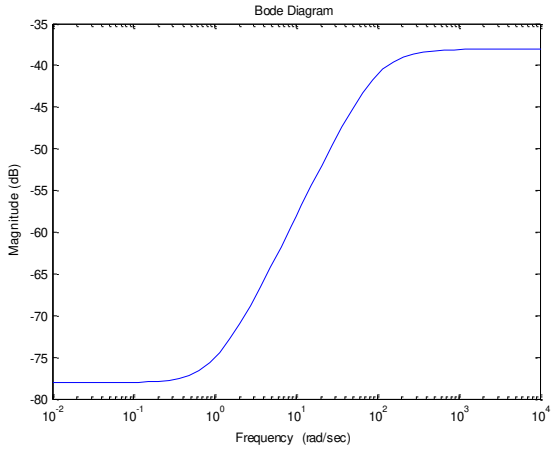

Figure 6
Amplitude frequency characteristics of the shaping filter

Required quality of controlling an aircraft with a control handle and pedals is achieved only when the difference between the required and actual value s is minimized, which is a feedback signal. The Wp filter shaper, which narrows the noise band down to $5\,\%$ difference with transfer function (Fig. 7, Fig. 8), Zero/Pole placement of the filters (12, 13) shows normal displacement in the negative part of the complex plane with conjugated complex roots with negative real parts:

$$W_p = \frac{0.05s^4 + 2.9s^3 + 105.9s^2 + 6.17s + 0.16}{s^4 + 9.19s^3 + 30.8s^2 + 18.83s + 3.95} \qquad (12)$$

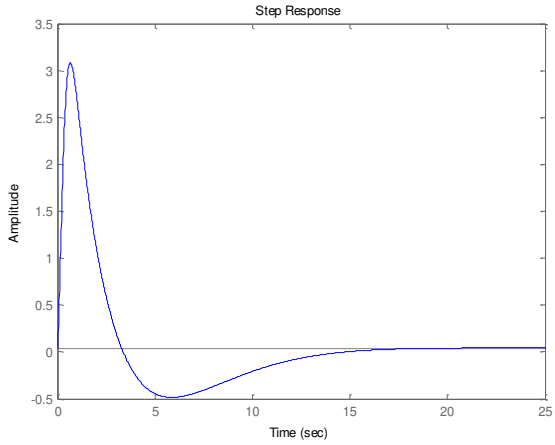

Figure 7
Step response of the Wp differential filter

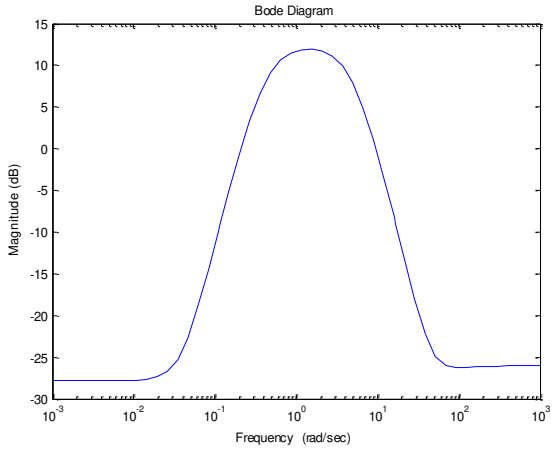

Figure 8
Amplitude frequency characteristics of the Wp differential filter

Directional control of aircraft is of higher quality, which is estimated by the multiple of 2, by which the filtration band is extended (Fig. 9). Then: $W\beta = 2 \cdot Wp$.

$$W_\beta = \frac{0.1s^4 + 5.8s^3 + 211.9s^2 + 12.34s + 0.32}{s^4 + 9.19s^3 + 30.8s^2 + 18.83s + 3.95} \tag{13}$$

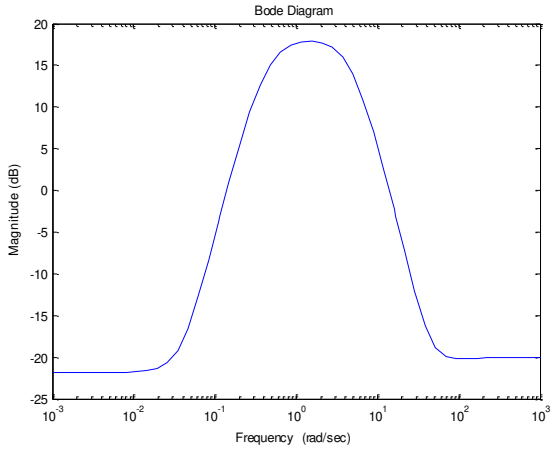

Figure 9
Amplitude frequency characteristics of the $W\beta$ differential filter

Weight functions of $Wact$, Wn, Wp, $W\beta$ are closing the circuit between external inputs and weight functions.

3.4 State Model of an Aircraft in Lateral Motion

Pilot exercises control of the aircraft by means of control stick handle and pedals, when the controlled inputs are: differential spoilers of lift (interceptors) marked as differential stabilizer deflection $\delta_{int}\left[deg\ rees\right]$, rudder deflection marked as $\delta_{rud}\left[deg\ rees\right]$.

The three outputs measured are: roll rate $p\left(deg\ rees\ per\ sec\ ond\right)$, yaw rate $r\left(deg\ rees\ per\ sec\ ond\right)$, lateral acceleration $y_{ac}\ \left(g\right)$ and computed outputs: sideslip angle β, bank angle $\phi\left(deg\ rees\right)$.

State variables are contained in the relation:

$$\begin{aligned}\dot{\boldsymbol{x}}\left(t\right)&=\boldsymbol{A}\boldsymbol{x}\left(t\right)+\boldsymbol{B}\boldsymbol{u}\left(t\right),\\ \boldsymbol{y}\left(t\right)&=\boldsymbol{C}\boldsymbol{x}\left(t\right).\end{aligned}\tag{14}$$

where, for the nominal model of the maneuvering aircraft (numerical values taken from [7]) can be set as:

$$\begin{pmatrix} \dot{v} \\ \dot{r} \\ \dot{p} \\ \dot{\phi} \\ \hline \beta \\ p \\ r \\ y_{ac} \end{pmatrix} = \left[\begin{array}{c|c} A & B \\ \hline C & D \end{array}\right] \begin{bmatrix} v \\ r \\ p \\ \phi \\ \hline \delta_{differ.} \\ \delta_{rud.} \end{bmatrix} \tag{15}$$

$$\left[\begin{array}{c|c} A & B \\ \hline C & D \end{array}\right] = \left[\begin{array}{cccc|cc} -0.116 & -227.3 & 43.02 & 31.63 & 0.062 & 0.101 \\ 0.003 & -0.26 & -0.14 & 0 & -0.005 & -0.011 \\ -0.021 & 0.67 & -1.37 & 0 & -0.047 & 0.004 \\ 0 & 0.19 & 1 & 0 & 0 & 0 \\ \hline 0.247 & 0 & 0 & 0 & 0 & 0 \\ 0 & 0 & 57.3 & 0 & 0 & 0 \\ 0 & 57.3 & 0 & 0 & 0 & 0 \\ -0.003 & -0.008 & 0.05 & 0 & 0.0029 & 0.002 \end{array}\right] \tag{16}$$

For lateral motion of the aircraft as a response to the aileron deflections, we get the following transfer functions including actuator dynamics models and are simulated in Figure 10 [7]:

$$\frac{v(s)}{\xi(s)} = \frac{0.01536s^3 - 0.1759s^2 - 0.1541s - 0.006312}{s^4 + 1.74s^3 + 2.151s^2 + 1.762s + 0.004} \tag{17}$$

$$\frac{r(s)}{\xi(s)} = \frac{-2.674s^3 - 1.28s^2 - 3.173s + 0.004062}{s^4 + 1.74s^3 + 2.151s^2 + 1.762s + 0.004} \tag{18}$$

$$\frac{p(s)}{\xi(s)} = \frac{-0.3009s^3 - 0.0491s^2 - 0.5575s - 0.02192}{s^4 + 1.74s^3 + 2.151s^2 + 1.762s + 0.004} \tag{19}$$

$$\frac{\phi(s)}{\xi(s)} = \frac{0.0028s^4 + 0.0025s^3 + 0.00708s^2 + 0.00409s + 0.00009}{s^4 + 1.74s^3 + 2.151s^2 + 1.762s + 0.004} \tag{20}$$

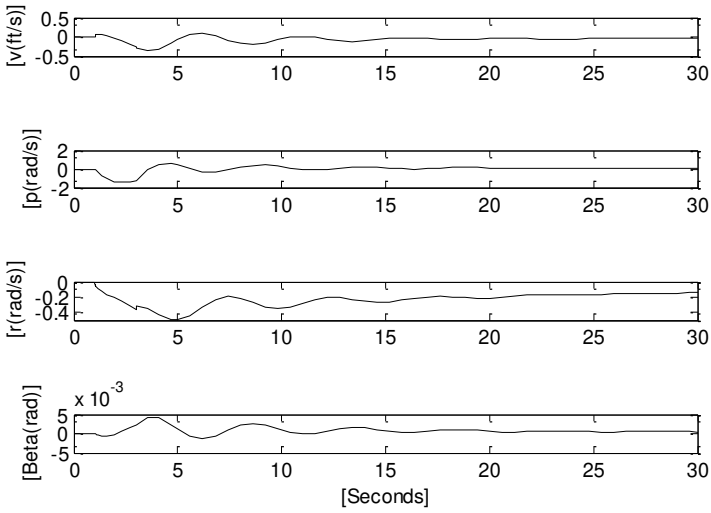

Figure 10
Nominal aircraft response to 1° 2s aileron pulse input

Lateral motion of aircraft as a response to the rudder deflection is described by the following transfer functions including actuator dynamics models and are simulated in Figure 11 [7]:

$$\frac{v(s)}{\zeta(s)} = \frac{0.025s^3 + 0.708s^2 + 0.830s + 0.0038}{s^4 + 1.74s^3 + 2.151s^2 + 1.762s + 0.004} \tag{21}$$

$$\frac{r(s)}{\zeta(s)} = \frac{0.208s^3 - 0.475s^2 - 3.026s + 0.0039}{s^4 + 1.74s^3 + 2.151s^2 + 1.762s + 0.004}$$

$$\frac{p(s)}{\zeta(s)} = \frac{-0.64s^3 - 0.9661s^2 - 0.626s - 0.212}{s^4 + 1.74s^3 + 2.151s^2 + 1.762s + 0.004} \tag{22}$$

$$\frac{\phi(s)}{\zeta(s)} = \frac{0.002s^4 + 0.003s^3 - 0.0035s^2 - 0.008s + 0.00005}{s^4 + 1.74s^3 + 2.151s^2 + 1.762s + 0.004} \tag{23}$$

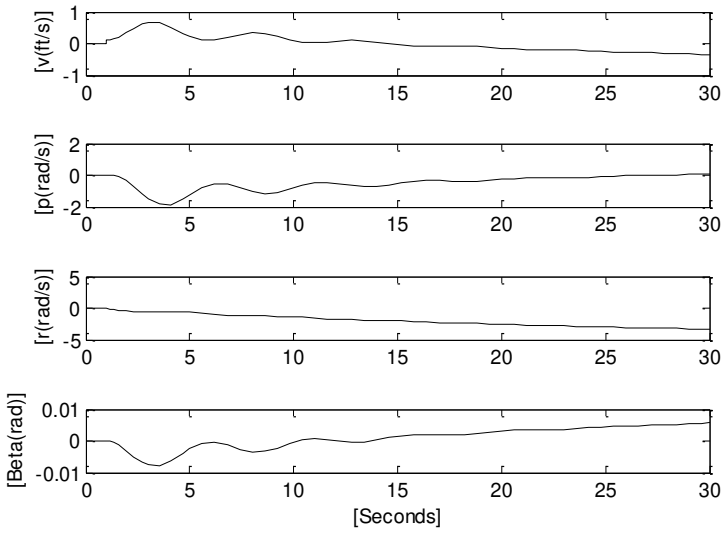

Figure 11
Nominal aircraft response to 1° rudder step input

The given model is further expanded by actuators A_{int}, A_{rud} with their respective transfer functions modeling system's dynamics with two transfer functions that are identical for rudder and interceptor:

$$A_{int_1} = \frac{25s}{s+25},\ A_{int_2} = \frac{25}{s+25},\ A_{int} = A_{rud} \tag{24}$$

Step responses of actuators representing the servo system of the rudder and interceptor drive are shown in Figure 12.

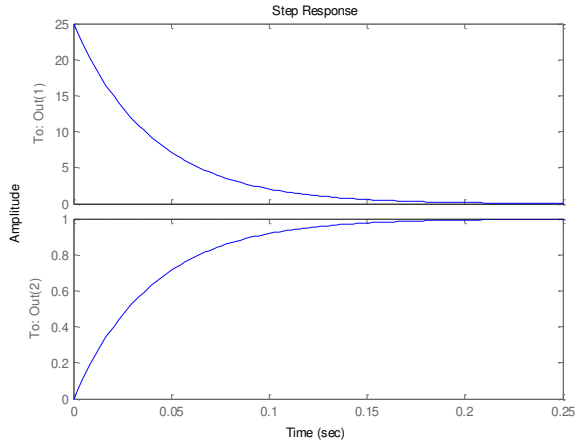

Figure 12
Step response of the actuators of the tail unit

3.5 Simulation Model Including Errors

Nominal model of the maneuvering aircraft is approximation from its real characteristics. Errors resulting from the difference are perceived by us as insensitivity, which is modeled by the product of aircraft uncertainties W_{ne} and the first frequency ΔG, which is the output of the weight filter: $W_{ne} \cdot G$.

The highest frequency of the weight filter W_n is carrying the uncertainty in aircraft control. Frequencies, which differentiate the model from the frequency of the signal of flight dynamics are generated by filters with transfer functions: $W_1 = \frac{2s+8}{s+160}$, $W_2 = \frac{1.5s+30}{s+200}$, [9, 11]. Error of the maneuvering aircraft model is expressed by frequency as in Fig. 13.

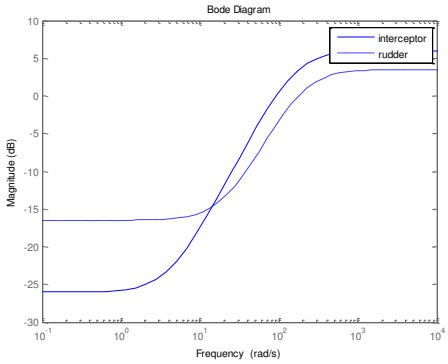

Figure 13
Error of the model of maneuvering aircraft dependant on flight dynamics expressed in frequency characteristics for rudder and interceptor

Weight filters W_{ne}, ΔG along with the acuators A_{int}, A_{rud} are bringing the simulation model closer to real aircraft characteristics.

3.6 Synthetic Model of a Maneuvering Aircraft

The synthetic model is formed by a complex scheme of filter transfer functions and actuators in MATLAB environemnt executed with "sysic" command. The main object of this analysis is dynamic behavior of the synthetic aircraft model with influence of errors on outer parameters of stick/pedal control shaping the ΔG. The signal has been processed by application of the MONTE CARLO method. As an example, the differential interceptor circuit was used with the uncertainty of weight W_1 with *5%* error, where the *100%* error corresponds to angular speed of *93 rad/sec.* The analysis is realized in the frequency area with application of Bode method and is done with 10 different noise signals which were selected from the performance spectrum of noises. Results representing all 10 different noise signals are shown in Figure 14. Figure 15 shows step response and frequency analysis concentrating on a single noise.

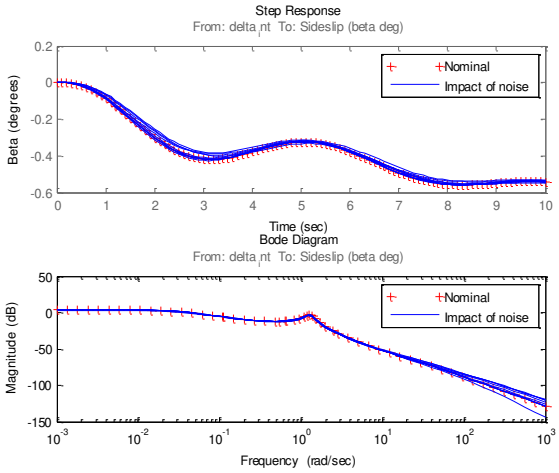

Figure 14

Analysis of 10 different applied noise samples in time domain (step response) and frequency domain (Bode plot)

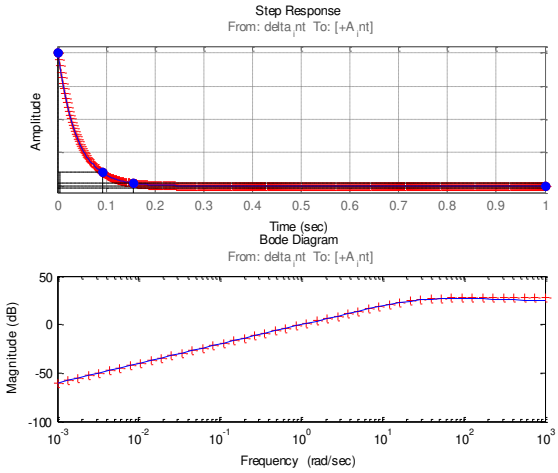

Figure 15

Analysis of the first noise sample in the time and frequency domain selected from the graph of the performance spectrum of noises of the differential interceptor circuit

3.7 Simulation Synthesis of the Robust Controller and the Lateral Control of Aircraft

The design is aimed at such a kind of robust controller, which will be sensitive to the errors being higher in value than the width of insensitiveness W_{ne}. In this process the 'sysic' command is used, which enables solution of the problem assuming higher number of outputs than inputs. The approximate status model of the controller generates the F14IC command, [6]. The closed feedback is completing the ADAD, which increases the quality of control. Further steps minimize the closed circuit of the H_∞ controller for controlling the nominal model of the maneuvering aircraft with the number of measurement sites at 5 and two control circuits. Using the 'hinfsyn' command helps calculate the controller, and on the command of 'kinf' the controller is adjusting the gain of the feedback. The size of the signal is somewhere between 0.67 < 1, in accordance with the model dynamics. By the method of μ - synthesis, we determine the robust circuit, through which the modeled errors or ΔG uncertainty are lead. Using the 'dksyn' command, the mentioned synthesis is performed; the width of the frequency band can be illustrated by using the 'dkitopts' command.

In this case, we compare the H_∞ robust controller and with the use of frequencies of feedback signals, their gain is set in a way to conform to each feedback.

By analyzing the sample of the frequency response from the band of feedback uncertainty, the uncertainty of the frequency response is created, [5]. The following figure (Fig. 16) shows obtained gains by both methods comparing the nominal plant and worst case scenario.

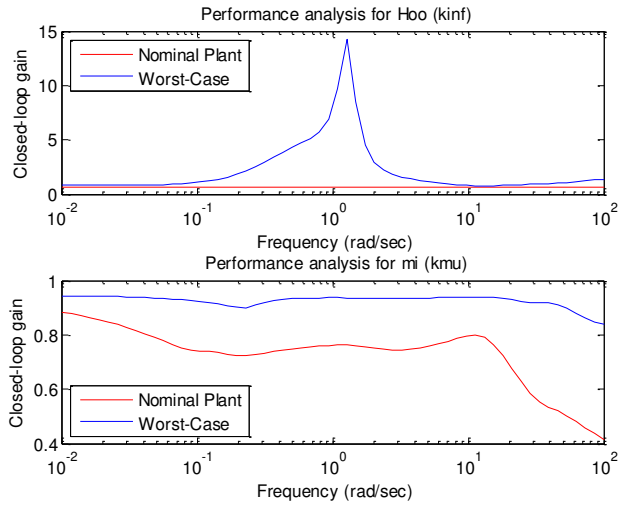

Figure 16
Comparing frequencies for amplification of the feedback for the designed types of controllers

3.8 Time Domains Validation of the Robust Controller

The test of the μ controller in time domain is done by comparison of its response on typical signal (Fig. 17). Three different models were tested – an ideal model, a nominal model with actuators, and disturbed model with actuators and disturbed dynamics by noise.

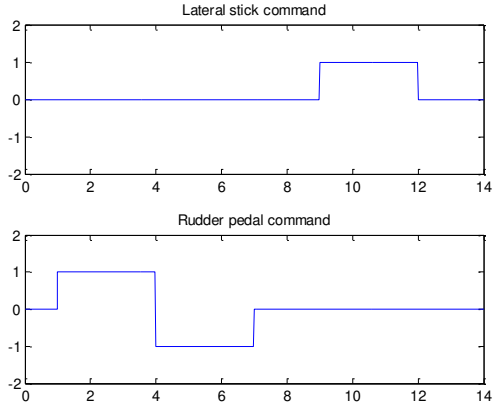

Figure 17
Input type signal for lateral control of aircraft

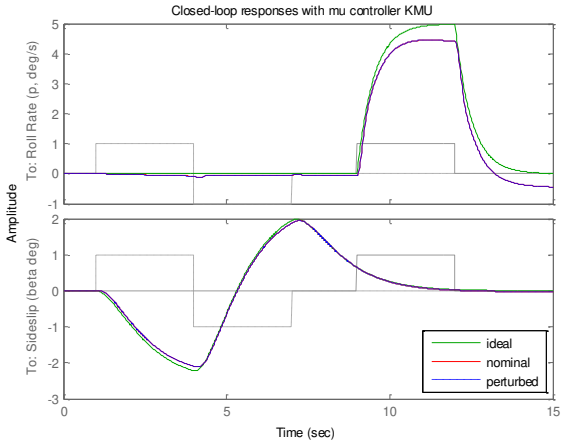

Figure 18

Comparing the response to the control action of the pilot from the closed circuit with the designed controller

Noise frequency was selected that produces worst aircraft behavior was selected and tested. As it is shown in Figure 18, the disturbed model with designed robust controller shows appropriate behavior with error not exceeding the value of 0.024 rad/sec.

Conclusions

ADAD systems, which are damping relaxation oscillations, are used to attenuate oscillation of aircraft in the circuit of rudder, where current aircraft, especially at medium altitudes are known for insufficient damping. When flying at large angles of attack, in landing mode, the effect is very small. It results from aerodynamic laws that the oscillation of aircraft in heading generates oscillations in the circuit of pitching, which is known for very high amplitudes. The value of the artificial attenuation constant introduced by the damper into the rudder circuit must be higher. Increase in the attenuation in the rudder circuit is positively reflected in the pitching circuit of the aircraft. Increasing the value of proportional damping of relaxation frequencies brings positive effects for aircraft flying in a turbulent atmosphere, in which the attenuator ensures „lower sensibility“ to wind. Apart from improving dynamic features of the aircraft, the ADAD system reduces the stabilized value of the angular velocity when deflecting the control stick by a single degree. Methods of analysis and synthesis helped us determine the parameters of the robust controller of the ADAD system for lateral control of high-maneuverability aircraft. The suggested H_∞ controllers shows the example of degradation in the frequency response of flight conditions of the model for the lateral movement of aircraft, when the value of gain is close to 15. By contrast, the

μ controller degrades flight characteristics, when compared to the H_∞ controller, as the gain of the feedback is only slightly exceeding the value of 1.25, consequently, the μ controller is better in compensating for control errors, if committed.

Acknowledgement

The work presented in this paper was supported by VEGA, Grant Agency of Ministry of Education and Academy of Science of Slovak Republic under Grant No. 1/0298/12 – "*Digital control of complex systems with two degrees of freedom*" and grant No. 1/1117/11 – *"Integration of automatic flight control algorithms with control algorithms of aircraft turbocompressor engines"*. The work presented in this paper was also supported by KEGA under Grant No. 018TUKE-4/2012 – "*Progressive methods of education in the area of control and modeling of complex systems object oriented on aircraft turbo-compressor engines*.

References

[1] ADAMS, Richard J. – BUFFINGTON, James M. – SPARKS, Andrew G. – BANDA, Siva S.: Robust Multivariable Flight Control. London: Springer-Verlag, 1994, ISBN 3-540-19906-3

[2] SONNEVELDT, L.: Nonlinear F-16 Model Description – Version 1.0: Delft:Control & Simulation Division, Faculty of Aerospace Engineering, Delft University of Technology, March 2010

[3] MACKENROTH, Uwe: Robust Control Systems. Berlin: Springer-Verlag, 2004, ISBN 3-540-20929-9-8

[4] SALIMBAHRAMI, Behnam: Multivariable Robust Control. Lehrstuhl für Regelungstechnik Technische Universität München, 2007

[5] SZÁSZI, István – KULCSÁR, Balázs: Robust Control and Fault Detection Filter Design for Aircraft Pitch Axis. Periodica Polytechnica, roč. 29, č. 1-2 (2001), s. 83-100

[6] Control of F-14 Lateral Axis Using mu-Synthesis. Matlab R2010b Help

[7] BALAS, Gary – CHIANG, Richard – PACKARD, Andy – SAFONOV, Michael: Robust Control Toolbox™ 3 – User's Guide. The MathWorks, Inc., April 2011

[8] ROSKAM, Jan: Airplane Flight Dynamics and Automatic Flight Controls - Part I, Third Printing. Lawrence, Kansas: DARcorporation, 2001, ISBN 1-884885-17-9

[9] ROHÁČ, J.; REINŠTEIN, M.; DRAXLER, K.: Data Processing of Inertial Sensors in Strong-Vibration Environment. In Intelligent Data Acquisition and Advanced Computing Systems (IDAACS). Piscataway: IEEE, 2011, Vol. 1, pp. 71-75, ISBN 978-1-4577-1426-9

[10] SOTÁK, Miloš – SOPATA, Milan – BRÉDA, Róbert – ROHÁČ, Jan – VÁCI, Ľuboš: Integrácia navigačných systémov. Monografia. Košice 2006, str. 64 – 65. ISBN 80-969619-9-3

[11] SOTAK, M.: Determining Stochastic Parameters Using an Unified Method. In: Acta Electrotechnica et Informatica. - ISSN 1335-8243, Vol. 9, No. 2 (2009)

[12] LAZAR, T., PASTOR, P.: Factors Limiting Controlling of an Inverted Pendulum. Acta Polytechnica Hungarica Vol. 8, No. 4, (2011), s 23-34

[13] VAŠČÁK, J., MADARÁSZ, L.: Automatic Adaptation of Fuzy Controllers. Acta Polytechnica Hungarica Vol. 2, No. 2, (2005), s 5-18

[14] DURHAM, W. C.: Aircraft Dynamics. Virginia: Virginia Polytechnic Institute &State University, 2002

[15] Richard J. ADAMS, James M. BUFFINKTON, ANDREW G. SPARKS and Siva S. BANDA: ROBUST MULTIVARIABLE FLIGHT CONTROL. Springer – Verlag, Berlin Heidelbeberg New Yourk. ISBN 3-540-19906-3

[16] R. P. G. Collinson: Introduction to Avionics. ISBN 0412-48250-9

Process-driven Approaches to Knowledge Transformation

Ján Paralič[1], František Babič[1], Marek Paralič[2]

[1] Department of Cybernetics and Artificial Intelligence,
[2] Department of Computers and Informatics,
Faculty of Electrical Engineering and Informatics,
Technical University Košice
Letná 9, 04200 Košice, Slovakia
E-mail: jan.paralic@tuke.sk, frantisek.babic@tuke.sk, marek.paralic@tuke.sk

Abstract: In this paper we focus on specific approaches to knowledge transformation within the educational domain. Our approaches can be briefly characterized as process-driven, because the core concepts are educational processes and semantic representations of them. In this paper we present two alternative ways of using process models for knowledge transfer in educational domain. First one is deductive approach, or top-down approach, where knowledge is captured from the very beginning and continuously upgraded with the repeated runs of educational processes. The second one is inductive approach, or bottom-up approach, where process logs are analyzed with the aim to derive useful knowledge patterns. We build on our experiences from more research and educational projects, where we have designed and developed information systems and services supporting these types of knowledge transformation.

Keywords: knowledge transformation; process model; ontology; process mining

1 Introduction

Knowledge transformation has been identified in [7] as the core approach when new knowledge is created. Nonaka and Takeuchi in their book identify four basic knowledge creation processes, whereas all of them are based on some form of transformation between two basic types of knowledge: explicit and tacit. The concept of tacit knowledge was first introduced by Polanyi in [10]. Nice article describing broadly area of knowledge management in the higher education context appeared in this journal [24], but we go much deeper into the educational processes proposing two different approaches to knowledge transformation.

The importance of process context is understood especially in the business area. Raghu and Vinze in [11] claim that the core of knowledge is defined in the

business process context and the knowledge is managed within the cyclical set of phases: knowledge storage and retrieval, knowledge sharing and knowledge synthesis. There is no doubt that process models are very useful and powerful means for knowledge capture, analysis and improvement of existing business processes. The question remains, to what extent created process models may be operationalized. Today's technologies (e.g. semantic technologies, workflows, various execution languages) provide quite straightforward tools for execution of well defined process models, which is often used in business [19], [20] but also in public sector [12], [3] where semantics is used to support automation of business processes. But what is the situation in educational processes? This article provides some possible answers on this question. In last seven years we had the chance to address the issues of knowledge creation and transformation in a couple of research and development projects. We designed and applied two different approaches for knowledge transformation, each of them being more suitable for different types of educational processes.

First approach, which we call deductive or top-down, is more suitable for relatively stable processes and is quite similar to the approaches used in business or public sectors mentioned above. But we also show how our operational environment provides enough flexibility to cope with process changes and improvements which are very typical in educational domain. Second approach, called inductive or bottom-up is aimed for very loosely-structured processes, typically of collaborative nature. Here the knowledge transformation is more about discovery of interesting knowledge patterns, using the information logged from the supporting educational (collaborative) information systems.

The rest of the article is organized as follows. We first present current state of the art in relevant areas in Section 2. Sections 3 and 4 create the core of this contribution. Our deductive approach to knowledge transformation is described in Section 3 and the inductive approach in Section 4. The paper concludes with a summary of main contributions of proposed approaches to knowledge transformation and recommendation for their usage.

2 Related Work

Semantic technologies have been used in various technology enhanced learning projects with different aims. Semantic models themselves are very good form of knowledge representation, which may be used also to achieve some level of operationalisation in educational processes. One of the first projects using this approach was PALETTE [21], where the solution is based on an expandable set of electronic services. Integration and interoperability was achieved by so called Cross Awareness Knowledge Base providing synchronization and searching functionalities for underlying services. Ontology models services, resources and

their actions. Similar recent approaches are e.g. [22] and [23]. Ontologies, methodologies, and other tools supporting technology enhanced learning applications were elaborated also within Kaleidoscope, a Network of Excellence project[1]. Semantic knowledge middleware infrastructure to support knowledge creation processes (also known as trialogical learning), was designed and developed in the integrated FP6 project KP-Lab [6]. Our approach described in the following Section 3 is to some extent similar, however, we handle the service integration by means of a more transparent and flexible approach of semantic process models.

Learning scenarios provide a basic structure (very similar to process-driven models) to support educational processes [4], [25]. The main challenge is to create an effective scenario reflecting actual education conditions, course's objectives, student's experiences and knowledge, teacher's expectations, available technical tools, etc. With the goal to help teachers in creating collaborative learning scenarios an intelligent authoring tool CHOCOLATO was implemented [4] that use ontologies for representation of relevant knowledge about various learning strategies and practices. Another ontological framework to support collaboration and interaction analysis is described in [13], which provides also means to automatic analyses of performed processes in groupware systems. Collaboration and interaction analysis represents a relatively new research area bringing new methods to investigate how users interact in virtual collaborative environment, supporting in such a way the knowledge transformation processes based on loosely structured collaborative processes or external examination of performed collaborative processes [14]. This approach was used also in [15] to design methods for enabling observation in CSCL (Computer-supported collaborative learning) environment in order to collect data for complex analyses of performed collaborative processes, focused on validity of used approaches to solve defined problems.

Different but interesting approach is described in [16]. Authors proposed a fuzzy expert system for evaluation of virtual collaboration and task implementation. This system is based on variables extracted from virtual collaborative system as fuzzy rules inputs that are further evaluated by predefined hierarchical fuzzy rules. The rules were created by experts with the objective to respect the subjective looks of involved experts and relative vague understanding of extracted characteristics. These fuzzy rules can be seen as a one possibility how to represent the transformed knowledge for loosely structured processes.

Another form of representation can be rules reflecting patterns of usage [9]. We present in Section 4 below here, what types of patterns can be used for knowledge transformation in loosely structured educational processes, how they can be defined and searched for.

[1] http://www.noe-kaleidoscope.org

3 Deductive Approach to Knowledge Transformation

Our deductive approach to knowledge transformation is based on carefully designed semantic models and their suitable operationalization, which is described in this section. In the center of deductive approach to knowledge transformation applied within the IT4KT – Information technology for knowledge transfer (ITMS project code: 26220220123) project are educational processes as they are conveyed during the university study. Altogether 11 courses and group of courses from the mathematical and computer science area at the Faculty of Electrical Engineering and Informatics, Technical University of Košice were analyzed. Small groups of teachers, process modelers and ontology engineers were created and crucial phases of the educational processes were formalized in the form of BPMN (Business Process Model and Notation) 2.0 process models. Created models represent an interesting combination of traditional learning scenarios and tacit teacher's knowledge acquired during previous instances of learning courses. This creation can be understood as complex transformation including all four knowledge creation processes from Nonaka and Takeuchi model:

- Externalization of tacit teacher's knowledge into relevant BPMN elements and relations between them.
- Combination of explicit knowledge representing identified traditional learning scenarios in the form of simple workflows.
- Internalization of collected explicit knowledge about various possible procedures, tools, methods, and data sources into teacher's tacit knowledge to create an effective structure (process model).
- Socialization representing a tacit to tacit knowledge transfer during face to face meetings of created groups.

By the selection of the modeled educational process phases beside importance from the knowledge transfer point of view, the perspective utilization of ICT was one of the most influential factors.

3.1 Modeling Particular Educational Processes

In the first phase, when the groups worked independently, more than 50 first and second level processes were designed. In order to begin the generalization process that could result in general schemes of knowledge transformation process, TEL (Technology-enhanced learning) ontology was applied to all process elements. TEL ontology created also within IT4KT project uses Activity, Actor/Agent, Role, Knowledge Artefact, Tool, Event and Condition elements. Relationships between these elements can be briefly characterized by the following sentence: the Actor of a given Role is using the Tool to create/manipulate a Knowledge Object within an Activity with specific characteristics given by Event and Condition concepts. More about the TEL ontology can be found in [8].

The following Table 1 summarizes the (by individual groups) identified processes and number of their occurrences either in the definition or usage form by the independent groups corresponding to a course or to a group of courses.

Table 1
Number of definitions and utilizations of identified process within modeled courses

Nr.	Name of the process	Nr. of def.	Nr. of usages
1.	Preparation of study materials for the course	4	3
2.	Generating and solving of tasks within and outside of the lab	3	4
3.	Generating, elaboration and evaluation of tests	5	1
4.	Automatic testing of programming tasks within LMS tests	5	1
5.	Lecture – including support of interactive materials	3	2
6.	Originality control of an assignment	1	4
7.	Correctness control of an assignment	1	4
8.	Management and control of assignments	3	1
9.	Controlled self-study	3	1
10.	Self-testing	2	2
11.	Support for semantic linking of lectures content, practical assignments and exam tests	1	3
12.	Introductory tests	1	3
13.	Support for creating lab materials based on practical programming assignments and their testing	3	0
14.	Exams – theoretical and practical, oral and written	2	1
15.	Questionnaires	2	1
16.	Management of individual and team based project	2	1
17.	Automatic update of university information system from LMS after finishing the test	1	2
18.	Utilization of on-line tools within interactive materials from LMS	2	0
19.	Design and publishing of scenarios	1	1
20.	Analysis of the incremental student's work at assignment	1	1
21.	Support for design and distribution of course packages containing the learning materials (teacher&student version)	1	1
22.	Support for design, maintenance and distribution of virtual engines specialized for given topic	1	0
23.	Collaborative commenting of scenarios	1	0
24.	Dynamic knowledge testing	1	0
25.	Management of programming assignments within LMS	1	0
26.	Creating of paper equivalents of electronic tests	1	0
27.	Integration of information systems involved in educational processes	0	1

3.2 Identification of Generic Processes

In the second phase all created processes were analyzed in detail and groups of processes were identified, in order to make the experiences, skills and practices of individual processes as generic as possible. Similarly the hierarchy of processes was established, because different groups by focusing on different aspects of the pedagogical process used different entry points to overall process structure. The results of the second phase are the following three generic processes, whereby the most of identified particular processes listed in Table 1 are covered within the generic process (those with higher number of definitions/usages were prioritized):

A. Preparing study materials for the course
   1) Lecture – materials including the interactive ones together with integrated on-line tools
   2) Labs – the process of task and assignment generation as well as their solving during the labs and at home
   3) Support of semantic interconnection of lectures content, practical examples at labs and test questions at exams
   4) Controlled self-study
   5) Creation, publication and collaborative commenting of scenarios
   6) Questionnaires – semantically aided feed-back
   7) Support and distribution of packages with learning materials and virtual machines

B. Support for student assignments
   1) Correctness control of the assignment solutions and detecting of solution plagiarism
   2) Assignment solutions storage and maintenance
   3) Support for individual and team based term projects
   4) Analyses of incremental work during the process of solving the assignment
   5) Support for material and test generation of practical labs based on annotated sample solution

C. Generation, developing and evaluation of tests including programming tasks
   1) Entry tests
   2) Self-testing
   3) Automatic control of programming tasks inside and outside of an LMS
   4) Dynamic tests of practical skills (e.g. SQL and relational algebra)
   5) System support for programming assignment variations
   6) Paper equivalents of electronic tests

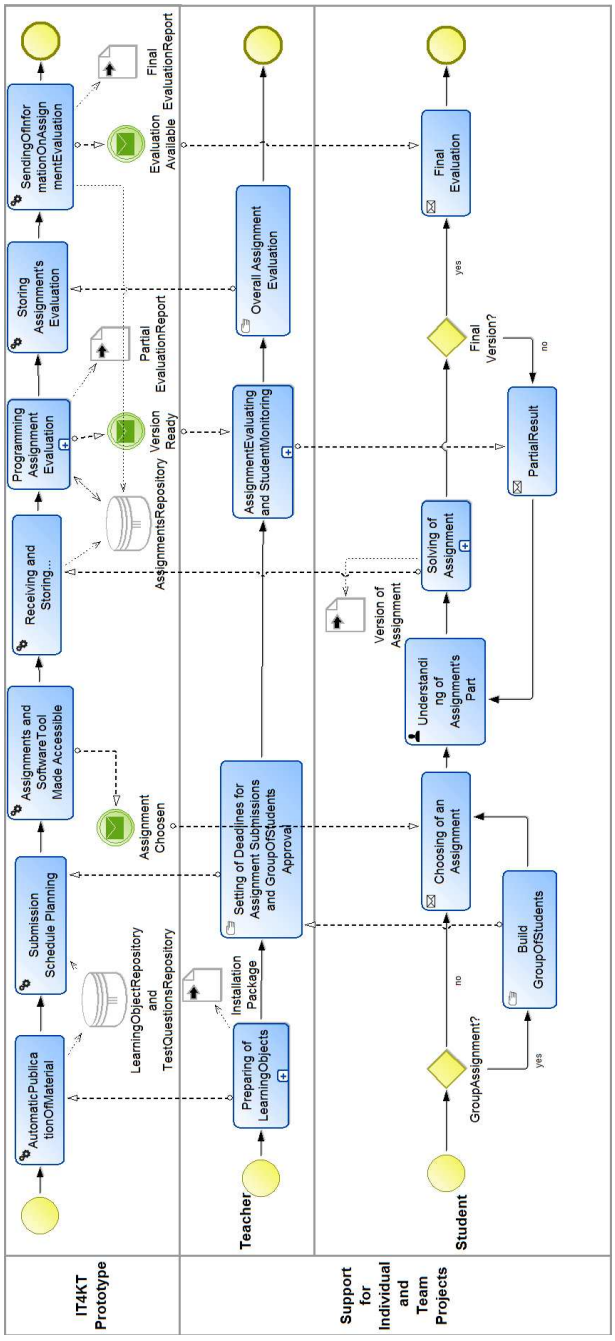

Figure 1
Top level process example - Support for Individual and Team Projects

Figure 1 depicts example of resulting generic process model at first level of modeling – Support for Individual and Team Projects (B3). It includes number of second level processes – e.g. Programming Assignments Evaluation or Preparing of Learning objects. All of them utilize concepts of TEL ontology [8] in order to describe an activity, repository or learning objects as input/output data.

3.3 Operationalization

Modeling of processes on one hand contributed to reveal tacit knowledge hidden behind individual teacher experiences and identify common services that could be supported by information and communication technologies (selected subset of identified services is shown in Table 2). On the other hand, the formalized form of processes as BPMN2.0 models that could be straightforward transformed into executable processes, contributed also to the architectural design of the IT4KT platform itself.

One way how to deal with such systems is to perceive them as process-driven service-oriented architecture (SOA) based systems. For such systems is important connecting process-oriented kernel with backend systems in flexible, scalable, maintainable and changeable way.

Table 2

Selected identified generic services which become electronic services

Generic process	Service
Preparing study materials for the course	Annotation of study materials
	Register of student profiles
	Evaluation and register of test results
	Generation of the list of practical exercises
	Verification of results of practical exercises
	Management of polls
Support for student assignments	Support for collection of assignments and projects
	Support for originality check
	Management of assignment registry
	Automatic system for validation of programming assignments
Generation, developing and evaluation of tests including programming tasks	Management of test bank, incl. programming tasks
	Evaluation of test task in LMS
	Evaluation of test task by external program
	Checking syntax of a program code fragment
	Statistical processing of test results
	Publishing of test results

In educational environment that we are focusing on, common backend systems are CMS systems (Content Management System) e.g. Joomla[2] or MediaWiki[3] and LMS systems (Learning Management System) like Moodle[4]. In order to support different technologies that should be connected to common platform and build SOA solution, the architectural pattern Process Integration Architecture [2] can be applied. According to [2] the following tiers could be distinguished:

- *Macroflow Tier* – educational processes can be hosted by different macroflow engines – in our case they should be able to run the BPMN 2.0 processes (e.g. Activiti BPM platform)
- *Macroflow Integration Tier* – contains one integration adapter per each macroflow engine. It integrates the process activities with the technical functions provided by services.
- *Microflow Tier* – a number of services is provided as well as the support for service orchestration
- *Backend Integration Tier* – integration adapters for needed backend systems
- *Backend Systems Tier* – systems that perform functions needed for running of educational processes – e.g. CMS, LMS.

4 Inductive Approach to Knowledge Transformation

Some types of educational processes (e.g. collaborative processes [4], or knowledge creation processes [17]) cannot be fully described by well-defined static process model, as presented by the deductive approach above. They change in time based on actual conditions, changes in participant's list, used procedures or methods and this dynamic aspect represents a very challenging task for modelling an implementation techniques.

The aim of our inductive approach is to trasfer the hidden knowledge in educational processes to the relevant users (learners, teachers, students) in suitable and easily understandable form. Such creative educational processes are usually supported by some suitable collaborative system offering various related end-user functionalities. In the KP-Lab project[5], the whole virtual collaborative system was mediated by ontology to support objects' semantic representation and software interoperability across the middleware layer [1]. The process part of ontology contained the basic elements as e.g. process, task, milestone, subject, deliverable

[2] http://www.joomla.org/
[3] http://www.mediawiki.org/wiki/MediaWiki
[4] https://moodle.org/
[5] www.kp-lab.org

and object creating a basic process model [5]. This structure can be extended by another elements from common KP-Lab ontology in order to model the complex educational processes with all characteristics [1].

Typical example of collaborative and loosely-structured educational process is work on team student assigment. The result of such an assigment can be understood as some new knowledge created in the process of knowledge transformation as combination of tacit knowledge of the students collaborating within the team and explicit knowledge represented by manuals, books, papers and other knowledge sources shared e.g. in some virtual space. Relevant activities are mediated by suitable information and communication solution, as students need collaborative space to share their inputs and contributions, to display their progress and to communicate and comment published versions of the assigment. The whole knowledge creation process consists of several phases and each of them requires interaction between participants based on their roles, experiences and theoretical background. Our inductive approach to knowledge transformation is based on tracing performed steps and visualizing them in suitable form (e.g. in form of some type of timeline) in order to provide historical overview in chronological order. Such visualization represents a historical projection of the realized educational process with all related objects (docs, tutorials, manuals, instructions, demos, etc.), involved subjects (students, teachers, instructors, etc.), created connections (between subjects, between objects or between both of these categories), etc. This type of projection can be used for collaborative analysis and reflexion to identify the key persons, important flows of information, interesting inputs for decissions or significant steps forward, etc.

We designed and implemented several necessary services to support the inductive approach, i.e. for logging, data management, extraction and visualization. Semi-automatic character of this approach can replace the often used manual methods of user behaviour evaluation that are much more time consuming and tedious for teachers or researchers. Reasons for that are e.g. necessary collection of all materials from students or laborious analysis of their communication channels, which causes difficulties by identification of the real involvement of each student. Suitable visualisation of automatically collected data with the possibility to define constraints based on users' needs provides easier approach, mainly in the case of large students' groups.

4.1 Data from Educational Processes

Source data recorded for historical projection represent actions/activities performed during educational processes. Each action or activity is monitored and logged in predefined format, e.g. if a user attaches a new tutorial to relevant task in order to help other students with this tasks; this action is logged and stored as new event in the log repository. Each event is described by specified parameters (log format) that provide complex data structure for visualization or analytical

purposes, i.e. timestamp, subject identifier, action type or related shared object. More details about used log format are presented in [9].

The implemented logging services were tested with three different colalborative systems to evaluate their adaptability and success in obtaining the required quality of data [18]. Moodle[6] was selected as typical representative of LMS in the conditions of Slovak education; KPE[7] as actual new software output of KP-Lab project offering an innovative look on knowledge creation processes called trialogical learning [6]; and Claroline[8] as potentially interesting candidate for execution of the various learning processes. The experiments realized within Moodle covered design and implementation of a new web service responsible for cooperation with internal Moodle logging system to transfer event logs from internal Moodle repository. In the case of KPE, logging procedure was integrated on the middleware layer to obtain data from user environment in cooperation with monitoring services on the GUI (Graphical user interface) level. The last experiment was not successful because it would require changes in internal Claroline logging API (Application programming interface), which was not accessible to our project team. Despite this fact, based on the two successful results mentioned above we can conclude that the integration of our inductive knowledge transfer tools with another collaborative educational systems is possible and straightforward if suitable API of original system is available.

Once the data from a collaborative or other educational supporting information systems is available, our approach offers a set of tools to their analysis supporting knowledge transfer. Simple examination of collected historical data from overall, quantitave point of view, can be performed with supporting tool offering a basic summary overview, see Figure 2.

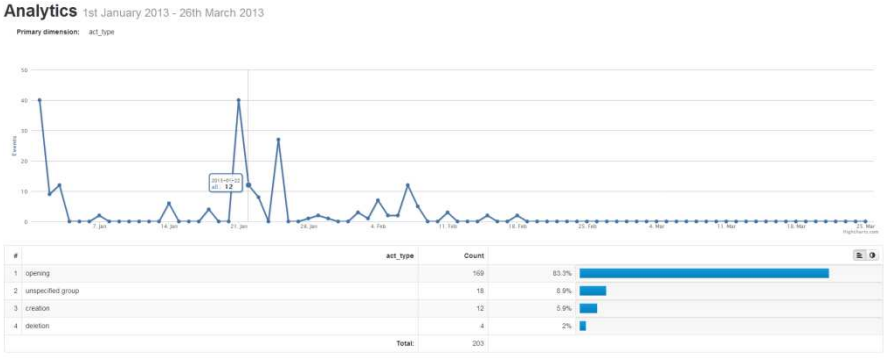

Figure 2
Example of simple summary visualization of collected historical data

[6] https://moodle.org/
[7] http://www.kp-lab.org/tools/knowledge-practices-environment
[8] http://www.claroline.net/

4.2 Tool Supporting Knowledge Transformation

The Timeline-based Analyzer (TLBA) is an application that visualizes selected historical events in chronological order, which is a natural way how to represent a collaborative or knowledge creation processes. TLBA in such a way gives the possibility to focus on potentially interesting sequences of activities and to reflect on the existing practices and in such a way to support knowledge transformation from loosely-structured educational proceses.

The main functionalities provided by the TLBA are the following:

- Timelines visualize sequences of performed events in chronological order. User can visualize more parallel timelines represented particular participats in the educational process. E.g. in case of team assignment each member of the team is represented by one timeline (see Figure 3).
- Visualised timelines contain all events from particular educational process (or its part). Authors of events are distinguished by particular parallel timelines, different types of events are distinguished by type of graphical icons used, e.g. star = modification or circle = opening. Consecutive events performed on the same knowledge object are connected with lines. In such a way all crutial information is placed into the view so users can explore and highlight events that are of particular interest to them.
- Basic timeline is constructed from automatically collected events which are stored in the event logs. If user needs to include important action/activity performed outside monitored virtual environment and relevant for investigated process, such an event can be inserted manually and stored in the log repository as so called external event and of course visualised on the timeline.
- Several supporting functions as commenting and filtering were implemented to support simple orientation and comprehensibility of visualized information for users.
- Reflexion over collected historical data is provided by definition of patterns representing a suitably generalised set of selected events or elements from timeline. These patterns are well formalized projections of interesting practices or parts of the whole educational processes (transformed knowledge).

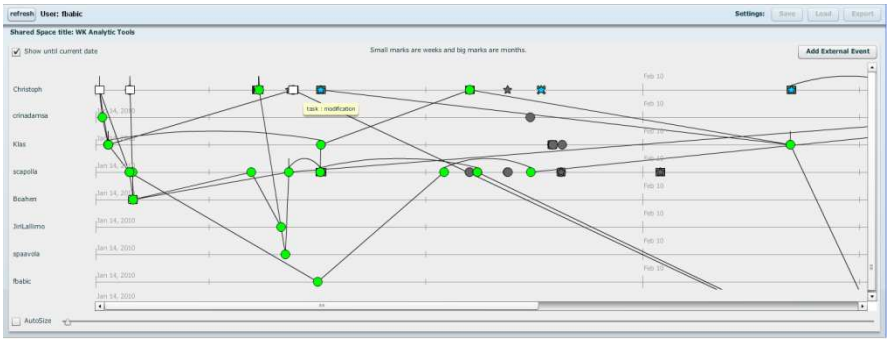

Figure 3
Example of timeline-based visualization

4.3 Knowledge Patterns

Knowledge patterns represent important mean to support knowledge transformation. It is a way how to identify interesting sequences of user actions during educational processes mediated by suitable information systems. The patterns usually describe situations that lead to some critical moments, which can mean a significant progress, discovery of new knowledge/method. However they can not only represent positive lessons learned, but on the other hand they also can reflect some negative lessons when a particular process was not successful or it finished untimely. Such kind of patterns may also conceptually represent interesting practices emerged within particular process or activity – either being positive (something like best practice), or negative (worst practices). The main issue in this case is the representation of the patterns and their identification.

Pattern can be understood as formalisation of captured tacit knowledge in the process realisation specified by user based on his experiences and own knowledge. Basically, it is some special type of knowledge transformation that connects two knowledge conversion processes from traditional model [7]: externalisation and combination. At first, user expresses her/his tacit knowledge (a kind of hypothesis) in order to verify a pattern that will be further evaluated over the collected historical data (externalisation). This pattern also represents an expected tacit knowledge hidden in investigated educational process or its part. If the subsequent evaluation of specified pattern will be successful, user verifies a new knowledge that can be further combined with existing ones to create the final transformed piece of knowledge (combination). Simple example of this transformation:

1. Teacher specified an assigment for students to solve some optimalisation task and provided also necessary detailed documentation.
2. As an inspiration teacher provided to students also some examples of traditional methods.

3. One group of students solved its task successfully, but they used different approach as it was originally expected by the teacher.
4. Teacher wanted to evaluate their approach based on collected historical data representing all performed steps.
5. He visualised on timeline all activities of the specific group and looked for specific sequences of activities describing the critical sequence of actions that led to the successful result trying to generalise them.
6. Created generalized pattern was evaluated over the relevant data sample (all other groups, possibly also from previous years) and all its occurrences in previous processes were found and can be displayed for detailed inspection.
7. This complex visualization provided for teacher all necessary information to decide if performed approach can be labelled as "good practice" or "bad practice". In the first case, teacher can update his set of possible procedures to solve this type of task for the future use. The second case indicates a potential cheating.

Based on this simple example we can propose a common worklow for our induction approach:

1. Understanding of problem's domain, formulation of hypothesis.
2. Acquiring logs of users' actions and basic understanding of them.
3. Preprocessing and creation of a filter in order to select and prepare suitable data set for analysis.
4. Construction of a pattern (hypothesis to be verified by its occurences).
5. Performing search for a pattern occurrences in given data set.
6. Interpretation of results, iteration *(back to step 3 or 4)*

The pattern can be defined either from scratch, or based on any subset of events presented on the timeline in TLBA with the possibility to relax some of the attributes of selected events, stating in such a way a set of constraints. The constraints can take one of the following alternative forms:

- Equality or inequality of properties of different events (e.g. different users performing event 1 and event 2, the same user performing events 2 and 3)
- Multiple occurrence of events (e.g. at least 2 comments have to be posted, for example by any user).
- Sequence of events (in given order e.g. first event, second event …).
- Specification of a timeframe between events (e.g. there should be a comment at least 48 hours after the creation of a document).

Each pattern element represents one generalized event, which is essentially a list of key-value pairs. User can specify the element based on any of the event's attributes. In these key-value pairs, user specifies which parts of the generalized event are important and which should be generalized. Simple example of pattern definition is presented below:

```
(def f1 {:actor :X :type "opening" :entity "doc1"})
(def f2 {:actor :X :type "creation" :entity :Y})
(def f3 {:actor :X :type "link" :entity :Y :link-to "doc1"})
(def pattern [f1 f2 f3])
(search data pattern)
```

This pattern represents a case in which user "X" created a new document "Y" after reading an existing document "doc", and then linked these two documents together. Defined pattern is matching with events stored in log repository to generate a searching tree in which obtained results are represented as leaf nodes at the lowest level of the tree, see Figure 4. In our case the search found two results (user a2 created documents doc4 and doc6 and linked both of them to doc1), depicted as green leaf nodes. Searching process operates with two variables X and Y, defined in the patterns above, which are bound to values as the search progresses. Depth-first search is used, with some optimizations which remembers environment (current parts and variable bindings) of traversed nodes and does not expand new nodes if they happen to have same environments as the failed ones (note that node u3 does not expand).

Pattern discovery service is implemented in the Lisp language called Clojure. This dynamic programming language for JVM (Java virtual machine) provides functional approach to the programming and usage of immutable data structures. In Clojure, collections are generalized into the sequences, for which most of the operations provides lazy evaluation. For each pattern element, pattern discovery service constructs an SQL query in order to find matching events in the log.

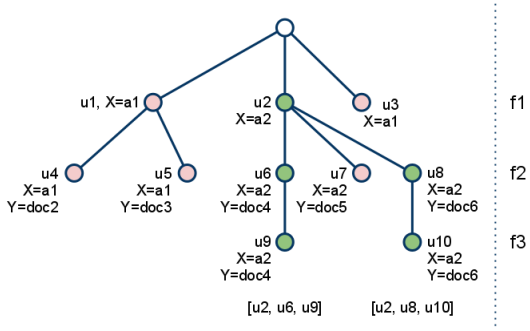

Figure 4
Resulting tree for pattern example

The lazy evaluation, easily achieved in Clojure, traverses only those parts of the result tree, which are actually used. This subsequently lessens the number of queries sent to the MySQL database, dramatically speeding up the whole matching process, if the user is interested only in small number of results.

Proposed inductive approach was tested in real conditions within the KP-Lab project focused mainly on various educational knowledge creation processes. Figure 5 displays an example from Austrian pilot case visualizing students' and teachers' activities within a collaborative learning environment KPE recorded over a period of 15 weeks. As a consequence, less time is needed to reconstruct the work processes and more efforts can be spent on the actual analysis of critical events.

Conclusions

In this article we described two alternative approaches to knowledge transformation in educational processes. Deductive approach is suitable for well structured processes, which is typically the case for more general processes like preparation of lectures, evaluation processes – tests or management of the whole lifecycle for student assignments. These processes are often used in many university courses and it is therefore efficient to design and implement supporting electronic services, which can be shared across various subjects. Proposed process-driven semantic approach makes it possible not only to model, but also support operationalization of selected parts of generic educational proceses in form of electronic services.

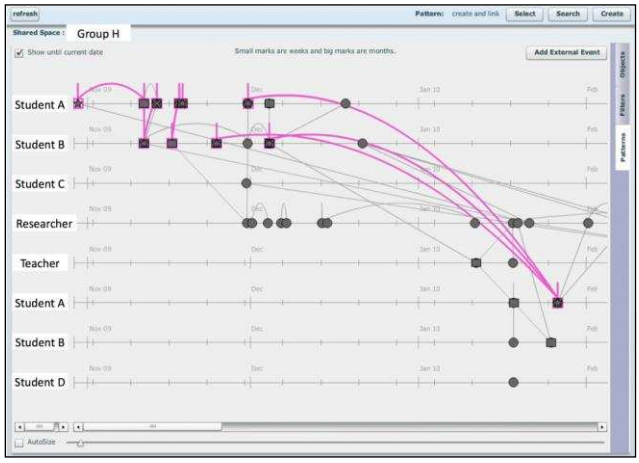

Figure 5
Screenshot of TBA displaying 27 matches of a defined simple pattern

Inductive approach is more suitable inside particular subjects, where educational processes are less structured and often highly specialised. These are e.g. various collaborative activities or knowledge creation processes. Nowadays even these

less structured processes can be traced to some extent thanks to the mediating information systems, which can generate logs of events. Proposed inductive approach provides formal as well as practical tools to represent interesting pieces of transformed knowledge in form of knowledge patterns.

Acknowledgement

This work was supported by the Scientific Grant Agency of the Ministry of Education, Science, Research and Sport of the Slovak Republic under the grant No. 1/1147/12 (50%). It is also the result of the project implementation: IT4KT - Information technology for knowledge transfer (project number: 26220220123) supported by the Research & Development Operational Program funded by the ERDF (50%).

References

[1] F. Babič, J. Wagner, J. Paralič: The Role of Ontologies in Collaborative Systems. SAMI 2008 6th IEEE International Symposium on Applied Machine Intelligence and Informatics - Proceedings, Herlany, Slovakia, January 2008, pp. 119-124

[2] C. Hentrich, U. Zdun: A Pattern Language for Process Execution and Integration Design in Service-oriented Architectures. Transactions on Pattern Languages of Programming, Vol. 1, Springer, 2009, pp. 136-191

[3] J. Hreňo, P. Bednár, K. Furdík, T. Sabol: Integration of Government Services Using Semantic Technologies. Journal of Theoretical and Applied Electronic Commerce Research, Vol. 6, Issue 1, April 2011, pp. 143-154

[4] S. Isotania, R. Mizoguchi, S. Isotani, O. M. Capeli, N. Isotani, A. R. P. L. de Albuquerque, Ig. I. Bittencourt, P. Jaques: A Semantic Web-based Authoring Tool to Facilitate the Planning of Collaborative Learning Scenarios Compliant with Learning Theories. Computers & Education, Volume 63, April 2013, pp. 267-284

[5] S. Jalonen, M. Lakkala, S. Paavola: Investigating Knowledge Creation Technology in an Engineering Course. Computers & Education, Volume: 57 (2011), Issue: 3, pp. 1930-1942

[6] M. Lakkala, S. Paavola, K. Kosonen, H. Muukkonen, M. Bauters, H. Markkanen: Main Functionalities of the Knowledge Practices Environment (KPE) Affording Knowledge Creation Practices in Education. Computer Supported Collaborative Learning Practices: CSCL2009 Conference Proceedings, pp. 297-306

[7] I. Nonaka, H. Takeuchi: The Knowledge Creating Company: How Japanese Companies Create the Dynamics of Innovation, New York: Oxford University Press, 1995, 284 p.

[8] J. Paralič, K. Furdík, M. Paralič, P. Bednár, P. Butka, J. Wagner: Semantic Support for Educational IT Services. Acta Electrotechnica et Informatica, Volume 12, No. 4, October – December 2012, pp. 39-46

[9] J. Paralič, C. Richter, F. Babič, J. Wagner, M. Raček: Mirroring of Knowledge Practices based on User-defined Patterns. Journal of Universal Computer Science. Volume 17, Issue 10, 2011, pp. 1474-1491

[10] M. Polanyi: The Tacit Dimension, University of Chicago Press: Chicago, 1966

[11] T. S. Raghu, A. Vinze: A Business Process Context for Knowledge Management. Decision Support Systems, Volume 43 (2007), Issue 3, pp. 1062-1079

[12] I. Savvas, N. Bassiliades: A Process-oriented Ontology-based Knowledge Management System for Facilitating Operational Procedures in Public Administration. Expert Systems with Applications, Volume 36 (2009), pp. 4467-4478

[13] R. Duque, C. Bravo, M. Ortega: An Ontological Approach to Automating Collaboration and Interaction Analysis in Groupware Systems. Knowledge-based Systems, Volume 37 (2013), pp. 211-229

[14] T. Bratitsis, et al.: Supporting Members of a Learning Community Using Interaction Analysis Tools: the Example of the Kaleidoscope NoE Scientific Network, in: Eighth IEEE International Conference on Advanced Learning Technologies, 2008, pp. 809-813

[15] R. Duque, C. Bravo, J. Gallardo, W. J. Giraldo, M. Ortega: Modelling and Capturing Users' Actions in CSCL Systems for Analysis Purposes. International Journal of Emerging Technologies in Learning (iJET), Volume 4 (2009), pp. 53-59

[16] S. Strigunaite, D. Kriksciuniene: Fuzzy Expert System for Virtual Team Collaboration and Work Evaluation. In Lecture Notes in Business Information Processing, Volume 127 LNBIP (2012), pp. 37-43

[17] S. Paavola, K. Hakkarainen: The Knowledge Creation Metaphor – an Emergent Epistemological Approach to Learning. Science and Education, Volume 14 (2005), pp. 535-557

[18] F. Babič, J. Wagner, S. Jadlovská, P. Leško: A Logging Mechanism for Acquisition of Real Data from Different Collaborative Systems for Analytical Purposes. SAMI 2010: 8th International Symposium on Applied Machine Intelligence and Informatics, Slovensko, IEEE, 2010, pp. 109-112

[19] M. Laclavík, Š. Dlugolinský, M. Šeleng, M. Ciglan, M. Tomášek, M. Kvassay, L. Hluchý: Lightweight Semantic Approach for Enterprise Search and Interoperability, Proceedings of the Fifth Interop-Vlab.It Workshop on Complexity of Systems, Complexity of Interoperability in Conjunction with itAIS 2012, Rome, CEUR-WS.org, Vol. 915, pp. 35-42

[20] A. Garcia-Crespo, B. Ruiz-Mezcua, J. L. Lopez-Cuadrado, I. Gonzalez-Carrasco: Semantic Model for Knowledge Representation in e-business. Knowledge-based Systems, Volume 24, Issue 2, March 2011, pp. 282-296

[21] J. Naudet et al, *First version of PALETTE services delivery framework (D.IMP.06)*,http://palette.ercim.org/images/stories/DocumentPDF/d.imp.06-final.pdf, 2008

[22] S. Heiyanthuduwage, R. Schwitter and M. A. Orgun, "Towards Ontology-driven E-Learning Information Systems", *Advances in Ontologies*, Proc. of 7th Australasian ontology workshop, Perth, Australia, pp. 21-26, 2011

[23] L. Romero, M. Gutierrez and M. L. Caliusco, "Conceptualizing the e-Learning Assessment Domain using an Ontology Network", *International Journal of Artificial Intelligence and Interactive Multimedia*, Vol. 1, No. 6, pp. 20-28, 2012

[24] F. Farkas, Á. Király: What Makes Higher Education Knowledge-Compatible? Acta Polytechnica Hungarica, Vol. 6, No. 3, 2009, pp. 93-104

[25] P. Tóth: Learning Strategies and Styles in Vocational Education. Acta Polytechnica Hungarica, Vol. 9, No. 3, 2012, pp. 197-216

Machine Vision-based Measurement System for Vehicle Body Inspection

András Rövid

Óbuda University, John von Neumann Faculty of Informatics
Bécsi út 96/B, 1034 Budapest, Hungary
rovid.andras@nik.uni-obuda.hu

Abstract: The main contribution of the paper is to propose a system for fast and easy measurement of car body parts to support their inspection. The proposed system is composed from a camera-projector (CP) subsystem and a multi-camera and active marker based tracking system (TS). During the reconstruction process „rotating" gray code pattern is projected onto the targeted surface which improves the robustness and accuracy of the measurement. Afterwards based on triangulation the 3D coordinates of surface points are estimated.

Keywords: 3D measurement; car-body; projector; point cloud; inspection

1 Introduction

Recently the number of applications where the 3D measurement plays crucial role is increasing more and more. As few examples the industrial applications can be emphasized such as product inspection, design and manufacturing of various components, etc. The required accuracy of the measurement and other prescribed properties depend on the particular application. As the technology evolves new possibilities are at hand, new technologies can be applied to improve the performance of the measurement.

There are numerous well known techniques to perform 3D measurement and reconstruct the surface of various objects. Among the most popular and most reliable approaches the structured light and laser based solutions can be emphasized, where a coded pattern, fringe pattern or laser stripe is projected onto the targeted surface and based on pattern analysis and subsequent triangulation the 3D surface can be reconstructed.

The main difference in these methods lies first of all in the type of projected sequence to solve the correspondence matching problem which is the most crucial issue during the reconstruction. Some techniques are using colors for coding [7],

while the others are based on binary code, Gray code [9] [10] or fringe pattern projection [1-3] [11-13], etc. Although the projection of pattern sequences is relatively time consuming process, by using high speed cameras and precise synchronization real-time reconstruction can also be achieved. For example certain phase shift based methods – which belong to the family of fringe analysis based solutions – can offer real-time reconstruction [14].

Among the hardware based solutions first of all the utilization of Time of Flight (TOF) cameras may be emphasized [4]. Furthermore one can find applications where the stereo imaging without pattern projection is applied, e.g. robotics, obstacle detection, etc. in which case the point correspondence matching may become ambiguous or imprecise, therefore the achievable precision of the measurement is relatively low. Beside the above mentioned techniques one can find in the literature other interesting approaches, as well. The selection of the most appropriate measurement method depends first of all on the application requirements. The main aim of our investigation was to design and implement a robust, low cost high precision 3D measurement system to ensure the measurement of car body elements and generate data appropriate for their inspection or to perform certain analysis.

Another consideration – related to 3D reconstruction – was the extension of the measurement range by maintaining the accuracy at acceptable level. There are various methods to achieve this goal, which aim is to extend the „working space" trough tracking the scanning device [8]. This goal can be achieved for example by attaching the scanning device to robot arm or tracking it by external cameras.

The primary application of the proposed system is to support the evaluation process of crash tested vehicles. Crash tested cars provide a lot of important data, which can be obtained through detailed measurements of the car-body. By using these data the mathematical models of deformation processes can be tuned or identified. Since the measurement of critical points manually is a time consuming process the necessity of the 3D reconstruction of crucial parts is important.

The main aim of the paper is to introduce a method based on machine vision and pattern projection together with a tracking system to enable quick and robust measurement of car body elements.

The paper is organized as follows: Section II describes the architecture of the proposed system, Section III deals with calibration related issues, Section IV describes how the markers used for tracking are detected and identified. Section V describes the reconstruction itself and finally results and conclusions as well as future works are reported.

2 The Architecture of the System

An important consideration during the development of the system was to ensure the acquisition of large objects (car body parts) and hidden or covered surfaces with high precision. For this purpose an active optical scanning technology was combined with a multi-camera based tracking system depicted by Fig. 1. The active optical scanner is composed from a camera and projector which is tracked by the multi-camera system (see Fig. 1). Thus the CP system can be repositioned to ensure the acquisition of complex surfaces, as well. To ensure easy tracking, active LED markers - controlled by the software - have been attached to the CP system. This solution supports their unambiguous identification even if the lighting conditions are not appropriate. The working principle of the system can be decomposed into following steps:

First of all the system has to be calibrated, i.e. the intrinsic and extrinsic parameters of the cameras and that of the projector (considered as an inverse camera model) are determined. At this stage the hand-eye problem has to be solved, as well. After the system calibration process the measurement can be started during which the below steps are performed:

The active markers are detected and identified followed by the estimation of their spatial location used to estimate the relative rotation and transition of the CP system with respect to an initial reference value.

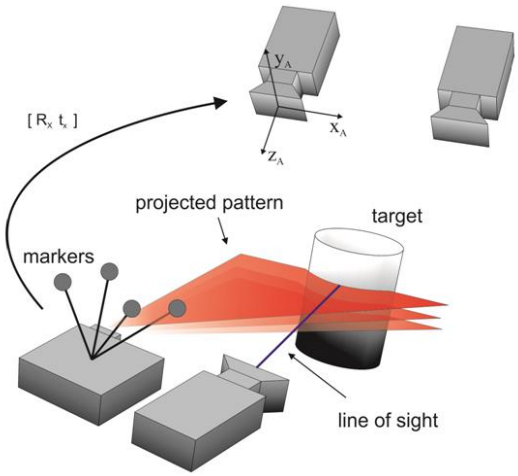

Figure 1
The architecture of the proposed system

Next, the so called rotated Gray code pattern is projected onto the targeted surface and based on ray-plane intersection the 3D coordinates of each projected pixel are determined. Accordingly the obtained 3D points are transformed into the world coordinate system.

Finally the point cloud is stored in a KD-tree structure and processed, i.e. the noise is eliminated and polynomial fitting is performed. In the upcoming section the main components of the system are described in more detail.

3 System Calibration

The calibration plays the most crucial part of the system. Since the proposed system has numerous components (cameras for tracking, projector, cameras for acquiring the illuminated surface), the accuracy strongly depends on the precision of the calibration of the mentioned elements as well as on the accuracy of the estimated relationships of coordinate systems. All these factors have significant impact on the output of the whole system therefore it is important consider them with high priority. The calibration of the system can be decomposed into three main parts, i.e. calibration of cameras; calibration of the projector and estimation of the relation between the probe and the world coordinate system (see Fig. 2).

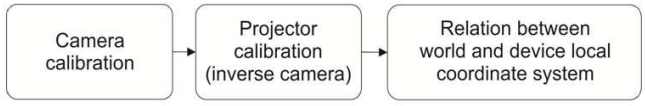

Figure 2
Flow of calibration

3.1 Camera Calibration

The intrinsic and extrinsic parameters of the cameras as well as the distortion coefficients of the applied lens were estimated by Zhang's method [5]. As calibration object a chessboard plate was used, which was acquired from various viewpoints by the cameras and based on the 3D coordinates of its corners and their projections onto the camera image plane the intrinsic as well as the extrinsic parameters of cameras can be determined (for more details see [5]).

3.2 Projector Calibration

The calibration of the projector is relatively more complex because in this case the 3D coordinates of the projected chessboard corners have to be estimated separately. The model of projector can be considered as an inverse camera model. As calibration pattern chessboard has been used. In order to estimate the intrinsic and extrinsic parameters of the projector, the first task is to get 3D-2D correspondences. In case of cameras the spatial coordinates of the chessboard

(calibration object of known dimensions) corners are known, their projections can be seen in the camera image. In case of a projector the situation is opposite, i.e. the coordinates of the corners projected onto a planar surface have to be estimated while the 2D coordinates of the corners in the image plane of the projector are known in advance.

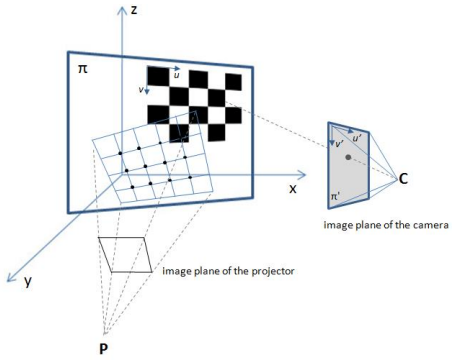

Figure 3

Illustration of projector calibration. (**P** – projector centre; **C** – camera centre). First the homography between $\boldsymbol{\pi}$ and $\boldsymbol{\pi}$**'** is estimated. Afterwards the u, v coordinates of projected corners are determined.

For estimating the coordinates of the projected corners first a chessboard pattern with known dimensions is attached to the planar surface. The top most horizontal and left most vertical edges represent the u and v axes of the reference coordinate system (see Fig. 3). As the coordinates of the physical chessboard corners in this coordinate system as well as the coordinates of their projections onto the camera image plane are known a homography can be estimated between the two projective planes [19].

By using the estimated homography the coordinates of the corners projected by the projector onto the planar surface (to which the chessboard pattern is attached) can be determined.

$$\begin{bmatrix} wu_b \\ wv_b \\ w \end{bmatrix} = \begin{bmatrix} h_{11} & h_{12} & h_{13} \\ h_{21} & h_{22} & h_{23} \\ h_{31} & h_{32} & h_{33} \end{bmatrix} \begin{bmatrix} u_a \\ v_a \\ 1 \end{bmatrix}, \tag{1}$$

where u_a, v_a and u_b, v_b stand for corresponding points in planes $\boldsymbol{\pi}$ and $\boldsymbol{\pi}$**'** respectively (see Fig. 3). **H** stands for the estimated homography matrix.

Accordingly the intrinsic and extrinsic parameters of the projector can be estimated - as in case of cameras - from known 3D→2D correspondences.

3.3 Hand-eye Calibration

The relation between the local coordinate system of the projector-camera subsystem and that of the world can be expressed as follows (see Fig. 4):

$$\begin{aligned} \mathbf{R}_A\mathbf{R}_X &= \mathbf{R}_X\mathbf{R}_B \\ (\mathbf{R}_A - \mathbf{I})\mathbf{t}_X &= \mathbf{R}_X\mathbf{t}_B - \mathbf{t}_A \end{aligned} \tag{2}$$

Here matrices $\mathbf{R}_A$, $\mathbf{R}_B$ and vectors $\mathbf{t}_A$, $\mathbf{t}_B$ stand for the transformation between two arbitrary positions and orientations of the projector-camera subsystem in the world coordinate system and the corresponding rotation and transition of the local coordinate system of the device (i.e. the coordinate system of the camera in the projector-camera subsystem).

$\mathbf{R}_X$ and $\mathbf{t}_X$ represent the unknown transformation from the local into the world coordinate system. After few steps of derivation we get the following minimization problem [6]:

$$f_1(\mathbf{R}_X) = \min_{\mathbf{R}_x} \sum_{i=1}^{n} \left\| \mathbf{n}_{Ai} - \mathbf{R}_X\mathbf{n}_{Bi} \right\|^2 \tag{3}$$

$$f_2(\mathbf{t}_X) = \min_{\mathbf{t}_x} \sum_{i=1}^{n} \left\| \mathbf{R}_X\mathbf{t}_B - (\mathbf{R}_A - \mathbf{I})\mathbf{t}_X - \mathbf{t}_A \right\|^2 \tag{4}$$

where $\mathbf{n}_{Ai}$ and $\mathbf{n}_{Bi}$ stand for the eigenvectors of $\mathbf{R}_{Ai}$ and $\mathbf{R}_{Bi}$ corresponding to the unit eigenvalue. $f_1(\mathbf{R}_X)$ can be solved for example by using quaternions together with langrange multipliers [6], while $f_2(\mathbf{t}_X)$ by least squares method.

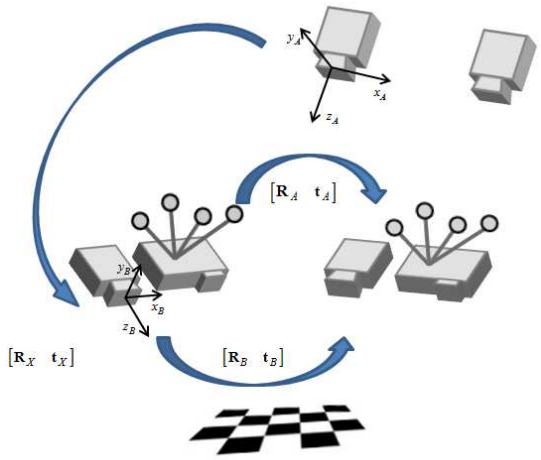

Figure 4
Illustration of the hand-eye problem

4 The Features of the Tracking Subsystem

In order to extend the range of measurement to ensure the reconstruction of large surfaces the camera-projector subsystem has to be tracked and the point clouds obtained from different locations of the CP subsystem can be combined in order to get a complete model and ensure the acquisition of hidden areas, as well. There are various techniques to perform the tracking. The proposed system uses multi-camera system to achieve this goal.

The CP subsystem is equipped with sequence coded active LED markers, which are controlled by the software and synchronized with the tracking subsystem. For this purpose a controller has been designed by the authors. The LED markers are turned on and off based on their assigned ID. Each state of the LED in the sequence represents one bit in the ID. An example of marker ID estimation can be followed in Fig. 5.

Let $\mathbf{a}_i$ and $\mathbf{b}_i$, i=1..N represent the 3D coordinates of markers corresponding to two different locations of the camera-projector subsystem. The transformation between the two states can be obtained as follows:

$f(\mathbf{R}) = \min_{\mathbf{R}} \sum_{i=1}^{N} \left\| (\mathbf{b}_i - \mathbf{q}) - \mathbf{R}(\mathbf{a}_i - \mathbf{p}) \right\|^2$ and the transition can be obtained simply as: $\mathbf{t} = \mathbf{q} - \mathbf{p}$, where $\mathbf{p} = \frac{1}{N}\sum_{n=1}^{N} \mathbf{a}_i$ and $\mathbf{q} = \frac{1}{N}\sum_{n=1}^{N} \mathbf{b}_i$.

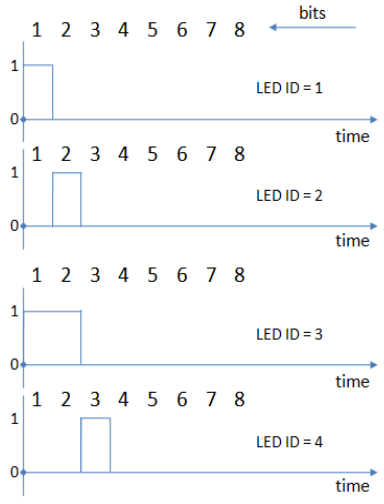

Figure 5
An example how the ID of each LED marker is determined (LED ON = 1; LED OFF = 0)

The algorithm used to detect the center of gravity of markers [15]:

Algorithm 1 Searching for COG of Markers in real-time

```
buffer_count := 0
Set every byte of the first row to 255
for y := 1 to image_height do
  for x := 1 to image_width do
    if I[x, y] > predefined_threshold then
      if ∀p ∈ N(x, y) : p := 255 then
        create_new_buffer
        I(x, y) := buffer_count
        buffer[buffer_count].AddItem(ActualPixel);
        buffer_count := buffer_count + 1;
      else
        I(x, y) := min{N(x, y)}
        if ∀p ∈ N(x, y) : p > I(x, y) then
          move items from buffer[p] into
          buffer[I(x, y)]
        end if
      end if
    end if
  end for
end for
for k := 1 to buffer_count do
  if buffer[k].itemcount > 0 then
    buffer.CalculateCOGofPixels
  end if
end for
```

5 Reconstruction

The main aim is to determine which projected column the camera sees in a given pixel. To identify the columns and rows in the image plane of the projector Gray coded sequence was projected onto the targeted surface (see Fig. 6). It can easily be recognized that in gray code sequence the consecutive codes differ only in one bit. In noisy images this kind of coding ensures more reliable identification.

The patterns are sequentially projected onto the targeted surface. Such a way for each camera image pixel the corresponding column in the projector image plane can be identified. Afterwards the 3D coordinates can be determined by the intersection of the line of sight corresponding to the pixel and the plane formed by the projected column (row) affecting the pixel (see Fig. 1).

In order to identify the planes the black and white regions of the projected patterns should be extracted from the camera image. This step is performed by subtracting the original image from the image taken when the target was fully illuminated and subsequently applying binarization based on thresholding. In order to increase the

robustness against the influence of external light sources, the pattern sequence is projected in various orientations onto the targeted surface. This first of all ensures more reliable acquisition and higher accuracy (see Fig. 7).

The results obtained by using different orientations of the pattern are averaged. The below diagram illustrates the steps of the reconstruction. The gray box represents the task performed by the camera-projector subsystem. The resulted point cloud is stored in KD-tree structure, which is a binary tree useful to organize finite set of points in the *k*-dimensional space [16] [18].

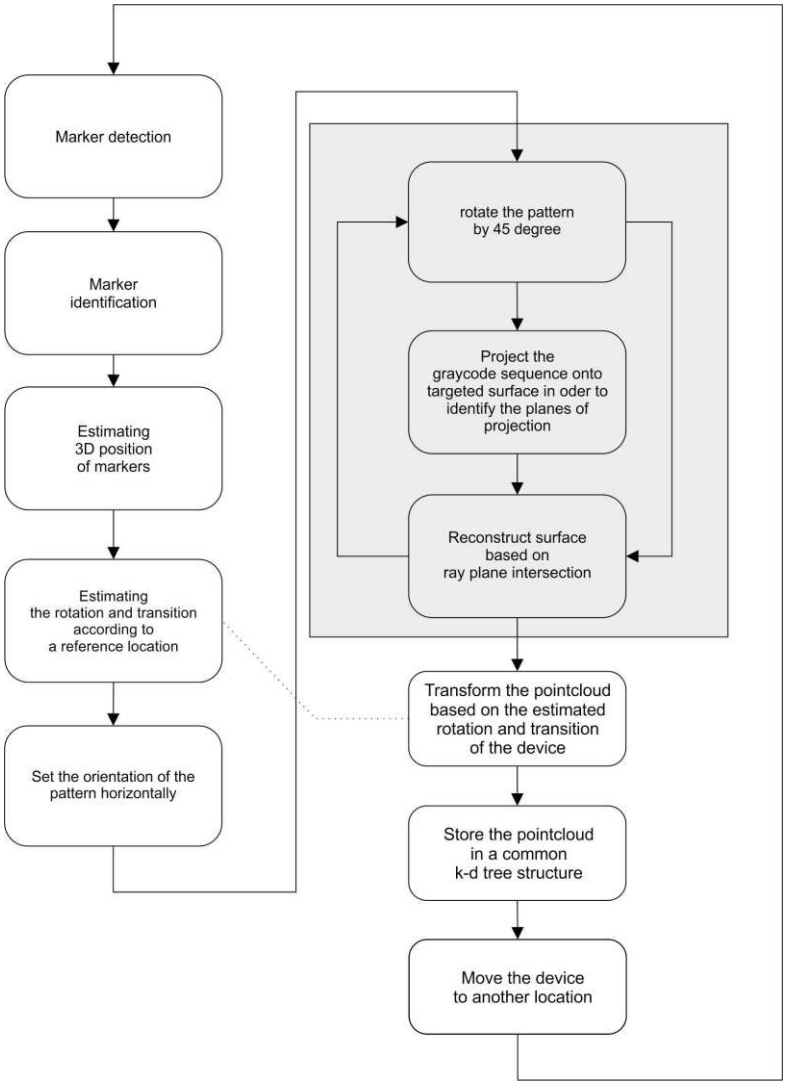

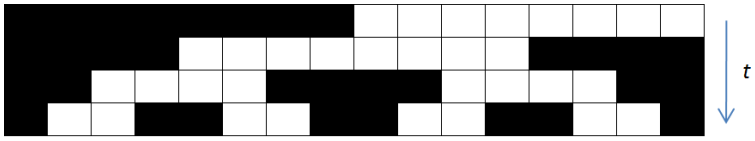

Figure 6
Illustration of a 4 bit gray code sequence. The horizontal patterns are projected onto the targeted surface sequentially (consecutive codes differ in one bit only). In the below example a 10 bit Gray code sequence was used.

Figure 7
Illustration of the projected pattern in different orientations

After relocating the projector-camera subsystem and performing another measurement from the new viewpoint we obtain a new surface segment which is placed in the same k-d tree structure as the segment from the previous measurement. This procedure has to be repeated in order to measure larger surfaces.

6 Results

The result below stands for a point cloud of a car door segment obtained by the proposed system. In Table 1 the specifications of the used hardware can be followed. For visualizing and processing the obtained point cloud data the Point Cloud Library (PCL) has been utilized.

Table 1

Properties	**Value**
Stereo-camera resolution	1024×768 pixels
Probe-camera resolution	1024×768 pixels
Projector resolution	1024×768 pixels
Frame rate	30 FPS
Number of LED markers	5

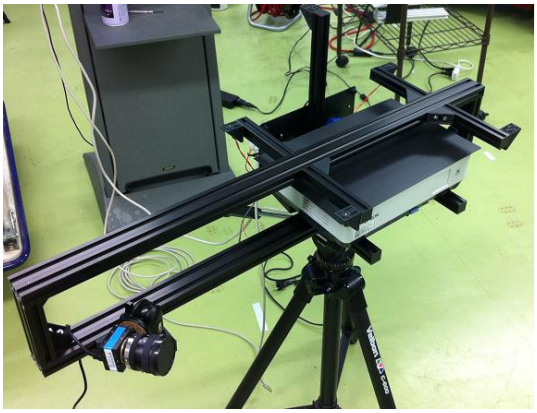

Figure 8
The hardware of the proposed camera-projector subsystem

Figure 9
The targeted surface (car door segment)

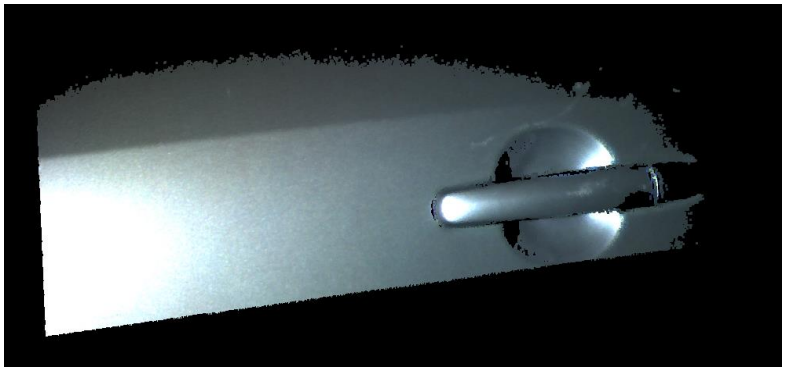

Figure 10
Result of the measured car door segment (View-1)

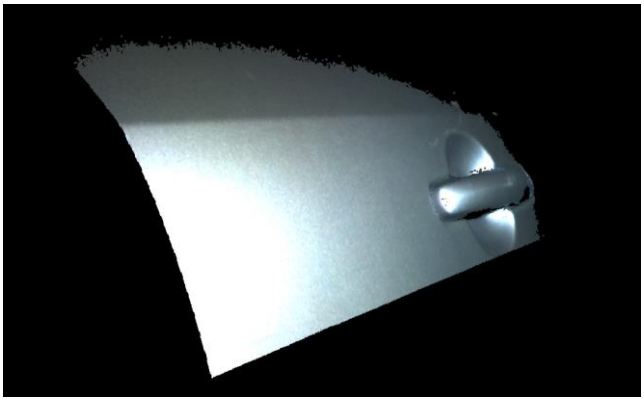

Figure 11
Result of the measured car door segment (View-2)

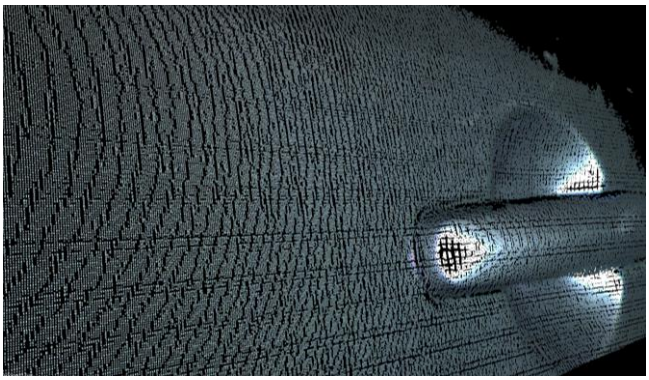

Figure 12
Enlarged point cloud (View-1)

Figure 13
Enlarged point cloud (View-2)

Conclusions and Future work

In the paper a tracked camera-projector based 3D measurement system has been proposed. The system is based on so-called “rotating” gray code pattern projection and a multi-camera based tracking system supporting the measurement of complex and large surfaces, as well. As future work the intensity of the projector light is going to be controlled based on the reflectance properties of the target surface. Thermal camera attached to the camera-projector subsystem will be used to perform higher level analysis of the targeted surface.

Acknowledgement

The project was realized through the support of European Union, with the co-financing of the European Social Fund TÁMOP-4.2.1.B-11/2/KMR-2011-0001

References

[1] M. Young, E. Beeson, J. Davis, S. Rusinkiewicz and R. Ramamoorthi, "Viewpoint-Coded Structured Light", IEEE Computer Society Conference on Computer Vision and Pattern Recognition, pp. 1-8, June 2007

[2] E. Lilienblum, B. Michaelis, "Optical 3D Surface Reconstruction by a Multi-Period Phase Shift Method,” Journal of Computers, Vol. 2, No. 2, pp. 73-83, 2007

[3] N. Karpinsky, S. Zhang, "High-Resolution, Real-Time 3D Imaging with Fringe Analysis," Journal of Real-Time Image Processing, Springer-Verlag, Vol. 7, Issue 1, pp. 55-66, 2010

[4] Yan Cui, Schuon, S., Chan, D., Thrun, S., Theobalt, C., "3D Shape Scanning with a Time-of-Flight Camera," 2010 IEEE Conference on Computer Vision and Pattern Recognition (CVPR), pp. 1173-1180, 13-18 June 2010

[5] Z. Zhang, "A Flexible New Technique for Camera Calibration," *IEEE Transactions on Pattern Analysis and Machine Intelligence*, 22(11):1330-1334, 2000

[6] Radu Horaud and Fadi Dornaika, “Hand-Eye Calibration,” *International Journal of Robotics Research* Vol. 14, No. 3, pp. 195-210, 1995

[7] Fang-Hsuan Cheng; Chien-Te Lu; Yea-Shuan Huang, "3D Object Scanning System by Coded Structured Light," *Electronic Commerce and Security (ISECS), 2010 Third International Symposium on* , Vol., No., pp. 213,217, 29-31 July 2010

[8] Huang Jin; Ma Zi; Hu Ying; Wang Yang, "Robotic 3D Structured Light Scanning System Based on External Axle," *Intelligent Computation Technology and Automation (ICICTA), 2008 International Conference on* , Vol. 1, No., pp. 1126,1129, 20-22 Oct. 2008

[9] H B Wu, Y Chen, M Y Wu, C R Guan and X Y Yu. 3D Measurement Technology by Structured Light Using Stripe-Edge-based Gray Code. Institute of Physics Publishing, 2006

[10] M. Gupta, A. Agrawal, A. Veeraraghavan, and S. G. Narasimhan. 2011. Structured light 3D scanning in the presence of global illumination. In Proceedings of the 2011 IEEE Conference on Computer Vision and Pattern Recognition (CVPR '11) IEEE Computer Society, Washington, DC, USA, 713-720

[11] Hani, A. F M; Khoiruddin, A. A.; Walter, N.; Faye, I.; Mun, T. C., "3D Reconstruction Using Spline Inverse Function Analysis," *Intelligent and Advanced Systems (ICIAS), 2012 4th International Conference on* , Vol. 1, No., pp. 324,327, 12-14 June 2012

[12] Nikolaus Karpinsky and Song Zhang. 2012. High-Resolution, Real-Time 3D Imaging with Fringe Analysis. J. Real-Time Image Process. 7, 1 (March 2012), 55-66

[13] M. Takeda, "Fourier Fringe Analysis and Its Application to Metrology of Extreme Physical Phenomena: a Review [Invited]," Appl. Opt. 52, 20-29 (2013)

[14] P. Huang and S. Zhang, "Fast Three-Step Phase-Shifting Algorithm," Appl. Applied Optics, Vol. 45, Issue 21, pp. 5086-5091 (2006)

[15] Rovid, A.; Szeidl, L.; Yamage, Y.; Takeshi, M.; Hashimoto, T., "Indoor Real-Time 3D Reconstruction of Crash-tested Car Cabins," *Intelligent Systems and Informatics (SISY), 2010 8th International Symposium on* , Vol., No., pp. 257,261, 10-11 Sept. 2010

[16] Li, B.; Holstein, H., "Using k-d Trees for Robust 3D Point Pattern Matching," *In Proc. of the Fourth International Conference on 3-D Digital Imaging and Modeling,* pp. 95-102, 6-10 Oct. 2003

[18] Zhou, Kun and Hou, Qiming and Wang, Rui and Guo, Baining, „Real-Time KD-Tree Construction on Graphics Hardware," *ACM Trans. Graph.*, Vol. 27, No. 5, ISSN 0730-0301, pp. 126:1-126:11, 2008

[19] Fernandez, S.; Salvi, J., "Planar-based Camera-Projector Calibration," *2011 7th International Symposium on Image and Signal Processing and Analysis (ISPA),* pp. 633-638, 4-6 Sept. 2011

Results and Experiences from the Application of Digital Image Correlation in Operational Modal Analysis

František Trebuňa, Róbert Huňady, Zdenko Bobovský, Martin Hagara

Technical University of Kosice, Faculty of Mechanical Engineering, Department of Applied Mechanics and Mechatronics, Letná 9, 042 00 Košice, Slovakia
frantisek.trebuna@tuke.sk, robert.hunady@tuke.sk, zdenko.bobovsky@tuke.sk, martin.hagara@tuke.sk

Abstract: Digital Image Correlation is a modern full-field optical method that is being used for measurement of 3D displacements and surface strains. The correlation systems using the high-speed digital cameras also allow perform dynamic measurements and vibration analysis. The paper deals with possibilities of using the high-speed correlation system Dantec Dynamics Q-450 for determination of modal parameters. Since, the correlation system does not have software tools for the evaluation of such type of measurement, the using of another post-processing application is necessary. The paper describes a conception and the basic functions of the software tool that is being developed for that purpose. The main attention of the paper is focused on Operational Modal Analysis.

Keywords: digital image correlation; Dantec Dynamics Q-450; operational modal analysis; Modan 3D

1 Introduction

Every structure has a tendency to vibrate under certain frequencies. This phenomenon is known as resonance. In the resonance state amplitudes can reach critical values. From this point of view, vibrations which occur in the majority of mechanical systems are undesirable not only because of the increased noise and dynamical stresses that can in some cases lead to malfunction or failure of a structure, but also due to loss of energy and decrease in efficiency. There are many cases known where excessive vibrations of one or several parts of the structure led to their damage or decreasing their lifetime. That is the reason why the dynamic analysis of a structure is part of its design process. After its completion and when putting the structure into operation, it is necessary to experimentally verify the assumptions of the analytical solution.

Experimental estimation of modal parameters from the measured data is known as modal testing or modal analysis. We distinguish two basic types. The first type, Experimental Modal Analysis (EMA), lies in the investigation of the relation between excitation and response of the object in the frequency domain. The second type, Operational Modal Analysis (OMA), allows determine modal parameters by only measuring the response of the structure without using an artificial excitation.

Sensors of acceleration are most often used for the measurement in the experimental testing. Thanks to progress achieved in the area of computer technology, modern optical systems which are becoming more common and increasingly available allow to provide high-speed contactless and blanket measurement of space displacements or velocities of an object. This category of measurement systems includes e.g. laser vibroscanners or digital image correlation.

2 Digital Image Correlation Method

Digital image correlation is an optical method based on correlation principle of a random black and white pattern created on an investigated object, which is sampled by CCD cameras during its loading. This pattern imitates the object contour, deforms and moves with it together. A comparison of acquired digital images, also called correlation, is performed gradually on small image elements called facets (Fig. 1). Minimal facet size is determined by a size of created pattern in such a way that every one facet has to contain white and black color in order to ensure proper correlation. Shape of these image elements use to be squared with usual size from 15x15 to 30x30 pixels [1].

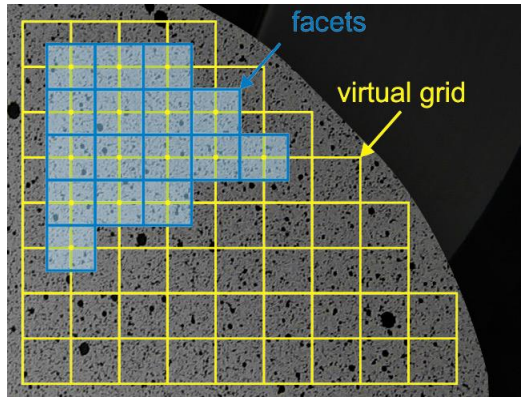

Figure 1
Virtual grid and facets on an object surface with created random black and white pattern

There are various ways to create finer or coarser pattern (using of a spray gun, an easy coating of Xerox toner on wet white surface, a manual painting by indelible ink felt pen or a chemical etching of metal materials), but the easiest and most popular as well is a creation of pattern by white and black spray color [1].

If the sampling process is performed by one CCD camera then the correlation is constrained only for planar objects situated parallel to camera image plane. For this instance it is not possible to perform spatial analysis but only a planar one (Fig. 2).

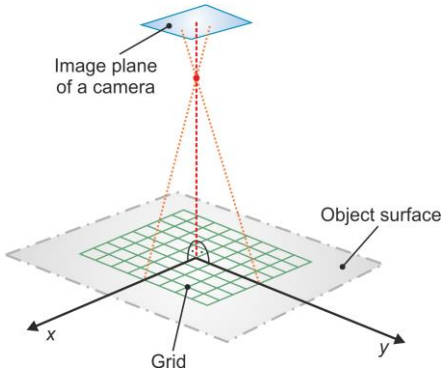

Figure 2
Principle of 2D Digital Image Correlation with one CCD camera

By a spatial analysis minimally a stereoscopic configuration of sensors is necessary. Providing that the object is observed from two different directions, the position of each object point is focused on a specific pixel of corresponding camera image plane (Fig. 3) [2]. If the cameras position, lens magnifications and all image parameters are known, it is possible to calculate the absolute three-dimensional coordinates of each object point and thus make its spatial contour [3].

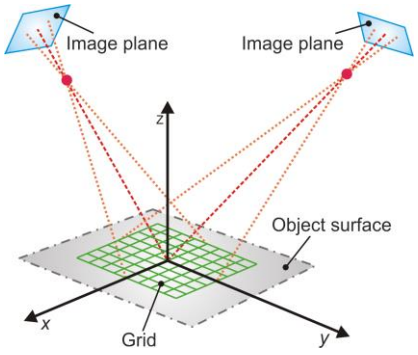

Figure 3
Principle of 3D Digital Image Correlation with two CCD cameras

Dantec Dynamics correlation systems realize calculations with the assistance of correlation algorithm based on pseudo-affine coordinates transformation of object points from one picture to the second one. If $a_0, a_1, \ldots, a_7$ are the transformation parameters of potential translation, stretch, shear and distortion (Fig. 4), the coordinate transformations can be expressed [4, 5]:

$$x_t(a_0, a_1, a_2, a_3, x, y) = a_0 + a_1 x + a_2 y + a_3 x y \tag{1}$$

$$x_t(a_0, a_1, a_2, a_3, x, y) = a_0 + a_1 x + a_2 y + a_3 x y \tag{2}$$

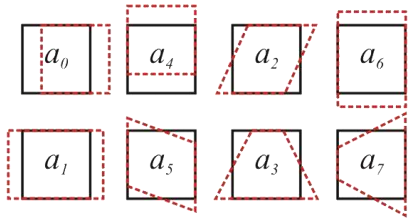

Figure 4
Transformation parameters

These parameters are determined by minimizing the distance between the observed grey pattern $G_2(x, y)$ in the second image and the original pattern $G_1(x, y)$ and by applying the photogrammetric corrections as follows [5]:

$$\min_{a_0, \ldots a_7, g_0, g_1} \sum_{x,y} \left\| G_1(x, y) - G_T(x, y) \right\|. \tag{3}$$

The term $G_T(x, y)$ represents an intensity change of grey points during loading and can be expressed:

$$G_T(x, y) = g_0 + g_1 . G_2(x_t(x, y), y_t(x, y)), \tag{4}$$

where g_0 and g_1 are the illumination parameters.

If the initial contour and displacement vectors of all element points are known, it is possible to compute its strains. Acquisition of strains is ensured either by differentiation of adjoining point displacements or by analysis of local facets curving used by correlation.

3 Background of Operational Modal Analysis

The dynamic behavior of any mechanical system can be described in frequency domain by Frequency Response Functions (FRFs). Consider the model of MDOF system with *N* degrees of freedom. Its FRFs can be written as a function of the complex poles as follows [6, 7]:

$$\mathbf{H}(j\omega) = \sum_{i=1}^{N} \left(\frac{\mathbf{R}_r}{j\omega - \lambda_r} + \frac{\mathbf{R}_r^*}{j\omega - \lambda_r^*} \right), \tag{5}$$

where $\mathbf{H}$ is the matrix of Frequency Response Functions.

The poles are expressed by equation:

$$\lambda_r = \sigma_r + j\omega_r ,$$

where σ_r is the damping factor, and ω_r is the damped natural resonance frequency.

If the poles are considered as eigenvalues of a system, its eigenvectors can be interpreted as the modal shapes, where each eigenvector corresponds with a specific eigenvalue. The residues, $\mathbf{R}_r$ are described by equation [6, 7]:

$$\mathbf{R}_r = \boldsymbol{\Psi}_r \boldsymbol{\gamma}_r^T ,$$

where $\boldsymbol{\gamma}_r$ is the modal participation vector, $\boldsymbol{\Psi}_r$ is the mode shape. All those parameters are specified for the r-th mode.

It is obvious that FRFs depend on the modal parameters, and modal parameters can therefore be extracted from the FRFs.

Frequency response function matrix can also be expressed as the ratio between output (response) and input (excitation) as a function of frequency:

$$\mathbf{H}(j\omega) = \frac{\mathbf{Y}(j\omega)}{\mathbf{X}(j\omega)} . \tag{6}$$

This concept is commonly used in practical applications of Experimental Modal Analysis. Excitation is any form of input that is used to create a response in a structural system. In Experimental Modal Analysis, there is controlled force signal used as input. The most commonly-used excitation signals are harmonic or periodic signals, random signals, impact (impulse) etc.

Operational modal analysis allows obtain a modal model of the system by using only the measured response and without explicitly knowing the excitation input. The relationship between input and output (eq. 6) can be also written in the following form [6, 7]:

$$\mathbf{G}_{yy}(j\omega) = \mathbf{H}(j\omega)^{*}\mathbf{G}_{xx}(j\omega)\mathbf{H}(j\omega)^{T}, \tag{7}$$

where $\mathbf{G}_{xx}(j\omega)$ is the input spectral density matrix and $\mathbf{G}_{yy}(j\omega)$ is the output spectral density matrix. Since $\mathbf{G}_{xx}(j\omega)$ is not known in OMA, it is necessary to make an assumption that input is represented by a white noise that has a flat power spectral density over the entire frequency spectrum [8]. Then spectral density matrix of the measured responses can be expressed as [6, 7]:

$$\mathbf{G}_{yy}(j\omega) = \sum_{r \in sub(j\omega)} \left(\frac{d_r \boldsymbol{\Psi}_r \boldsymbol{\Psi}_r^{T}}{j\omega - \lambda_r} + \frac{d_r^{*} \boldsymbol{\Psi}_r^{*} \boldsymbol{\Psi}_r^{*T}}{j\omega - \lambda_r^{*}} \right), \tag{8}$$

where d_r is a scalar constant and $sub(j\omega)$ is the set of modes that contribute at the particular frequency.

In a practical measurement, output spectral density matrix is defined as follows [6]:

$$\mathbf{G}_{yy}(j\omega) = \begin{bmatrix} g_{11}(j\omega) & g_{12}(j\omega) & \dots & g_{1n}(j\omega) \\ g_{21}(j\omega) & g_{22}(j\omega) & \dots & g_{2n}(j\omega) \\ \vdots & \vdots & \ddots & \vdots \\ g_{n1}(j\omega) & g_{n2}(j\omega) & \dots & g_{nn}(j\omega) \end{bmatrix}_{n \times n}, \tag{9}$$

where each element g_{ij} is a spectral density function. The diagonal elements are the power spectral densities (PSD) of the corresponding response, the off-diagonal elements are the cross spectral densities (CSD) between the individual responses. Output spectral density matrix (for a certain frequency) is Hermitian ($n \times n$), where n being the number of measured responses.

The most important step of operational modal analysis is to extract modal parameters from the measurement data. Brincker et al. introduced method called Frequency Domain Decomposition (FDD) [9-11] that is based on the singular value decomposition of the output PSD matrix:

$$\mathbf{G}_{yy}(j\omega) = \mathbf{U}(j\omega)^{*}\mathbf{S}(j\omega)\mathbf{V}(j\omega)^{H}, \tag{10}$$

where $\mathbf{U}(j\omega)$ and $\mathbf{V}(j\omega)$ are unitary matrices of singular vectors, and $\mathbf{S}(j\omega)$ is a diagonal matrix of singular values. In this special case, $\mathbf{U}(j\omega)$ and $\mathbf{V}(j\omega)$ are identical because $\mathbf{G}_{yy}(j\omega)$ is normal.

This technique allows us to identify possible coupled modes that are often indiscernible in the frequency spectrum. If only one mode is dominating at a particular frequency, then only one singular value will be dominating at this frequency and the corresponding singular vector is an estimate of the mode shape for that resonance frequency. Therefore, the first singular vector is a good

approximation of the mode shape. In the case of close or repeated modes, there will be as many dominating singular values as there are close or repeated modes [6]. The plot of the first four or five singular values depending on frequency is sufficient to detect resonance peaks (Fig. 5). The frequency domain decomposition provides very good results for the resonance frequencies and the mode shapes. It is important to note that the obtained mode shapes are not true mode shapes because residues are not scaled to the input force.

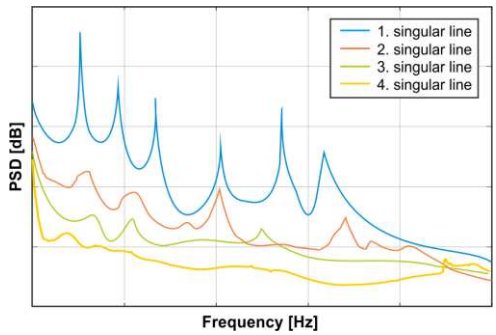

Figure 5
Plot example of singular values

It is also possible to obtain damping characteristics of each mode and more precise resonance frequencies by using the Enhanced Frequency Domain Decomposition (EFDD) based on the determination of the correlation functions [12]. The correlation function is being obtained from the power spectral density function by using the inverse Fast Fourier Transformation [13] and represents the free-decay of an equivalent SDOF oscillator. Fig. 6 shows an example of spectral Bell identification. This is the first step how to obtain a correlation function. Frequency band around the selected peak is defined by using Modal Assurance Criterion (eq. 13) of which value is greater than 0.9 [6-8]. Correlation function subsequently obtained by inverse FFT is shown in Fig. 7.

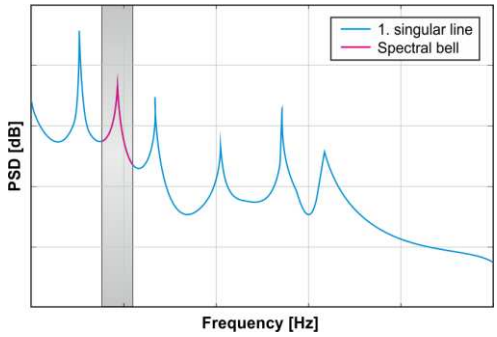

Figure 6
The identification of SDOF Bell function

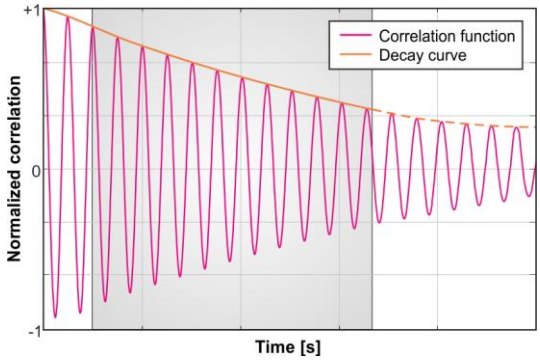

Figure 7
Correlation function of estimated SDOF Bell function

The resonance frequency is simply obtained by counting the number of times the correlation function crosses the zero axis. Damping is estimated by the logarithmic decrement technique and the logarithmic plot of decay curve [12] (Fig. 8). The logarithmic decrement δ is given by the equation [6, 7]:

$$\delta = \frac{2}{n} \ln \left| \frac{r_0}{r_n} \right|, \tag{11}$$

where r_0 is the initial value of the correlation function and r_k is the k-th extreme. Thus, logarithmic decrement and the initial value of the correlation function can be found by linear regression on $k\delta$ and $2\ln|r_n|$. The damping ratio for the mode k is given by the well-known formula [6, 7]:

$$\xi_k = \frac{\delta_k}{\sqrt{\delta_k^2 + 4\pi^2}}. \tag{12}$$

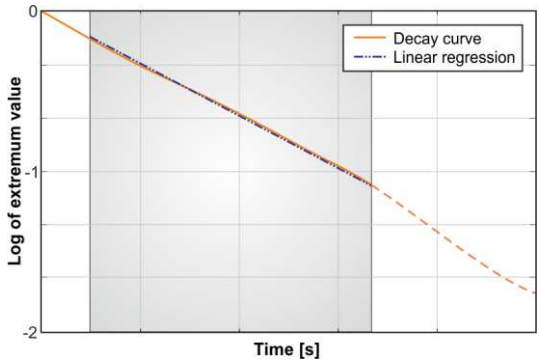

Figure 8
Estimation of damping ratio

As Fig. 8 shows, only the part of the correlation function is used for the estimation, because they are dominated nonlinearities at the beginning and the end of correlation function.

The Modal Assurance Criterion (MAC) can be also used to investigate the validity of estimated modes. MAC is a mathematical tool to compare two vectors to each other. The MAC value between two mode shape vectors $\boldsymbol{\Psi}_r$ and $\boldsymbol{\Psi}_s$ is calculated as [14]:

$$\mathrm{MAC}_{r,s} = \frac{\left|\boldsymbol{\Psi}_r^H \boldsymbol{\Psi}_s\right|^2}{\boldsymbol{\Psi}_r^H \boldsymbol{\Psi}_r \boldsymbol{\Psi}_s^H \boldsymbol{\Psi}_s}. \tag{13}$$

The MAC takes the values from the interval (0, 1). If the MAC is equal to 1, mode shape vectors $\boldsymbol{\Psi}_r$ and $\boldsymbol{\Psi}_s$ are the same mode shape. If they are different the MAC value should be low, due to the orthogonality condition of the mode shapes.

4 Experimental Determination of Modal Parameters by using DIC Method

The using of DIC method in Operational Modal Analysis is based on post-processing of the measurement data. Since, most correlation systems do not have software tools for the evaluation of such type of analysis, it is needed to use another post-proccessing application. Modan 3D is a modal analysis software tool intended for the high-speed digital image correlation system Dantec Dynamics Q-450. It is being developed at the Department of Applied Mechanics and Mechatronics, Faculty of Mechanical Engineering, Technical University of Košice, Slovakia [1, 15, 16].

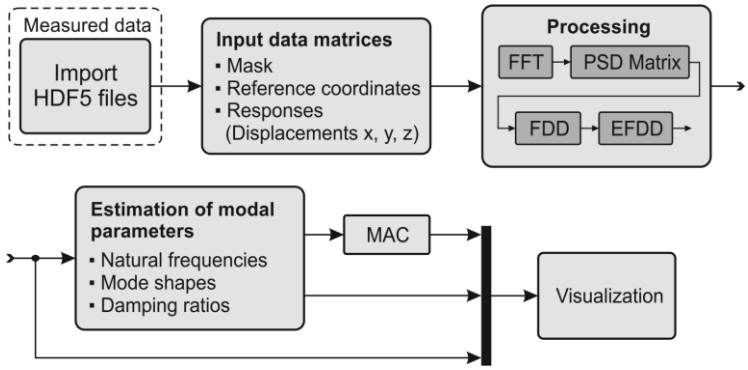

Figure 9
Principle scheme of Modan 3D software as a tool for operational modal analysis

Modan is being programmed in Matlab because of easy transfer and processing of measurement data exported from Istra 4D (software application of the system Q-450). Modan 3D has two main parts, of which one provides the evaluation for operational modal analysis measurements. This part uses functions and algorithms described in the previous chapter. The block diagram in Fig. 9 shows the basic principle of Modan 3D as a tool for operational modal analysis. Measured data exported from Istra4D are contained in the HDF5 files. The number of files corresponds to the number of time data. Each file contains the information about the surface mask and surface point displacements that represent measured responses. Modan enters these data into the relevant matrices. Subsequently, Power Spectral Density Matrix is being obtained by using Fast Fourier Transformation. PSD Matrix is important for the identification and estimation of modal parameters. Modan uses the algorithm of Frequency Domain Decomposition to determine natural frequencies and mode shapes. Damping ratio is being determined by Enhanced Frequency Domain Decomposition. The results of evaluation can be exported in graphical and text form.

The object of measurement was a steel specimen of fan blade shape with thickness of approximately 0.4 mm. The specimen was fixed on the tapering side. For the purposes of image correlation, a black and white speckled pattern was sprayed onto the investigated surface. The specimen was acoustically excited by using the powerful sound system (Fig. 10) and white noise was used as the excitation signal. The measurement has been performed by using the correlation system Q-450 with two IDT NanoSense cameras.

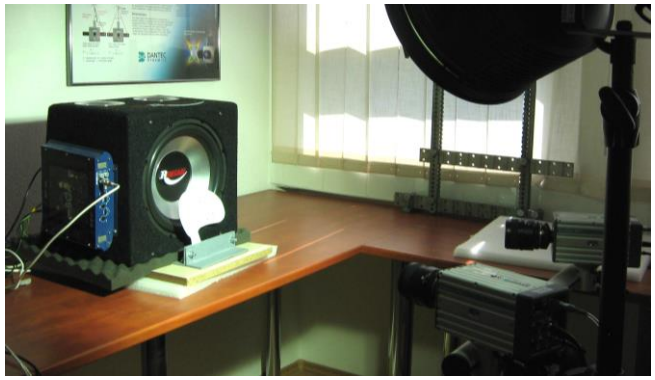

Figure 10
Experimental setup during the measurement

The sampling frequency was 1000 fps and the total acquisition time was 1 second. Coordinates and spatial displacements of all surface points were determined in image correlation process in every single time step. The correlation results have been exported from Istra4D in HDF5 file format and subsequently processed in Modan 3D.

The reference specimen shape shown in Fig. 11 is the result of the image correlation and contains 1831 mesh points. Computer memory size is the limiting factor in creating of spectral density matrices. When we used all points, the only one complete spectral density matrix had more than 1.3 billion elements. For this reason, Modan 3D had to reduce the number of the input data. The size of the matrices used in the experiment was $237 \times 237 \times 500$.

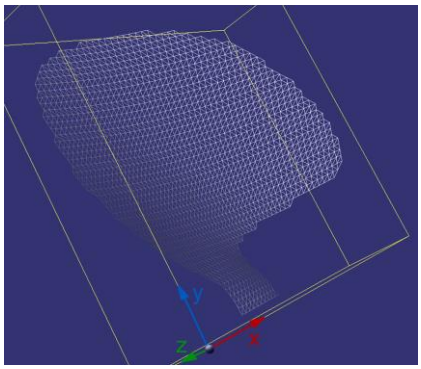

Figure 11
The reference shape of specimen

Fig. 12 shows the first four singular lines obtained by the singular value decomposition of the output spectral density matrix for vibration measured in z-direction. Potential resonance frequencies were determined from the first singular line by peak-picking method. Their mode shapes vectors were subsequently compared to each other by using MAC (Fig. 13).

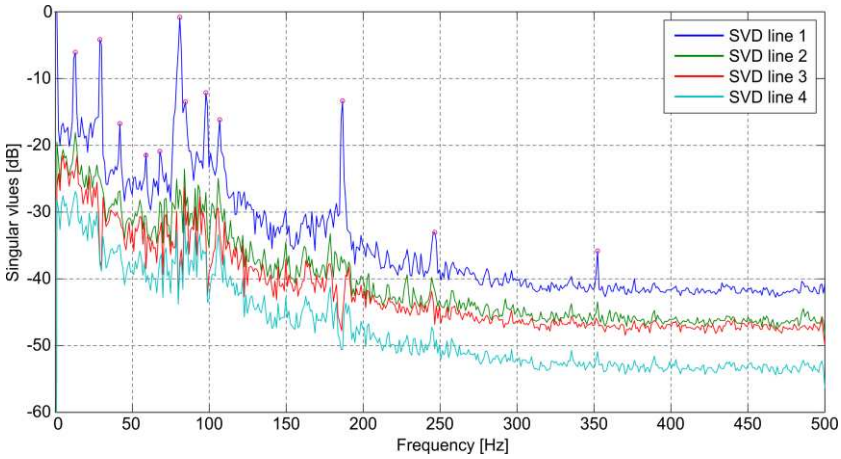

Figure 12
Singular lines for vibration measured in z-direction

Figure 13
Auto MAC matrix

In frequency range up to 500 Hz, there have been identified the first 7 modes. The individual resonance frequencies and their mode shapes obtained by Modan 3D are shown in Tab. 1.

The results of the modal analysis performed in the Modan 3D have been verified by using the finite element method (see Tab. 1). Istra4D allows to export obtained geometry to STL (STereoLithography) file format. Spatial contour of the specimen was imported to SolidWorks as an object of the type "surface". There were defined material properties and thickness of the imported surface. SHELL elements were used to meshing.

Table 1
Resonance frequencies and mode shapes of the specimen

Modan 3D	FEA
1. Mode 12.98 Hz	1. Mode 11.65 Hz
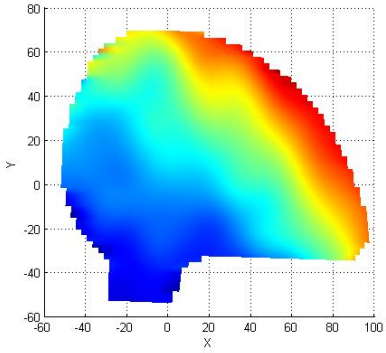	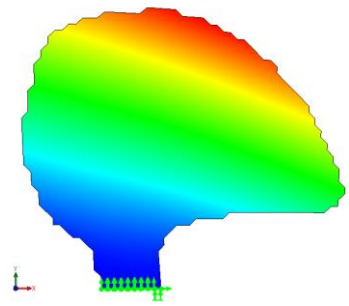

Table 1 (continue)
Resonance frequencies and mode shapes of the specimen

2. Mode 28.94 Hz	2. Mode 29.97 Hz
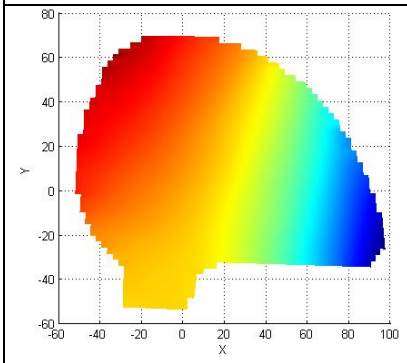	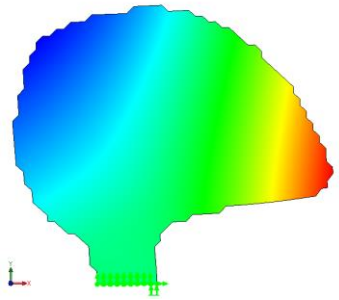
3. Mode 80.84 Hz	3. Mode 75.71 Hz
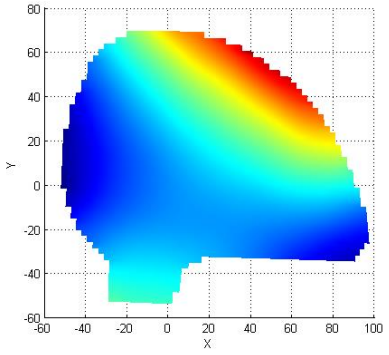	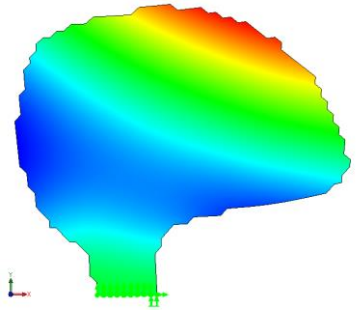
4. Mode 97.8 Hz	4. Mode 96.02 Hz
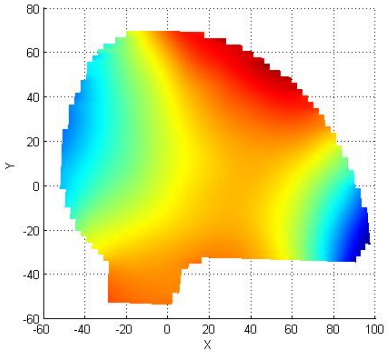	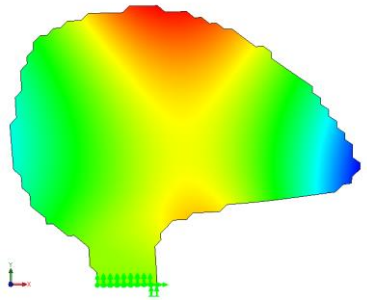

Table 1 (continue)
Resonance frequencies and mode shapes of the specimen

5. Mode 186.6 Hz	5. Mode 194.3 Hz
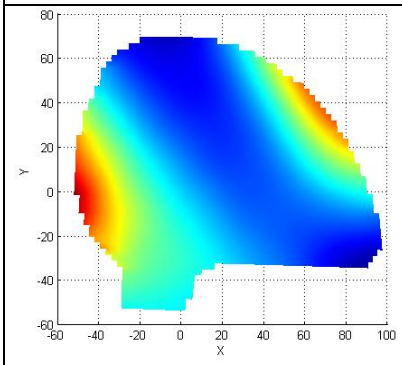	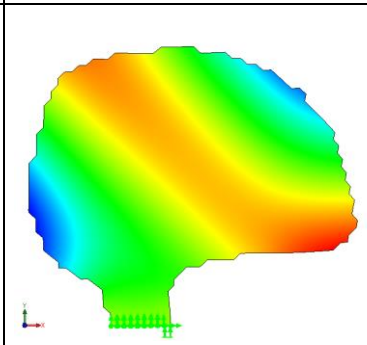
6. Mode 246.5 Hz	6. Mode 249.7 Hz
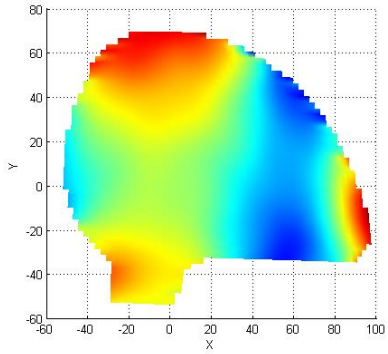	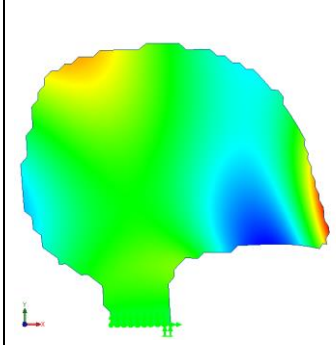
7. Mode 351.3 Hz	7. Mode 365.9 Hz
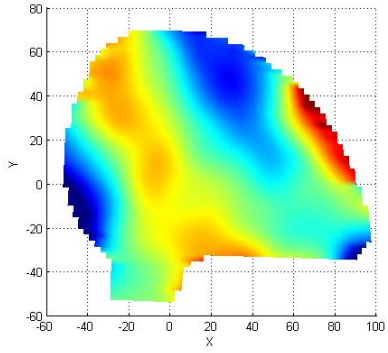	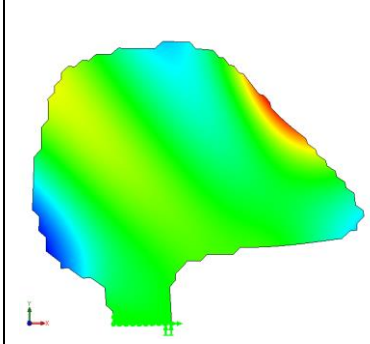

Modal parameters obtained by the measurement are in relatively good agreement with the results of numerical analysis. The differences in the mode shapes and frequency values may be caused by the fact that boundary conditions considered in the simulation are ideal – not real. In addition, the accuracy of the measurement depends on the measurement system sensitivity and on the parameters of FFT analyzer.

Conclusions

The flexible design of digital image correlation systems opens a wide range of their applications. Due to rapid new developments in high resolution digital cameras and computer technology, systems with high-speed cameras have proven to be a flexible and useful tool for vibration analysis and dynamic measurements. But, the full utilization of DIC method in Operational Modal Analysis or Experimental Modal Analysis requires the use of appropriate software application for the post-processing of the measurement data. In the paper, there was described a software tool called Modan 3D that is able to determine modal parameters by using the system Q-450. Modan 3D is actually not finished as well as some functions mentioned in the paper. There is needed to finalize algorithms for damping ratio estimation, perform complex verification of evaluation results and create a Graphical User Interface.

Acknowledgement

This work is supported by the projects VEGA 1/0937/12, VEGA 1/0289/11 and APVV-0091-11.

References

[1] M. Hagara, F. Trebuňa, R. Huňady, M. Kalina, M. Schrötter: Experimental Identification of Modal Parameters of Thin Metal Sheets by Using of DIC. In: Procedia Engineering 48, 2012, pp. 180-188

[2] M. Kalina, F. Šimčák, M. Hagara, M. Schrötter, M. Štamborská: The Use of the Experimental Optical Technique for Investigation of Shear Strains of the Samples Exposed to Shear Stress Beyond the Yield Point. In: Procedia Engineering 48, 2012, pp. 264-272

[3] C. Dudescu, A. Botean, M. Hardau: Application of Digital Image Correlation for Measuring E-Modulus of Wood Beams. In. Annals of DAAAM for 2009 & Proceedings of the 20th International DAAAM Symposium, Vol. 20, No. 1, Vienna, Austria, 2009

[4] T. Siebert, K. Splitthof, S. Stecklum, Ch. Herbst: New Features in Digital Image Correlation Techniques. In: 22nd Danubia-Adria Symposium on Experimental Methods in Solid Mechanics, Parma, Monticelli Terme, 2005

[5] T. Siebert, T. Becker, K. Splitthof: Analysis of Advanced Materials under Load. In: SPIE – The International Society for Optical Engineering, November 2006, SPIE Newsroom <http://spie.org/x8594.xml>

[6] M. Batel: Operational Modal Analysis – Another Way of Doing Modal Testing. In: Sound and Vibration, August, 2002, pp. 22-27 <http://www.sandv.com/downloads/0208batl.pdf>

[7] B. MacMillan, M. Batel, E. Dascotte, B. Verbeeck: OMA Testing by SLDV with FEM Pre- and Post-Test Analysis. In: Proceedings of the 22th International Modal Analysis Conference (IMAC), January 2004, Detroit, Michigan <http://www.femtools.com/download.php?id=imac2004b&dl=no>

[8] C. Rainieri, G. Fabbrocino, G. Manfredi, M. Dolce: Robust Output-Only Modal Identification and Monitoring of Buildings in the presence of Dynamic Interactions for Rapid Post-Earthquake emergency Management. In: Engineering Structures 34, 2012, pp. 436-446

[9] R. Brincker, C. E. Ventura, P. Andersen: Damping Estimation by Frequency Domain Decomposition. In: Proceedings of IMAC 19: A Conference on Structural Dynamics, Hyatt Orlando, Kissimmee, Florida, 2001, Society for Experimental Mechanics, 2001. pp. 698-703

[10] R. Brincker, L. Zhang, P. Andersen: Modal Identification From Ambient Responses Using Frequency Domain Decomposition. In: Proceedings of The 18th International Modal Analysis Conference (IMAC), San Antonio, Texas, 2000, pp. 625-630

[11] N. J. Jacobsen, P. Andersen, R. Brincker: Using EFDD as a Robust Technique to Deterministic Excitation in Operational Modal Analysis. In: Proceedings of The 2nd International Operational Modal Analysis Conference (IOMAC), Copenhagen, Denmark, 2007

[12] F. Gomaa, M. Tayel, K. Kandil, G. Hekal: Validation Study Illustrates the Accuracy of Operational Modal Analysis Identification. In. International Journal of Emerging Technology and Advanced Engineering, Vol. 2, Issue 11, November 2012 <http://www.ijetae.com/files/Volume2Issue11/IJETAE_1112_103.pdf>

[13] E. Reynders: System Identification Methods for (Operational) Modal Analysis: Review and Comparison. In: Archives of Computational Methods in Engineering, Vol. 19, Issue 1, March 2012 pp. 51-124

[14] R. J. Allemang: The Modal Assurance Criterion – Twenty Years of Use and Abuse. In: Sound and Vibration, August, 2003, pp. 14-21

[15] R. Huňady, M. Hagara, M. Schrötter: Using High-Speed Digital Image Correlation to determine the Damping Ratio. In: Procedia Engineering 48, 2012, pp. 242-249

[16] F. Trebuňa, R. Huňady, Z. Bobovský, M. Hagara: An Application of High-speed Digital Image Correlation in Determination of Modal Parameters. In: Acta Mechanica Slovaca, Vol. 15, No. 4, 2011, pp. 6-12

Double Fuzzy Point Extension of the Two-step Fuzzy Rule Interpolation Methods

Zoltán Krizsán, Szilveszter Kovács

University of Miskolc
Egyetemváros
3515 Miskolc, Hungary
krizsan@iit.uni-miskolc.hu, szkovacs@iit.uni-miskolc.hu

Abstract: The "Double Fuzzy Point" rule representation opens a new dimension for expressing changes of fuzziness in fuzzy rule-based systems. In the case of standard "Fuzzy Point" rule representations, it is difficult to describe fuzzy functions in which crisp observations are required to have fuzzy conclusions, or in which an increase in the fuzziness of observations leads to reduced fuzziness in conclusions. These problems are mainly due to a lack of information. A fuzzy point rule determines the connection between a pair of fuzzy sets taken from the domain and the range of the rule. Expressing the fuzzy function through a set of fuzzy points and fuzzy interpolation between pairs of those points, each fuzzy point can be considered as a node point with given location and fuzziness. In common, sparse rule-base definitions, these node points are usually disjunctive on the domain, defining only single antecedent-consequent fuzziness connections at the location of the fuzzy points. However, this kind of information is insufficient when the goal is to express changes in the fuzziness of a given location in the domain. One solution to this problem is the double fuzzy point rule representation concept. Double fuzzy points are pairs of fuzzy points which share the same reference locations, but have different fuzziness properties. The existence of two different fuzziness values in a single location within the domain creates new possibilities for introducing fuzzy interpolation methods capable of interpolating not only between locations, but between changes in local fuzziness values as well. The main goal of this paper is to discuss how two-step Fuzzy Rule Interpolation methods can be adapted to be able to handle the double fuzzy point concept. To this end, an approach referred to as the Generalized Double Fuzzy Point Methodology (GDFPM) is proposed.

Keywords: fuzzy rule interpolation; interpolation of the fuzziness; fuzzy function; double fuzzy point rule representation

1 Introduction

There are numerous Fuzzy Rule Interpolation (FRI) methods which have appeared in the literature. One of the first methods was published by Kóczy and Hirota (KH method [1]). The KH method can only handle convex and normal fuzzy (CNF) sets in single dimensional antecedent universes, determining the conclusion from the α-cuts of the two rules which immediately surround the observation. The KH method inspired many subsequent approaches, such as the modified α-cut based interpolation (MACI) method [2]. MACI transforms fuzzy sets into vector representations, computes the conclusion based on those representations, and finally transforms the conclusion back to the original space. The first FRI method capable of explicitly dealing with "fuzziness" appeared in the "conservation of relative fuzziness" (CRF) method, which was proposed by Kóczy et al. in [3] for single antecedent dimensions. CRF uses the two closest surrounding rules to the observation. It stipulates that the rate of the left (right) fuzziness of the conclusion and the fuzziness of the rule consequents should be the same as the rate of the right (left) fuzziness of the observation and the fuzziness of the two surrounding rule antecedents. A multidimensional extension of the CRF method, known as IMUL, was proposed in [4] ("An improved fuzzy interpolation technique for multidimensional input spaces"). IMUL is a combination of CRF and the multidimensional MACI methods.

In parallel with these developments, a rather different two-step method was proposed by Bouchon-Meunier et al. [5], [6]. At the first step their "analogy-based interpolation" calculates the reference point of the conclusion. This step is simple interpolation based on the reference point distances of the observation and the rule antecedents. In the second step the FRI method constructs the shape of the conclusion according its similarity (distinguishability) to the rule consequents to be the same as the similarity (distinguishability) of the corresponding rule antecedents and the observation. Another two-step method concept is presented in the "General Methodology" (GM suggested by Baranyi et al. in [7]). GM extends the first step of the original analogy-based interpolation to the generation of interpolated "intermediate rules" in the reference point position of the observation. In the second step, a single rule reasoning method (revision function) is applied to determine the final fuzzy conclusion based on the similarity of the fuzzy observation and an "interpolated" observation. In this way, GM can handle arbitrarily shaped fuzzy sets. An extension of GM appeared in the work of Shen et al. [8]. The suggested "scale and move transformation" extends GM with extrapolation. Practical applications of GM appear in the "Least Squares Method" ("LESFRI"), in the "FRI based on Subsethood Values" ("FRISUV") as well as in the "Polar a Cut" interpolation ("FRIPOC") suggested by Johanyák et al. in [9], [10], [11] and [12]. As a single rule reasoning step FRIPOC calculates the similarity of fuzzy sets based on their polar cuts.

In the remainder of the paper, the above "two-step" methods will be studied in detail, with the goal of extending them to be able to adopt the "double fuzzy" point rule representation concept. An improvement, referred to as the Generalized Double Fuzzy Point Methodology (GDFPM), is proposed for the case of SISO Mamdani fuzzy systems (i.e., Mamdani systems with one input and one output dimension).

Many of the above mentioned FRI methods and a sparse fuzzy model identification tool are available as open source code MATLAB Toolbox (Johanyák et al. [13], [14], [15]). Systematic model-based fuzzy control approaches are presented in [16].

2 Definitions and Notations

This section introduces elementary definitions and concepts and notations utilized in later parts of the paper. Scalar values are denoted by lowercase letters, e.g. $\{a, b, c, ratio, \dots\}$; fuzzy sets are denoted by capital letters, e.g. $\{A, B, P, Q, \dots\}$; and the letter R is reserved to denote fuzzy rules of the form IF x=A , THEN y=B, or $R: A \rightarrow B$ for short. The letters X, Y, and S are reserved for the input–output universes and for the third dimension of geometrical representations, respectively (see later). x and y are used to denote the observation and the conclusion. Antecedent fuzzy sets are denoted by A ($A \in L^X$); consequent sets by B ($B \in L^Y$) where L^X and L^Y are fuzzy spaces on X and Y, respectively.

There are some common concepts which are followed by all of the FRI methods when calculating the similarity between fuzzy sets. Many of the FRI methods define similarity as distances in every important α value ($\alpha = [0..1]$) of the α-cuts. As this similarity concept requires all of the α-cuts to be known in advance, its use is restricted to CNF sets (e.g. LESFRI [9]). Another possible fuzzy set similarity calculation is based on the polar coordinate system and polar cuts. This method has the advantage that it is also suitable for calculating the similarity of subnormal fuzzy sets. The FRIPOC method, introduced by Johanyák in [10], is currently the only FRI method in the literature which uses this technique. The method calculates the consequent for every θ angle ($0 \leq \theta \leq 180$) in the domain where the reference point of the fuzzy set (e.g. the centre of the core, or the centre of gravity) is also the reference point of the polar coordinate system. Further methods for calculating the similarity of fuzzy sets include the "scale and move transformation" [8], which is based on the parameters of scaling and translation necessary to transform one fuzzy set into the shape of the other.

It can be stated that at the moment there is no common, universally accepted method used to represent the similarity of two arbitrarily shaped fuzzy sets. In the remainder of the paper, methods applying α-cuts and polar cuts for similarity calculations will be studied in more detail.

Finally, there are some common guidelines followed by all of the FRI methods, which make up the "axiomatic approach of fuzzy interpolation" (an overview can be found in [17], [18] and [19]). Two of these axioms – "avoiding invalid conclusions" and "preserving linearity" – will be studied in this paper. The axiom of "avoiding invalid conclusions" (also referred to as "validity of the mapping" in [19]) stipulates that the conclusion generated by the FRI method should be a valid fuzzy set. The axiom of "preserving linearity" (also referred to as "shape invariance of the mapping" in [19]) stipulates that the conclusion generated by the FRI should have a piecewise linear shape, provided that the observation is based on linguistic terms with piecewise linear shapes.

Definition 1 (fuzziness): Several fuzziness definitions can be found in the literature. An easily interpretable definition was introduced by Kóczy, Hirota and Gedeon in [3] in the following form:

$$f_{A,L} = inf\{[A]_1\} - inf\{[A]_{0+}\}, \quad (1)$$

$$f_{A,U} = sup\{[A]_{0+}\} - sup\{[A]_1\}, \quad (2)$$

where $f_{A,L}$ and $f_{A,U}$ are the "lower" and "upper" fuzziness values, $[inf\{[A]_1\}, sup\{[A]_1\}]$ is the core, and $[inf\{[A]_{0+}\}, sup\{[A]_{0+}\}]$ is the support of fuzzy set A.

In later parts of this paper, the concept of fuzziness will be used in terms of definition 1.

Definition 2 (double fuzzy point rule): A double fuzzy point rule consists of two overlapping fuzzy rules (P,Q) with the same reference points [20].

3 The Double Fuzzy Point Rule Representation

A number of Fuzzy Rule Interpolation (FRI) methods exist which use a variety of different computational concepts, but most of them handle changes in fuzziness in similar ways. This is because of the "Monotonicity" condition, which was first defined in [18] (condition "I2") for the single dimensional antecedent case, and was extended in [19] ("Property 6.") to multidimensional antecedents in the following manner: If $f_{A^*I} < f_{A^*II}$ in all dimensions (such that A^*I is more specific than A^*II) then $f_{B^*I} < f_{B^*II}$ holds as well. According to the condition, it is not possible to reverse changes of fuzziness in the conclusion. Moreover, a singleton conclusion $f_{B^*I} = 0$ can be gained only if the observation is a singleton as well (i.e., $f_{A^*I} = 0$).

The "double fuzzy point" rule representation was proposed in [20] in order to extend the classical fuzzy point concept so that changes of fuzziness in fuzzy rules could also be expressed. The "double fuzzy point" rule is an extension of the single fuzzy point rule representation to two overlapping fuzzy rules (cf.

Definition 1). The fuzzy rule pairs share the same reference points, i.e. in both rules, the corresponding antecedent and consequent fuzzy sets have the same reference points, but apart from this condition, they can have different fuzziness properties. Differences in antecedent fuzziness define the domain, and differences in consequent fuzziness define the range of the fuzziness interpolation [20].

The i[th] rule of the double fuzzy point rule representation has the following form:

$$A_i^{p,q} \rightarrow B_i^{p,q}, \tag{3}$$

which combines two overlapping fuzzy rules: $A_i^p \rightarrow B_i^p$ and $A_i^q \rightarrow B_i^q$, such that both the antecedent and the consequent fuzzy sets in the overlapping rules have the same reference point. Details depend on the way in which reference points are defined, e.g. in triangular linguistic terms the reference point might be the core of the fuzzy set. In this case, the conditions core(A_i^p) = core(A_i^q), core(B_i^p) = core(B_i^q) would hold (see e.g. on Fig. 1 and on Fig. 2).

Based on the above, the double fuzzy point rule-base $R^{p,q}$ can be considered as the superposition of two overlapping rule-bases, R^p and R^q.

According to the double fuzzy point rule representation concept [20], fuzziness interpolation requires an observation A^* within the fuzziness domain of the double fuzzy point rule:

$$f_{A^*} \in [f_{A^q}, f_{A^p}] \tag{4}$$

and it generates a conclusion B^* within the fuzziness range of the double fuzzy point rule:

$$f_{B^*} \in [f_{B^q}, f_{B^p}] \tag{5}$$

Depending on the p, q part of the double fuzzy point rule, the direction of change in fuzziness can remain the same, or may be reversed. The direction of change in fuzziness remains the same (see e.g. on Fig. 1) if:

$$f_{A^q} \leq f_{A^*} \leq f_{A^p} \text{ and } f_{B^q} \leq f_{B^*} \leq f_{B^p}, \tag{6}$$

or

$$f_{A^q} \geq f_{A^*} \geq f_{A^p} \text{ and } f_{B^q} \geq f_{B^*} \geq f_{B^p}, \tag{7}$$

The direction of change in fuzziness is reversed (see e.g. on Fig. 2) if:

$$f_{A^q} \leq f_{A^*} \leq f_{A^p} \text{ and } f_{B^q} \geq f_{B^*} \geq f_{B^p}, \tag{8}$$

or

$$f_{A^q} \geq f_{A^*} \geq f_{A^p} \text{ and, } f_{B^q} \leq f_{B^*} \leq f_{B^p}. \tag{9}$$

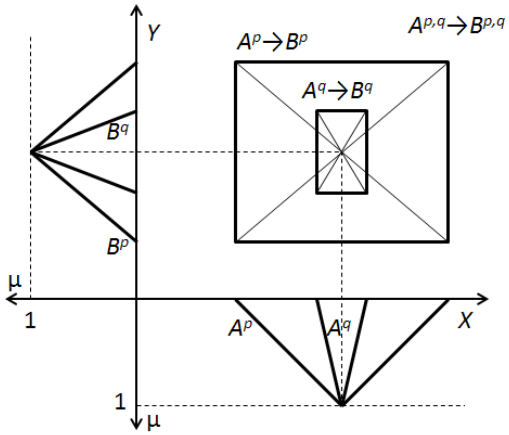

Figure 1

"Double fuzzy point" rule representation when the direction of change in fuzziness remains the same [20]

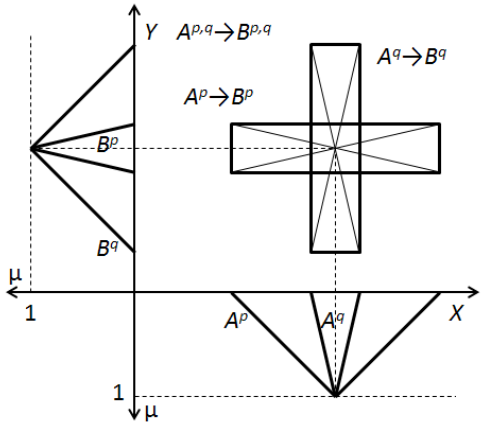

Figure 2

"Double fuzzy point" rule representation when the direction of change in fuzziness is reversed [20].

4 Double Fuzzy Point Extension of Two Step FRI Methods

In this section, a novel extension of the two-step FRI method concept (following the generalized methodology [7]) is introduced to support double fuzzy point rule representations. Some additional properties of the newly obtained family of two-step double fuzzy point FRI methods are also examined, such as the validity of the conclusion and the preservation of linearity.

The proposed "Generalized Double Fuzzy Point Methodology" (GDFPM) can be applied as a guideline for the double fuzzy point adaptation of any two-step FRI method.

GDFPM can be used to extend any two-step FRI method with the ability to handle the $R^{p,q}$ double fuzzy point rule-base, and with a special additional step enabling the interpolation of fuzziness for the final conclusion. As GDFPM is based on two-step FRI methods, the limitations and preconditions of the original two-step FRI method used will be inherited by GDFPM.

The first step of two-step FRI methods is the generation of a temporal interpolated fuzzy rule at the reference point of the observation. In the case of double fuzzy point extended FRI methods (GDFPM), a temporal interpolated fuzzy rule pair is generated, one for each of the two fuzzy rule sets R^p and R^q in the position of the observation. If the observation is within the fuzziness domain (4) covered by the antecedent fuzzy sets A_i^p, A_i^q in every input dimension, then the fuzzy conclusion can be obtained through interpolation. In other cases, the fuzzy conclusion can be considered as an extrapolation of fuzziness. In this paper, extrapolation is not discussed.

The second step of the GDFPM method proposed here is the determination of the conclusion based on the observation (A^*) and the temporal interpolated rule pair ($A_i^p \rightarrow B_i^p, A_i^q \rightarrow B_i^q$) generated in the previous step. The concept of double fuzzy rule representation suggests that the property of "fuzziness similarity ratio preservation" should hold between the triplets A_i^p, A^*, A_i^q and B_i^p, B^*, B_i^q. Therefore, as a final step of GDFPM, the single rule reasoning step of the original two-step method is replaced with a new "fuzziness similarity ratio preservation reasoning" step.

The "fuzziness similarity ratio preservation reasoning" step is an extension of the common single rule reasoning concept. Rather than preserving the fuzzy similarity of the observation and the rule antecedent to the conclusion and the rule consequent, it preserves the fuzziness similarity ratio of the observation and the two antecedents of the double fuzzy rule to the conclusion and the two corresponding consequents. Generally speaking, the fuzziness similarity ratios must be equal on both the antecedent and the consequent sides:

$$fuzzinessRatio(A^{p,q}, x) = fuzzinessRatio(B^{p,q}, y). \quad (10)$$

This "fuzziness similarity ratio" is calculated in the same manner in which fuzzy similarity was calculated in the single rule reasoning step of the original two-step method, but this time it is calculated based on the double fuzzy rule. Therefore, as discussed earlier, the interpretation of the similarity ratio preservation strongly depends on the FRI technique used. In the following, the previously mentioned α-cut based and polar cut based fuzzy similarity calculations will be studied in more detail.

When using α-cut based methods (e.g. LESFRI [9], [10]), the similarity ratio can be determined based on the rate of α-cut distances (d_α) (see Fig. 3):

$$fuzzinessRatio_L(A^{p,q},x)_\alpha = \frac{d_\alpha(K^p_{AL},K_{xL})}{d_\alpha(K_{xL},K^q_{AL})}, \tag{11}$$

$$fuzzinessRatio_U(A^{p,q},x)_\alpha = \frac{d_\alpha(K^p_{AU},K_{xU})}{d_\alpha(K_{xU},K^q_{AU})},$$

where "*L*" denotes the lower, and "*U*" denotes the upper α-cut endpoint distances.

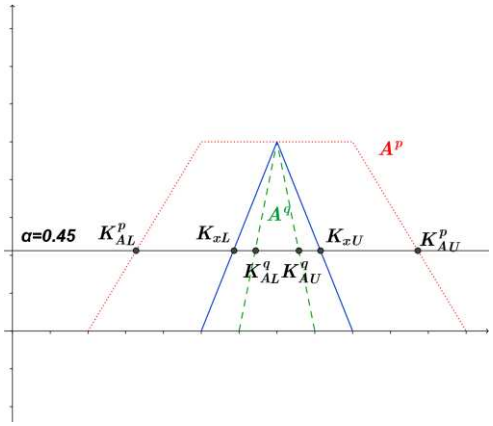

Figure 3
"α-cut based" fuzziness similarity ratio

When using polar cut based methods (e.g. FRIPOC [12]), the similarity ratio can be determined based on the rate of polar distances (d_θ) (see Fig. 4):

$$fuzzinessRatio(A^{p,q},x)_\theta = \frac{d_\theta(K^p_A,K_x)}{d_\theta(K_x,K^q_A)} \tag{12}$$

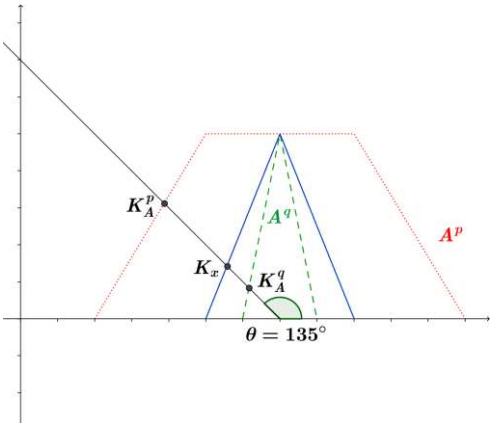

Figure 4
"Polar cut based" fuzziness similarity ratio

Finally, the conclusion y can be determined based on requirement of equality between the antecedent and consequent side fuzziness similarity ratios. In the case of α-cut based methods (see e.g. on Fig. 5 and Fig. 6):

$\forall \alpha \in (0,1]$:

$$fuzzinessRatio(B^{p,q}, y)_\alpha = fuzzinessRatio(A^{p,q}, x)_\alpha, \tag{13}$$

$$\frac{d_\alpha(K^p_{BL}, K_{yL})}{d_\alpha(K_{yL}, K^q_{BL})} = \frac{d_\alpha(K^p_{AL}, K_{xL})}{d_\alpha(K_{xL}, K^q_{AL})}, \tag{14}$$

$$\frac{d_\alpha(K^p_{BU}, K_{yU})}{d_\alpha(K_{yU}, K^q_{BU})} = \frac{d_\alpha(K^p_{AU}, K_{xU})}{d_\alpha(K_{xU}, K^q_{AU})}.$$

In the case of polar cut based methods (see e.g. on Fig. 7 and Fig. 8):

$\forall \theta \in [0°, 180°]$:

$$fuzzinessRatio(B^{p,q}, y)_\theta = fuzzinessRatio(A^{p,q}, x)_\theta \tag{15}$$

$$\frac{d_\theta(K^p_B, K_y)}{d_\theta(K_y, K^q_B)} = \frac{d_\theta(K^p_A, K_x)}{d_\theta(K_x, K^q_A)}. \tag{16}$$

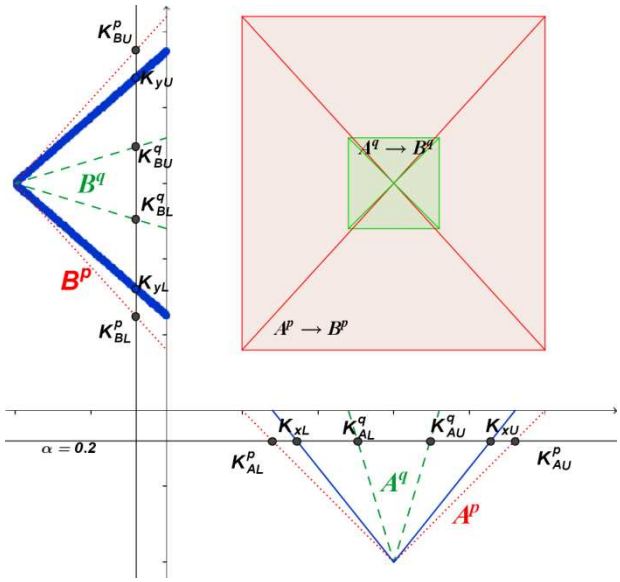

Figure 5

An example of the GDFPM α-cut based fuzziness similarity ratio preservation reasoning step, in which the conclusion is valid, and the direction of change in fuzziness remains the same

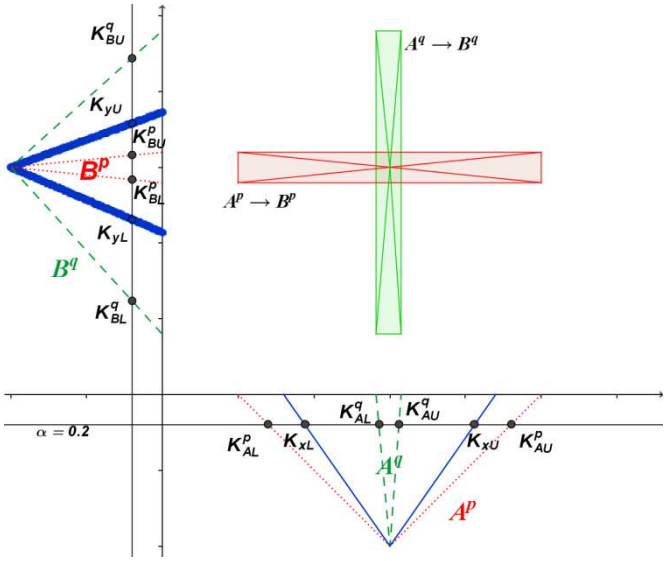

Figure 6

An example of the GDFPM α-cut based fuzziness similarity ratio preservation reasoning step, in which the conclusion is valid, and the direction of change in fuzziness is reversed

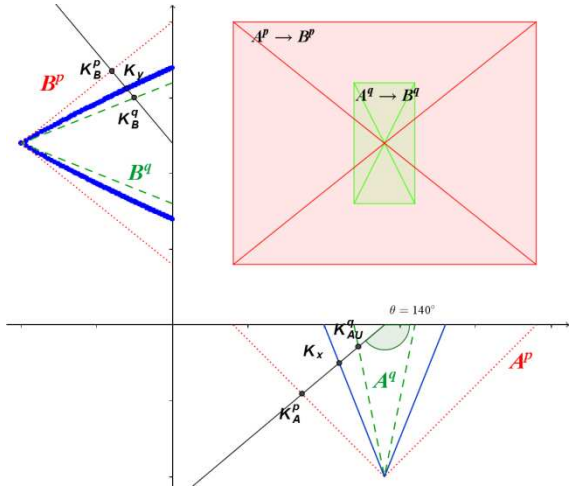

Figure 7

An example of the GDFPM polar cut based fuzziness similarity ratio preservation reasoning step, in which the conclusion is valid, and the direction of change in fuzziness remains the same

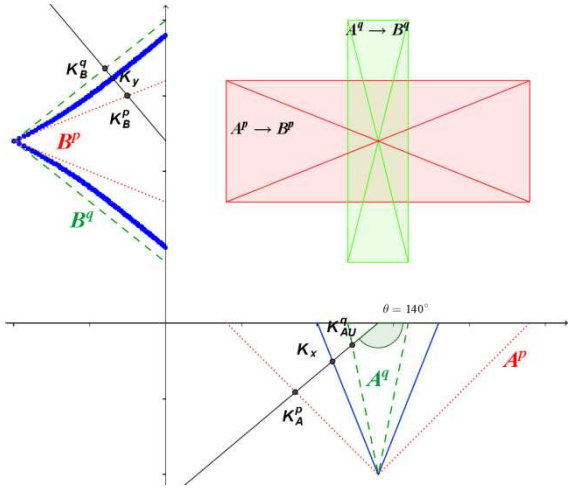

Figure 8

An example of the GDFPM polar cut based fuzziness similarity ratio preservation reasoning step, in which the conclusion is valid, and the direction of change in fuzziness is reversed

4.1 Validity and Shape of the Conclusion

The aim of this section is to briefly check the validity and the shape of the conclusion, i.e. to check whether or not the generated conclusion is a valid fuzzy set in general, and whether or not it preserves the piecewise linear shape of the terms. The validity of a fuzzy set can be defined as the validity of the membership function [19]. A fuzzy set A is valid if:

$$\forall \alpha, \alpha_1 < \alpha_2 \in (0,1]: inf\{[A]_\alpha\} \leq sup\{[A]_\alpha\} \text{ and} \quad (17)$$

$$inf\{[A]_{\alpha_1}\} \leq inf\{[A]_{\alpha_2}\} \text{ and } sup\{[A]_{\alpha_2}\} \leq sup\{[A]_{\alpha_1}\}.$$

Remark 1 The conclusion of GDFPM is not always valid. See e.g. the example on Fig. 9.

Remark 2 GDFPM does not preserve the piecewise linear shape of the terms. See e.g. the examples on Figs. 8, 10, 11 and 12.

Remark 3 In the α-cut based GDFPM fuzziness similarity ratio preservation reasoning step, if all fuzzy sets involved (i.e., rule antecedents, consequents and the observation) are restricted to normal triangular shaped membership functions, the conclusion will also be a valid triangular shaped fuzzy set. See e.g. the examples on Figs. 5 and 6.

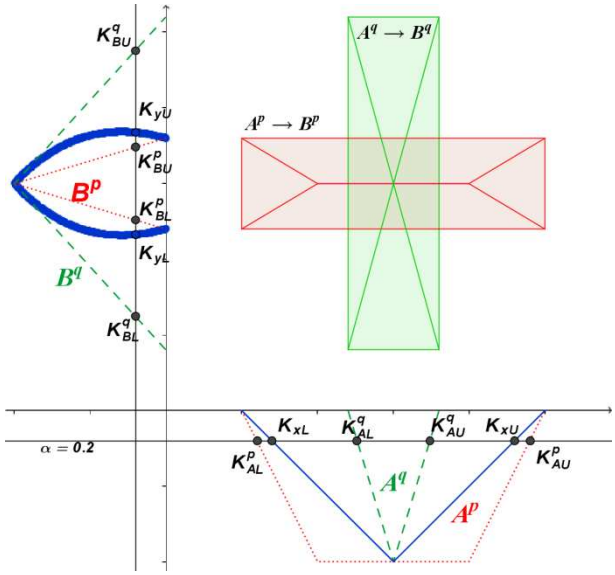

Figure 9

An example of the GDFPM α-cut based fuzziness similarity ratio preservation reasoning step, in which the conclusion is invalid, and the direction of change in fuzziness is reversed

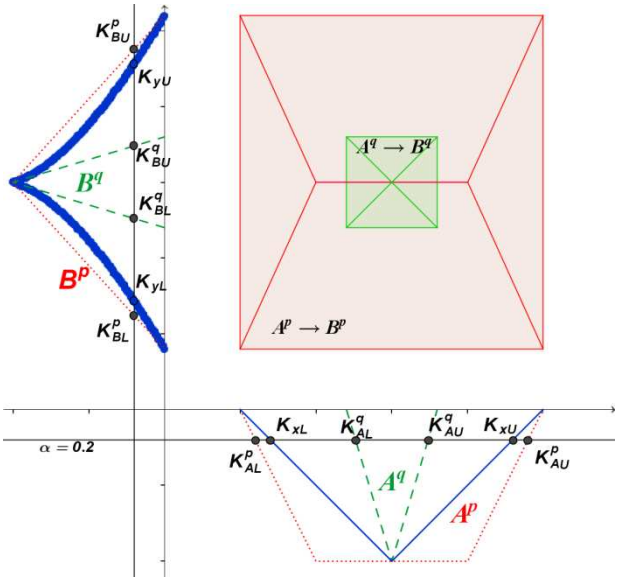

Figure 10

An example of the GDFPM α-cut based fuzziness similarity ratio preservation reasoning step, in which the conclusion is valid, but piecewise linearity is not preserved

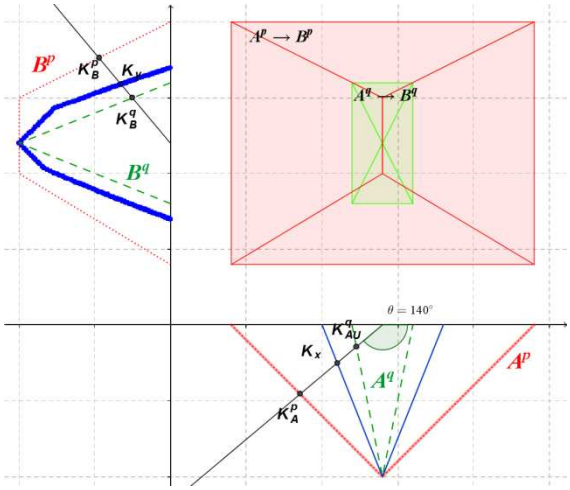

Figure 11

An example of the GDFPM polar cut based fuzziness similarity ratio preservation reasoning step, in which the direction of change in fuzziness remains the same, the conclusion is valid, and piecewise linearity is preserved

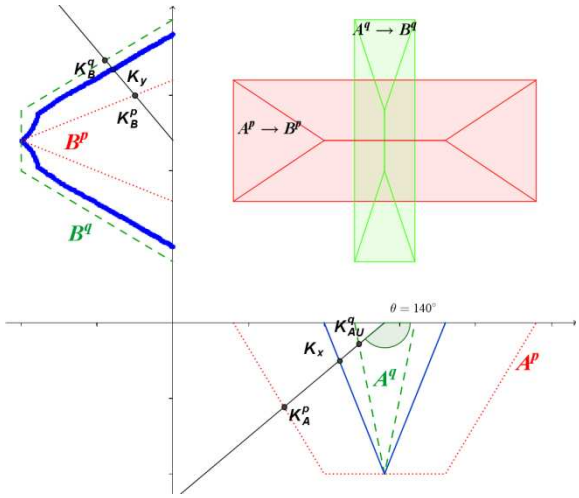

Figure 12

An example of the GDFPM polar cut based fuzziness similarity ratio preservation reasoning step, in which the direction of change in fuzziness is reversed, the conclusion is valid, but piecewise linearity is not preserved

Conclusions

In this paper, a common "Generalized Double Fuzzy Point Methodology" (GDFPM) is introduced, which can be applied as a guideline for the double fuzzy point adaptation of any two-step FRI method. Compared to the original two-step FRI method, the first step of the proposed GDFPM approach consists of the generation of a temporal interpolated double fuzzy point rule (this is a pair of rules: one for each of the fuzzy rule sets R^p and R^q) in the position of the observation. The second step of the proposed GDFPM approach consists of the determination of the conclusion based on the observation (A^*) and the temporal interpolated double fuzzy point rule ($A_i^{p,q} \rightarrow B_i^{p,q}$). In the latter step, GDFPM replaces the single rule reasoning step of original two-step method with a new "fuzziness similarity ratio preservation reasoning" step. As a demonstrative example, the "Least Squares Method" ("LESFRI" [9], [10]) and the "Polar a Cut" interpolation ("FRIPOC" [12]) methods were adapted to "fuzziness similarity ratio preservation reasoning" in this paper. The questions of validity of conclusion and linearity preservation in the case of the obtained two-step double fuzzy point FRI methods were also briefly examined.

Acknowledgement

This research was supported by the Hungarian National Scientific Research Fund grant no: OTKA K77809. This research was carried out as part of the TAMOP-4.2.2.C-11/1/KONV-2012-0002 project with support by the European Union, co-financed by the European Social Fund.

References

[1] L. T. Kóczy and K. Hirota, "Rule Interpolation by α-level Sets in Fuzzy Approximate Reasoning," BUSEFAL, Vol. 46, No. Automne, pp. 115-123, 1991

[2] P. Baranyi, D. Tikk, Y. Yam, L. T. Kóczy and L. Nádai A New Method for Avoiding Abnormal Conclusion for alpha-cut Based Rule Interpolation, 8th IEEE International Conference on Fuzzy Systems (FUZZ-IEEE'99), Seoul, Korea, 22-25August, 1999, pp. 383-388

[3] L. T. Kóczy, K. Hirota, and T. D. Gedeon, "Fuzzy Rule Interpolation by the Conservation of Relative Fuzziness," Hirota Lab, Dept. of Comp. Intelligent and Sys. Sci., Tokyo Institute of Technology, Yokohama, Japan, Technical Report 97/2, 1997

[4] K. W. Wong, D. Tikk, T. D. Gedeon, and L. T. Kóczy, "Fuzzy Rule Interpolation for Multidimensional Input Spaces With Applications", IEEE Transactions on Fuzzy Systems, Vol. 13, No. 6, December, 2005, pp. 809-819

[5] B. Bouchon-Meunier, J. Delechamp, C. Marsala, N. Mellouli, M. Rifqi, and L. Zerrouki, "Analogy and Fuzzy Interpolation in Case of Sparse Rules," Proceedings of the EUROFUSE-SIC Joint Conference, pp. 132-136, 1999

[6] B. Bouchon-Meunier, C. Marsala, and M. Rifqi, "Interpolative Reasoning Based on Graduality," Proc. of the 9th IEEE Int. Conf. on Fuzzy Systems (FUZZ-IEEE'00), Vol. 1, pp. 483-487, May 6-10, 2000

[7] P. Baranyi, L. T. Kóczy, and T. D. Gedeon, "A Generalized Concept for Fuzzy Rule Interpolation," IEEE Trans. on Fuzzy Systems, Vol. 12, No. 6, pp. 820-837, December 2004

[8] Z. Huang and Q. Shen, "Fuzzy Interpolative Reasoning via Scale and Move Transformations," IEEE Trans. on Fuzzy Systems, Vol. 14, No. 2, pp. 340-359, April 2006

[9] Zs. Cs. Johanyák and S. Kovács, "Fuzzy Rule Interpolation by the Least Squares Method", 7th International Symposium of Hungarian Researchers on Computational Intelligence (HUCI 2006), November 24-25, Budapest. pp. 495-506, 2006

[10] Zs. Cs. Johanyák, "Performance Improvement of the Fuzzy Rule Interpolation Method LESFRI", in Proceeding of the 12th IEEE International Symposium on Computational Intelligence and Informatics, Budapest, Hungary, November 21-22, 2011, pp. 271-276

[11] Zs. Cs. Johanyák, Fuzzy Rule Interpolation based on Subsethood Values, in Proceedings of 2010 IEEE Interenational Conference on Systems Man, and Cybernetics (SMC 2010), 10-13 October 2010, pp. 2387-2393

[12] Zs. Cs. Johanyák and S. Kovács, "Fuzzy Rule Interpolation Based on Polar Cuts", Advances in Soft Computing, Computational Intelligence, Theory and Applications, Bernd Reusch (Ed.), Springer Germany, pp. 499-511, 2006

[13] Zs. Cs. Johanyák, D. Tikk, S. Kovács, and K. W. Wong, "Fuzzy Rule Interpolation Matlab Toolbox – FRI Toolbox," Proc. of the IEEE World Congress on Computational Intelligence (WCCI'06), 15th Int. Conf. on Fuzzy Systems (FUZZ-IEEE'06), pp. 1427-1433, July 16-21, 2006

[14] Zs. Cs. Johanyák, "Sparse Fuzzy Model Identification Matlab Toolbox - Rulemaker Toolbox," Proceedings of IEEE 6th International Conference on Computational Cybernetics ICCC, pp. 69-74, 2008

[15] Zs. Johanyák. Fuzzy Rule Interpolation Matlab Toolbox Website. [Online]. Available: http://fri.gamf.hu

[16] R.-E. Precup, S. Preitl and P. Korondi, "Fuzzy Controllers with Maximum Sensitivity for Servosystems", IEEE Transactions on Industrial Electronics, Vol. 54, No. 3, 2007, pp. 1298-1310

[17] I. Perfilieva, et al., “Interpolation of Fuzzy Data: Analytical Approach and Overview”, Fuzzy Sets and Systems, 2010, doi:10.1016/j.fss.2010.08.005

[18] S. Jenei, “Interpolating and Extrapolating Fuzzy Quantities Revisited – an Axiomatic Approach”, Soft Comput., Vol. 5., 2001, pp. 179-193

[19] D. Tikk, Zs. Cs. Johanyák, Sz. Kovács, K. W. Wong, “Fuzzy Rule Interpolation and Extrapolation Techniques: Criteria and Evaluation Guidelines”, Journal of Advanced Computational Intelligence and Intelligent Informatics, Vol. 15, No. 3, 2011, pp. 254-263

[20] S. Kovács, “Extending the Concept of Fuzzy Rule Interpolation with the Interpolation of the Fuzziness,” Proceedings of the WCCI 2012 IEEE World Congress on Computational Intelligence, pp. 1106-1113, June 2012

Sensing System for Intra-Abdominal Pressure Measurement

Teodor Tóth, Monika Michalíková, Jozef Živčák

Technical University of Košice, Faculty of Mechanical Engineering, Department of biomedical engineering and measurement, Letná 9, Košice, 04200 Slovakia
teodor.toth@tuke.sk; monika.michalikova@tuke.sk; jozef.zivcak@tuke.sk

Richard Raši

Louis Pasteur University Hospital, Rastislavova 43, Košice, 04 001 Slovakia
rasi@unlp.sk

Abstract: The development of technology and information technology offers new possibilities for detecting intra-abdominal pressure (IAP) in critically ill patients. Presently, non-invasive measuring through the monitoring of pressure in the bladder has begun to be promoted. Studies on monitoring pressure in the urinary tract point to a high level of correlation with pressure in the abdominal cavity. These measures are currently conducted in the majority of workplaces by manual measurement in specified time intervals. In this article the verification of a monitoring system for measuring IAP is described, which is part of a proposed system for automatisation of IAP detection.

Keywords: intra-abdominal pressure; measurement; sensors

1 Reasons for the Origin of IAH

The reasons for the origin of inter-abdominal hypertension can be divided into a number of groups based on the aetiology of origin:

1. post-traumatic – the reason for origin is a traumatic mechanism with subsequent damage to individual organs: massive multi-organ disabling, burning, intra-abdominal or retroperitoneal bleeding (a traumatic rupture of the aorta, bleeding from the spleen), massive contusion of the body (anti-shock trousers), swelling of tissues after a massive intake of fluids during resuscitation, [12]

2. on the basis of disease and disease complications – infection of the abdominal cavity (stercoraceus or biliary peritonitis), a place of abscess, acute pancreatitis, decompensation cirrhosis with ascites, edema and ascites after a massive intake of fluids, hemoperitoneum or hemoretroperitoneum, [12]
3. as a response to therapeutic procedures – peritoneal dialysis, artificial lung ventilation [12]
4. surgical procedures and their complications – laparoscopic surgery with enforced creation of pneumoperitonea, a large stomach operation, diaphragmatic hernia, application of an abdominal belt after an operation, post-operative bleeding, closing of the abdominal wall caused by pulling, oedema after a major operation (oncological operations). Acute post-operative dilation of the stomach; this is possible also after undergoing a gastrofibroscopic examination. [12]

Massive influx of fluids with forced volume therapy works on the abdominal wall in several ways. It leads to dilation of the veins in the area of the abdominal wall, becoming an oedema of the intestinal walls with increased pressure on the venous and lymphatic system with a resultant worsening of drainage. The stagnation of fluids in the intestinal wall endures with the development of tissue hypoxia. A vicous cycle begins; blood gets into the intestinal wall but does not reach the drainage of the venous system; the oedema grows. A decline in kidney function follows. According to recent studies close monitoring of the inflow and outflow of fluids is appropriate. [6, 7, 12]

2 Treatment of ACS

In clinical practice we have been coming across occurrences of ACS for a long time, and history has recorded data in which increased IAP in critically ill patients leads to a growth in morbidity and mortality. [1, 2, 5, 7]

At present the occurrence of ACS is connected with repeated use of an old-new conception of treatment of serious traumatic injuries. In this strategy of treatment algorithm, a multi-stage procedure, described by different authors as Staged Laparotomy (Morris,1993), Planned Reoperation (Hisrhberg,1994), Abbreviated Laparotomy (Brenneman,1994) and Damage Control Laparotomy (Ivatury, 1997), is again fully acceptable. [1, 2, 12]

The essence of this approach is the carrying out of an immediate introductory laparotomy with necessary treatment of the organs and by stopping the life-endangering bleeding. The aim is to anticipate the origin of irreversible coagulopathy, because coagulopathy worsened by hypothermia and acidosis is considered as a primary factor in the timely death of patients after a serious abdominal injury. [12]

3 Verification of Measuring System

The testing device for verifying the pressure sensor consists of two parts (Fig. 3). In the first a model of the abdomen is made from a 250 ml saline bag (in the place of the bladder). This saline bag is placed in the bottom of a 35L container which allows pressure to be built up to 25 mmHg. Velcro is used to anchor the bag to the bottom of the container. [8, 10]

For determining the impact of the anchoring of the model of the bladder two versions of the clamp were tested. In the first version, the bag for the saline was anchored with two Velcro fastener strips along its full length in the middle. Upon testing it was determined that the edges of the bag have a tendency to lift and thus shift the zero point for measurement. To prevent such lifting of the bag edges, Velcro strips were attached to the inside of the container and to the four corners of the bag (Figure 4). [8, 10, 11]

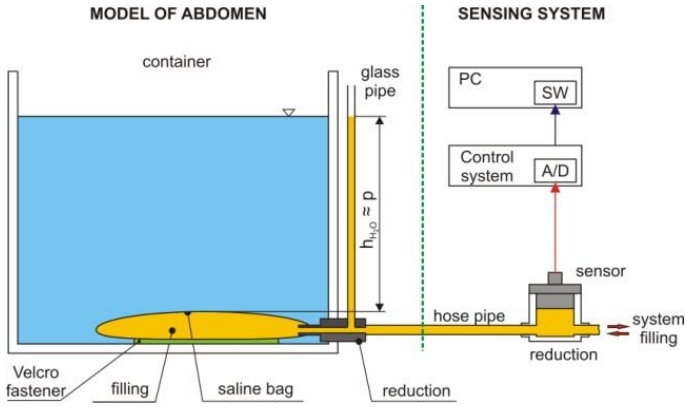

Figure 3
Schematic representation of sensing system [8, 10]

The second part is the sensing system.

The selection of an inter-abdominal pressure sensor is subject to strict hygienic and safety conditions. Among the most basic are that it be possible to disinfect the sensor and that upon its being damaged no contamination of the measuring space can occur. [8, 10, 11]

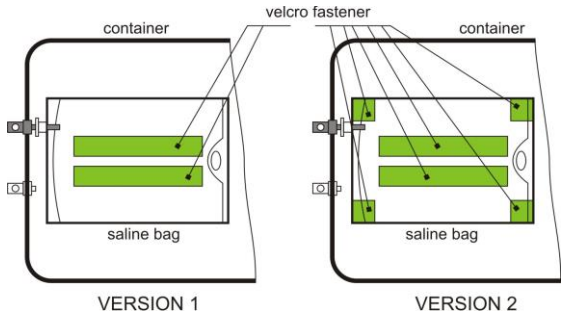

Figure 4
Versions of the clamp

On the basis of the given criteria the selected sensor was model number DMP 331 P from the company BD SENSORS. The sensor is also supplied in a variant filled with edible oil. The basic parameters of the sensor are presented in Table 2. [8]

The measuring range (0-0.1) bar corresponds to 10 kPa or 75 mmHg, while 3.3 kPa or 25 mmHg is desirable. The sensor, therefore, has sufficient reserve for measuring. The sensor has an output of (0 – 5) V, thus it is possible to connect it directly into the microcontroller. [8]

Table 2
Basic parameter of DMP 331 P sensor [8]

	Value
Measuring range [bar]	0 – 0,1
Accuracy	0,5% from measuring range
Output [V]	0-5
Cover	IP 65
Material of the sensor body	stainless steel
Filling	edible oil

The sensing system is connected to a reduction through tubing of 4mm inner diameter [10].

The measurement was performed as follows:

- the saline bag was filled with 100 ml of water
- 5 mmHg pressure was created through the water column, and the value was read from the level gauge,
- stabilization of the water level (15 - 20) s,
- measuring process (Figure 5),
- increasing the pressure up to 25 mmHg stepwise by 5 mmHg per step, measuring after each increment,

- decreasing the pressure after reaching 25 mmHg stepwise by 5 mmHg steps, measuring after each decrement,
- 20 measurement packs were obtained with this approach, and each pack contained 5 levels of measurement (5 – 25 mmHg with 5 mmHg steps) (Figure 5) (Table 3) (Table 4) [9, 10].

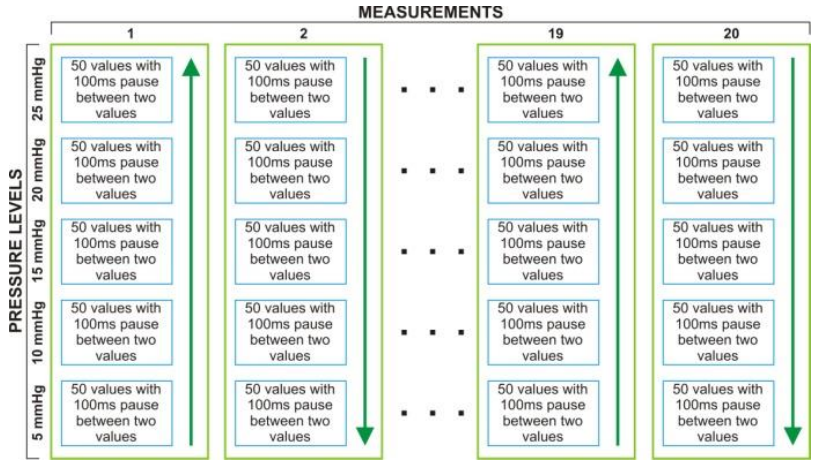

Figure 5
Schematic representation of measuring process [9, 10]

Each measurement contains 50 values with 100 ms pause between two values. The pressure sensor has an analog output (0 – 5V), which is processed in a PIC microprocessor. The program in the PIC was designed to read data from the sensor, perform the A/D conversion (10-bit) and then send the data to a PC. [8, 10]

The outcome consists of data in a range from 0 to 1023, which represents the total range of the sensor (0 – 75) mmHg or (0 – 0.1) bar. These are subsequently converted to a pressure value through the relation [8]

$$p_{BD} = measured\_value.\frac{75}{1023}[\text{mmHg}]$$

The surface tension of the water in the container is reduced by adding washing up liquid, which allows for a more exact filling of the container to the desired level. [8, 10]

Table 3
Table of the recalculated pressure values for version 1 [8, 10]

i	Pressure [mmHg]				
	$p(5)_i$	$p(10)_i$	$p(15)_i$	$p(20)_i$	$p(25)_i$
1	5,413	10,326	15,180	20,084	24,889
2	5,368	10,194	15,072	19,870	24,834
3	5,408	10,267	15,154	19,950	24,845
4	5,377	10,232	15,113	19,978	24,821
5	5,411	10,284	15,157	20,001	24,840
6	5,430	10,249	15,114	19,944	24,886
7	5,430	10,273	15,255	19,985	24,817
8	5,403	10,214	15,075	19,911	24,837
9	5,368	10,267	15,075	19,933	24,817
10	5,443	10,236	15,092	19,762	24,824
11	5,422	10,271	15,114	19,982	24,804
12	5,421	10,226	15,041	19,889	24,839
13	5,361	10,227	15,095	19,960	24,786
14	5,371	10,254	15,051	19,905	24,826
15	5,431	10,249	15,063	19,971	24,783
16	5,491	10,309	15,097	19,997	24,905
17	5,504	10,352	15,166	20,006	24,853
18	5,415	10,283	15,107	20,026	24,865
19	5,472	10,279	15,157	20,015	24,837
20	5,443	10,315	15,135	20,006	24,861
Mean $\bar{p}$	5,419	10,265	15,116	19,959	24,838
Standard deviation s_p	0,040	0,040	0,052	0,069	0,032
$\bar{p}+3s_p$	5,538	10,384	15,270	20,166	24,934
$\bar{p}-3s_p$	5,300	10,146	14,961	19,752	24,743

The values from the A/D converter are recalculated to a pressure value (Table 3, Figure 6). Data evaluation was performed in Microsoft Excel 2003. [8, 10]

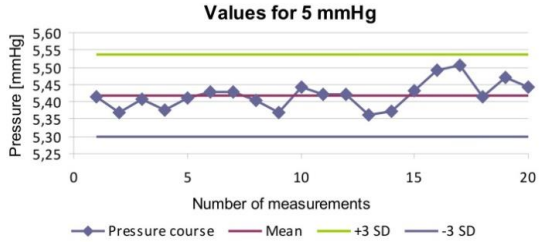

Figure 6
Trend for 5 mmHg, SD – standard deviation [8, 10]

The dependency of the measured values on the expected values is linear (Fig. 7), with a correlation coefficient from 0.98 to 1. [8, 10]

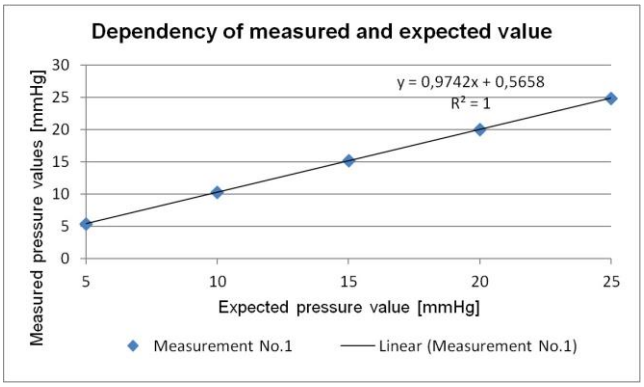

Figure 7
Dependency of the measured values on the expected values

Differences in the measured values upon comparison of both variants for solving the anchoring of the bag of saline solution are greater than 0.5 mmHg for each range. (Table 4, Table 5)

Table 4
Table of the recalculated pressure values for version 2 [8, 10]

	Pressure [mmHg]				
i	$p(5)_i$	$p(10)_i$	$p(15)_i$	$p(20)_i$	$p(25)_i$
1	4,799	9,713	14,472	19,274	24,258
2	4,799	9,809	14,414	19,403	23,965
3	4,826	9,638	14,367	19,346	23,978
4	4,821	9,701	14,522	19,518	23,993
5	4,771	9,463	14,430	19,304	24,000
6	4,786	9,691	14,589	19,424	23,930
7	4,837	9,521	14,422	19,334	23,936
8	4,805	9,691	14,518	19,397	24,006
9	4,779	9,641	14,434	19,333	24,021
10	4,779	9,645	14,469	19,384	23,877
11	4,757	9,570	14,346	19,264	23,874
12	4,736	9,658	14,431	19,204	23,963
13	4,691	9,567	14,447	19,315	23,930
14	4,716	9,638	14,427	19,367	24,028
15	4,701	9,644	14,458	19,321	24,019
16	4,680	9,560	14,446	19,292	23,977
17	4,685	9,685	14,475	19,296	23,950

18	4,676	9,616	14,378	19,219	23,897
19	4,691	9,543	14,386	19,267	23,908
20	4,692	9,632	14,302	19,368	23,924
Average $\bar{p}$	4,751	9,631	14,437	19,332	23,972
Standard deviation s_p	0,055	0,078	0,065	0,074	0,082
$\bar{p}+3s_p$	4,918	9,865	14,631	19,553	24,218
$\bar{p}-3s_p$	4,585	9,397	14,242	19,110	23,725

The following table (Table 5), which determines the difference of a nominal (reference) value versus a measured value, serves for determining the better variant.

Table 5

Pressure differences between two variants

i	Pressure [mmHg]				
	$p(5)_i$	$p(10)_i$	$p(15)_i$	$p(20)_i$	$p(25)_i$
1	0,6139	0,6134	0,7079	0,8098	0,6309
2	0,5689	0,3846	0,6585	0,4668	0,8692
3	0,5825	0,6292	0,7874	0,604	0,867
4	0,5559	0,5311	0,591	0,4604	0,8283
5	0,6397	0,8207	0,7274	0,6975	0,84
6	0,6441	0,5584	0,5246	0,5202	0,9564
7	0,5928	0,7525	0,8327	0,6507	0,8815
8	0,598	0,5234	0,5574	0,5136	0,8311
9	0,5894	0,6262	0,641	0,6002	0,7965
10	0,6644	0,5908	0,6228	0,3778	0,9472
11	0,6654	0,7006	0,768	0,7181	0,9301
12	0,6849	0,5676	0,6099	0,6852	0,8757
13	0,6704	0,6596	0,6478	0,6448	0,8564
14	0,6555	0,6162	0,6243	0,5384	0,7981
15	0,7301	0,6053	0,6055	0,6499	0,7639
16	0,8106	0,7489	0,6513	0,7052	0,9285
17	0,8192	0,6672	0,6909	0,7098	0,9029
18	0,739	0,6672	0,7287	0,8075	0,9676
19	0,7814	0,7365	0,7714	0,7481	0,9294
20	0,7509	0,683	0,8329	0,638	0,9372
Mean	0,6678	0,6341	0,6790	0,627	0,86689
Standard deviation s_p	0,0804	0,0975	0,0881	0,1171	0,0803

The individual values are calculated as follows:

Deviation 1 = Absolute value (*nominal value* – v*alue of "version 1"*).

Total deviation for the selected version = the sum of all deviations for selected version. (Table 6), (Figure 8)

Table 6
Calculation of fifferences between two variants

Nominal Value	Version 1	Version 2	Deviation 1	Deviation 2
5	5,419	4,751	0,419	0,249
10	10,265	9,631	0,265	0,369
15	15,116	14,437	0,116	0,563
20	19,959	19,332	0,041	0,669
25	24,838	23,972	0,162	1,028
Total deviation			1,003	2,8779

From the results it is obvious that the total deviation for Variant 2 is nearly 3-times the total deviation for Variant 1. Fom this it follows that anchoring the bag of saline solution using Variant 1 is more suitable.

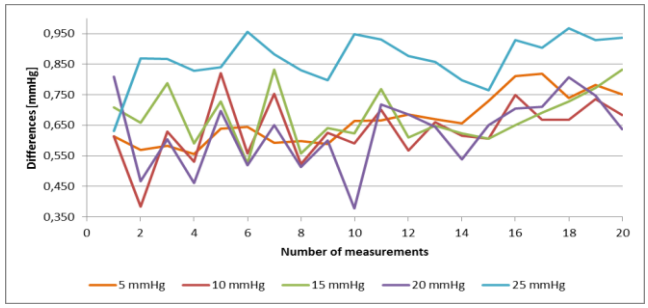

Figure 8
Values for differences between two variants

3.1 Measurement Error Determination

The total error measurement is given by the error of the sensor and the error of the converter.

The error of the sensor is given by the manufacturer and represents 0.5% of the measuring range, which is, to the extent required, a precision of measuring to a whole number; the sensor also satisfies this condition. [8]

$$\varepsilon_s = \frac{\text{sensor\_range}}{100}.sensor\_error = \frac{10000\,\text{Pa}}{100}.0{,}5 = 50\,\text{Pa} \quad \text{resp.} \quad 0{,}375\,\text{mmHg}$$

For digitalisation of the pressure from the sensor, an integrated 10-bit converter is used. [8]

The sensitivty of the converter *LSB* (Least Significant Bit) can be calculated from the relation:

$$LSB = \frac{FS}{2^n} = \frac{5\,\mathrm{V}}{2^{10}} = 0{,}00488\,\mathrm{V}$$

where *FS* (Full Scale) is the range of the converter and n is the number of bits.

A quantization error represents the theoretical maximum difference between the value of the analogue parameter and its maximum value corresponding to the given code word; it is given by the relation:

$$QE = \frac{LSB}{2} = \frac{0{,}00488\,\mathrm{V}}{2} = 0{,}00244\,\mathrm{V}$$

The accuracy of the pressure measurement for a measuring a range of 0.1 bar, i.e. 75 tors, can be calculated from the relation:

$$\frac{LSB}{FS}.sensor\_range = \frac{0{,}00488\,\mathrm{V}}{5\,\mathrm{V}}.75\,\mathrm{mmHg} = 0{,}0732\,\mathrm{mmHg}$$

If a sensor error reaches the maximum allowable value and at the same time a quantization error is also expressed, then there is a total error of measurement:

$$\varepsilon = \varepsilon_s + \varepsilon_p = \varepsilon_s + \frac{QE}{FS}.sensor\_range =$$

$$= 0{,}375\,\mathrm{mmHg} + \frac{0{,}00244\,\mathrm{V}}{5\,\mathrm{V}}.75\,\mathrm{mmHg} = 0{,}41\,\mathrm{mmHg} \quad \text{resp.} \quad 54{,}66\,\mathrm{Pa}$$

Because intra-abdominal pressure is measured for an entire unit, this error is below the margin of acceptability. Its value can be lowered by use of a converter with higher resolution capability. The total error of measurement for a 16-bit converter is on the level of the sensor error. [8]

$$\varepsilon = \varepsilon_s + \varepsilon_p = \varepsilon_s + \frac{\frac{1}{2}\frac{FS}{2^n}}{FS}.sensor\_range =$$

$$= 0{,}375\,\mathrm{mmHg} + \frac{\frac{1}{2}\frac{5\,\mathrm{V}}{2^{16}}}{5\,\mathrm{V}}.75\,\mathrm{mmHg} = 0{,}376\,\mathrm{mmHg} \quad \text{resp.} \quad 50{,}13\,\mathrm{Pa}$$

Conclusion

A proposed measuring device for medical applications must satisfy the appropriate conditions for safety and for reliable use. The sterilisation of all parts which come into contact with body fluids (urine) is one of these conditions. This condition has a basic effect during sensor selection.

In the course of testing the system's sensor two methods of anchoring the bag for saline solution were verified. The methodology for testing was the same in both cases. In view of the principles of the measurement (measuring with a column of water) it was necessary to measure under stable weather conditions, because a change in atmospheric pressure can influence the measured values. The difference between the two methods of anchoring for pressures of 5 – 20 mmHg is approximately 0.65 mmHg and for a range of 25 mmHg it is approximately 0.87 mmHg. Because when measuring internal-abdominal pressure measuring in units of mmHg is sufficient, the measuring of intra-abdominal pressure is within the tolerance limits for both Variants. From an evaluation of the results, it follows that measuring using Variant 1 is more precise.

The total error of the sensing system is on a level of 0.41 mmHg. For decreasing the total error of measurement it is possible to use a stand-alone 16-bit A/D converter. The total error in this case will be equal to the sensor error.

Acknowledgement

This contribution is the result of the project implementation: Center for research of control of technical, environmental and human risks for permanent development of production and products in mechanical engineering (lTMS:26220 120060) supported by the Research & Development Operational Programme fund ed by the ERDF.

References

[1] Malbrain, ML., Cheatham, ML., Kirkpatrick, A., Sugrue, M., Parr, M., De Waele, J., Balogh, Z., Leppäniemi, A., Olvera, C., Ivatury, R., D'Amours, S., Wendon, J., Hillman, K., Johansson, K., Kolkman, K., Wilmer, A.: Results from the International Conference of Experts on Intra-abdominal Hypertension and Abdominal Compartment Syndrome. I. Definitions, Intensive Care Med. 2006 Nov; 32(11):1722-32. Epub 2006 Sep 12

[2] Malbrain, ML., Cheatham, ML., Kirkpatrick, A., Sugrue, M., Parr, M., De Waele, J., Balogh, Z., Leppäniemi, A., Olvera, C., Ivatury, R., D'Amours, S., Wendon, J., Hillman, K., Wilmer, A.: Results from the International Conference of Experts on Intra-abdominal Hypertension and Abdominal Compartment Syndrome. II. Recommendations. Intensive Care Med. 2007 Jun; 33(6):951-62. Epub 2007 Mar 22

[3] Malbrain, ML., Deeren DH.: Effect of Bladder Volume on Measured Intravesical Pressure: a Prospective Cohort Study, Critical Care 2006, 10:R98, http://ccforum.com/content/10/4/R98

[4] Efstathiou, E., Zaka, M., et al.: "Intra-Abdominal Pressure Monitoring in Septic Patients." Intensive Care Medicine 31, 2005, Supplement 1(131): S183, Abstract 703

[5] Kinball, EJ.: IAP Measurement: Bladder Techniques, WCACS,, Antwerp, 2007

[6] Malbrain ML, Cheatham ML, Kirkpatrick A, Sugrue M, De Waele J, Ivatury R.: Abdominal Compartment Syndrome: it's Time to Pay Attention!, Intensive Care Medicine, Volume 32, Number 11, November 2006, pp. 1912-1914(3)

[7] Ivatury, R., Cheatham M., Malbrain, M., Sugrue, M.: Abdominal Compartment Syndrome, Landes Biosciences, ISBN 978-1-58706-196-7

[8] Toth, T.: Návrh zariadenia na meranie intra – abdominálneho tlaku, Doktorandská dizertačná práca, Košice, 2009

[9] Tóth, T., Michalíková, M., Bednarčíková, L., Petrík, M., Živčák, J.: Verification of Measuring System for Automation Intra – Abdominal Pressure Measurement, In: MEDICON 2010 : 12 Mediterranean Conference on Medical and Biological Engineering and Computing 2010 : May 27-30. 2010, Chalkidiki, Greece. - s.l. : Springer, 2010 P. 513-516. - ISBN 978-3-642-13038-0

[10] Tóth, T., Živčák, J., Liberko, I.: Verification of Measuring System for Intra – Abdominal Pressure Measurement, SAMI 2010, 8th International Symposium on Applied Machine Intelligence and Informatics, January 28-30, 2010, Herľany, Slovakia, pp. 297-299, ISBN 978-1-4244-6423-4

[11] Tóth, T., Michalíková, M., Tkáčová, M., Živčák, J.: Overenie snímacieho systému na meranie intra-abdominálneho tlaku, Trendy v biomedicínském inženýrství: 21. - 23.září, 2011, Rožnov pod Radhoštěm. – Ostrava, pp. 134-137, ISBN 978-80-248-2479-6

[12] Liberko, I.: Neinvazívne meranie vnútrobrušného tlaku pri kompartment syndróme brušnej dutiny : doktorandská dizertačná práca Košice, 2010

Investigation of Localization Accuracy for UWB Radar Operating in Complex Environment

Jana Rovňáková, Dušan Kocur, Peter Kažimír

Department of Electronics and Multimedia Communications,
Faculty of Electrical Engineering and Informatics, Technical University of Košice,
Park Komenského 13, 041 20 Košice, Slovak Republic
jana.rovnakova@tuke.sk, dusan.kocur@tuke.sk, peter.kazimir@tuke.sk

Abstract: The aim of this paper is to investigate localization accuracy of ultra wideband (UWB) radar with a minimal antenna array taking in the account complexity of the real environment (extended and multiple targets, presence of wall or other obstacle in the line of sight, practical restrictions of antenna setting). Simulation-based results show how the localization accuracy depends on the radar range resolution, deployment of the radar antennas and the accuracy of ranges estimated between transmitting antenna-target-receiving antenna. As the output, the distributions of the average localization errors in the monitored area are obtained. Their correctness is demonstrated by processing of the signals acquired by two M-sequence UWB radars with different range resolution and coverage.

Keywords: localization accuracy; UWB radar; antenna setting; complex environment; TOA measurement

1 Introduction

Detection and localization of people by an ultra wideband (UWB) radar has numerous practical applications including anti-terror or anti-drug operations, victim search and rescue following an emergency or interior monitoring for aged people helping to ensure their health and safety [5], [16].

The minimal amount of radar antennas required for passive (uncooperative) target localization in two dimensional (2D) space by means of trilateration principles is one transmitting antenna (Tx) and two receiving antennas (Rx_1, Rx_2). UWB radars with such small antenna array usually utilize less complex signal processing, are cheaper and more flexible during measurement than the radars with multiple antennas or the sensor networks. On the other hand their localization accuracy and maximal range are limited.

The localization accuracy performance is in the literature evaluated from many aspects. In most cases, the Cramér Rao Lower Bound (CRLB) is used to assess the localization accuracy which can be attained with the available measurement set, e.g. [6], [7], [12], [17]. From them, [7] presents an analysis of target localization accuracy, attainable by the use of multiple-input multiple-output (MIMO) radar systems, configured with multiple transmit and receive sensors, widely distributed over an area. In [12] the authors investigate and compare the precision of selected localisation methods with respect to the wireless sensor network (WSN) geometry and highly inaccurate distance measurements. [17] analyzes the achievable accuracy of a new localization system, designed by the authors, using time-difference-of-arrival (TDOA) measurements by covering the sources for time measurement errors like thermal noise, timing jitter, and multi-path propagation. The authors of [6] interestedly stated that the CRLB is more pertinent for outdoor applications where low-scattering channels prevail but not necessarily so for strong-scattering channels that characterize dense-multipath indoor environments in emerging commercial applications of UWB radios.

In latter papers, even derivation of a new CRLB based on a distance-dependent noise variance modelling is introduced for time-of-arrival (TOA) and TDOA measurements in [8] and [9], respectively. The authors demonstrate that the distance-dependent variance model impacts the derivation of the Fisher information matrix, eventually leading to a CRLB different from the existing derivations.

The localization accuracy can be evaluated by means of simulation results, too [1], [19]. For example in [19], the accuracy enhancement for 3D indoor localization has been demonstrated with the use of 4, 5, and 6 base stations. [1] deals with the 2D indoor localization accuracy of the short-range UWB radar acquiring TOA measurement with a minimal antenna array, what is exactly application on which we focus. In [1], though, the accuracy was investigated under ideal conditions, i.e. a pinpoint target, no multiple reflections, no additional noise, etc. It was demonstrated that the quantization effect by itself results in the localization error up to 2.5 m, the largest target position estimation errors are located along the straight lines between *Tx* and all *Rx* antennas and that the ideal distance between antennas of UWB radar system with the range resolution of 1.7 cm and coverage up to 8.5 m should be set to 5 m.

However, in a real measurement it is not very functional to have the antennas so far each other. Many times the character of monitored area does not allow it, e.g. the short length of wall through which the targets are tracked. More important is flexibility loss of the portable device and loss of radar data similarity resulting from small and symmetric distance between antennas utilizable for data association. These practical restrictions of antenna setting together with presence of wall or other obstacle in the line of sight as well as challenging nature of human targets create a complex environment which should be taken into account while investigating the localization accuracy of the UWB radar. It is the main goal of

this paper. For that purpose the simulation based considerations, extending the ideas and results provided in [1], will be given in Section 2. Consequently they will be validated by the experimental results provided in Section 3. Finally, the concluding remarks will be summarized in the last section.

2 Localization Accuracy

To understand the distribution of average localization errors inside a monitored area two things need to be explained. The first one relates to regular organization of the estimated positions which is described in Section 2.1. The second topic is about manifestation of measurement and processing errors further discussed in Section 2.2. After that the localization accuracy of UWB radar system with small antenna array will be shown in the form of localization error maps in Section 2.3.

2.1 Rays Formed from Estimated Locations

As the considered UWB radar system works with the minimal amount of radar antennas (*Tx, Rx1, Rx2*), the target locations are estimated by the direct method of localization [1]. The input data to this algorithm has a form of time-of-arrival (TOA) of signals propagating between *Tx*-target-Rx_k, $k=1,2$. The correctly estimated and associated TOA couples from both receivers produce, after localization process, the true target positions and no false targets (ghosts). On the basis of the triangle inequality arising from the antenna layout and an arbitrary target position, difference between TOA estimated from both receivers and belonging to the same target fulfil the following inequality:

$$\left|TOA_1 - TOA_2\right| c \le 2d \tag{1}$$

where TOA_k represents TOA estimated by the receiver Rx_k, c is the speed of light and $d = dist(Tx, Rx_1) = dist(Tx, Rx_2)$ is the distance between adjacent antennas. The foundation of (1) is illustrated in Figure 1 and in detail derived in [15].

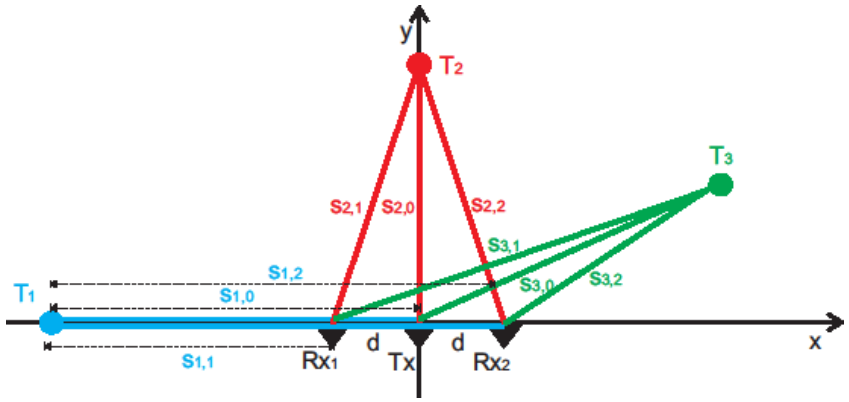

Figure 1

Scheme of the layout of the radar antennas and the targets in a monitored area. Target T_1 located on *x*-axis has TOA difference equal to $2d/c$, target T_2 located on *y*-axis has TOA difference equal to 0 and target T_3 located neither on *x*-axis nor on *y*-axis has TOA difference lesser than $2d/c$.

If $2d$ is small (e.g. less than 1 m), the TOA difference can be used for simple, yet efficient data association [15]. Moreover if $2d$ is divided by the theoretical maximal radar range resolution $S_r = \frac{c}{2f}$ and properly adjusted according the relation

$$N = \text{int}(\frac{2d}{S_r}) + 1 \qquad \text{if } \text{int}(\frac{2d}{S_r}) \text{ is even number,} \tag{2}$$

$$N = \text{int}(\frac{2d}{S_r}) \qquad \text{if } \text{int}(\frac{2d}{S_r}) \text{ is odd number} \tag{3}$$

(f – radar frequency, $\text{int}(x)$ - the integer part of x),

then the quantity N represents number of TOA couples which meets (1). Consequently, if from these TOA couples are computed target locations, they are regularly spread in the radar coverage on the N rays rising from the segment between Rx_1-Tx-Rx_2 (Figure 2). The distance between the adjacent positions located on the same ray is equal to the range resolution S_r and their total number on the ray corresponds to the total number of samples (chips) of the radar signal.

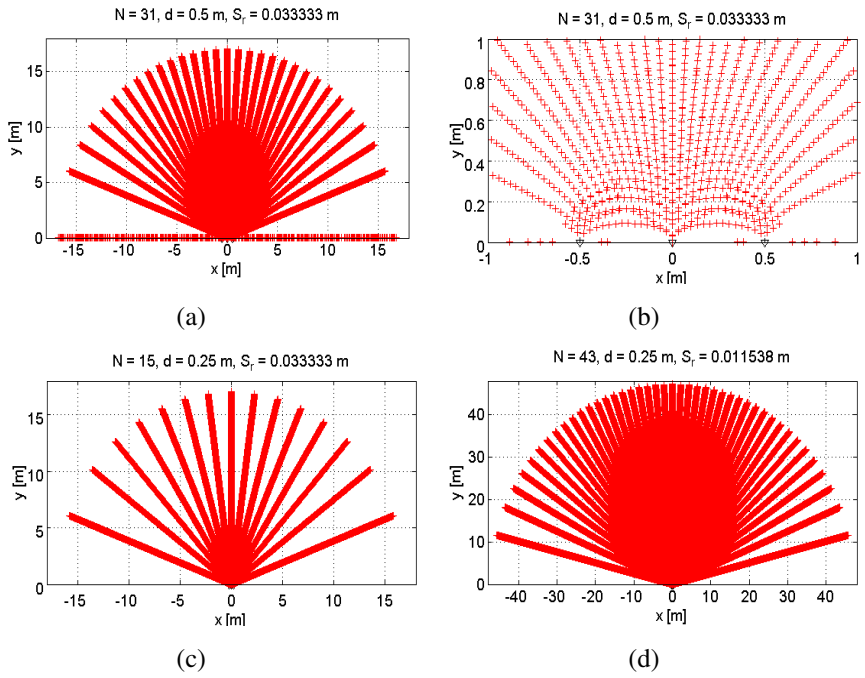

Figure 2

Rays formed from estimated locations: (a) *N=31* obtained for *d=0.5 m* and S_r*=0.0333 m*, (b) zoom in the segment between Rx_1-Tx-Rx_2, (c) *N=15* obtained for *d=0.25 m* and S_r*=0.0333 m*, (d) *N=43* obtained for *d=0.25 m* and S_r*=0.0115 m*

From (2) and (3) can be easily implied that N increases with bigger d (Figure 2(c) vs. 2(a)) and finer S_r (Figure 2(c) vs. 2(d)). From Figure 2 can be also seen that the biggest localization errors are in the surrounding of the *x*-axis and at the end of coverage area when the rays retreat from each other.

The relation between the number of rays *N*, the antenna distance *d* and the radar range resolution S_r is illustrated in Figure 3. It can be observed from there that notable increase of N is achievable with $S_r = 0.01m$. The values $S_r \geq 0.07m$ provide almost comparable values of N for $d \in \langle 0,1 \rangle m$. It naturally holds - the larger N, the better localization accuracy.

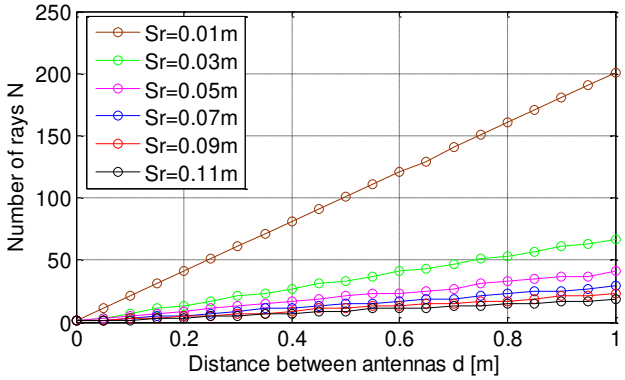

Figure 3

The relation between the number of rays N, the antenna distance d and the radar range resolution S_r.

2.2 Measurement Errors and Processing Errors

The localization accuracy is influenced by measuring and processing errors. According [3], the measurement errors can be classified to following groups:

- S/N-dependent random measurement error,
- random measurement error having fixed standard deviation, due to noise sources in the latter stages of the radar receiver,
- bias error associated with the radar calibration and measurement process,
- errors due to radar propagation conditions,
- errors from interference sources such as radar clutter and radar jamming signals.

These errors depend mostly on properties of employed UWB radar system and can be partially reduced by a careful calibration.

The sources of processing errors accumulate with a complexity of the environment. The localization errors are particularly massive in the cases when is needed to monitor crowded full-furnished areas containing strong reflectors, moreover through some obstacle (e.g. wall or walls) with unknown parameters. All such conditions influence the target range estimation and consequently the target localization accuracy. Considering UWB radar signal processing aimed at localization of people, the following error sources need to be especially treated within the particular processing phases:

- time zero setting during pre-processing phase – incorrect finding of the first bigger peak indicating crosstalk results in a bias range error [18],

- loss of reflections from motionless or mutually shadowed persons during background subtraction phase – missing data for localization [10],
- evaluation of a strong reflector gradually shadowed by a moving person as another target during detection phase – false target detection [11],
- replacement of extended targets (human body has radar cross section larger than the UWB radar range resolution) by simple targets (one value of time of arrival (TOA) on the path *Tx-target-Rx* for every target) and their association through all receivers during TOA estimation phase – incorrect replacement results in target range errors and incorrect association causes generation of the ghost targets [15],
- wall parameter estimation and not exact methods of correction during wall effect compensation phase – bias range error due to unknown wall parameters or residual error due to approximate compensation methods [14],
- arrangement of the computed locations on the limited number of rays during localization phase – localization errors if target is located outside the rays (Section 2.1),
- distinction of crossing targets, slow change of direction for fast manoeuvring targets and track maintenance during tracking phase – despite of many advantages of tracking systems, improper setting of tracking parameters can lead to aggravation of the localization results [2].

Taking into account all the measuring and processing errors occurring in the complex environment, it is realistic to expect the target range error as several multiples of the maximal range resolution. Said by other quantities, TOA is estimated with error of few T_s, where $T_s = 1/f$ represents a sample period.

Figure 4 illustrates the increasing of localization error with the increasing of TOA error given by the standard deviation of a Gaussian distribution expressed in multiple of T_s. The figure has form of an empirical Cumulative Distribution Function (CDF). Here, CDF is defined by $CDF(E) = P(E \leq e)$ where $P(E \leq e)$ is a probability that the localization error E is less than or equal to e. The CDF in Figure 4 were calculated for the antenna distance $d = 0.5m$, the range resolution $S_r = 0.0333m$ and the standard deviations $STD \in \{0, 1T_s, 2T_s, 3T_s, 4T_s\}$. The case $STD = 0$ means that TOA was estimated, except for the quantization error, accurately. Then, the localization errors observable in Figure 4 for the red curve line results only from limited number of rays formed from estimated locations. The maximal error around 6 m appertains to the positions located near the *x*-axis what corresponds with Figure 2(a). From the red CDF from Figure 4 can be also seen that 90% of all estimated locations has localization error less than 2 m. The increasing of the standard deviation leads to increasing of the maximal

localization error gradually up to 26 m. The localization error for 90% of all estimated locations rises with every consequent value of STD approximately about 2 m (Figure 4).

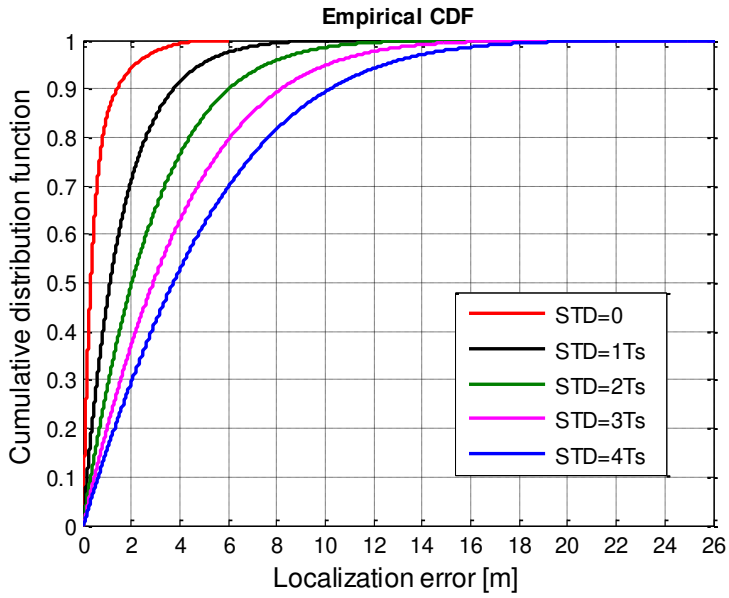

Figure 4

Illustration of the localization error increasing with the increasing of TOA error given by the standard deviation of a Gaussian distribution expressed in multiples of the sample period T_s by means of the cumulative distribution function

2.3 Maps of Average Localization Errors

Distribution of the localization errors in a monitored area can be demonstrated through the maps of average localization errors. The map is created in the following steps:

- the monitored area is divided to subregions,
- from every subregion is randomly generated K positions,
- for them is calculated exact TOA as round trip time between Tx-the kth position-Rx_i for $k=1,2,...,K$ and $i=1,2$,
- every exact TOA is rounded (quantization error) and increased about the expected STD of a Gaussian distribution expressed in multiples of T_s (measuring and processing error),
- from the couples of such TOA are computed the position estimates,

- the difference between the true and estimated position express the localization error,
- for every subregion is computed the average localization error,
- finally, all the subregions are depicted in a common map where according to color is possible to distinguish regions with different localization errors.

The illustration of three various visual display of the localization error distribution is given in Figure 5 and Figure 6. The first figure depicts accumulation of the localization errors under the same scale of colours expressing the average error from interval $\langle 0,10 \rangle m$. The maps from Figure 5(a) to Figure 5(f) demonstrate the extension of the localization error due to increasing of TOA error. The results complement the information provided by the CDF from Figure 4.

Figure 6 represents a decrease of the localization error depending on the increasing of the distance between antennas. The colour scale adapts to maximal attained localization error. The maps from the first column are depicted also in the form of contour maps in the second column of Figure 6. The contour maps provide a clear understanding of the mutual relation between a given deployment of radar antennas and the achievable accuracy at various target locations. From Figure 6 can be observed the changing shape of the most precise areas.

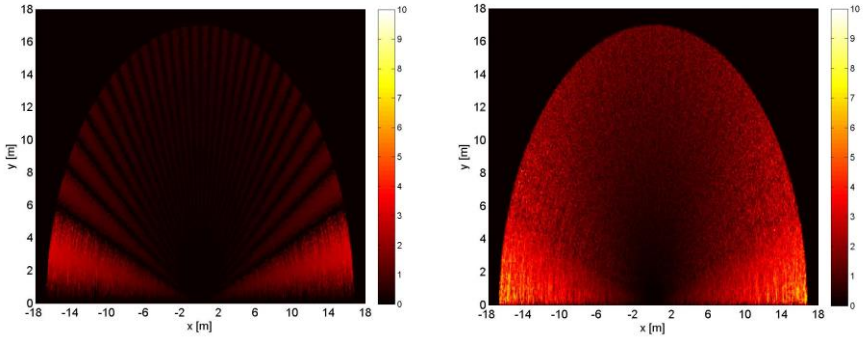

(a) (b)

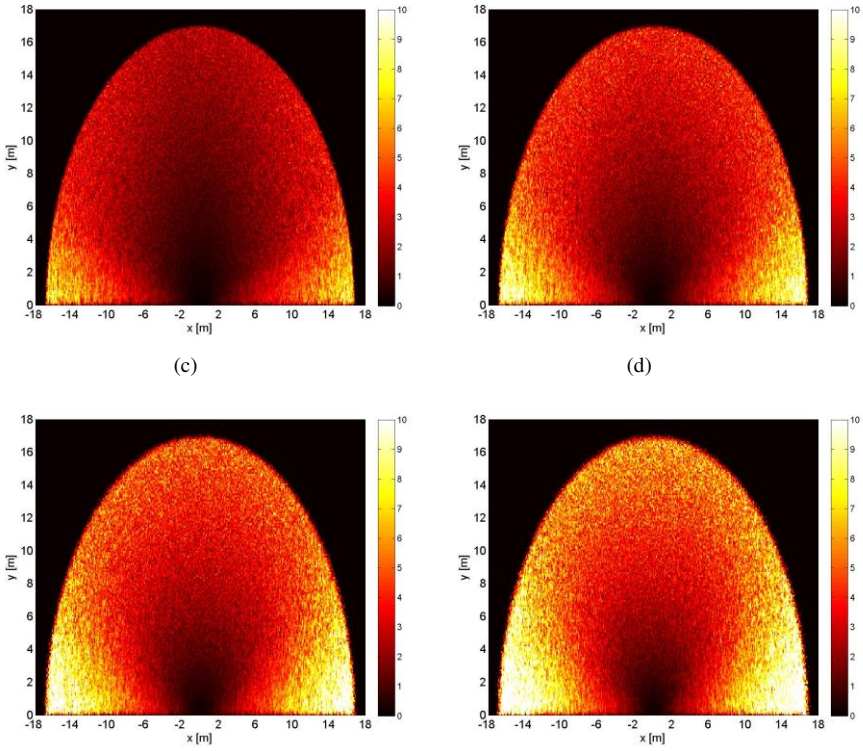

(c) (d)

(e) (f)

Figure 5

The maps of average localization errors obtained for *d=0.5 m*, *Sr=0.0333 m* and changing TOA error expressed as STD of a Gaussian distribution expressed in multiples of *Ts* (a) *STD=0*, (b) $STD=1T_s$, (c) $STD=2T_s$, (d) $STD=3T_s$, (e) $STD=4T_s$, (f) $STD=5T_s$.

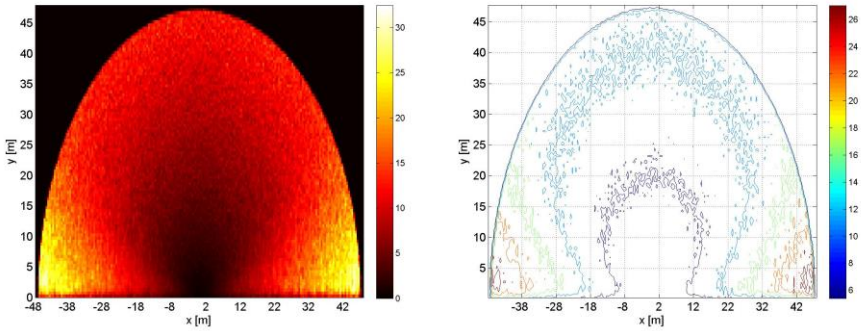

(a) (b)

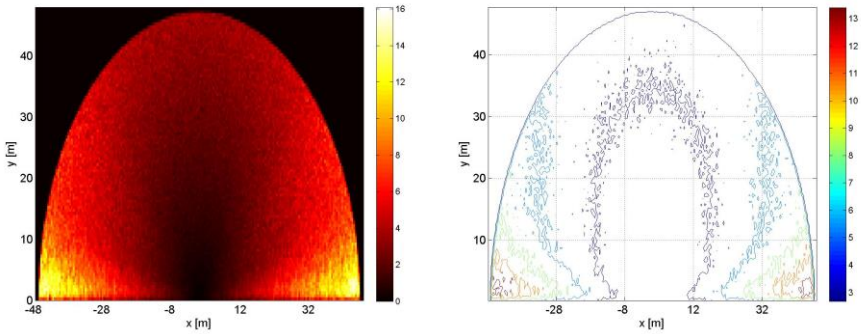

(c)

(d)

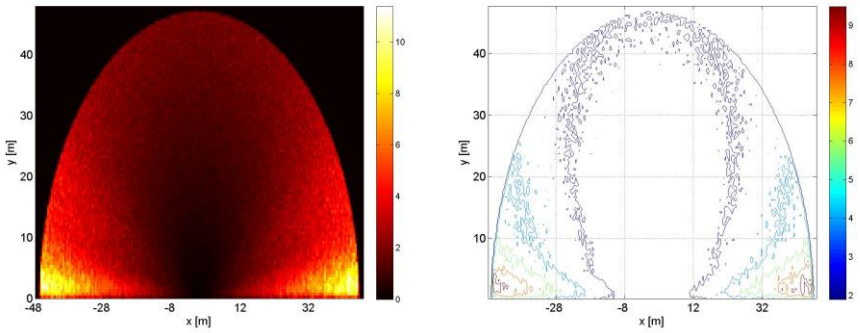

(e)

(f)

Figure 6

The maps of average localization errors obtained for *Sr=0.0115 m, STD=3T*$_s$ and changing *d* (a) *d=0.1 m*, (b) the contour map for *d=0.1m,* (c) *d=0.5 m*, (d) the contour map for *d=0.5 m,* (e) *d=1 m*, (f) the contour map for *d=1 m*

3 Experimental Results

The validation of presented simulation results concerning the localization accuracy of UWB radar operating in complex environment is demonstrated by processing of the signals acquired by two M-sequence UWB radars with different range resolution and coverage [4], [16]. The first UWB radar system, depicted in Figure 7(a), has the range resolution 0.0115 m and coverage of 47 m. The remaining basic parameters are 13 GHz chip clock rate and 4095 impulse response samples regularly spread over 315 ns. During measurement, the radar was equipped with one transmitting and two receiving opened horn antennas (Figure 7(a)).

The second M-sequence UWB radar, depicted in Figure 7(b), has the range resolution 0.0333 m and coverage of 17 m. The remaining basic parameters are 4.5 GHz chip clock rate and 511 impulse response samples regularly spread over 114 ns. During measurement, the radar was equipped with one transmitting and two receiving closed horn antennas (Figure 7(b)).

(a) (b)

Figure 7
M-sequence UWB radars with: (a) the range resolution 0.0115 m and coverage of 47 m, (b) the range resolution 0.0333 m and coverage of 17 m

3.1 Measurement I

The first measurement was realized without an obstacle in the line of sight. The M-sequence radar with the coverage of 47 meters was located together with antennas in the long corridor. The distance between antennas was set to 0.42 m, because the area was narrow, with Tx between Rx_1 and Rx_2. The measurement scenario was simple – a person was walking from the position in front of Tx 40 m straight and then back with short stopping every 5 m.

The localization results obtained by the signal processing procedure for the detection, localization and tracking of moving targets, described in [13], are depicted in Figure 8(a). Here can be observed that despite of the scenario simplicity the localization errors reach the values above the 20 m. However, such results are consistent with the expected distribution of average localization errors represented in Figure 8(b).

The localization error map was computed for the parameters S_r*=0.0115 m, d=0.42 m* and $STD=9T_s=0.69\ ns$. The value of *STD* was found for the used M-sequence UWB radar experimentally on the basis of various measurements. According the environment complexity, average TOA errors recomputed to ranges reach the values between 0.2 m to 0.3 m for human targets. It corresponds with $STD \in \langle 9T_s, 13T_s \rangle$ for $T_s = 0.0769ns$. As the considered measurement was realized without an obstacle in the line of sight, $STD=9T_s$.

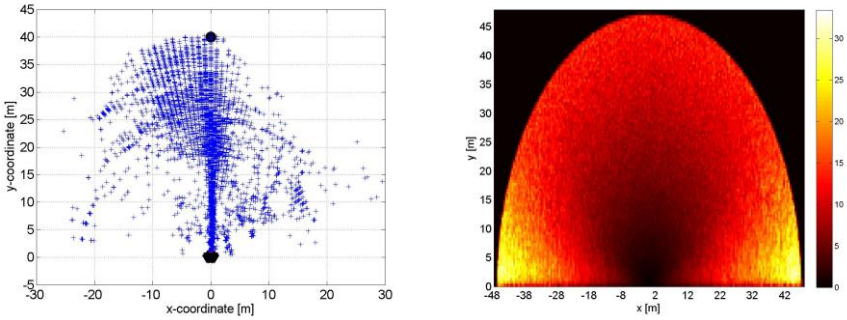

(a) (b)

Figure 8

Measurement I: (a) estimated target positions, (b) expected localization errors for the parameters S_r=0.0115 m, d=0.42 m, STD=9T_s=0.69 ns

3.2 Measurement II

The second measurement was more challenging. The M-sequence UWB radar with the coverage of 17 m was located behind 0.17 m thick concrete wall (Fig. 9). The distance between adjacent antennas was set to 0.38 m (maximal distance enabled by the used tripod), 0.14 m from the wall (Figure 9(a)). The monitored area was short corridor with a staircase depicted in Figure 9(b). During measurement, a person was walking along the corridor up the stairs and then back through the reference positions P1-P2-P1 marked in Figure 9(c).

The localization results obtained by the same signal processing procedure as in the first measurement are depicted in Figure 9(d). As the relative permittivity of the wall was not known, the wall effect compensation phase was omitted. As result, the bias error shifted all the estimated positions further from the radar antennas

(a) (b)

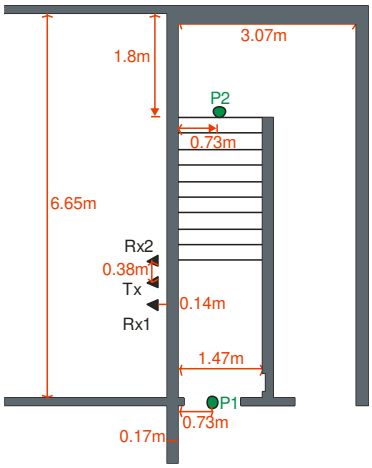

(c)

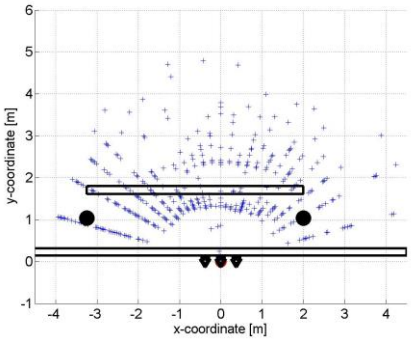

(d)

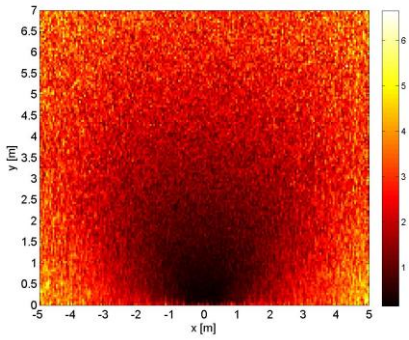

(e)

Figure 9

Measurement II: (a) the antenna deployment behind the wall, (b) interior of monitored area, (c) scheme of the measurement scenario, (d) estimated target positions, (e) expected localization errors for the parameters S_r=0.0333 m, d=0.38 m, $STD=5T_s$= 1.11 ns

(Figure 9(d)). In addition, the movement near by the rear wall caused the multiple reflections visible in Figure 9(d) for y-coordinate above 2 m.

The best localization accuracy of the target trajectory was achieved in the area 1 m to the left and to the right from Tx. The further parts of target trajectory was estimated with the error higher than 1 m, whereas when the person was walking up and down the stairs the localization error exceeded 2 m (Figure 9(d)).

These results correspond with the expected distribution of average localization errors represented in Figure 9(e). The localization error map was computed for the parameters S_r=0.0333 m, d=0.38 m and $STD=5T_s$=1.11 ns. Analogous to the

previous case, for the used M-sequence UWB radar holds that for human targets the average TOA errors recomputed to the ranges reach the values between 0.2 m to 0.3 m depending up the environment complexity. It corresponds with $STD \in \langle 3T_s, 5T_s \rangle$ for $T_s = 0.222ns$. As the considered measurement was realized through concrete wall with unknown parameters, the standard deviation of the TOA error was chosen $5T_s$.

Finally, the tracking results from both considered scenarios are depicted in Figure 10. It can be seen from there that the correctly adjusted tracking system can considerably decrease the localization error.

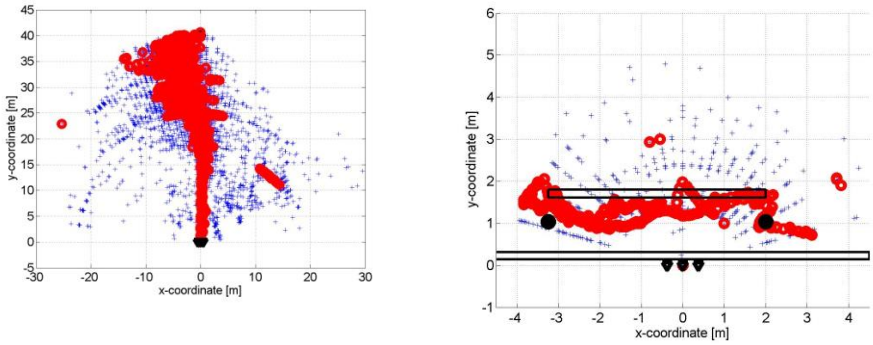

(a) (b)

Figure 10

The target track estimated for scenario from: (a) measurement I, (b) measurement II

Conclusions

The simulation and experimental results presented in this paper provide practical view on the localization accuracy of UWB radars with minimal antenna array. The obtained maps of the localization errors enable to plan the emplacement of the antenna system depending on the monitored area in advance. They also help to decided about the suitability of the chosen UWB radar for some considered application. The introduced investigation of the localization accuracy taking into account the complexity of the monitored environment can serve as the basis for the analysis of localization accuracy for a sensor network consisted from independent UWB radar systems.

Acknowledgement

This work was supported by the VEGA grant agency under contract No. 1/0563/13 and by the Slovak Cultural and Educational Grant Agency under contract No. 010TUKE-4/2012.

References

[1] Aftanas M., Rovňáková J., Rišková M., Kocur D., Drutarovský M.: An Analysis of 2D Target Positioning Accuracy for M-sequence UWB Radar System under Ideal Conditions, The 17th International Conference Radioelektronika, Brno, Czech Republic, pp. 189-194, April 2007

[2] Blackman S. S., Popoli R. Design and Analysis of Modern Tracking Systems, Artech House Publishers, 1993

[3] Curry G. R.: Radar System Performance Modeling, second edition, Artech House, 2005

[4] Daniels D. J.: Ground Penetrating Radar, 2nd ed. London, UK: The Institution of Electrical Engineers; 2004, chapter M-sequence radar written by Sachs J.

[5] Geogiadis A., Rogier H., Roselli L., Arcioni P.: Microwave and Milimeter Wave Circuits and Systems – Emerging Design, Technologies and Applications, John Wiley & Sons, Ltd., Chichester, November 2012

[6] Gezici S., Tian Z., Giannakis G. B., Kobayashi H., Molisch A. F., Poor H. V., Sahinoglu Z.: Localization via Ultra-Wideband Radios: A Look at Positioning Aspects for Future Sensor Networks, IEEE Signal Processing Magazine, Vol. 22, No. 4, pp. 70-84, July 2005

[7] Godrich H., Haimovich A. M., Blum R. S.: Target Localization Accuracy Gain in MIMO Radar-based Systems, IEEE Transactions on Information Theory, Vol. 56, No. 6, pp. 2783-2803, June 2010

[8] Jia T., Buehrer R. M.: A New Cramer-Rao Lower Bound for TOA-based Localization, IEEE Military Communications Conference (MILCOM), San Diego, CA, pp. 1-5, November 2008

[9] Kaune R., Horst J., Koch W.: Accuracy Analysis for TDOA Localization in Sensor Networks, Proc. of the 14th International Conference on Information Fusion (FUSION), Chicago, IL, pp. 1-8, July 2011

[10] Kocur D., Rovňáková J., Urdzík D.: Short-Range UWB Radar Application: Problem of Mutual Shadowing between Targets, Elektrorevue, ISSN 1213-1539, Vol. 2, No. 4, pp. 37-43, December 2011

[11] Leung S. W., Minett J. W., Chung C. F.: An Analysis of the Shadow Feature Technique in Radar Detection, IEEE Trans. Aero. Elec. Sys., Vol. 35, No. 3, 1999, pp. 1104-1106

[12] Niemeyer F., Born A., Bill R.: Analysing the Precision of Resource Aware Localisation Algorithms for Wireless Sensor Networks, Accuracy Symposium, pp. 41-44, July 2010, Leicester, UK

[13] Rovňáková J.: Complete Signal Processing for through Wall Tracking of Moving Targets, LAP LAMBERT Academic Publishing, Germany, September 2010

[14] Rovňáková J., Kocur D.: Compensation of Wall Effect for Through Wall Tracking of Moving Targets, Radioengineering journal: Special Issue on Workshop of the COST Action IC0803, Vol. 18, No. 2, pp. 189-195, June 2009

[15] Rovňáková J., Kocur D.: TOA Estimation and Data Association for Through Wall Tracking of Moving Targets, EURASIP Journal on Wireless Communications and Networking, The special issue: Radar and Sonar Sensor Networks, Volume 2010, pp. 1-11, September 2010

[16] Sachs J.: Handbook of Ultra-Wideband Short-Range Sensing, Wiley-VCH, December 2012

[17] Tüchler M., Schwarz V., Huber A.: Accuracy of an UWB Localization System Based on a CMOS chip, Proc. of the 2nd Workshop on Positioning, Navigation and Communication (WPNC) & 1st Ultra-Wideband Expert Talk (UET), pp. 211-220, 2005

[18] Yelf, R: Where is True Time Zero?, Proc. of the 10th International Conference on Ground Penetrating Radar, Vol. 1, pp. 279-282, June 2004

[19] Zhang C., Kuhn M., Merkl B., Fathy A. E., Mahfouz M.: Accuracy Enhancement of UWB Indoor Localization System via Arrangement of Base Stations, Proc. GA, 2008

Application of Optimization Techniques in the Power System Control

Péter Kádár

Power System Department Faculty of Electrical Engineering, Óbuda University, Bécsi út 96/b, H-1034 Budapest, Hungary
e-mail: kadar.peter@kvk.uni-obuda.hu

Abstract: In this paper we introduce some of the power systems' control and operation problems. The management of the modern power system faces mainly optimization tasks. We show some single and multi objective optimization solutions, these are: Decision making; Optimization of the schedule of renewable sources; Energy storage problems; Optimization of the network structure; Definition of the right power mix in single and also multiobjective case, Regional energy trade. A large variety of applied technologies is described. In the industry the fast and robust methods are favored.

Keywords: power system; optimization problems; single and multi objective optimization

1 Introduction

The electric (and heat) power generation are more than a century old technology but each element of the system contains high-tech solutions (power plant technology, generators, transformers, power lines, power electronic devices, Supervisory Control And Data Acquisition, etc.) The controlled elements are several millions so the system operation, stability, control, balance, optimization, settling is a really complex and distributed task.

1.1 Challenges

In spite of the clear technical knowledge and the capability of the full control of the system elements a lot of new and vague non technical questions emerged. In the following section some current topics are mentioned:

Monopoly and Deregulation

> Most of the power systems start off as monopoly. The monopoly provided the secure and relative cheap energy – and an uncontrollable bureaucratic organization. The deregulation philosophy broke the monolithic power

sector into distinct parts, as generators, transmission, distribution, trader, etc. After the liberalization problems emerged in the supply, investment and price side. The state stepped back to control the uncontrolled free market

Profitability

In the monopolistic case the organization prospers, the energy is supplied. If the company makes a loss, it will be covered by the state/owner. Normally the prices contain the reserves for long-term investment, some profit and the cost of the huge organization. In the deregulated environment the profit is the only driver. There is no investment without the hope of return and there is no energy supply if it is not profitable.

Investment and Development

In the present deregulated market operation there is a lack of long term investments. The profitable developments are made by private companies, the low ROI[1] high costs constructions (e.g. nuclear power plant) stay public.

Fossil, Nuclear or Renewable Sources

A really hot topic is the modification of the actual power mix, the search for the appropriate energy resource. The main decision maker in this question is the government but the lobbies, the greens have their votes, too. The environmental consequences are clear but the long term interests often go by the board of the daily politics.

Distributed and Centralized Generation

The "traditional" centralized energy generation methods are replaced or completed by distributed generation as the gas engines, PVs [2] or small hydros, etc. It poses several issues as the controllability of the net, the standardized design and operation, scale of economics, etc.

Who Rules the System?

The right operation of the power system must incorporate the triumvirate of legal regulation, the technical and trading approaches. The parties concerned work on different time scales (from the long term planning to the intraday market operations).

[1] Return On Investment
[2] PhotoVoltaics

Demand Growth and/or Efficiency

By the traditional paradigm all the energy demands are fulfilled by the producers. The customer has no interest to decrease its consumption. The present trend is the introduction of low-energy-need technologies and the better efficiency of the usage.

Smartening the System

Because of the drastic fall of the reliability of the old networks a new trend emerged that contains a lot of switches and meters outside the substations, open for the small scale bidirectional energy trade, ready for the Demand Side Management. The traditional heavy current power system is completed by Information and Communication Technologies.

Out of Control? Overcontrolled System?

The traditional, centralized power system control philosophy and the market philosophy don't match. The emerging complexity of the (intercontinental) networks and the subtle control system augurs large black-outs (greater area/cost/volume). The reliability and network security can be kept only by huge investments. The life cycle of the early devices in the system was over 50 years (e.g. electromechanical protections) but today the over computerized systems can't work over 10 years. The huge amount of the acquired on-line data overloads the dispatchers. It can be alleviated by some AI applications.

1.2 Tasks and Techniques

The numerous activities related to the operation of multilevel continent wide power system(s) require some optimum searching techniques [1] [2]:

Preparation and planning

- Prioritizing investments in distribution network
- Optimal protection and switching device placement
- Generation scheduling
- Maintenance scheduling
- Power mix planning

Operative control

- Constrained load flow
- Power plant operation optimizer
- Unit commitment – economic dispatch

- Optimal power flow
- FACTS (Flexible AC Transmission System) control
- Voltage/VAr and loss reduction
- Dynamic load modeling
- Short-Term load forecast
- Network reconfiguration and load reduction
- Market operations, etc.

The area of the optimizing methods is one of the most diversified areas of applied mathematics.

"Traditional" techniques

- Weighting Objectives
- Goal programming
- Constraint programming
- Stochastic
- Linear Programming
- Gradient Based/Hill Climbing
- Sequential Optimization, etc.

AI solutions

- Evolutionary Computation
- Genetic algorithms
- Particle swarm optimization
- Fuzzy Set Theory
- Ant colony search algorithm
- Simulated Annealing
- Pareto multi objective Optimization

Solving the problem by different techniques we should arrive at the same conclusion. The difference of the approaches can be characterized by the time spent for the prototyping, the robustness in industrial environment.

1.3 The Optimization Problem

In case of optimization some parameters are set between predefined limits. Typically we look for the minimum or the maximum of the objective (or cost) function. In a simple case we have only one cost function, we call it Single Objective Optimization – SOO, in other cases we look for the optimum of more values. This is the Multi Objective Optimization – MOO. In the complicated energy sector we face mainly the MOO, e.g. the energy strategy.

Nowadays dozens of tools stay at disposal to solve the large optimization tasks by computer. In our case we concentrate on the problem definition and problem mapping.

In the Single Objective Optimization (SOO) we look for min or max of a cost function (1) taking into account constraints:

$$Min/Max\ F(X) \tag{1}$$

where F(X) is the cost or objective function.

In MOO case the general formalization is [3]:

$$Minimize\ F(x) = [F_1(x), F_2(x), F_3(x), \dots, F_k(x)]^T \tag{2}$$

2 Optimization Solutions in the Power System Area

The development and operation problems of the power systems are mostly optimization tasks.

2.1 Decision Making

The power generation, transmission and service projects beyond the technical aspects are influenced by social-economy view points. A typical question to decide is: "To build or not to build a large hydro dam?" "construct or not a fossil or nuclear plant?" There is no good or bad choice but all the choices have effects on dozens of different aspects. We developed a weighting methodology that measures if we are getting closer or not to the optimal market conditions. The market is measured by heuristic Key Performance Indicators based on qualitative functions.

This method [4] is a possible solution if we have a complex incomprehensible problem space that cannot be handled analytically, where we must take into account e.g. the STEPLE framework (Social – Technological – Economic – Political – Legislation – Environmental aspects).

$$\text{Outcome} = w_1 * f_A(x_1) + w_2 * f_B(x_1) + \dots + w_{i-1} * f_P(x_n) + w_i * f_Q(x_n) \tag{3}$$

where

f_{A-Q} = qualitative functions

$x_{1\ldots n}$ = influence variables

$w_{1\ldots i}$ = weight factors

A decision at a place/date and time is better

IF

$$\text{Outcome (Option}_A\text{)} > \text{Outcome (Option}_B\text{)} \quad (4)$$

THEN

Option A is recommended

KPI function matrix	← *Independent variables*	**Social**	Employment	Right to the energy	Value of human positions	Social mission	**Technology**	Energy security	Quality	Efficiency	Standardisation	Integrity	**Economy**	Costs	Price of the energy	Growth rate	Profitability, ROI	Investment/development	Life time of the assets	**Political**	State decision
weight factors →		W_s	w_1	w_2	w_3	w_4	…														
Monopolistic or deregulated structures (level of unbundling)	x_1		B	B	C	C		B	A	G	B	B		B	B	-	A	C	B		C
From fossil toward the nuclear plants	x_2		C	E	B	-		G	E	E	G	G		B	B	E	D	E	D		E
Level of network development	x_3		E	E	E	-		E	H	E	E	E		E	E	-	C	E	E		-
Level of maintenance	x_4		E	E	E	-		G	G	G	G	G		G	G	-	H	G	G		-
From traditional towards the distributed gener.	x_5		G	G	G	G		G	G	H	G	G		G	G	G	H	G	H		-
From traditional to renewable sources	x_6		G	G	G	G		H	H	G	G	G		G	G	G	H	G	-		G
OPP price	x_7		H	H	-	G		-	-	-	-	-		-	G	H	G	G	-		G
Tariffs (net/ISO/PX)	x_8		G	H	G	G		G	G	-	G	G		G	G	-	G	G	G		-
Level of the general investment	x_9		G	G	G	G		G	G	G	G	G		G	H	G	G	G	G		G
Level of the import	x_{10}		H	G	H	H		-	G	-	-	-		H	H	G	H	H	H		G
Level of the control (raising)	x_{11}		G	G	G	G		G	G	G	G	G		G	G	-	H	G	G		-

Figure 1
Part of the qualitative weight table

2.2 Optimization of the Schedule of Renewable Sources

In vehicles, spaceships but also in island mode power systems the load maximum, minimum, battery capacity and also some production forecast are known (e.g. wind and PV, fuel-cell, battery status). [5] [9] [10]

The objective function is the continuous power supply by minimal costs. The sources have different costs, as the "cheap" wind and PV but the fuel cell operation should be minimized.

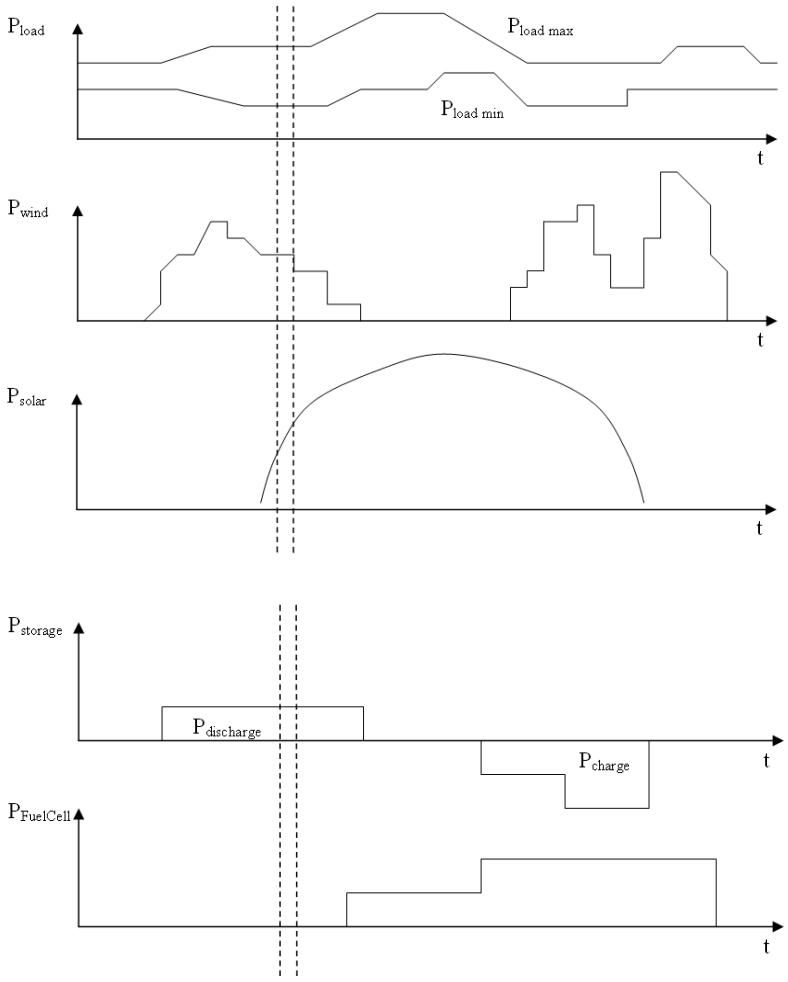

Figure 2
The load limits and the different generation curves

The constraints of the problem are the load limits, the actual generation capabilities, the status of the battery, the forecasted production schedule.

We assigned production costs to each type of generators, also to the battery. The time line is split into short periods. The objective function is:

$$C_p = \sum_{i=1}^{n} C_{source} \tag{5}$$

where

C_p - energy costs during the period

C_{source} - generation cost of the i [th] device

The objective function of the linear program is to find the least cost.

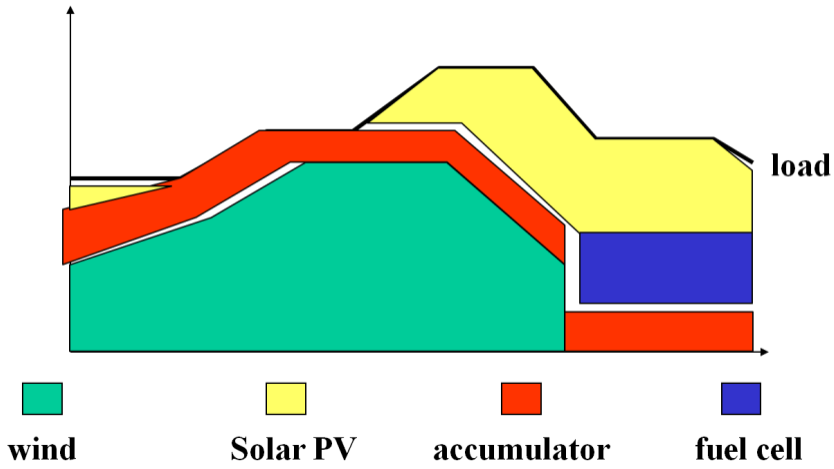

Figure 3
The Tetris[3] problem

2.3 Energy Storage Problems

In the energy market the players are the generation, consumer and trader entities. [7] The deal is the profit maximization. If a generation company has renewable generation capability and also storage possibility it is hard to say, when to store the energy and when to sell directly to the market.

A rule based system was developed to make decisions when to sell/buy/store in function of renewable production possibility and market price.

An example from the rules:

Generate AND store IF (6)

There is renewable potential

AND there is storage capacity

AND Prod. Cost + Cost of Storage is remarkable lower than the Selling Price$_{average}$

[3] Tetris (trademark of The Tetris Company)

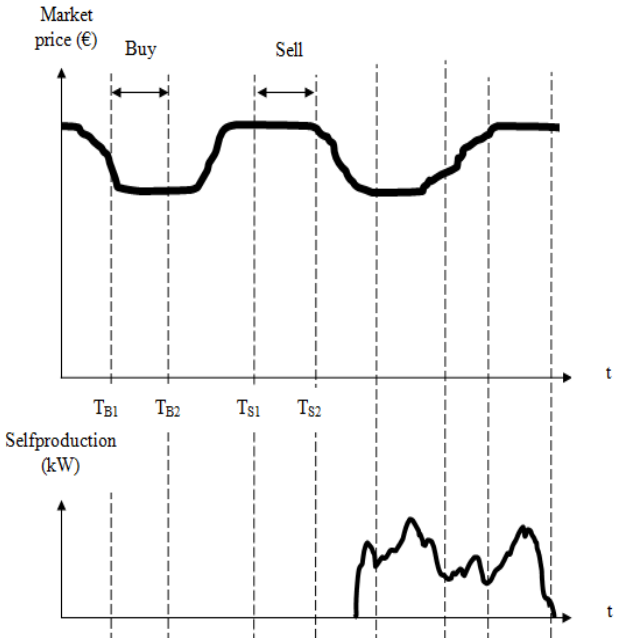

Figure 4a
A possible dynamic operation schedule

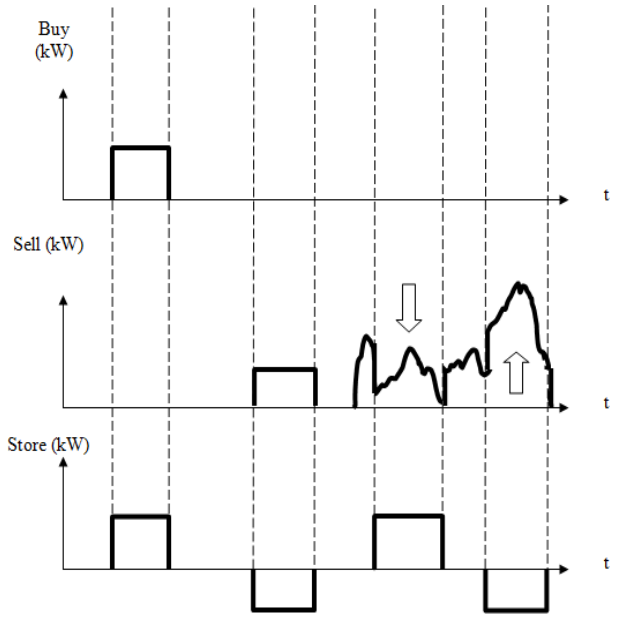

Figure 4b
A possible dynamic operation schedule

2.4 Optimization of the Network Structure

The „Smart" network means that there are renewable sources, adaptive protections, on-the-line switches, intelligent meters, on-the-line metering devices, etc. But how many smart devices should be built in the network? [6]

The reliability raise of the network means the reduction of the amount of the non-delivered energy.

Reliability can be increased by building in primary and secondary gauges, remotely controlled line breakers, redundant network parts or reconstructing parts of the old network. These measures have different costs and results.

The objective is the not-lost-energy maximization.

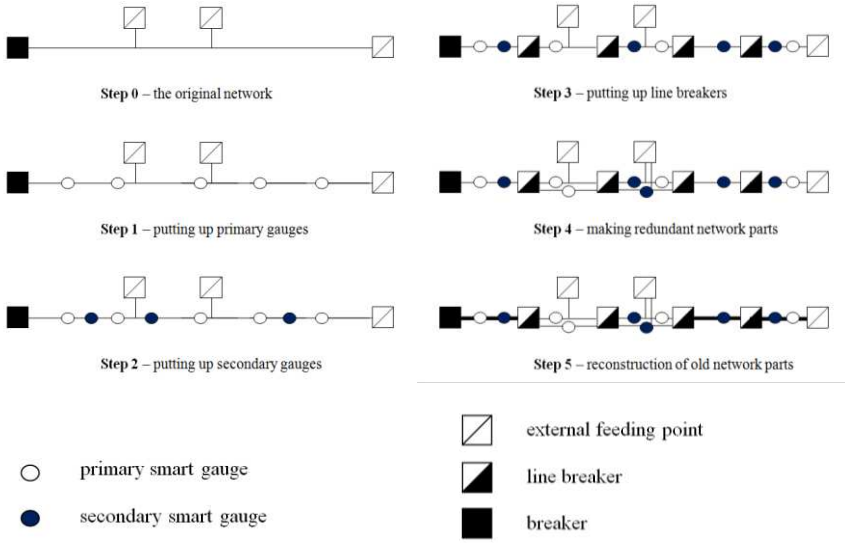

Figure 5
Options to improve the network's reliability

2.5 Definition of the Right Power Mix

The problem is to define the relatively cheap, low CO_2 emission, secure and sustainable power plant portfolio for a country or for continental communities (EU/Russia/USA, etc.). We investigated only the electricity generation, but for the CO_2 emission it can be stretched to the heat generation, traffic and the transportation. [11] [12] [14]

The options are to construct or replace fossil (oil, coal, gas), nuclear, renewable (wind, hydro, PV, geothermal) sources.

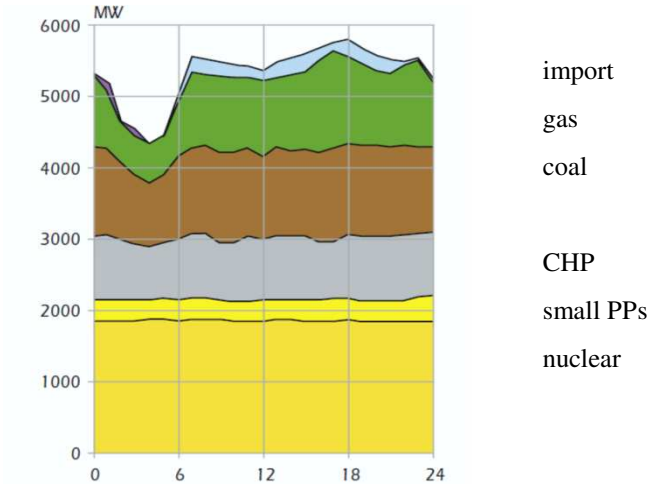

Figure 6
Daily generation portfolio[4]

The simplified SOO problems are solved by linear programming but the mathematically optimal solutions in the practice are often contradictory – as the cheapest OR lowest emission OR best fit to the social expectations.

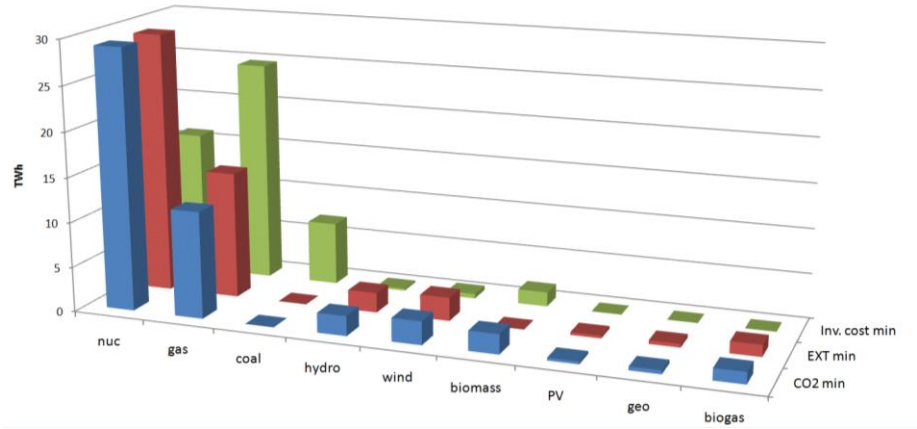

Figure 7
Visualization of generation ratios in different optimization alternatives

[4] source: MAVIR – Hungarian transmission operator

Facing the real MOO problem we developed the Reverse Weighted MOO [18]. In this method we applied the following steps:

1) defined independent SOO-s for each objectives for measuring the maximal "space"
2) identified the difference between the actual and optimal values of the objectives (actual – one-step-reachable SO Optimum)
3) by a priority list we define percentages for the different objectives as fixed constraint
4) we create a SOO for the last, non fixed objective beside fixed constraints

"Reverse" means that we apply the weights only after a series of SOO-s. The advantage of the method is the possibility to define the preferences (before the optimization). The different units (Mt, MEUR) are getting the same neutral percentage (%) dimension.

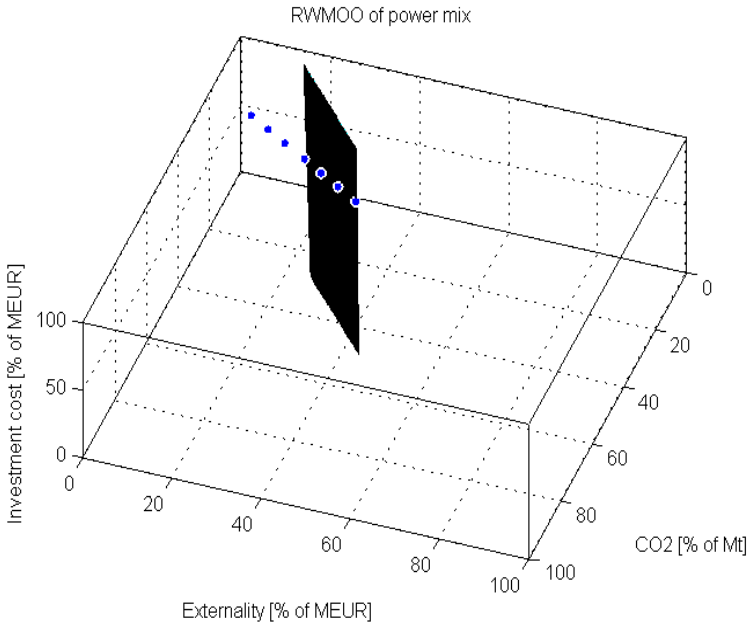

Figure 8
Optimal points by three variables as – CO_2 – Externality – Investment cost

2.6 Regional Energy Trade

The energy flows on the interconnected European network strongly depend on the traders' actions [16] [17]. The energy traders' tasks are to gain profit, to keep the margin high, to get cheaper energy. The local price consists of production price and transfer costs.

$$P_e = Q_e * \left(P_p + P_{CBTe} + \sum_{i=1}^{n} P_{bc\,i} + P_{CBT\,i} \right) \tag{7}$$

where

P_e - local energy price

Q_e - quantity of the energy originating from a distinct location

P_p - production price

$P_{CBT\,e}$ - CBT fee of the exporteur

$P_{bc\,i}$ - border cross fee on the i th border

$P_{CBT\,i}$ - CBT fee of the importeur

The traders want to minimize it, so the paths from the cheap sources to the high priced regions are crowded.

The trade has a lot of physical constraints, such as the cross border capacities, the generation capacities, legal obstacles. The load of the border crossing network can be simulated by the profit maximization objectives of the traders.

We minimized the total market costs (the sum of all national energy costs).

$$C_t = \sum_{i=1}^{n} C_{nat\,i} \tag{8}$$

where

C_t - Total energy costs

$C_{nat\,i}$ - energy cost in the i th country.

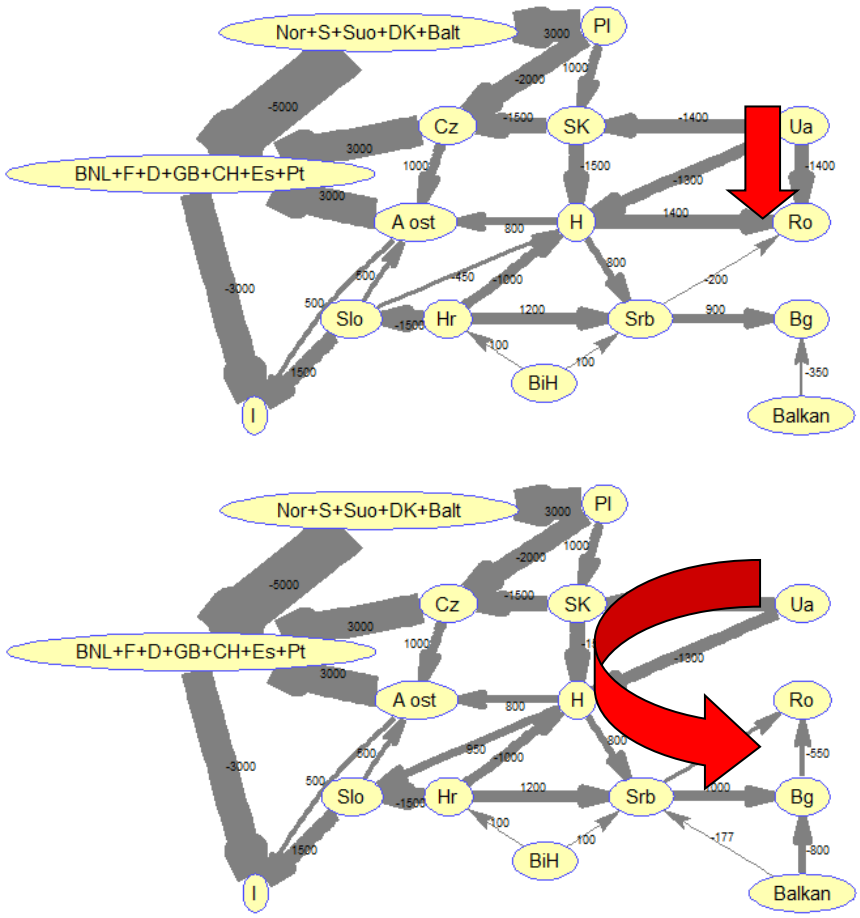

Figure 9
Shortest and cheapest path solutions

Conclusions

The examples have shown that in power systems there are a numerous complex tasks to be supported by computer control. Since the energy industry plays with large amounts of money, the optimization, moreover the profit optimization have high importance. A large variety of applied technologies have been described. In the industry the fast and robust methods are favored. At Óbuda University we developed several optimization solutions applying linear programming, constraint programming, weighting methods and rule based systems.

References

[1] Kwang Lee – ElSharkawi: Modern Heuristic Optimization Techniques, Wiley, 2008

[2] A. Gomez-Expósito – J. Conejo – C. Cannizares: Electric Energy Systems; CRC 2008

[3] R. T. Marler and J. S. Arora: Survey of Multi-Objective Optimization Methods for Engineering; Struct Multidisc Optim 26, 369-395 (2004) DOI 10.1007/s00158-003-0368-6; Springer-Verlag 2004 *and* R. T. Marler. "Survey of multi-objective optimization methods for engineering", Structural and Multidisciplinary Optimization, 04/01/2004

[4] Péter Kádár: Seeking for the Optimal Market; 4th Slovakian – Hungarian Joint Symposium on Applied Machine Intelligence; Herl'any, Slovakia January 20-21, 2006, proceedings pp. 234-246

[5] Péter Kádár: Scheduling of the Generation of Renewable Power Sources; 5th Slovakian – Hungarian Joint Symposium on Applied Machine Intelligence, Poprad, Slovakia January 25-26, 2007, proceedings pp. 255-263

[6] Peter Kadar: Multi Objective Optimalisation of Smartgrid Structure; 15th International Conference on Intelligent Systems Application to Power Systems; Curitiba, Brasilia, November 8-12, 2009

[7] Peter Kadar: Storage Optimization in a Liberalized Energy Market; 7th International Symposium on Applied Machine Intelligence and Informatics; Herl'any, Slovakia January 30-31, 2009

[8] Peter Kadar: "Multi Objective Optimization of Smart Grid Structure", 2009 15th International Conference on Intelligent System Applications to Power Systems, 11/2009

[9] Hugo Morais, Péter Kádár, Pedro Faria, Zita A. Vale, H. M. Khodr: Optimal Scheduling of a Renewable Micro-Grid in an Isolated Load Area Using Mixed-Integer Linear Programming; Elsevier Editorial System(tm) for Renewable Energy Magazine Volume 35, Issue 1, pp. 151-156; April, 2010

[10] Khodr, H.M.; Vale, Zita A.; Ramos, Carlos; Soares, J. P.; Morais, H.; Kadar, Peter: Optimal Methodology for Renewable Energy Dispatching in Islanded Operation; Transmission and Distribution Conference and Exposition, 2010 IEEE PES Digital Object Identifier: 10.1109/TDC.2010.5484411

[11] Peter Kadar: Power Generation Portfolio Optimization by Externality Minimization; Acta Electrotechnica et Informatica; Faculty of Electrical Engineering and Informatics, Technical University of Kosice, SK; April-June 2010, Vol. 10. No. 2, 2010, ISSN 1335-8243, pp. 5-9

[12] Peter Kadar: Multi Objective Power Mix Optimization; 8th International Symposium on Applied Machine Intelligence and Informatics (SAMI 2010) Herl'any, Slovakia January 28-30, 2010

[13] Petar Čisar, Sanja Maravić Čisar: Optimization Methods of EWMA Statistics; Acta Polytechnica Hungarica; Volume 8, Issue Number 5, 2011

[14] Peter Kadar: The Climate Change and the Power Industry; chapter in book Climate Change - Research and Technology for Adaptation and Mitigation ISBN 978-953-307-621-8; Edited by: Juan Blanco; Publisher: InTech, September 2011

[15] Zita Vale: "Computational Intelligence Applications for Future Power Systems", Computational Intelligence for Engineering Systems, 2011

[16] Peter Kadar: "Regional Power Trade Modeling", 2011 16th International Conference on Intelligent System Applications to Power Systems, 2011

[17] Peter Kadar and Andrea Varga: "Power Trade Simulation", 2012 IEEE 16th International Conference on Intelligent Engineering Systems (INES), 2012

[18] Peter Kadar: Reverse Weighted Multi Objective Optimization; INES 2013, San-José, Costa Rica June 19-21